Related titles

Understanding the Rheology of Concrete
(ISBN: 978-0-85709-028-7)

Non-Destructive Evaluation of Reinforced Concrete Structures: Deterioration Processes and Standard Test Methods
(ISBN: 978-1-84569-560-6)

Toxicity of Building Materials
(ISBN: 978-0-85709-122-2)

Woodhead Publishing Series in Civil and Structural Engineering: Number 61

Corrosion of Steel in Concrete Structures

Edited by

Amir Poursaee

AMSTERDAM • BOSTON • CAMBRIDGE • HEIDELBERG
LONDON • NEW YORK • OXFORD • PARIS • SAN DIEGO
SAN FRANCISCO • SINGAPORE • SYDNEY • TOKYO
Woodhead Publishing is an imprint of Elsevier

WP
WOODHEAD
PUBLISHING

ELSEVIER

Notices
Knowledge and best practice in this field are constantly changing. As new research and experience broaden our understanding, changes in research methods, professional practices, or medical treatment may become necessary.

Practitioners and researchers must always rely on their own experience and knowledge in evaluating and using any information, methods, compounds, or experiments described herein. In using such information or methods they should be mindful of their own safety and the safety of others, including parties for whom they have a professional responsibility.

To the fullest extent of the law, neither the Publisher nor the authors, contributors, or editors, assume any liability for any injury and/or damage to persons or property as a matter of products liability, negligence or otherwise, or from any use or operation of any methods, products, instructions, or ideas contained in the material herein.

For information on all Woodhead Publishing publications
visit our website at https://www.elsevier.com/

Working together
to grow libraries in
developing countries

www.elsevier.com • www.bookaid.org

List of contributors

C. Andrade Institute of Construction Science "Eduardo Torroja" (IETcc) of the National Research Council of Spain; Consejo Superior Investigaciones Científicas (CSIC), Madrid, Spain

T. Barrett Purdue University, West Lafayette, IN, USA

O. Burkan Isgor Oregon State University, School of Civil and Construction Engineering, Corvallis, OR, USA

M. ElBatanouny Wiss, Janney, Elstner Associates, Inc., Northbrook, IL, USA

C.M. Hansson Mechanical and Mechatronics Engineering, University of Waterloo, Waterloo, ON, Canada

R.B. Holland Simpson Gumpertz & Heger, Waltham, MA, USA

L.F. Kahn Georgia Institute of Technology, Atlanta, GA, USA

K.E. Kurtis Georgia Institute of Technology, Atlanta, GA, USA

I. Lasa Florida Department of Transportation, Gainesville, FL, USA

K. Lau Florida International University, Miami, FL, USA

D.B. McDonald Epoxy Interest Group of the Concrete Reinforcing Steel Institute, Schaumburg, IL, USA

G. Moriconi Università Politecnica delle Marche, Italy

Amir Poursaee Clemson University, Clemson, SC, USA

C. Qiao Purdue University, West Lafayette, IN, USA; University of Science and Technology Beijing, Beijing, China

R. Spragg Purdue University, West Lafayette, IN, USA

J. Weiss Oregon State University, Corvallis, OR, USA

S.R. Yeomans School of Engineering and Information Technology, University of New South Wales at the Australian Defence Force Academy, Canberra, Australia

P. Ziehl University of South Carolina, Columbia, SC, USA

Woodhead Publishing Series in Civil and Structural Engineering

Preface

The low cost of steel-reinforced concrete and the ready availability of raw materials with which it is formed make it the most widely used structural material available. Many critical infrastructure facilities are made of steel-reinforced concrete, and since they are under constant degradation from the aggressive environments, they suffer from durability issues, particularly the corrosion of the steel bars within such structures. Corrosion is the main deterioration mechanism of those structures which significantly reduces the service life, reliability, functionality of structures, and safety. This corrosion in turn has created a multi-billion-dollar infrastructure deficit. Given the indisputable societal and economical importance of the impact of corrosion when developing advanced structures, it is quite surprising that the study of corrosion in infrastructure facilities receives little to no attention in most civil engineering curricula at both undergraduate and graduate levels! It is obvious that better education for the nation's engineers is essential to improving corrosion control and management practices throughout the national infrastructure. However, to become a fully qualified civil or mechanical engineer usually requires at most a one-semester course in materials, one in which the subject of corrosion is rarely mentioned! Civil engineering education and the profession are confronting a challenging crossroads and undergoing revolution. Nevertheless, the seeming lack of ability of civil engineers to thoroughly understand corrosion and its impact on the service lives of these structures, and its role in designing materials that are adaptable to today's challenging world, hinders progress toward addressing 21st-century challenges. Therefore, there is a critical need to deliver such education to future engineers. This book aims to be a handbook for civil engineers who are involved in design and maintenance of steel-reinforced concrete structures as well as a textbook for upper-level undergraduate- and graduate-level students, specifically in the civil engineering discipline.

This book discusses not only all the important aspects of the field of corrosion of steel-reinforced concrete, but also new topics and future trends. The contributions in this book cover all the important aspects in the field of corrosion and corrosion protection of reinforced concrete, such as the theory and mechanisms of corrosion of steel bars in concrete, different measurement and assessment techniques, the effects of concrete properties on corrosion, repair and rehabilitation, modeling, different corrosion prevention and protection methods, and modeling. It should be acknowledged that

this project was only possible due to the support of the contributors to this book, and I am grateful to them.

I dedicate this book to the memory of my parents and to my wife, Neda, who gave me love beyond measure.

I hope you will enjoy the book and find it useful!

Amir Poursaee
Clemson University, USA

An introduction to corrosion of engineering materials

<div style="float:right">**1**</div>

C.M. Hansson

Mechanical and Mechatronics Engineering, University of Waterloo, Waterloo, ON, Canada

1.1 Introduction—the ubiquitous nature of corrosion

With isolated exceptions, metals exist in Earth's crust as minerals such as carbonates, sulfides, sulfates, or oxides formed over billions of years. These compounds are therefore considered to be in their equilibrium state—that is, their lowest energy state. Extracting the metals from these compounds requires a significant amount of energy in the form of heat or electrical power. Once extracted, the metals and alloys are in a thermodynamically metastable state and depending on the environment, they will always attempt to revert to a lower energy compound, usually by corrosion or oxidation. Since the Earth's atmosphere contains water and oxygen, and coatings and other barriers are inherently imperfect, it is impossible to completely prevent corrosion. Consequently, all metals and alloys in use today are in a metastable condition.

1.2 Thermodynamics are on the side of corrosion

The stability of a metal is usually described in terms of its electrochemical potential, a thermodynamic function that may be defined in the context of corrosion as "the ease of ionizing an atom of the metal." Potentials are dependent on the pH of the environment and factors such as oxygen availability. Potentials cannot be determined absolutely, and are generally defined as the potential difference between the metal of interest and that of a reference electrode so chosen to have a stable potential (Revie and Uhlig, 2008). The "standard hydrogen electrode" (SHE) is the reference electrode against which all other electrodes are measured and is given the electrochemical potential of 0.00 V. It is designed so that the reaction: $2H^+ + 2e^- = H_2$ is in equilibrium at pH 0 (i.e., 1 M acid solution), 1 atm hydrogen gas, and 25 °C. Because the hydrogen electrode is cumbersome to operate and transport, other electrodes consisting of a metal in contact with a saturated solution of its ions, such as $Cu/CuSO_4$, are used. The different common reference electrode potentials relative to that of the SHE are given in Table 1.1, and conversions are illustrated in Figure 1.1 (Roberge). These electrodes are not generally suitable for embedding in concrete because they become unstable over a short period of time at high pH levels. Therefore, an Mn/MnO_2 electrode has been developed specifically for use in concrete (Arup et al., 1997).

Table 1.1 Characteristics of common reference electrodes (Roberge)

Electrode type	Equilibrium reactions Nernst equation	Conditions (activity)	Potential V vs SHE	Temp. coefficient mV/°C
Standard hydrogen electrode (SHE)	$2H^+ + 2e^- = H_2$ $E^0 = 0.059\,pH$	$pH = 0$		
Silver chloride	$AgCl + e^- = Ag + Cl^-$ $E^0 = 0.059\log_{10}(a_{Cl-})$	$a_{Cl-} = 1$	0.2224	−0.6
		0.1 M KCl	0.2881	−0.6
		1.0 M KCl	0.235	−0.6
		Saturated KCl	0.199	−0.6
		Seawater	∼0.250	−0.6
Calomel	$Hg_2Cl_2 + 2e^- = 2Hg + 2Cl^-$ $E^0 - 0.059\log_{10}(a_{Cl-})$	$a_{Cl-} = 1$	0.268	
		0.1 M KCl	0.3337	−0.06
		1.0 M KCl	0.280	−0.24
		Saturated KCl	0.241	−0.65
Mercurous sulfate	$Hg_2SO_4 + 2e^- = 2Hg + SO_4{}^{2-}$ $E^0 - 0.0295\log_{10}(a_{SO_4{}^{2-}})$		0.6151	
Mercuric oxide	$HgO + 2e^- + 2H^+ = Hg + H_2O$ $E^0 - 0.059\,pH$		0.926	
Copper sulfate	$Cu^{2+} + 2e^- = Cu$ (SO_2 solution $E^0 + 0.0295\log_{10}(a_{Cu}{}^{2+})$	$a_{Cu} = 1$ Saturated	0.340 0.318	
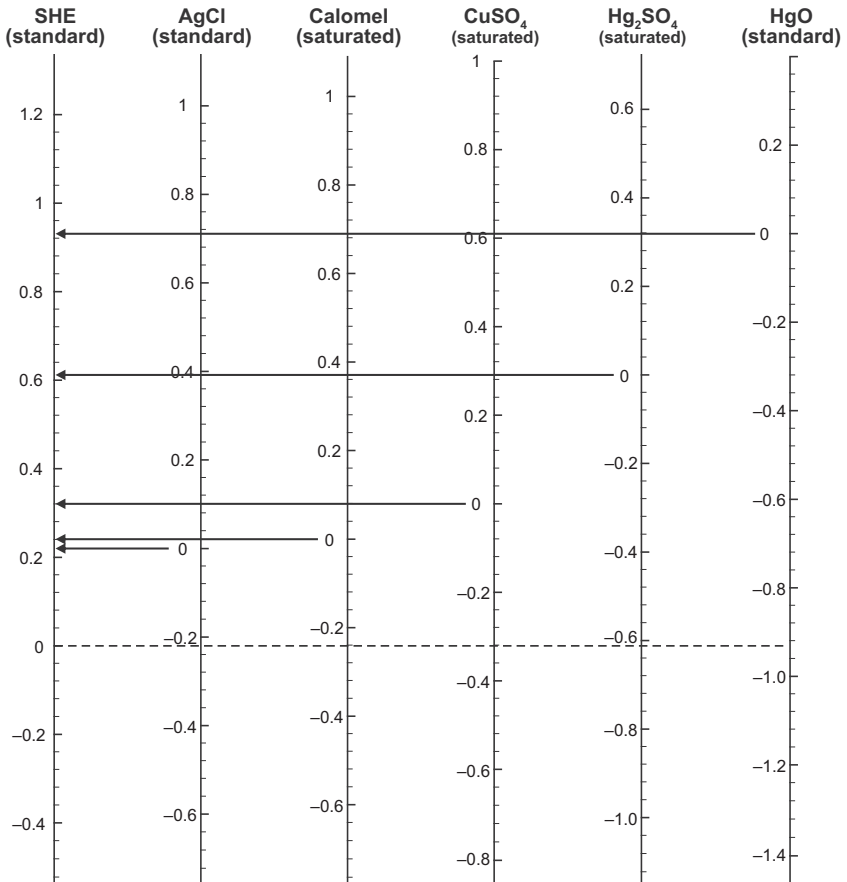
Figure 1.1 Comparison of potentials from different reference electrodes. Reproduced with permission from Roberge.

The ranges of electrochemical potential and pH in which the products of corrosion are either dissolved ions—for example, Fe^{2+} or Cr^{3+}—or solid oxides or hydroxides are given in the "Atlas of Electrochemical Equilibria" (Pourbaix, 1974) for each metal in aqueous solutions. The solid products may protect the metal from further rapid corrosion and are then known as "passive films." The simplified "Pourbaix diagrams" for iron and zinc given in Figure 1.2 indicate the regions of potential and pH in which the metals are immune from corrosion, will actively corrode, or will form passive films.

The dashed lines labeled (a) and (b) in each diagram in Figure 1.2 represent the equilibria for the reactions:

1. $2H^+ + 2e^- = H_2$
2. $O_2 + 2H_2O + 4e^- = 4(OH)^-$
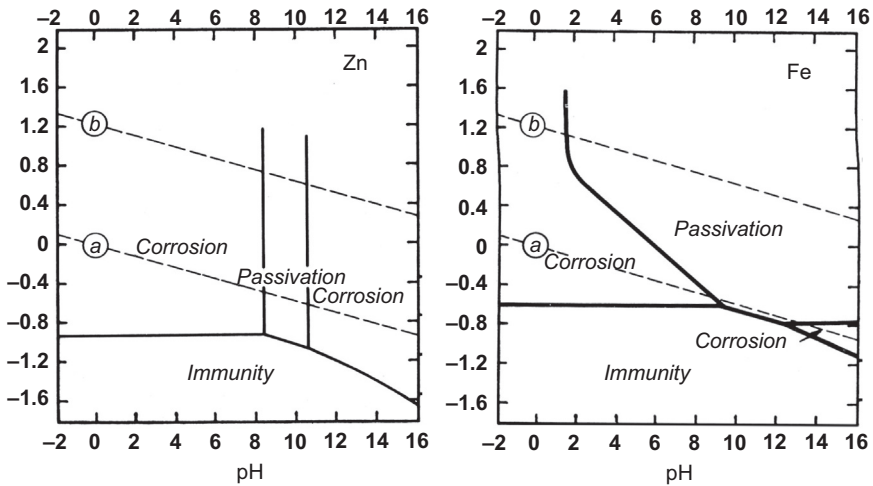
Figure 1.2 "Pourbaix diagrams" for zinc and iron, showing regions of pH and potential in which each metal is passive; that is, the corrosion products are solid and protect the metal from active corrosion (Pourbaix, 1974).

The dissolution or oxidation of a metal (e.g., $M \rightarrow M^{2+} + 2e^{-}$) constitutes the anodic half-cell reaction, and the electrons released are immediately consumed, usually by one of the two cathodic half-cell reactions (a) or (b). In low pH conditions and with little available oxygen, reaction (a) is the most likely cathodic reaction, whereas with more oxygen and/or at neutral or high pH, reaction (b) is more likely.

The limitations of these diagrams are that they consider only pure metals, water and oxygen as the electrolyte, and are calculated only for 25 °C. Research is only fairly recently being conducted to calculate comparable electrochemical phase diagrams for alloys and for different environments using computational methods (Bale et al., 2009; Andersson et al., 2002) or by experiment, for example (Beverskog and Puigdomenech, 1999a,b; Nishimura and Kodama, 2003; Gimenez et al., 1981).

1.3   Kinetics are on the side of the metals

First and foremost, only about 1 in 10 million atoms in a metal or alloy is on the surface and exposed to the environment, and therefore susceptible to corrosion. Second, although these surface atoms react, many of the reactions result in a solid oxide or hydroxide that protects the underlying metal from further rapid corrosion. The solid generally forms a very thin film on the order of a few to a few hundred nanometers and consisting of multiple layers (Oranowska and Szklarska-Smialowska, 1981; Albani et al., 1986). It is described as a passive film rather than a coating, and is discussed in detail in Chapter 2. Because corrosion involves the exchange of electrons between the metal (the anode) and the cathodic species (e.g., hydrogen ions or dissolved oxygen), it is described as an "electrochemical process," and measurement of the current flowing between anode and cathode is a direct measure of the rate of dissolution or
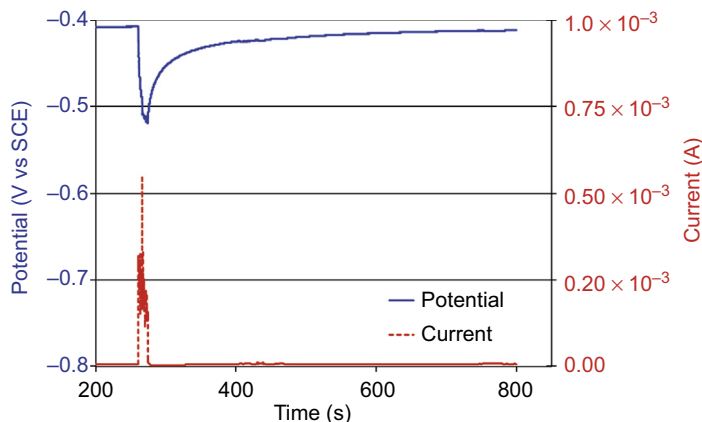
Figure 1.3 Recovery time of passive film on S2205 duplex stainless steel when immersed in synthetic pore solution and scratched (Hansson and Mammoliti, 2004).

oxidation of the metal, known as the corrosion current. The passive film is not perfect, and behaves as a leaky capacitor with some metal ions being transported through the film. Thus, corrosion is not zero but at a level considered insignificant relative to the expected service life of the part. Another major feature of natural passive films is their ability to recover after being damaged mechanically. This is illustrated in Figure 1.3, which shows corrosion current and potential excursions for a sheet of grade UNS S2205 duplex stainless steel immersed in a synthetic concrete pore solution (pH ∼ 13.5) and scratched with a knife. Note that the current recovered after ∼ 15 s, but the potential drifted much more slowly to its original level.

Unfortunately, while metals and alloys may exhibit passive behavior resulting in a loss of material of less than 1 μm/year, in practice that passive film can be breached, causing corrosion rates several orders of magnitude higher. A prime culprit in passive film failure is the chloride ion, which causes major problems in marine environments and in regions where deicing salts are used, as well as in some industrial regions. Other less well-understood culprits are microbes such as bacteria as well as molds (Stott, 1993; Lane, 2005; Sooknah et al., 2007), which are a major cause of blockage and corrosion in pipelines.

1.4 Forms of corrosion

There are many forms of corrosion (Revie and Uhlig, 2008; ASM, 1990), but only those most commonly encountered in concrete structures are discussed here.

1.4.1 General corrosion

General corrosion occurs in regions of potential and pH in which the corrosion products are either dissolved ions or nonprotective oxides/hydroxides. The rust produced on steel in the outdoor atmosphere is a typical example. In concrete, general corrosion can result from a decrease in pH to a range where the passive film is not stable and

breaks down, leaving the steel to either dissolve (in very low pH solutions) or form a nonprotective oxide/hydroxide. This form of corrosion can result in a general thinning of the metal or alloy, and eventually failure of the part.

1.4.2   Pitting corrosion

Pitting corrosion or localized corrosion, examples of which are shown in Figure 4.10, is usually limited to those metals with passive films such as aluminum, titanium, or zinc in neutral solutions, or steel at high pH. The most common cause is very localized break-down of the passive film by chlorides, typically from seawater and deicing salts, but also from industry and even household salt use. There have been many studies of the break-down of passive films, but because the films are so thin, the initiation of pit cannot be observed directly. It is generally agreed that the first step is by adsorption of chloride or other halide ions. For the next step, theories diverge from the adsorption-induced devel-opment of mechanical stresses in the film to a local thinning of the film, thereby increasing the potential gradient across the film and local "dielectric breakdown" (Sato, 1990; Szklarska-Smialowska, 2002). A recent model including the role of the oxide nanolayer is given in Marcus et al. (2008). The semiconducting nature of the passive film is discussed in Chapter 2.

Once pits are formed, however, there is a general consensus that they create a local "differential environmental cell" in which the electrolyte in the pit becomes depleted in oxygen and more acidic than the solution adjacent to the nonpitted passive film. Moreover, the growth of the pit becomes autocatalytic because the chloride ions are not consumed in the process; they react with the metal, but the metal chloride complex becomes unstable and reacts further, releasing the chloride ions to combine with other metal ions. The sequence of reactions is as follows:

$$M \rightarrow M^{n+} + ne^-$$

$$M^{n+} + nCl^- \rightarrow MCl_n$$

$$MCl_n + nH_2O \rightarrow M(OH)_n + nCl^-$$
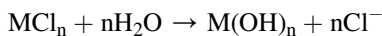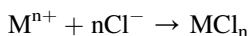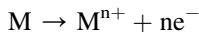
The electrons released in the first of these reactions travel through the metal as shown in Figure 1.4, and react with water and oxygen to create hydroxyl ions.

A third form of corrosion, which is not a concern for reinforcing bars but can be a problem for prestressed or post-tensioned steel, is environmentally assisted cracking that comprises stress corrosion cracking and/or hydrogen embrittlement. These phenomena are discussed in Chapter 3.

1.5   A brief history of corrosion of reinforcing steel

The problem of rebar corrosion has been recognized for over a century. In 1911, a report in the *Proceedings of the American Institute of Electrical Engineers* (Magnusson and Smith, 1911), based on laboratory studies of a few years
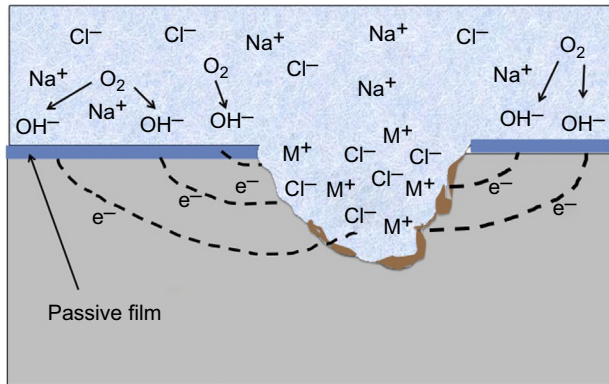
Figure 1.4 Schematic representation of chloride-induced pitting corrosion of a passivated metal (Hansson, 2011).

earlier, stated: "While reinforced concrete was coming into general use as a structural material much space in the technical press was given to discussions and reports on the durability of the encased iron. The results from a large number of experiments gave fairly conclusive evidence that under ordinary conditions the iron is protected, and that even if it was rusty when placed in the concrete, it will be free from the oxide after remaining in the concrete for some time. The time test on the durability of practical structures is, of course, the final arbiter, and for each year the increasing data bears out the assumption that properly constructed concrete-steel structures will stand indefinitely."

Nevertheless, in 1911, there were two reports of electrolytic corrosion (currently known as "stray current corrosion"). The first (Brown, 1911) involved damage to a large reinforced concrete (RC) packing house outside New York City. It was originally attributed to stray current from a nearby electric railway, but subsequently was found to be caused by a short between the DC electric light circuit and a water pipe, but "*only where the concrete was damp and the pipe had an electric potential positive to ground.*" At that time, "*none thought it possible that electricity could leak to steel deeply buried in beams and girders and split the concrete apart*" (Brown, 1911). The second report followed inspection of four RC structures in the harbor in Southampton, United Kingdom (Bamber et al., 1911). One of the structures, a small jetty, built in 1899 and believed to be the oldest such structure in the country, was found to be in excellent condition. Two other structures, a coal barge jetty and a quay, built in 1908, were showing significant deterioration: rusting of the steel and cracking and spalling of the concrete. This problem too was traced to the return wire of the electric lighting circuit, which was earthed (ground) to a metal plate on the deck of the jetty with a path to the sea through the concrete. Both of these studies used electrical potential difference measurements between the lighting wires, the rebar, and the ground in order to identify the cause of deterioration.

Much of the concern for the next few decades appears to have been focused on electrolytic, or stray current, corrosion. In 1949, a study of the stray-current corrosion of steel embedded in concrete and buried in soil adjacent to an electrified railroad

(which produced the stray current) concluded that (a) a large (300 mm) concrete cover provided some but not complete protection from corrosion; (b) the electrochemical potentials produced attracted sulfate ions from the soil that deteriorated the concrete; (c) AC currents did not produce any degradation; (d) stainless steel bars were not corroded. and (e) an asphalt coating on the concrete was effective in protecting the rebar (Magee, 1949).

There was, however, an early realization of the destructive influence of chlorides. In 1917, practically all marine concrete structures in the United States were inspected (Wig and Ferguson, 1917). It was found that the majority of them, with ages ranging from 1 to 10 years, were showing some signs of deterioration or failure due to corrosion of the rebar above the waterline. For some structures, seawater had been used as mixing water, but for most, freshwater was used. After eliminating the possibility of "electrolysis" (stray current corrosion), it was concluded that the cause was accumulation of salts in the concrete pores above the waterline by capillarity and evaporation—a process widely accepted today. It was also noted that when steel corrodes, it occupies about twice its previous volume, causes stresses to develop in the concrete, and results in cracking and spalling. The role of preexisting cracks and those caused by corrosion was also discussed. It was concluded that preexisting cracks would be a large contributing factor but not a necessary one—a topic still under discussion today in Chapter 8. The recommended solutions were increasing the concrete cover and the use of galvanized steel—again a current topic, discussed in Chapter 6.

A recognition of concrete as an electrolyte was reported in *Corrosion* in 1957 (Stratfull, 1957). This paper concerned the deterioration of a seven-mile-long causeway in California, United States, and is believed to be the first structure in which the areas of corrosion were identified by electrochemical corrosion mapping—a technique in routine use today by transport authorities around the world for condition monitoring. The map for one pile in 1957 is shown in Figure 1.5.

The use of this mapping technique for other structures was initiated in Europe in the 1970s after an apartment balcony in Copenhagen collapsed, killing several people. There were approximately 6000 balconies of similar design and age, and potential mapping was used to identify those in need of immediate attention (Grønvold and Arup, 1979).

1.6 The magnitude of the corrosion issue in general

The cost of corrosion can be measured in social, environmental, and financial terms (Hansson, 2011). There have been a number of projects aimed at estimating the financial costs, but there has been much less attention given to the social and environmental impacts. For example, a corrosion-induced oil pipeline failure in which the oil contaminates the surrounding ground and water, is described in terms of the cleanup and repair costs, but not in terms of the impact on the neighboring population, flora, and fauna, and the time for these to return to their former states. Fortunately, few corrosion-induced failures result directly in human deaths, but the resulting environmental contamination can cause death to countless other species, and future sickness

Concrete cracked & steel rusted 2" below top of pile
on North side
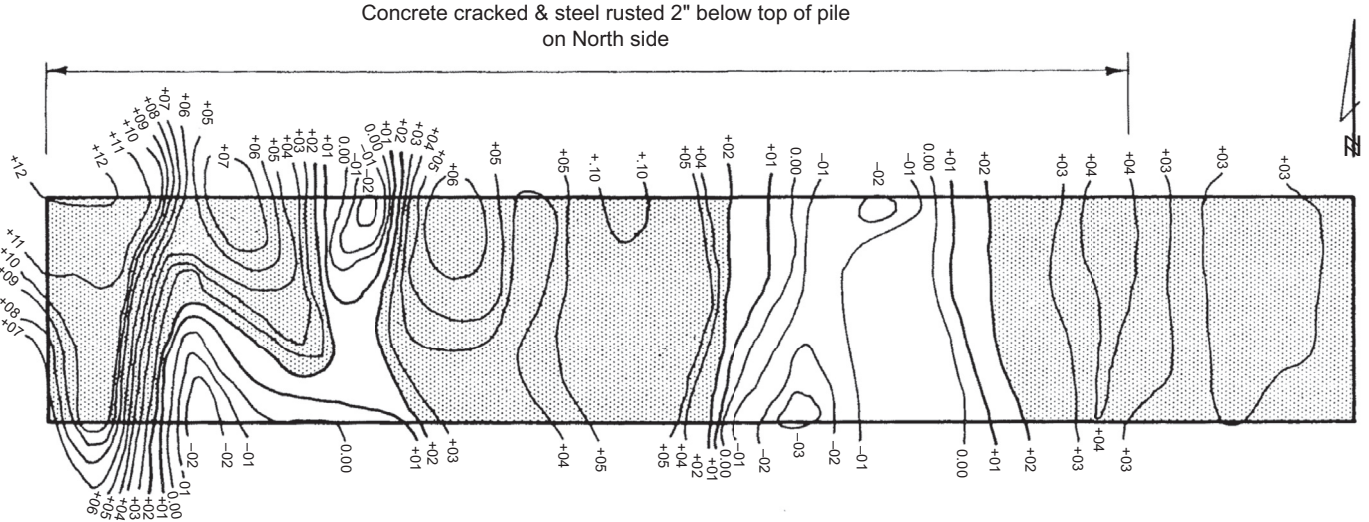
Figure 1.5 Equipotential contours of surface potential differences for Pile A of the San Mateo Highway Bridge. Shaded sections represent anodic areas while white areas represent cathodic areas. Potentials are between Cu/CuSO$_4$ electrodes on the concrete and on the soil. Scale: 1 in = 8 ft longitudinally; 1 in = 2 ft laterally (Stratfull, 1957).

and suffering for the human population. The worst example of this was the Bhopal disaster of 1984 that resulted in the release of toxic gases and the immediate deaths of over 8000 people, but also longer-term health problems for a half-million people (Brown, 2009; Peterson, 2009). Another insidious form of corrosion is the long-term slow release of metallic ions, which can have unpredicted health impacts (Bertling et al., 2006a,b; Dietrich et al., 2004), particularly in the case of microbially induced corrosion (Costerton et al., 1987).

To quote George Hayes, director general of the World Corrosion Organization (Hays, 2010):

> The public hears about bridges and piers that collapse due to corrosion and environmental damage caused by pipeline failures, but does it ever hear about the loss of potable water from water main corrosion or environmental damage caused by corroded sewer lines? The answer is no. Neither news media nor government agencies find such events sufficiently newsworthy to alert the public. Yet in many countries, the cost of water and wastewater system failures is far greater than any other single sector of the economy.
>
> Corrosion knows no national boundaries. Acid rain generated in one country pollutes the environment and causes corrosion damage far beyond that country's borders and even beyond the borders of its neighbors. Toxic materials, released from corroded equipment in one area, pollute the air and water far beyond one country's borders. And toxic material released into the world's waterways poisons sea life, killing many species and making others toxic to humans.

Table 1.2 Estimated costs of corrosion in different countries (Biezma and San Cristóbal, 2005)

References	Year	Country	% GNP	Cost
Zhu (1986)	1986	China		
Cherry and Skerry (1983)	1983	Australia	1.5	US$2 B
Al-Kharafi et al. (1995)	1995	Kuwait	5.2	US$1 B
Tullmin (2015)	1996	Switzerland	3−5	10−15 B Swiss Fr.
JSCE (2001)	2001	Japan	0.77	3938 B Yen
Tullmin (2015)	2008	Australia	2	Aus. $1−$5 B
Koch et al. (2002)	2002	United States	3.1	US$276 B
Sastri et al. (2003)	2003	Canada		CAD$32.8 B
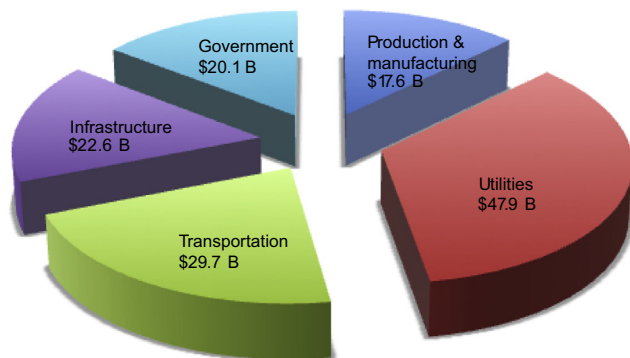
Figure 1.6 Direct annual costs of corrosion in the United States (Koch et al., 2002).

While little attention has been paid to the social costs, the financial costs of corrosion have received a huge amount of attention in recent years, largely in an attempt to draw the attention of decision makers to the magnitude of the problem. The general conclusion is that corrosion is consuming approximately 3% of the world's gross domestic product (GDP)—that is, about US$2.2 trillion (Hays, 2010). The estimates of the financial cost to several nations are given in Table 1.2, modified from Biezma and San Cristóbal (2005).

For the United States in 2002, the *direct* annual costs of corrosion were estimated at $137.9 B, broken down into sectors in Figure 1.6. When the *indirect* costs were included, this total became $276 B—or 3.1% of US GDP.

1.7 The magnitude of the corrosion issue specifically related to RC structures

Concrete in the early part of the last century was relatively simple, as illustrated in Figure 1.7(a). Today's concrete is a very sophisticated blend. Figure 1.7(b) shows how the proportions of the basic constituents can be tailored to the specific application and "seasoned" with a number of chemical and mineral admixtures to enhance performance, as described further in Chapter 7. Consequently, the diffusion of deleterious species through today's concrete pores is a very slow process (Sandberg et al., 1998; Stanish et al., 1997). Unfortunately, all structural concrete is cracked, and ingress is significantly faster through the cracks than through the pores (Jacobsen et al., 1966; Wang et al., 1997). The impact of the cracks on the time required to initiate corrosion of the rebar and on subsequent corrosion rates is discussed in detail in Chapter 8.

According to Davis and Goldberg (2013), most bridges in the United States were designed for a 50-year service life, and their average age is now 45 years. The number of these bridges described as structurally deficient in 2012 was 66,405, and they had an average age of 65 years. It is clear that this number is likely to increase significantly in the future, raising the annual cost to far beyond the 2002 estimate of $8.3 B.

(a)

(b)
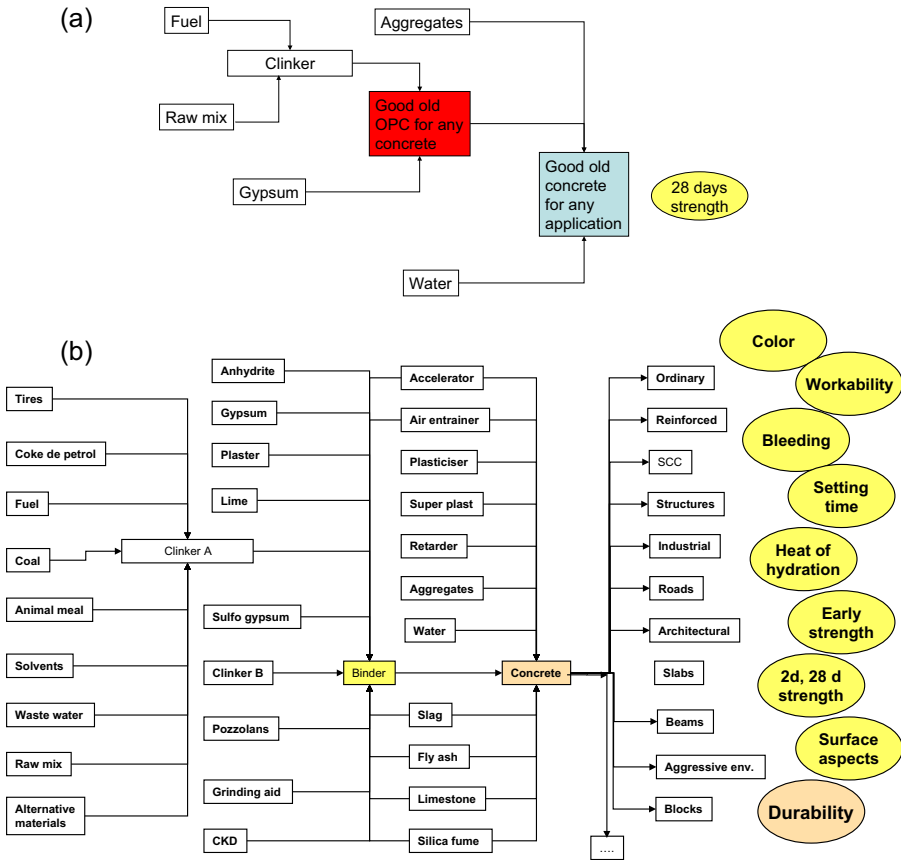
Figure 1.7 Concrete constituents (a) at the beginning of the last century and (b) today. Courtesy: Y. Guitton-Fumet, Lafarge Central Research Laboratory.

The age of the infrastructure in Canada, as a percentage of its useful life in 2007, is given in Figure 1.8, showing that the average age of all sectors except water supply systems exceeds 50% (Gagnon et al., 2007). In Ontario, this translates to 2600 of the provincial bridges in a 2000 survey having reached an average of more than 80% of their planned service lives. Although there are many factors contributing to the "end of life" for RC bridges, corrosion of the reinforcing steel is by far the most common.

The total (direct plus indirect) annual cost of corrosion of the (largely RC) infrastructure in the United States was estimated in 2002 as $63.6 B and was broken down in sectors as given in Table 1.3 (Koch et al., 2002). Note the huge cost to the drinking water and sewage sector with respect to the comments of Mr Hayes, quoted above.
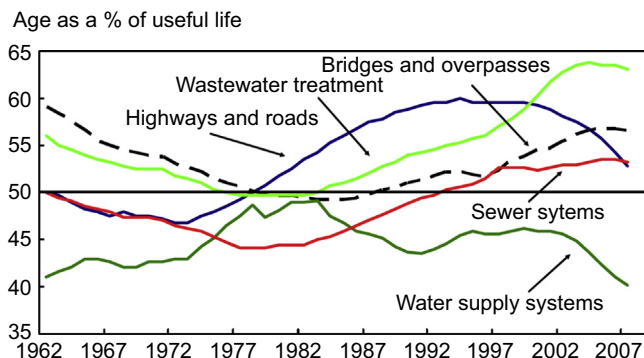
Figure 1.8 Age of Canadian infrastructure as a function of its useful life (Gagnon et al., 2007).

Table 1.3 **Cost of corrosion in the infrastructure section in the United States (Koch et al., 2002)**

Sector	Annual cost
Highway bridges	$8.3 B
Gas and liquid pipelines	$7.0 B
Waterways and ports	$0.3 B
Hazardous materials storage	$7.0 B
Gas distribution	$5.0 B
Drinking water and sewer	$36.6 B

1.8 Conclusion

Corrosion is here to stay. The goal for the corrosion science and engineering community must be to slow the corrosion rate sufficiently enough that the part or structure remains serviceable for its specified service life. This requires a thorough understanding of the nature of corrosion and of the materials comprising the part or structure. The remaining chapters in this book are aimed at explaining the fundamentals, methods, and materials to achieve this goal.

For most engineering applications, alloys should be selected that are passive in the environment in which they will operate in service or are provided with adequate protection for the expected useful life. Unfortunately, most engineers select materials for their functional properties, such as mechanical strength or electronic capabilities, without regard to the potential hazards of the service environment. To quote (Koch et al., 2002): "Corrosion research has, over the years, suffered from inadequate industry and government funding, especially given the cost and inconvenience associated

with corrosion of water mains, bridge structures, automobiles, airplanes, and pipelines. In contrast, physicists and biologists have captured the attention of the public and Congress by describing the dynamics of high-energy physics and biotechnology. While not as noteworthy to the popular press as some other technologies, corrosion research has much to contribute to delivering social services more efficiently and more reliably while lowering the costs of many of the products and services purchased by the public."

To conclude, there is one final objective: to educate the design and engineering community in order to break the "corrosion cycle" defined by J.C. Bowles, former president of NACE International (Tullmin, 2015):

- **Phase 1—Neglect**: Corrosion control is ignored; this may be "tempting" to (poor) management, as corrosion problems may not show up immediately. It is easy to be lulled into a false sense of security.
- **Phase 2—Panic**: The previously hidden corrosion danger becomes apparent, possibly with disastrous financial consequences and safety hazards. It is not easy to combat corrosion rationally and effectively in a state of panic.
- **Phase 3—Learning Curve**: In dealing with the serious corrosion problems, effective corrosion control measures are eventually introduced, and failure rates are reduced to manageable levels. Considerable effort (and time) may be required before effective solutions are found, qualified, and implemented.
- **Phase 4—Unlearning Curve**: Once the initial crisis is over, there is a risk that corrosion control will be neglected again, and that hard lessons learned in the past will be forgotten. This is when the corrosion cycle starts all over again, with the neglect stage reestablishing itself.

References

Al-Kharafi, F., Al-Hashem, A., Matrouk, F., 1995. Economic Effects of Metallic Corrosion in the State of Kuwait. KISR Publications.

Albani, O.A., Zerbino, J.O., Vilche, J.R., Arvia, A.J., 1986. A comparative electrochemical and ellipsometric study of iron electrodes in different alkaline electrolytes. Electrochimica Acta 31, 1403−1411.

Andersson, J.-O., Helander, T., Höglund, L., Shi, P., Sundman, B., 2002. Thermo-calc & Dictra, computational tools for materials science. CALPHAD 26, 273−312.

Arup, H., Klinghoffer, O., Mietz, J., 1997. Long Term Performance of MnO_2-Reference Electrodes in Concrete. Corrosion 97. NACE.

ASM, 1990. Metals Handbook−Tenth Edition−Corrosion. ASM International, Materials Park.

Bale, C.W., Bélisle, E., Chartrand, P., Decterov, S.A., Eriksson, G., Hack, K., Jung, I.-H., Kang, Y.-B., Melancon, J., Pelton, A.D., Robelin, C., Petersen, S., 2009. FactSage thermochemical software and databases−recent developments. CALPHAD 33, 295−311.

Bamber, H.H.G., Marsh, C.F., Wentworth-Sheild, F.F., 1911. A British example of electrolytic corrosion of steel in a reinforced concrete structure. Engineering News Record 66.

Bertling, S., Wallinder, I.O., Berggren Kleja, D., Leygraf, C., 2006a. Long-term corrosion-induced copper runoff from natural and artificial patina and its environmental impact. Environmental Toxicology and Chemistry 25, 891−898.

Bertling, S., Wallinder, I.O., Leygraf, C., Berggren Kleja, D., 2006b. Occurrence and fate of corrosion-induced zinc in runoff water from external sources. Science of the Total Environment 367, 908−923.

Beverskog, B., Puigdomenech, 1999a. Revised pourbaix diagrams for Zn. Corrosion Science 39, 107−114.

Beverskog, B., Puigdomenech, I., 1999b. Pourbaix diagrams for the ternary system of iron-chromium-nickel. Corrosion 55, 1077−1087.

Biezma, M.V., San Cristóbal, J.R., 2005. Methodology to study cost of corrosion. Corrosion Engineering, Science and Technology 40, 344−352.

Brown, H.H., 1911. Serious injury to a reinforced concrete building by electrolysis. Engineering News Record 65.

Brown, M., 2009. Bhopal Gas Disaster Legacy Lives on 25 Years Later. Online. The Daily Telegraph. Available: http://www.telegraph.co.uk/news/worldnews/asia/india/5978266/Bhopal-gas-disasters-legacy-lives-on-25-years-later.html (accessed 18.07.10).

Cherry, B.W., Skerry, B.S., 1983. Corrosion in Australia. Australian National Centre of Corrosion Prevention and Control Feasilbility.

Costerton, J.W., Cheng, K.-J., Geesey, G.G., Ladd, T.I., Nickel, J.C., Dasgupta, M., Marrie, T.J., 1987. Bacterial biofilms in nature and disease. Annual Review of Microbiology 41, 435−464.

Davis, S., Goldberg, D., 2013. The Fix We're in for: The State of Our Nation's Bridges 2013 (Washington, DC).

Dietrich, A.M., Glindemann, D., Pizarro, F., Gidi, V., Olivares, M., Araya, M., Burlingame, G.A., Khiari, D., Edwards, 2004. Health and aesthetic impacts of copper corrosion on drinking water. Water Science and Technology 49, 55−62.

Gagnon, M., Gaudreault, V., Overton, D., 2007. Age of Public Infrastructure: A Provincial Perspective (Ottawa, Canada).

Gimenez, P., Rameau, J.J., Reboul, M.C., 1981. Experimental pH potential diagram for aluminium for sea water. Corrosion 37.

Grønvold, F., Arup, H., 1979. Localization of corroding reinforcement by electrochemical potential surveys. In: RILEM Symposium on Quality Control of Concrete Structures, pp. 251−258 (Stockholm, Sweden).

Hansson, C.M., 2011. The impact of corrosion on society. Metallurgical and Materials Transactions A 42A, 2952−2962.

Hansson, C.M., Mammoliti, L., August 2004. Alternative pretreatments of 316LN and 2205 stainless steel reinforcing bars. University of Waterloo. Report No.: MTO Project HIIFP #152A222.

Hays, G.F., 2010. Corrosia. Fall 2010. World Corrosion Organization (National Association of Corrosion Engineers Europe Board).

Jacobsen, S., Marchand, J., Boisvert, L., 1966. Effect of cracking and healing on chloride transport in OPC concrete. Cement and Concrete Research 26, 869−881.

JSCE, 2001. Committee on Corrosion Loss in Japan, vol. 50, 490−512.

Koch, G.H., Brongers, M.P.H., Thompson, N.G., Virmani, Y.P., Payer, J.H., 2002. Corrosion Cost and Prevention Strategies in the United States. Federal Highway Administration, McLean VA.

Lane, R.A., 2005. Under the microscope: understanding, detecting and preventing microbiologically influenced corrosion. Journal of Failure Analysis and Prevention 5 (5), 10−12.

Magee, G.M., 1949. Electrolytic corrosion of steel in concrete. Corrosion 5, 378−382.

Magnusson, C.E., Smith, G.H., 1911. Electrolytic corrosion of reinforced concrete. Proceedings of the American Institute of Electrical Engineers 30.

Marcus, P., Maurice, V., Strehblow, H.-H., 2008. Localised corrosion (pitting): a model of passivity breakdown including the role of the oxide nanostructure. Corrosion Science 50, 2698−2704.

Nishimura, T., Kodama, T., 2003. Clarification of chemical state for alloying elements in iron rust using a binary-phase potential−pH diagram and physical analyses. Corrosion Science 45, 1073−1084.

Oranowska, H., Szklarska-Smialowska, Z., 1981. An electrochemical and ellipsometric investigation of surface films grown on iron in saturated calcium hydroxide solution with or without chlorides. Corrosion Science 21, 735−747.

Peterson, M.J., 2009. Bhopal Plant Disaster. Online. Available: http://www.umass.edu/sts/ethics.

Pourbaix, M., 1974. Atlas of Electrochemical Equilibria in Aqueous Solutions. National Association of Corrosion Engineers, Paris, France.

Revie, R.W., Uhlig, H.H., 2008. Corrosion and Corrosion Control. John Wiley & Sons, Hoboken, NJ, USA.

Roberge, P.R., Corrosion-Doctors.org (accessed 14.05.15).

Sandberg, P., Tang, L., Andersen, A., 1998. Recurrent studies of chloride ingress in uncracked marine concrete at various exposure times and elevations. Cement and Concrete Research 28, 1489−1503.

Sastri, V.S., Elboujdaini, M., Perumareddi, 2003. Economics of corrosion and wear in Canada. In: Li, J., Elboujdaini, M. (Eds.), International Conference on Environmental Degradation of Metals. Metallurgical Society of the Canadian Institute of Mining, Vancouver, Canada.

Sato, N., 1990. An overview of the passivity of metals. Corrosion Science 31, 1−19.

Sooknah, R., Papavinasam, S., Revie, R.W., 2007. Monitoring Microbiologically Influenced Corrosion: A Review of Techniques. Corrosion 2007. National Association of Corrosion Engineers, Nashville, TN.

Stanish, K., Hooton, R.D., Thomas, M.D.A., 1997. Testing the Chloride Penetration Resistance of Concrete: A Literature Review. University of Toronto, Toronto.

Stott, J.F.D., 1993. What progress in understanding of microbially induced corrosion has been made in the last 25 years? A personal viewpoint. Corrosion Science 35, 667−673.

Stratfull, R.F., 1957. The corrosion of steel in a reinforced concrete bridge. Corrosion 13 (3), 43−48.

Szklarska-Smialowska, Z., 2002. Mechanism of pit nucleation by electrical breakdown of the passive film. Corrosion Science 44, 1143−1149.

Tullmin, M., 2015. Corrosion-Club.com (accessed 02.08.15).

Wang, K., Jansen, D.C., Shah, S.P., 1997. Permeability study of cracked concrete. Cement and Concrete Research 27, 381−393.

Wig, R.J., Ferguson, L.R., 1917. Reinforced concrete in sea water fails from corroded steel. Engineering News Record 79 (15), 689−693.

Zhu, R., 1986. International approaches to reducing corrosion costs. Corrosion 86 (Houston, TX. National Association of Corrosion Engineers).

Corrosion of steel in concrete structures

2

Amir Poursaee
Clemson University, Clemson, SC, USA

2.1   Introduction

The low cost of steel-reinforced concrete and the ready availability of raw materials with which it is formed make it the most widely used structural material available. The durability of structures made from steel-reinforced concrete is related to its ability to impede or greatly reduce the rate of moisture transport or the ingress of aggressive ions. However, because many existing concrete structures are under constant degradation from aggressive environments, they suffer from durability issues, particularly corrosion of the steel bars within such structures. This corrosion in turn has created a multi-billion-dollar infrastructure deficit. Unfortunately, sequestration, with its adverse impact on discretionary revenues, has alarmingly reduced the revenues necessary for repairing US infrastructures, which become more degraded by the day (Thompson, 2013). Currently, one in nine of the nation's bridges is deemed structurally deficient (ASCE, 2013). Indeed, the FHWA report on corrosion protection of concrete bridges estimated in 2002 that the average direct cost of corrosion for highway bridges was $8.3 billion per year (Yunovich et al., 2001). Considering inflation, this cost is much higher in 2016. Given the current state of US infrastructure, there is a critical need to undertake corrosion research for a nation in desperate need of such services. The corrosion of reinforcing steel in concrete is a serious problem from the perspective of both safety and economy and can directly affect the sustainability of the infrastructure.

2.2   Passivation/depassivation

Concrete provides physical corrosion resistance to steel reinforcement by acting as a barrier, and chemical corrosion resistance as a result of its high pH. Concrete that is not exposed to any external influences usually exhibits a pH between 12.5 and 13.5 (Hansson, 1984). As shown in the Pourbaix diagram (Figure 2.1), which defines the range of electrochemical potential and pH for the Fe-H_2O system in an alkaline environment, at potentials and pHs normally found within the concrete, a protective passive layer forms on the surface of steel.

It is believed that this layer is an ultrathin (<10 nm) protective oxide or hydroxide film that decreases the dissolution rate of steel to negligible levels (Zakroczymski

Corrosion of Steel in Concrete Structures. http://dx.doi.org/10.1016/B978-1-78242-381-2.00002-X
Copyright © 2016 Elsevier Ltd. All rights reserved.
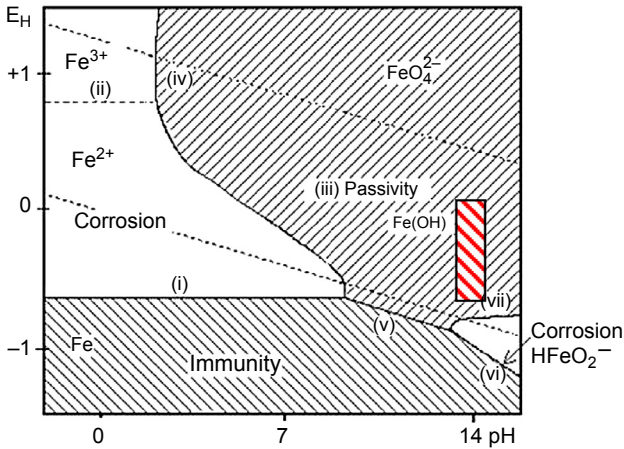
Figure 2.1 Pourbaix diagram for Fe-H$_2$O at 25 °C (Pourbaix, 1974). Hatch area shows the pH and potential region of steel in concrete.

et al., 1985; Montemor et al., 1998; Carnot et al., 2002). However, the partial or complete loss of the passive layer, known as depassivation, leads to the active corrosion of steel bars. The corrosive products of iron are expansive, and their formation can cause cracking and further deterioration in concrete.

Limited research has been carried out on the formation and breakdown of the passive layer. It has been observed that the oxidation state of the iron passive layer varies across the layer. It is assumed that the outer layer that is mainly composed of Fe^{3+} rich oxides and hydroxides is nonprotective, and that the inner oxide layer adjacent to the steel that is rich in Fe^{2+} is protective (Ghods et al., 2009). It is also known that the Fe^{3+}/Fe^{2+} ratio increases in the presence of chloride ions (Gunay et al., in press). It was hypothesized that when chloride ions diffuse through the nonprotective outer layer and come into contact with the inner layer, they convert some Fe^{2+} oxides/hydroxides to Fe^{3+} oxides/hydroxides that reduce the protective nature of the inner layer (Ghods et al., 2009; Gunay et al., in press).

Chloride ions that come mostly from deicing salts or seawater, and carbon dioxide from the atmosphere, are two major factors that can break the passive film on the surface of steel and initiate corrosion. Insufficient oxygen to preserve the passive film, galvanic cell formation from the contact of different metals, and stray currents are the other factors that may cause active corrosion in reinforced-steel structures.

2.2.1 Semiconductive behavior of passive layers

Due to the nature of passive layers on metals, they usually exhibit the electrochemical properties of a semiconductor (Morrison, 1981; Bard and Mirkin, 2001). The electronic structure of these solids is usually discussed in terms of energy bands. The highest occupied and lowest unoccupied levels, called the valence band and

the conduction band, respectively, are of interest. The gap between these bands determines the properties of the material. Conductivity of a solid-state material is achieved by occupancy of the conduction band. For semiconductors, the band gap (E_B) is not as large, and electrons can be moved into the conduction band (Bard and Mirkin, 2001). The movement of electrons leaves a positively charged vacancy in the electrical valence, which is referred to as a hole (Morrison, 1981). Holes are considered to be mobile and to cause conduction. Doping, another method for generating charge carriers (using electrons or holes) within a semiconductor, involves the addition of a different element, dopant, into the semiconductor (Morrison, 1981). Doped semiconductors, in which the majority of charge carriers are electrons, are n-type semiconductors, whereas those in which holes are the majority of charge carriers are p-type semiconductors. The generation of charge carriers requires the presence of dopants. The dopants must be able to: give off electrons to the conduction band, in which case they are called donors (they provide free electrons to n-type semiconductors); or give off holes to the valence band, in which case they are called acceptors (they provide free holes to p-type semiconductors). When a semiconductor contacts an electrolyte, electrical charges are transferred between the semiconductor phase and the solution phase. The electrochemical potential of the solution is determined by the redox potential of the electrolyte solution (Uhlig, 1985), and the redox potential of the semiconductor is determined by the Fermi level, which is defined as the energy level at which the probability of occupation by an electron is 50% (Morrison, 1981; Bard and Mirkin, 2001). If the redox potential of the solution and the Fermi level do not lie at the same energy level, a movement of charge between the semiconductor and the solution is required in order to equilibrate the two phases. For a semiconductor, the excess charge extends into the electrode for a significant distance (Morrison, 1981). This region is referred to as the space charge region and is composed of two double layers: the interfacial (electrode/electrolyte) double layer and the space charge double layer (C_{SC}). At a certain potential, the Fermi level lies at the same energy level as the solution redox potential; there is no net transfer of charge, hence there is no band bending. This potential is known as the flat-band potential, E_{fb}. The charge distribution at the interface between a semiconductor and an electrolyte is often determined by measuring the capacitance of the C_{SC} as a function of the electrode potential (E). When the space charge double layer serves as a depletion layer, the relation of the capacitance and the potential follows the Mott−Schottky equation (Morrison, 1981; Sukhotin et al., 1989):

$$\left\{ \frac{1}{C_{sc}^2} = \frac{2}{\varepsilon\varepsilon_0 qN} \left(E - E_{fb} - \frac{kT}{q} \right) \right\} \tag{2.1}$$

The Mott−Schottky relationship ($1/C_{sc}^2$ vs E plot) expresses the potential dependence of the C_{SC} of a semiconductor electrode under depletion types, where N represents the donor (N_D) or acceptor density (N_A), ε is the dielectric constant of the passive layer, ε_0 is the vacuum permittivity, q is electron charge of an electron, E_{fb} is the

flat-band potential, k is the Boltzmann constant, and T is the absolute temperature. N_D and N_A can be determined from the slope of the experimental $1/C_{sc}^2$ vs E plots, while E_{fb} comes from the extrapolation for $1/C_{sc}^2 = 0$.

The characteristics and roles of passive layers on Fe base metal and alloys have been one of the most important subjects of study in corrosion science. Since the passive layer on the surface of steel could be interpreted in terms of a semiconductive layer (Paola et al., 1986; Sunseri et al., 1987; Paola, 1989; Simoes et al., 1990; Schmuki and Böhni, 1992; Belo et al., 1999), its electronic properties play an important role in the corrosion resistance of the steel. Mott−Schottky analysis has been successfully used to investigate the semiconductive properties of passive layers on metals, specifically in obtaining the type of the semiconductor, donor density (N), and the flat-band potential (E_{fb}) (Harrison and Williams, 1986; Burleigh and Latanision, 1987; Paola, 1989; Simoes et al., 1990; Paola and Shukla, 1991; Schmuki and Böhni, 1992). However, the number of studies on the semiconductive properties of the passive layer in an alkaline concrete environment is very limited. In their study of the semiconductive behavior of the passive layer of steel in chloride-free and chloride-contaminated concrete pore solutions, Zhang and Li concluded that the passive layer on a steel bar in concrete is a highly disordered n-type semiconductor (Paola and Shukla, 1991). They also found that in the presence of chloride ions, the semiconductive behavior of the passive layer changes, thus causing a decrease in corrosion resistance and a thinner passive layer on rebar. They did not, however, investigate the semiconductive properties of the passive layer under different loading types. In the examination of the semiconductive behavior of the passive layer on steel under different loading types, Zhang and Poursaee (in press) found that, irrespective of the type and magnitude of the applied load, the passive layer on rebar in a concrete simulate pore solution was a highly disordered n-type semiconductor. In all specimens tested, they observed that the presence of chloride ions increased the slope of the Mott−Schottky plots and decreased both the donor density and the space charge layer thickness. This increase in slope and decrease in donor density and charge layer thickness in turn led to a thinner passive layer, which degraded much faster and was much more vulnerable to active corrosion.

2.2.2 Reinforcing steel passivation time

Portland cement concrete pore solution mainly consists of saturated $Ca(OH)_2$ (pH = 12.6), but the presence of NaOH and KOH increases the pH to more than 13 (Poursaee, 2010). In concrete structures, the steel normally has many years to develop a protective passive film over its surface before chlorides penetrate the concrete cover. This is not the case in laboratory specimens. Nevertheless, Poursaee and Hansson (2007) showed that steel bar in mortar and pore solution does need a significant amount of time for passivation. For the corrosion rate of steel in mortar to drop to a rate typically considered passive takes approximately seven days, but the corrosion rate continues to decrease slowly for a long period after that. For steel in pore solution, the corrosion rate took about three days to drop to passive levels, and again continued to decrease very slowly thereafter.

2.3   Chloride-induced corrosion

Chloride ions can be present in the concrete due to the use of chloride-contaminated components, the use of $CaCl_2$ as an accelerator when mixing the concrete, or diffusion into the concrete from the outside environment (Thuresson, 1996). Use of deicing salts during the wintertime is the largest source of chlorides in Ontario, Canada.

A localized breakdown of the passive layer occurs when a sufficient amount of chlorides reach reinforcing bars, and the corrosion process is then initiated. Chlorides in concrete can be either dissolved in the pore solution (free chlorides) or chemically and physically bound to the cement hydrates and their surfaces (bound chlorides). Only the free chlorides dissolved in the pore solution are responsible for initiating the process of corrosion (Martin-Perez et al., 2000).

There are three theories about the chloride attack (ACI Committee 222, 1996):

1. Penetration of chloride ions to the oxide film on steel through pores or defects in the film is easier than penetration of other ions.
2. Chloride ions are adsorbed on the metal surface in competition with dissolved O_2 or hydroxyl ions.
3. Chloride ions compete with hydroxyl ions for the ferrous ions produced by corrosion and a soluble complex of iron chloride forms that can diffuse away from the anode, destroying the protective layer of $Fe(OH)_2$ and permitting corrosion to continue.

The current approach to quantify chloride-induced rebar depassivation in concrete is in the form of defining chloride threshold values, certain critical concentrations at which the passive film is damaged and corrosion is initiated. Hausmann, in his article that was appropriately titled "Three Myths About Corrosion of Steel in Concrete" (Hausmann, 2007), identified three misconceptions ("myths") with the current understanding of steel corrosion in concrete. The first two myths that are relevant to this project are: (1) "passivating film on steel in concrete is destroyed when high concentrations of chloride ions reach the steel surface"; and (2) "to prevent chloride-induced steel corrosion in concrete, the soluble chloride content should not exceed 0.06% of cement weight in prestressed concrete and 0.15% in reinforced concrete exposed to chlorides in service." Although there is a general acceptance of the chloride threshold value theory qualitatively, the above-mentioned myths, and uncertainty in existing chloride threshold data (Hansson and Sørensen, 1990; Zhang, 2008; Angst et al., 2009) are clear indicators that scientists and engineers still do not have a clear understanding of why, how, and when steel bar depassivates in concrete exposed to chloride ions.

2.4   Carbonation-induced corrosion

When concrete is exposed to air, the calcium hydroxide reacts with water and carbon dioxide in the air:

$$Ca(OH)_2 + CO_2 \rightarrow CaCO_3 + H_2O \qquad (2.2)$$

   The effect of carbonation is to reduce the pH value of the surface layer of the concrete to less than 8.3. This pH is sufficient to make the passive layer on the reinforcement rebar unstable (Allen and Forrester, 1983). The depth of carbonation increases with time, and the rate at which it advances is a function of relative humidity (RH): the penetration of the CO_2 into the concrete is highest at low RH, but the reaction with the $Ca(OH)_2$ takes place in solution and is therefore highest in saturated concrete. The net result of these two factors is that carbonation is most rapid in the 50−70% RH range (Tuutti, 1980, 1982). The carbonation front penetrates the concrete at an ever-decreasing rate because of three factors. First, the gas has to penetrate further into the concrete. Second, the concrete continues to hydrate and becomes more impermeable as it ages. Finally, carbonation itself decreases permeability, both by the precipitation of the carbonate in the existing pores and because the reaction releases water, which could result in increased hydration (Hansson et al., 2007). When the carbonation front reaches the reinforcement, the passive film is no longer stable and active corrosion initiates. Unlike chloride-induced corrosion, the corrosion process is generalized and relatively homogeneous. Moreover, the corrosion products tend to be more soluble in the neutral carbonated concrete, and may diffuse to the surface as rust stains on the concrete rather than precipitating in the concrete cover and causing stresses and cracking. Corrosion rates of carbonation are lower than those of chlorides, but over a long period, the cross section of the rebar can be reduced significantly even while there is little visible damage to the concrete. Although an intermediate RH provides the highest rate of carbonation, active corrosion of any significance does not occur in that humidity range (Rosenberg et al., 1989). Consequently, the most aggressive environment for carbonation-induced corrosion is alternate semidry and wet cycles (Tuutti, 1980). Carbonation can therefore be a major factor in the durability of concrete in hot climates, where the concrete is easily dried out and periodically subjected to saturation by rainstorms. Chloride attack and carbonation can act synergistically, and are responsible for major problems in hot coastal areas. Carbonation-induced corrosion is not found to be a major problem in northern North America, where adequate concrete cover over steel is used.

2.4.1   Carbonation depth measurement

Carbonation depth is the average distance from the surface of concrete or mortar where carbon dioxide has reduced the alkalinity of the hydrated cement (NORDTEST, 1989). Depending on the concrete quality and curing condition, the carbonation depth varies. The depth of carbonation can be determined by different techniques. Microscopic observation of $CaCO_3$, which is the main chemical product of carbonation, is one technique that can be used for this purpose (ASTM, 2004). As mentioned before, carbonation reduces pH, and therefore examination of the internal pH of the concrete by applying pH-sensitive liquid indicators such as phenolphthalein to the freshly fractured or freshly cut surface of concrete can be used to estimate the depth of carbonation. Upon application of phenolphthalein, noncarbonated areas turn red or purple, while carbonated areas remain colorless. The maximum color change

to deep purplish-red occurs at pH of 9.8 or higher. Below 9.8, the color may be pink, and at pH of 8, colorless (Verbeck, 1995). The Rainbow Indicator® (Germann Instruments Inc., 2006) is a combination of specific chemicals that produces a range of color based on the different pH when sprayed on a freshly broken concrete surface (Campbell et al., 1991).

2.5 Mechanism of corrosion in reinforced concrete

Corrosion is an electrochemical reaction that consists of anodic and cathodic half-cell reactions. Microcell corrosion is the term given to the situation where active dissolution and the corresponding cathodic half-cell reaction take place at adjacent parts of the same metal part. For a steel reinforcing bar (rebar) in concrete, this process always occurs in practice. The surface of the corroding steel can act as a mixed electrode containing both anode and cathode regions connected by the bulk steel. Macrocell corrosion can also form on a single bar exposed to different environments within the concrete or where part of the bar extends outside the concrete. In both cases, concrete pore solution functions as an electrolyte. Figure 2.2 shows a schematic illustration of corrosion in concrete-reinforcing steel.

For steel embedded in concrete, based on the pH of the concrete (electrolyte) and the presence of aggressive ions, the following would be the possible anodic reactions (Hansson, 1984; Ahmed, 2003):

$$3Fe + 4H_2O \rightarrow Fe_3O_4 + 8H^+ + 8e^- \tag{2.3}$$

$$2Fe + 3H_2O \rightarrow Fe_2O_3 + 6H^+ + 6e^- \tag{2.4}$$

$$Fe + 2H_2O \rightarrow HFeO_2^- + 3H^+ + 2e^- \tag{2.5}$$

$$Fe \rightarrow Fe^{2+} + 2e^- \tag{2.6}$$
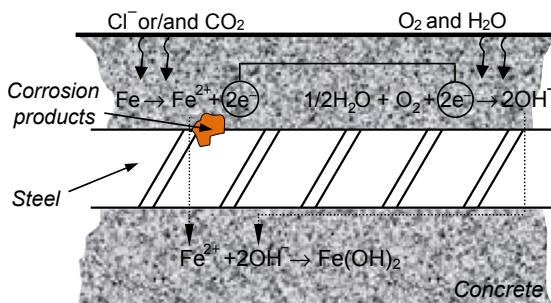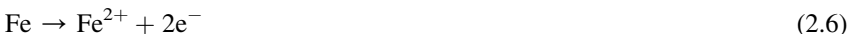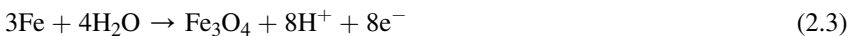
Figure 2.2 Schematic illustration of the corrosion of reinforcement steel in concrete (Ahmed, 2003).

The possible cathodic reactions depend on the availability of O_2 and on the pH near the steel surface. The most likely reactions are as follows (Hansson, 1984; Ahmed, 2003):

$$2H_2O + O_2 + 4e^- \rightarrow 4OH^- \tag{2.7}$$

$$2H_2O + 2e^- \rightarrow H_2 + 2OH^- \tag{2.8}$$
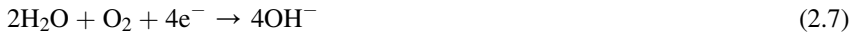
The corrosion products occupy a greater volume than the steel itself, and this causes internal expansion and stress. The stress can destroy the concrete and expose the steel to more aggressive factors.

2.6 The influence of concrete parameters on rebar corrosion

Chloride ions or carbon dioxide penetrates the concrete cover depth to reach the surface of the reinforcing steel by a number of mechanisms. The surface of the concrete may be dry, allowing the dissolved chlorides or carbon dioxide to be absorbed by capillary action together with moisture through the interconnected pores in the cement paste. At deeper levels, concrete rarely dries out in the atmosphere (Hong and Hooton, 1999), so the continued penetration by aggressive ions is by diffusion through the pores, which is a much slower process than absorption.

Porosity in cement paste consists of capillary pores, gel pores, and calcium silicate hydrate (C−S−H) interlayers (Soroka, 1979). Capillary pores are the remains of originally water-containing spaces between cement particles that have not been filled up by products of hydration (Powers, 1960). They are the largest with a diameter >5 nm (Mehta, 1986), and their number and interconnectivity control the ingress of chloride ions, carbon dioxide, oxygen, and moisture into concrete (Jensen et al., 1999). Gel pores and interlayer spaces are believed to be too small and disconnected to contribute to transport. Two factors that significantly influence capillary porosity in concrete are the water-to-binder (w/b) ratio (Kosmatka et al., 2002) and the use of supplementary cementing materials (Oh et al., 2002). Practically, a w/b ratio of 0.42 is required for the complete hydration of cement. However, hydration is a gradual process, and the unused mixing water is retained in the capillary pores (Aïtcin et al., 1997). Higher w/b ratios, traditionally used to give a workable mixture, increase the amount and interconnectivity of capillary porosity in the cement paste, allowing for greater diffusion. With the advent of high-range water-reducing agents, much lower w/b ratios are now possible and significantly limit the penetration of chloride ions and carbon dioxide. There are other factors that can affect the diffusion of the chloride ions and carbon dioxide (Verbeck, 1995):

- Inadequate cover provides shorter path for diffusion and is regularly associated with areas of high corrosion risk due to both carbonation and chloride ingress.
- The age of the concrete is another factor affecting the diffusion of aggressive ions. With passing time, the curing process continues and diffusion becomes harder. In addition, diffusion is a function of time, and thus its rate decreases with time.

- Curing is another parameter that changes the diffusion of chloride ions and carbon dioxide into concrete (Balayssac et al., 1995; Lo and Lee, 2002). Better curing causes lower permeability, better hydration, more CH, and consequently less carbonation and chloride diffusion.
- Temperature and RH are additional factors that can affect the diffusion of aggressive species into concrete (Jones et al., 1995; Andrade et al., 1999; Khatib and Mangat, 2002; Woo-Yong et al., 2003). Diffusion is a function of temperature. For carbonation, there is a critical point that allows for the evaporation of water released by carbonation reactions, but does not result in enough drying out of the concrete to stop the reaction. RH (Gonzalez and Andrade, 1982), wind, direction of sunlight, and the type of environment (e.g., pollutant and costal regions) are the other effective factors.

2.7 Corrosion products

The volume of corrosion products directly affects the proportion of concrete damage and consequently plays an important role in modeling structural performance and service life prediction. As can be seen in Figure 2.3 (Lide, 1999), different corrosion products of steel occupy different volumes.

Suda et al. (1993) detected Fe_3O_4 (magnetite), α-FeOOH (goethite), and γ-FeOOH (lepidocrocite), while Jaffer and Hansson identified γ-Fe_2O_3 (maghemite) (Jaffer and Hansson, 2009). The most expansive corrosion product detected to date in reinforced concrete is β-FeOOH (akaganeite), which is approximately 3.5 times the original volume of iron (Marcotte and Hansson, 1998, 2003). The reasons for such variance in observations remain unclear, however. The lack of information on the mechanism of depassivation of steel bars in the presence of chloride ions, and the interaction between passive and active regions (anode to cathode ratio) at the nano/micro scale, may be one reason. One difficulty in determining the type of corrosion products,
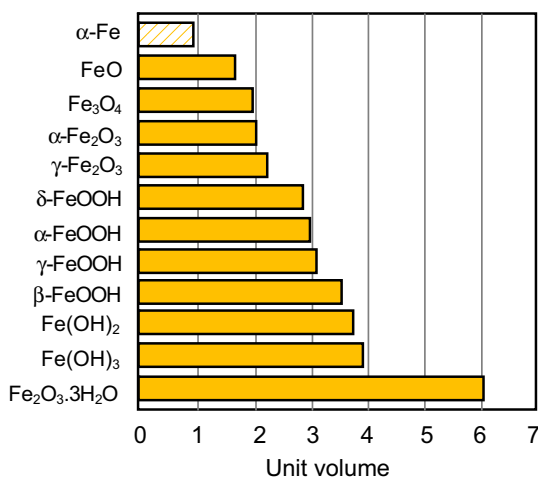
Figure 2.3 Volume of corrosion products relative to iron.

and consequently the volume of products, is that the corrosion product from the steel is unstable in air and changes almost immediately upon exposure to the atmosphere for laboratory analysis. An in situ study of corrosion products (e.g., with Raman spectroscopy and scanning electrochemical microscopy) would be advantageous because it would provide more precise information on the volume and distribution of corrosion products.

2.8   Macrocell and microcell corrosion

Microcell corrosion is the term given to the situation where the active dissolution and corresponding cathodic half-cell reaction (the reduction of dissolved oxygen) take place at adjacent parts of the same bar, as illustrated in Figure 2.4(a). This process always occurs in practice, and in most cases is the dominant corrosion process. Macrocell corrosion can occur when the actively corroding bar is coupled to another bar that is passive because of either its different composition or its different environment. For
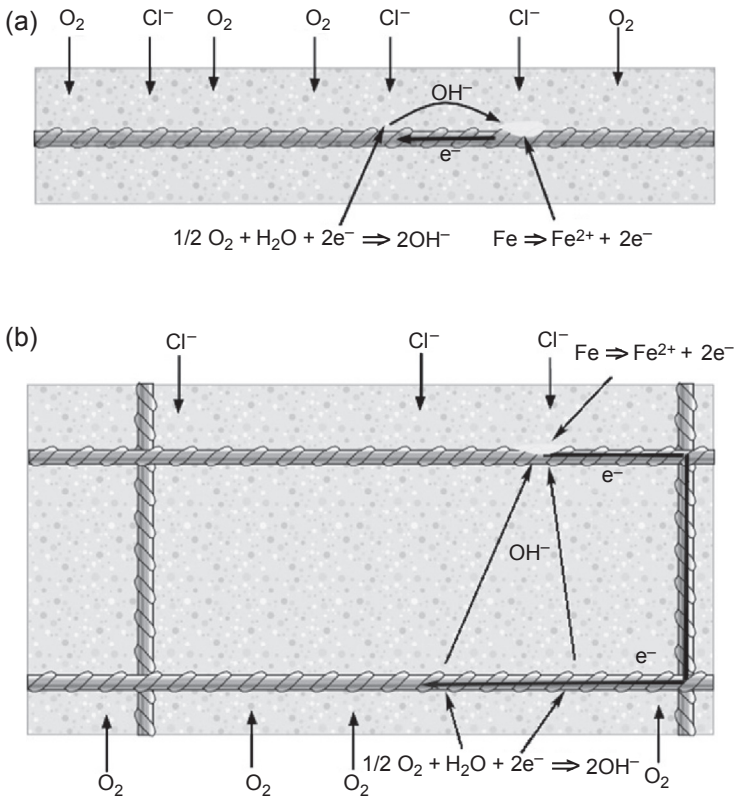
Figure 2.4 Schematic illustration of (a) microcell corrosion and (b) macrocell corrosion.

example, the former situation might occur when black steel is in contact with stainless steel, and the latter when a top mat in chloride-contaminated concrete is coupled to a bottom mat in chloride-free concrete, as in Figure 2.4(b).

Macrocells can also form on a single bar exposed to different environments within the concrete or where part of the bar extends outside the concrete. The process is the same in all cases, and in all cases the corrosive action of the macrocell is added to those of the microcells. It should be emphasized that the simplified view of the "active steel becoming the anode and the passive steel becoming the cathode" is not actually correct. In each case, anodic and cathodic reactions occur on both metal surfaces; when the two metals are coupled, anodic corrosion of the active metal increases and anodic corrosion of the passive metal decreases. While macrocell corrosion can be measured directly, the same is not true of microcell corrosion, and most investigators choose to neglect the microcell component. This has led to the general assumption that macrocell corrosion is always the dominant component.

In the study by Hansson et al. (2006), it was concluded that for carbon steel in Ordinary Portland Cement (OPC) concrete with a relatively low electrical (ionic) resistance, the macrocell and microcell corrosion components were of the same order of magnitude and could be added together to provide the total corrosion rate on the actively corroding bar. In this case, the total corrosion rate was approximately three times that of the macrocell rate alone. In contrast, the macrocell corrosion of carbon steel in concrete with fly ash, silica fume, and slag was negligible, and corrosion was limited to the microcells on the top bar by the ionic resistance of the concrete. Therefore, care must be taken in using the results of macrocell measurements. The absence of macrocell corrosion cannot be taken as an indicator that microcell corrosion is not occurring.

2.9   Corrosion under load

Two electrically connected dissimilar metals in contact with an electrolyte can form a galvanic cell to produce a corrosive attack. Alternatively, either one metal or two similarly coupled metals immersed in two different environments can form a galvanic cell, as can applied stress (Uhlig, 1985; Jones, 1995).

In their use of steel bars in simulated concrete pore solutions to determine passive behavior under loads and repassivation after loads were removed, Feng et al. (2011) noted much more severe damage to passive layers under higher loads, which were hardly affected by the loading time change. In these applications of various loads, they also observed that steel under lower loads did indeed repassivate after the load was removed, but did not behave similarly under higher loads, which resulted in plastic deformation. They did not determine, however, how compressive stress loads and chloride ions affect depassivation, and their experimental procedure was questionable. Specifically, this investigation was flawed in that the samples were immersed in a concrete pore solution for 24 h to form the passive layer, which based upon the previous experience is insufficient time for forming a protective layer (Poursaee and Hansson, 2007). Also, the cold-air drying of samples rendered them vulnerable to a pH of less

than 9, at which point the steel loses its passivity, meaning that the layer on the steel surface is a poor representation of the passive layer of steel within concrete. Finally, neither the presence of chloride ions nor their synergic effect on loading was considered when studying the depassivation of steel.

Zhang and Poursaee (2014, in press) also studied carbon steel passivation and depassivation from chloride attack in concrete simulated pore solution under different loading types. They determined that in a chloride-free pore solution, the corrosion rate in a passive state is less for specimens under tensile stresses than for specimens under compressive stresses. Specifically, we determined that the passivation of steel under tensile stress occurs more rapidly than it does under compressive stress, and that the electrode potential of the specimens under tensile stresses becomes more noble with increasing tensile stress. Conversely, an increase of the compressive stress caused a minor decrease in the nobility of the potential. In pore solutions contaminated with chloride ions, we observed that in spite of more rapid passivation and more protective passive layers formed during applications of tensile stress, specimens (previously passivated in chloride-free pore solution) under tensile stresses corroded faster than those under either compressive stresses or no stress. Zhang and Poursaee (2014) also noted that specimens exposed to chloride ions under compressive stresses exhibited superior performance compared with specimens under tensile load or no loading. Regardless of later placing protective passive layers under tensile stresses in the absence of chloride ions, this layer cannot protect the steel effectively when exposed to such chloride ions, thus showing that the degree of tensile stress has a greater impact on corrosion than does the passive layer's ability to protect steel against it.

References

ACI Committee 222, 1996. 222R-96: Corrosion of Metals in Concrete.

Ahmed, S., 2003. Reinforcement corrosion in concrete structure, its monitoring and service life prediction-a review. Cement and Concrete Composite 30 (4−5), 459−471.

Aïtcin, P.C., Neville, A.M., Acker, P., 1997. Integrated view of shrinkage deformation. Concrete International 19, 35−41.

Allen, R.T.L., Forrester, J.A., 1983. In: Crane, A.P. (Ed.), The Investigation and Repair of Damaged Reinforced Concrete Structures. Society of Chemical Industry, London, pp. 193−222.

Angst, U., Elsener, B., Larsen, C.K., Vennesland, Ø., 2009. Critical chloride content in reinforced concrete − a review. Cement and Concrete Research 139 (12), 1122−1138.

ASCE, 2013. 2013 Report Card for American's Infrastructure. ASCE.

ASTM, 2004. C856-04: Standard Practice for Petrographic Examination of Hardened Concrete.

Andrade, C., Sarria, J., Alonzo, C., 1999. Relative humidity in the interior of concrete exposed to natural and artificial weathering. Cement and Concrete Research 29 (8), 1249−1259.

Balayssac, J.P., Detriche, C.H., Grandet, J., 1995. Effect of curing upon carbonation of concrete. Construction and Building Materials 9 (2), 91−95.

Bard, A.J., Mirkin, M.V. (Eds.), 2001. Scanning Electrochemical Microscopy. Marcel Dekker AG, Basel, Switzerland.

Belo, M.D.C., Hakiki, N.E., Ferreira, M.G.S., 1999. Semiconducting properties of passive films formed on nickel−base alloys type Alloy 600: influence of the alloying elements. Electrochimica Acta 44 (14), 2473−2481.

Burleigh, T.D., Latanision, R.M., 1987. The use of photocurrents to characterize anodic films on Ti, Zr, Cu, and 304 stainless steel. Journal of Electroanalytical Society 134 (1), 135−141.

Campbell, D.H., Sturm, R.D., Kosmatka, S.H., 1991. Detecting carbonation. Concrete Technology Today. PL911. http://www.portcement.org/pdf_files?PL911.pdf_12.

Carnot, A., Frateur, I., Marcus, P., Tribollet, B., 2002. Corrosion mechanisms of steel concrete moulds in the presence of a demoulding agent. Journal of Applied Electrochemistry 32, 865−869.

Feng, X., Tang, Y., Zuo, Y., 2011. Influence of stress on passive behaviour of steel bars in concrete pore solution. Corrosion Science 53, 1304−1311.

Germann Instruments Inc., 2006. http://www.germann.org/Pages/Products/index.htm.

Ghods, P., Isgor, O.B., McRae, G., Miller, T., 2009. The effect of concrete pore solution composition on the quality of passive oxide films on black steel reinforcement. Cement and Concrete Composites 31, 2−11.

Gonzalez, J.A., Andrade, C., 1982. Effect of carbonation, chlorides and relative ambient humidity on the corrosion of galvanized rebars embedded in concrete. British Corrosion Journal 17 (1).

Gunay, H.B., Ghods, P., Isgor, O.B., Carpenter, G.J.C., Wu, X., 2013. Characterization of atomic structure of oxide films on carbon steel in simulated concrete pore solutions using EELS. Applied Surface Science, 274 (1 June), 195−202.

Hansson, C.M., 1984. Comments on electrochemical measurements of the rate of corrosion of steel in concrete. Cement and Concrete Research 14, 574−584.

Hansson, C.M., Poursaee, A., Jaffer, S.J., 2007. Corrosion of Reinforcing Bars in Concrete. Portland Cement Association (PCA). PCA R&D Serial No. 3013.

Hansson, C.M., Poursaee, A., Laurent, A., 2006. Macrocell and microcell corrosion of steel in ordinary Portland cement and high performance concretes. Cement and Concrete Research 36, 2098−2102.

Hansson, C.M., Sørensen, B., 1990. The threshold concentration of chloride in concrete for the initiation of reinforcement corrosion. Corrosion Rates of Steel in Concrete. Baltimore, MD, ASTM STP 1065.

Harrison, J.A., Williams, D.E., 1986. How does the electrochemical behavior of stainless steel reflect that of its constituent elements. Electrochimica Acta 31 (8), 1063−1072.

Hausmann, D.A., 2007. Three myths about corrosion of steel in concrete. Materials Performance 46 (7), 70−73.

Hong, K., Hooton, R.D., 1999. Effects of cyclic chloride exposure on penetration of concrete cover. Cement and Concrete Research 29, 1379−1386.

Jaffer, S.J., Hansson, C.M., 2009. Chloride-induced corrosion products of steel in cracked-concrete subjected to different loading conditions. Cement and Concrete Research 39, 116−125.

Jensen, O.M., Hansen, P.F., Coats, A.M., Glasser, F.P., 1999. Chloride ingress in cement paste and mortar. Cement and Concrete Research 29 (9), 1497−1504.

Jones, D.A., 1995. Principles and Prevention of Corrosion. Prentice Hall.

Jones, M.R., Dhir, R.K., Gill, J.P., 1995. Concrete surface treatment: effect of exposure temperature on chloride diffusion resistance. Cement and Concrete Research 25 (1), 197−208.

Khatib, J.M., Mangat, P.S., 2002. Influence of high-temperature and low-humidity curing on chloride penetration in blended cement concrete. Cement and Concrete Research 32, 1743−1753.

Kosmatka, S.H., Kerkhoff, B., Panarese, W.C., MacLeod, N.F., McGrath, R.J., 2002. Design and control of mixtures. Cement Association of Canada, Ottawa, ON, Canada.

Lo, Y., Lee, H.M., 2002. Curing effects on carbonation of concrete using a phenolphthalein indicator and Fourier-transform infrared spectroscopy. Building and Environment 37, 507−514.

Lide, D.R., 1999. CRC Handbook of Chemistry and Physics. CRC Press, New York, NY.

Marcotte, T.D., Hansson, C.M., 1998. A comparison of the chloride-induced corrosion products from steel-reinforced industrial standard versus high performance concrete exposed to simulated sea water. In: International Symposium on High Performance and Reactive Powder Concretes. University of Sherbrooke, Sherbrooke, Canada.

Marcotte, T.D., Hansson, C.M., 2003. The influence of silica fume on the corrosion resistance of steel in high performance concrete exposed to simulated sea water. Journal of Materials Science 38, 4765−4776.

Martin-Perez, B., Zibara, H., Hooton, R.D., Thomas, M.D.A., 2000. A study of the effect of chloride binding on service life predictions. Cement and Concrete Research 30 (8), 1215−1223.

Mehta, P.K., 1986. Concrete Structure, Properties and Materials. Prentice-Hall Inc., Englewood Cliffs, NJ, USA.

Montemor, M.F., Simoes, A.M.P., Ferreira, M.G.S., 1998. Analytical characterization of the passive film formed on steel in solutions simulating the concrete interstitial electrolyte. Corrosion 54 (5), 347−353.

Morrison, S.R., 1981. Electrochemistry at Semiconductor and Oxidized Metal Electrodes. Plenum Press, New York.

NORDTEST, 1989. NT BUILD 357: Concrete, Repairing Materials and Protective Coating. UDC 691.32:658.588 carbonation resistance. NORDTEST.

Oh, B.H., Cha, S.W., S.Jang, B., Jang, S.Y., 2002. Development of high-performance concrete having high resistance to chloride penetration. Nuclear Engineering and Design 212, 221−231.

Paola, A.D., 1989. Semiconducting properties of passive films on stainless steels. Electrochimica Acta 34 (2), 203−210.

Paola, A.D., Quarto, F.D., Sunseri, C., 1986. A photoelectrochemical characterization of passive films on stainless steels. Corrosion Science 26 (11), 935−948.

Paola, A.D., Shukla, D., 1991. Photoelectrochemical study of passive on stainless steel in neutral solutions. Electrochimica Acta 36 (2), 345−352.

Pourbaix, M., 1974. Atlas of Electrochemical Equilibria in Aqueous Solutions. National Association of Corrosion Engineers, Houston, TX.

Poursaee, A., 2010. Corrosion of steel bars in saturated $Ca(OH)_2$ and concrete pore solution. Concrete Research Letters 1 (3), 90−97.

Poursaee, A., Hansson, C.M., 2007. Reinforcing steel passivation in mortar and pore solution. Cement and Concrete Research 37, 1127−1133.

Powers, T.C., 1960. Properties of cement paste and concrete. In: Chemistry of Cement: Fourth International Symposium. National Bureau of Standards, U.S. Department of Commerce, Washington, DC, USA.

Rosenberg, A., Hansson, C.M., Andrade, C., 1989. Mechanisms of corrosion of steel in concrete. In: Skalny, J. (Ed.), The Materials Science of Concrete, vol. 1. The American Ceramic Society, pp. 285−313.

Schmuki, P., Böhni, H., 1992. Metastable pitting and semiconductive properties of passive films. Journal of Electroanalytical Society 139 (7), 1908−1913.

Simoes, A., Ferreira, M., Rondot, B., Belo, M., 1990. Study of passive films formed on AISI 304 stainless steel by impedance measurements and photoelectrochemistry. Journal of Electrochemical Society 137 (1), 82−87.

Soroka, I., 1979. Portland Cement Paste and Concrete. The Macmillan Press Ltd, Surrey, England.

Suda, K., Misra, S., Motohashi, K., 1993. Corrosion products of reinforcing bars embedded in concrete. Corrosion Science 35 (5−8), 1543−1549.

Sukhotin, A.M., Grilikhes, M.S., Lisovaya, E.V., 1989. The influence of passivation on the kinetics of the dissolution of iron − I. Outer layer of the passivating film as a heavy doped thin semiconductor and M-S equation. Electrochimica Acta 34 (2), 109−112.

Sunseri, C., Piazza, S., Dipaola, A., Diquarto, F., 1987. A photocurrent spectroscopic investigation of passive films on ferritic stainless steels. Journal of Electrochemical Society 134 (10), 2410−2416.

Thompson, D., 2013. The Falling-bridge Lesson: The U.S. Infrastructure Failure Is Still Totally Inexcusable. The Atlantic, Washington, DC.

Thuresson, T.I., 1996. Electrochemical Monitoring of the Influence of Concrete Quality on the Reinforcing Steel Corrosion in Industrial Effluent. Queen's University. MA. Sc.

Tuutti, K., 1980. Service life of structures with regard to corrosion of embedded steel. In: International Conference on Performance of Concrete in Marine Environment. American Concrete Institute, St. Andrews By-the-Sea, Canada.

Tuutti, K., 1982. Corrosion of Steel in Concrete. CBI Research Report No. 4.82. Swedish Cement and Concrete Research Institute, Stockholm, Sweden.

Uhlig, H.H., 1985. Corrosion and Corrosion Control: An Introduction to Corrosion Science and Engineering. Wiley, New York; Toronto.

Verbeck, G.J., 1995. Carbonation of Hydrated Portland Cement. Research Department Bulletin RX087, Portland Cement Association.

Woo-Yong, J., Young-Soo, Y., Young-Moo, S., 2003. Predicting the remaining service life of land concrete by steel corrosion. Cement and Concrete Research 33, 663−677.

Yunovich, M., Thompson, N.G., Balvanyos, T., Lave, L., 2001. Corrosion Costs and Preventive Strategies in the United States, Appendix D: Highway Bridges. Federal Highway Administration (FHWA), Office of Infrastructure Research and Development, Washington, DC.

Zakroczymski, T., Fan, C.-J., Szklarska-Smialowska, Z., 1985. Kinetics and mechanism of passive film formation on iron in 0.05M NaOH. Journal of Electrochemical Society 132 (12), 2862−2867.

Zhang, J.Y., 2008. Corrosion of Reinforcing Steel in Concrete Structures: Understanding the Mechanisms. National Research Council (NRC)-Institute for Research in Construction, Ottawa.

Zhang, Y., Poursaee, A., 2014. Study the passivation and corrosion activity of carbon steel in concrete simulated pore solution under tensile and compressive stresses. ASCE Journal of Materials in Civil Engineering 04014234.

Zhang, Y., Poursaee, A., 2015. Study the semi-conductive behavior of the passive film on carbon steel in simulated concrete pore solution under stress. Anti-Corrosion Methods and Materials 62 (6), online.

Corrosion of prestress and post-tension reinforced-concrete bridges

3

K. Lau [1], *I. Lasa* [2]
[1]Florida International University, Miami, FL, USA; [2]Florida Department of Transportation, Gainesville, FL, USA

3.1 Introduction

Implementation of prestressed concrete elements in highway bridges is an engineering practice that has continued from the late twentieth century into the present. The application of prestress techniques to concrete has allowed for greater structural design considerations by bridge engineers (Naaman, 2004; Hewson, 2003). Light and slender prestressed structural elements provide advantages for long bridge spans. The integration of precast concrete elements in prestress techniques provides good quality control during element casting and erection. Furthermore, prestressed concrete provides nice aesthetics for public use and the appreciation of highway bridges. Several decades of experience with the technique, and continued improvements and innovations in its application, have further helped garner acceptance of prestressed concrete by bridge engineers and owners. In contrast to the advantages and general good use of prestressed concrete for over 60 years, documented durability problems and component failures in arguably isolated cases continue to illustrate difficulties in bridge applications. Unfortunately, corrosion concerns over the steel components of prestressed concrete bridges have persisted.

Prestressed bridge systems are complicated, and many structural, construction, material, and environmental factors can be involved in corrosion development. The use of prestressing techniques for concrete bridges is diverse and has been used for bridge superstructure and substructure elements. Examples of prestressed concrete elements are shown in Figure 3.1. Extensive information on the current practice and structural applications of prestressed concrete for highway bridges can be found in guidelines, handbooks, and other publications from state transportation departments, the Federal Highway Administration (FHWA) (Corven and Morenton, 2013), trade organizations promoting the construction, and from materials providers. These include the Precast/Prestressed Concrete Institute, the Post-Tensioning Institute, and the American Concrete Institute (PCI, 2010; PTI M55.1-12, 2012; ACI-318R, 2014; ACI-222.2, 2014). For brevity and in the context of case studies of corrosion development, prestress applications can be broadly categorized by two prestressing methods, pretensioning and posttensioning. Pretensioning of high-strength steel wires prior to encapsulation in concrete, and releasing after concrete hardening, is commonly associated with prefabricated prestressed beams
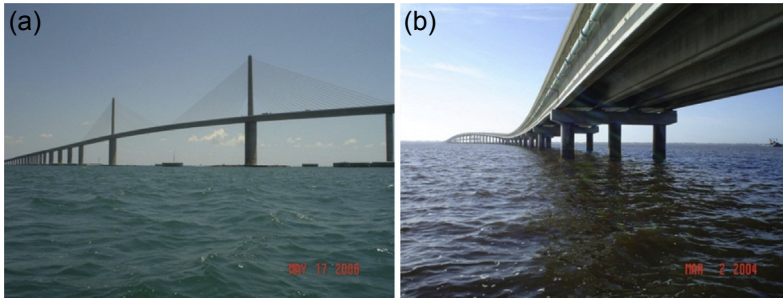
Figure 3.1 Examples of prestressed concrete elements. (a) Sunshine Skyway Bridge, FL (segmental box girders and columns). (b) St. George Island Bridge, FL (concrete cylinder piles and girders).

and prestressed piles for bridge applications. Posttensioning of high-strength steel, as its name implies, occurs after the concrete element (often precast) has been fabricated. The concrete element typically contains embedded duct conduits where the prestressing steel is subsequently placed and stressed. The assembly of prestressed steel and other relevant hardware components is called a tendon. Posttensioned tendons are differentiated as being bonded or unbonded, where in the former, the prestress steel is permanently set in an injected cementitious grout to prevent movement relative to the concrete. Prestressing forces can be developed along the length of the steel in bonded tendon systems to transfer the forces onto the surrounding concrete. Posttensioned tendons are further identified as being internal or external, where the former are cast within the concrete of the structural element and the latter have free spans external to the structural concrete. Posttensioned tendons have been commonly associated with bridge superstructure box girders, but other bridge components such as columns and caps have been designed as well.

3.2 Materials

The variety of materials and hardware components used in prestressed concrete is wide, as are the many applications for bridge components. Specification changes, technology innovations, and economic conditions continue to allow for the introduction of new components and materials. Constructability and bridge durability concerns also provide opportunities for new materials and designs. For brevity, the reader is referred to literature available from FHWA, trade organizations, and materials providers for detailed descriptions of important hardware components. This section highlights select materials and components that are relevant to later discussion on corrosion development in select prestressed concrete systems.

3.2.1 Prestressing steel

Effective prestressing in practice requires steel with high strength and high elongation. Other important steel characteristics include elastic behavior and ductility at stress levels at loading, low relaxation of tension, resistance to stress corrosion cracking,
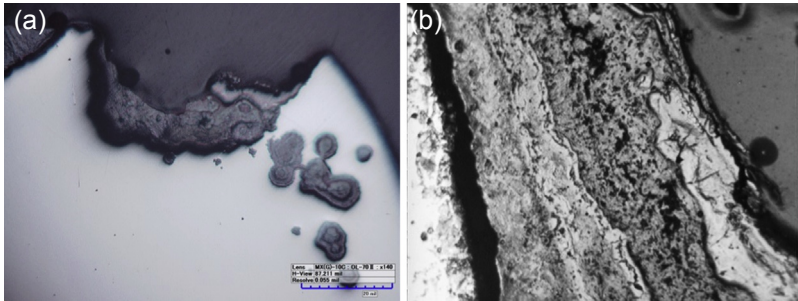
Figure 3.2 Micrographs of corrosion. (a) Wire from posttensioned strand (unetched). (b) Rebar (etched with 2% Nital).

and resistance to hydrogen embrittlement. Wires and strands are typically high-carbon steel with applications of cold-work and thermal treatment to attain desired material characteristics. Standard specifications for prestress wire, strand, and bar can be found in ASTM A421, A416, and A722. An example of corrosion of a wire from a posttensioned strand compared with rebar corrosion is shown in Figure 3.2. Vertical and horizontal pitting corrosion on the wire is seen in Figure 3.2(a), and corrosion progression into the microstructure of the rebar steel is shown in Figure 3.2(b). Prestressed concrete, similarly to conventional reinforced concrete, can be susceptible to chloride- and carbonation-induced corrosion in aggressive exposure environments. Like conventional reinforced concrete, alternative materials to prestressed steel have been presented. Epoxy-coated strand is specified in ASTM A882. Work on applications of austenitic and duplex stainless steel (Mullins et al., 2014; Moser, 2013) and carbon fiber composite cables (CFCCs) (ACI 440.4R, 2004; Roddenberry et al., 2014) has been recently reported. Stainless steels are expected to provide greater resistance to chloride-induced corrosion, but issues regarding stress corrosion cracking, mechanical properties, and costs require further deliberation. Mechanical performance, detailing, and costs are issues to be resolved for CFCC wire and strand.

3.2.2 Prestressing components and materials

Innovations in tendon detailing and design, including strand configuration to address tendon corrosion durability, have also been presented. Electrically isolated tendons, among others, have been presented as a useful design for health monitoring of the system. More generally, appropriate material selection and design of the other prestress system components are important to mitigate corrosion development. Examples of bonded posttensioned tendon components are shown in Figure 3.3. The tendon duct for posttensioned concrete systems not only provides the form for the continuous longitudinal space for the prestressing steel, but also serves as an outer barrier to environmental contaminants including moisture and salt. The duct can be made out of galvanized steel, plastic, or high-density polyethylene pipe (HDPE) depending on its application. Corrugated galvanized steel and plastic (polyethylene or polypropylene) pipe are often used for internal tendons. Galvanized pipe can be used for
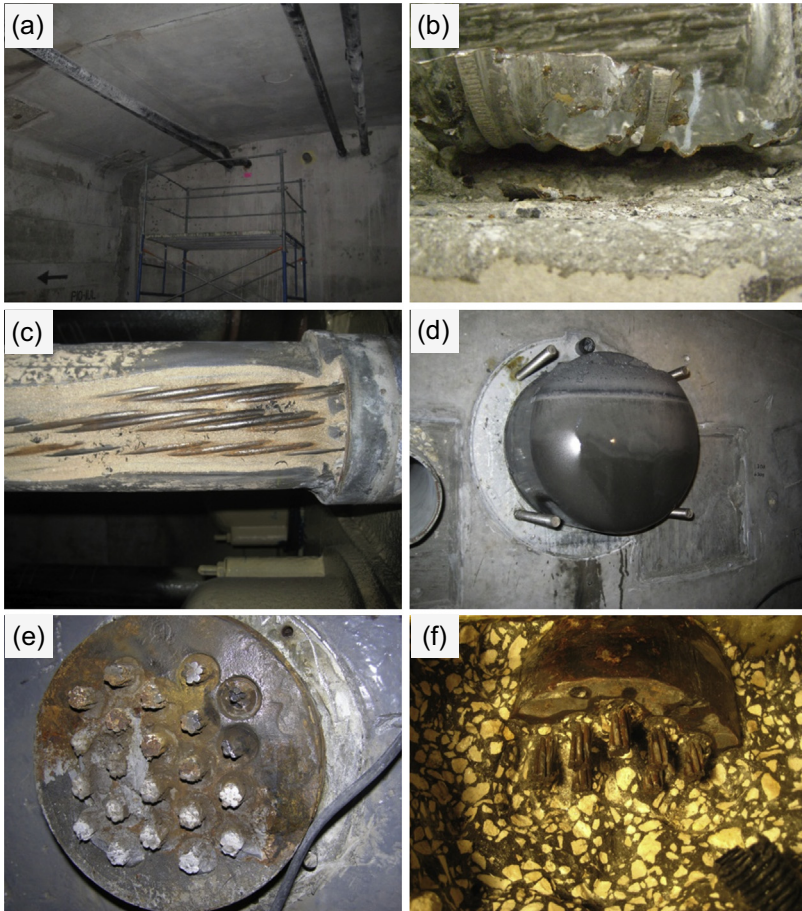
Figure 3.3 Examples of bonded posttensioning components and materials with corrosion-related degradation and deficiency. (a) Damaged external tendon. (b) Corroded steel duct. (c) Corroded strand in tendon with sand contamination. (d) Segregated grout in anchor cap. (e) Corroded strand, wedges, and wedge plate. (f) Surface corrosion on anchor in pour-back.

tendon portions through deviators and diaphragms. HDPE pipe is common for external tendons. Tendon systems contain valve inlets and outlets to allow for proper grout injection. Those same locations should contain appropriate plugs during and after construction to minimize exposure to the external environment including moisture, salt, and atmospheric carbon dioxide. Posttensioned concrete steel anchors also require appropriate design and material selections to account for possible tendon deficiencies, especially for bonded tendons where proper grouting is vital to mitigate corrosion development. The anchorage system typically consists of the trumpet, bearing plate, wedge plate, individual strand wedges, and an outer permanent protective cap. Materials can vary depending on design and make; different metallic components in the

prestress anchor may introduce aggravating galvanic interactions. The anchorage trumpet can be of ductile iron, galvanized steel, or plastic.

Appropriate design details and materials selection of the prestressed concrete elements, the joints, and pour-backs are also important to avoid premature corrosion. For example, direct moisture and chloride penetration may occur at the joints between concrete segments. To minimize potential for corrosion of internal tendons in segmental box bridge construction, epoxy-resin joints have been generally used to good effect (Trejo et al., 2009a,b) compared with dry joint construction (although record of flawed sealing have also been documented in the former). Similarly, shrinkage cracks and other degradation of cementitious materials can occur at the concrete pour-back possibly allowing intrusion of moisture and salts. Epoxy grout encapsulating material and concrete seal coatings have been used in practice over pour-back areas to act as barrier coating. Use of plastic ducts at joints and permanent grout caps further prevent exposure to external contaminants.

For posttensioned tendons, materials for duct couplings and fittings should be compatible to the duct material and duct filler, resilient to degradation and mechanical damage, provide unobstructed internal space, and provide protection for leaks and exposure to external contaminants. Various duct couplers and connection techniques are prescribed based on design and use. Use of heat fusion welding techniques for plastic pipes, polymer boots (ethylene propylene diene monomer), shrink sleeves, and duct couplers are used in practice. Poor construction practices of using adhesive tape and cloth should be avoided.

3.2.3   Concrete, grouts, and filler material

The concrete for the prestressed structural elements especially for locations that embed or cover prestressing steel provide some level of protection from external environmental exposure. For external tendons, the concrete sections can minimize direct exposure of the tendons from salt spray and deicing salts in applications where the tendons are located inside the structure (segmental bridges). For pretensioned wire and posttensioned internal tendons, the concrete clear cover provides barrier for aggressive chemicals such as chloride ions and atmospheric carbon dioxide to diffuse in the same manner as that for conventionally reinforced concrete elements. High performance concretes with low permeability provide good corrosion durability of the embedded steel elements.

The cementitious grout used in bonded posttensioned tendons has received significant attention in the past 20 years because of its association with severe corrosion in a number of bridges in Florida and elsewhere, despite its intended function to provide corrosion protection of the prestressing steel. The grout in current practice is essentially Portland cement and can include supplemental cementitious materials (such as slag, silica fume, and fly ash), admixtures (for set-control, air-entraining, antibleeding, and corrosion inhibition), and fine-sized aggregates. In earlier practices, expansion-causing admixtures were used, but have subsequently been shelved after revisions to grout specifications, particularly due to durability concerns. Prior to specification changes in the first decade of the twenty-first century, posttension grouts

were neat grouts and were documented to have challenges due to the excess formation of bleed water and resulting in grout void formation and severe corrosion of tendons in a number of bridges. In response to that corrosion development in the late 1990s, posttensioning systems in recent practice have used prepackaged thixotropic grouts with low-bleed water formation—unfortunately, recent developments since 2011 have shown that challenges in corrosion mitigation persists for these grouts as well. In specifications, the allowable grouts are grouped into four categories depending on tendon exposure conditions, thixotropic property of the grout, and prepackaging.

Construction of bonded posttensioned tendons in aggressive environments in the past 15 years has typically used prepackaged thixotropic grouts to incorporate qualified grout products with expected good quality control and low-bleeding characteristics. Low bleed characteristics are typically defined by bleed tests such as the wick-induced bleed test and Schupak pressure bleed test. Other tests prescribed in Europe include inclined-tube tests (VSL, 2002). As alluded to earlier, qualified grouts used in construction and conforming to the revised grout specifications had a few documented incidences of severe deficiency (nominally called soft grout) and in some cases directly associated with fast and severe corrosion of the prestressing steel in the absence of chloride contamination and grout pore water carbonation (Lau et al., 2013a). The deficient grout was characterized as having poor cohesive bulk properties, high moisture content, and enhanced level of sulfate ion concentrations in the pore water. Another recent development of quality control issues not directly related to soft grout development of some prepackaged grout used in construction included the presence of enhanced chloride presence in the cement component (Gee, 2011). Many questions concerning these cases are still to be resolved, and concerns about grout material quality control (grout contamination), product packaging quality control (underweight bags), grout robustness (segregation), construction practices (excess moisture), and corrosion development (corrosion initiation in chloride-free alkaline environments) are currently being addressed. Other grout material parameters that have received recent attention include chloride threshold concentrations in prepackaged grouts and segregation testing (Lee and Zielske, 2014). Some construction issues related to grout quality that have received recent attention include mandates for rigorous personnel qualifications, grout shelf life expiration, and the use of field mockup tests. The Virginia Department of Transportation, as part of the construction of a recent posttensioned concrete bridge, required full-scale test mockups to qualify grout material.

Filler materials such as waxes and greases have been used for protection of cables for utilities and in the application of posttensioned concrete elements in nuclear facilities. Flexible fillers for posttensioned concrete bridges have been adopted in Europe because of corrosion associated with bleeding and void formation in cementitious grouts. In current practice in Germany and France, filler wax material was thought to have good stability at high temperatures (Parsons Brinckerhoff, 2012). Wax filler heated above its congealing point is injected into the tendon with the intent to completely encapsulate the prestressing steel. Acceptable wax materials (bitumastic petroleum-based waxes) and oil-based greases specified in the European Organization

for Technical Approval ETAG 013 (2012) have minimum-material-required criteria for material stability, separation, penetration, aggressive ion content, and corrosion protection. The wax and grease material is intended to provide corrosion protection by encapsulating the prestressing steel and acting as a physical barrier. European standards require minimum corrosion resistance in spray tests, including salt spray. Unlike cementitious grout (where the normally high pH pore water solution provides conditions for steel passivation), the grease and wax material itself is not necessarily intended to provide corrosion mitigation, but rather to provide a barrier against the elements. The European standards have stipulations to specify the corrosivity of the wax by copper-strip corrosion tests at $100\,^{\circ}\mathrm{C}$, and of the grease by Emcor tests. In the United States, Florida has recently begun taking steps for implementation of flexible fillers for some posttensioned bridge applications in order to provide alternative means of corrosion protection for the prestressing steel (Robertson, 2015). Concerns with issues in structural design and detailing of nonbonded tendons in bridges, construction and injection procedures with flexible fillers, and possible durability concerns for highway bridge applications are still to be resolved before wide adoption of the technique and its materials.

3.3   Overview of corrosion mechanisms

The corrosion mechanisms of prestressing steel in highway bridges can vary with many complicating factors involving structural components, prestressing techniques, construction practices, deficiencies in building materials, and natural and service environments. As such, only select topics that have been of recent interest in bridge durability are presented here. Corrosion of prestressing steel encapsulated in cementitious grout and concrete, as in pretensioned concrete and bonded posttensioned concrete, is in general similar to that of conventional reinforced concrete; however, the structural implications of even minor cross-sectional loss of prestressing wire may be more consequential than those for reinforced concrete. Other factors such as the use of high-strength steel and multiwire strand, presence of a prestress force, presence of segment joints, use of cementitious grout, and presence of other building materials further complicate the system. Possible hydrogen embrittlement and stress-corrosion cracking with the use of high-strength steels and the presence of the prestress force can be a concern in certain environments.

3.3.1   Pretensioned steel concrete

Prestressing steel in pretensioned concrete bridge girders and piles are exposed to the environment in ways similar to those of conventional reinforced concrete. Bridge structural elements can be exposed to deicing salts, marine splash, or soils. The prestressing steels in these systems are not surrounded by ducts as in posttensioned concrete components, and may be susceptible to corrosion by exposure to aggressive chemical species through the concrete cover. Transport of aggressive chemical species such as chloride ions can occur through the concrete cover at a rate that depends on the

Figure 3.4 Longitudinal crack in prestressed concrete cylinder pile.

quality of the concrete and environmental conditions. As with conventional reinforced concrete, chloride- or carbonation-induced corrosion can occur.

Detailed descriptions of chloride- and carbonation-induced corrosion can be found in Chapter 2 and elsewhere (Bentur et al., 1997; Bertolini et al., 2004). Various changes in the cement pore water can allow for depassivation of the steel to occur, but corrosion has commonly been attributed to the enhanced presence of chloride ions and pore water carbonation. The maximum chloride limits for prestressed concrete prescribed by ACI 318 and ACI 222 are 0.06 percent by weight of cement (water soluble chloride ion) and 0.08 percent by weight of cement (acid soluble chloride ion) (ACI-318R, 2014; ACI-222.2, 2014). Carbonation of the cementitious material at the prestressing steel interface causing drop in pore water pH below 12 will allow depassivation of the steel. A larger concrete cover and the use of less permeable concrete should provide longer bridge service times. Enhanced transport of moisture, chlorides, and atmospheric carbon dioxide can occur at localized cracks that may be present in components of prestressed concrete depending on its exposure to moisture, salty humid air, water, and soil. Cracks in prestressed concrete components in bridge substructures such as piles (Figure 3.4) can occur during installation. Work by Lau and Sagüés (Lau and Sagüés, 2009) indicated that isolated cracking in conventionally reinforced concrete should create topical corrosion damage, but adverse crack conditions could cause increased damage.

3.3.2   Posttensioned steel concrete

Corrosion damage to the prestressing steel of posttensioned concrete components can occur by different mechanisms, depending on prestressing configuration and environmental exposure. Use of a visual guide for acceptance of corroded strand was proposed by Sason (1992), particularly for corrosion that formed prior to construction. The steel strand may be exposed to moisture, sea spray, and other deleterious environmental

contamination during transport and storage. The significant presence of corrosion pitting can reduce the structural capacity of the strand, and may result in failure during stressing or in service (Trejo et al., 2009a; Sason, 1992).

After construction, unbonded posttensioned tendons rely on fillers such as grease and wax to provide encapsulation of the steel and a barrier to environmental exposure. The authors were not aware at the time of writing of any cases of strand corrosion in the contemporary filler materials used in Europe for unbonded bridge tendons. Corrosion of steel strand prior to wax injection is expected to be similar to that of bonded tendons prior to group pumping.

During the construction sequence of bonded posttensioned tendons, the strand is installed through the ducts of aligned concrete segments and then stressed prior to grouting. The time until grouting may be delayed by complications during construction. The time limit for grouting in humid and marine environments is 7 days (PTI M55.1-12, 2012) (20−40 days in dry environments), but may be extended with the use of additional means for corrosion protection upon approval by the construction engineer. Runoff water may become entrapped in ducts if they are not properly sealed during construction delays. Corrosion activity in near-neutral pH or even slightly elevated pH can be further exacerbated with the presence of chloride ions (and other aggressive ions) and possible carbonation in the latter case. Internal ducts were left ungrouted for up to 15 months during the construction of the San Francisco−Oakland Bay Bridge in 2006, and runoff water from the deck entered the duct through unsealed grout tubes (Reis, 2006, 2007a,b). Strands with moderate corrosion and indications of shallow pitting were observed, and some failed to meet specified tensile strength and ductility requirements. Transverse cracks and fractures in some wires in strands touching a duct hard-point (metal duct defect caused during construction) may have been associated with environmentally assisted cracking. Research in 2011 and 2014 (Sagüés et al., 2011; Fernandez et al., 2014) indicated that no significant corrosion of steel strands in sheltered marine exposures was observed, and only minor pitting in closed systems containing some water occurred in stressed tendon mockups exposed for 4 weeks and unstressed tendons exposed for up to 9 months. Superficial deposition of salt resulted in early enhanced corrosion in the closed system containing water (exposed for 4 weeks). In all cases, no loss of tensile strength was measured. Greater hydrogen buildup was measured in the closed system containing water than in the open exposed and dry closed systems.

Due to a variety of material- and construction-related issues, portions of bonded posttensioned tendons may be inadvertently left ungrouted, therefore creating large void spaces that can expose steel strands for long periods. Also, movement of air and water during grouting can leave a bleed trail that results in similar improper encapsulation of the strand in cementitious material. Barring other chemical deficiencies of the grout and other interactions with free moisture availability (discussed later), the void space itself may or may not create a region where steel can experience severe corrosion, but may still be considered a deficiency. With the simplifying assumption that no other chemical interactions are important, possible corrosion of the exposed steel in the void space can be generically viewed as being exposed to atmospheric conditions. In that scenario, the major factors involved include the time of wetness,

relative humidity, temperature, and presence of contaminants such as salts (Roberge and Revie, 2011; Revie and Uhlig, 2008; Jones, 1996). Sufficient moisture film on the steel surface is needed to provide the electrolyte for the electrochemical reactions. Stability of that moisture film depends on the humidity level, temperature, and level of pollution (i.e., sulfur dioxide) in the duct. Significant corrosion occurs above a critical relative humidity level (reported to be >75% (Matsushima and Revie, 2011)) that in turn is dependent on the extent of surface contaminants on the metal surface. Hygroscopic salts such as chlorides can promote water condensation from the air at lower relative humidity than in noncontaminated conditions and thus increase the time of wetness and corrosion development. Also, surface contamination (i.e., chlorides and sulfates) can result in greater corrosion development due to the formation of nonprotective corrosion product films. In practice, inspection of voided tendons with dry internal conditions often reveals minor to no corrosion development.

In other documented cases, voids have been associated with severe corrosion, but other tendon or material deficiencies were often also related (Powers, 1999; Corven Engineering, 2001; Hartt and Venugopalan, 2002). Corrosion of strands in the void spaces created by the formation of grout bleed water has been widely discussed in posttensioned tendon failures in the past 20 years. Prior to the use of low-bleed prepackaged thixotropic grouts, plain cement grouts with expansive agents were commonly used. Case studies revealed the tendency of those materials to form bleed water, thus leading to subsequent changes in grout material specifications and testing methodologies for bleed water formation. Capillary action through the narrow interstitial spaces of the strand, and vertical deviation of draped tendons, allowed for accumulation of the bleed water at high points such as at the anchorage assemblies. The movement of air and bleed water, followed by grout subsidence/segregation, allows for voids to expose the strand in a mixed environment of grout, bleed water, and air. Severe corrosion of strands exposed to bleed water may still occur, even though the pH of the bleed water itself can be alkaline (pH > 12). It has been proposed that corrosion can occur as a result of carbonation of the bleed water and grout by the presence of CO_2, or by intrusion of CO_2 at the grout-to-air interface, where pH can drop to 8 (Hartt and Venugopalan, 2002). At these pH levels, active corrosion of the steel at the carbonated grout can develop. After formation of the void, the level of bleed water can diminish either by reentering the grout pore space or by drying and evaporative processes. The corrosion rate may diminish in dry conditions; however, corrosion of the strand in the void space and in the grout-to-air interface may continue if moisture becomes available in periods when the relative humidity is high and condensation of moisture occurs (Hartt and Venugopalan, 2002), or generally if external moisture seeps through improperly sealed or defective posttensioning components (Wang et al., 2005). Furthermore, the pore water residuals and corrosion products may be hygroscopic, allowing moisture condensation at lower relative humidity levels. The large movement of water to accumulate bleed water would likely aggregate chloride and other aggressive ionic chemical species. Indeed, even the vestigial amount of chlorides in the raw grout materials meeting specification limits may allow for sufficient aggregation of chloride ions at the defect location (Wang et al., 2005). The enhanced

chloride content in the grout at the void location in conjunction with carbonation of the grout would create situations where the $[Cl^-]/[OH^-]$ threshold is exceeded and steel passivity breakdown can occur. The level of corrosion is most severe at the grout-to-air interface, due to not only active corrosion by grout carbonation and chloride enhancement, but also aggravating macrocell development between the anodic regions at the grout-to-air interface and the rest of the passive strand in otherwise normal grout. Furthermore, adverse macrocell development can occur between the strand and the rest of the anchorage assembly (Wang et al., 2005).

Since 2011, isolated cases of severe corrosion of steel strand in deficient grout not directly associated with voids, bleed water, carbonation, and chlorides were reported in Europe and Florida (Lau et al., 2013a; Bertolini and Carsana, 2011; Carsana and Bertolini, 2015). In those accounts, the grout was described as having poor cohesive bulk properties, high moisture content, high alkali content, and high sulfate ion concentrations. In the European case, failure of a bridge prestressing cable occurred in less than 2 years of service. In Florida, two posttensioned bridges with less than 8 years in service had severe steel corrosion in grouts with these characteristics, but unexpectedly it occurred in the newer low-bleed prepackaged thixotropic grouts. The grout anomalies in prepackaged thixotropic grouts were also documented in Texas (Merrill, 2010). Research is ongoing on the cause of the grout deficiency in the prepackaged grout products (Hamilton, 2014), but early indicators attributed the failure in part to excess water and materials intolerant to excess water. The lack of supporting evidence of significant chloride presence and carbonation, and the inconsistent association of severe corrosion to void spaces, would indicate different corrosion mechanisms than those conventionally associated with the corrosion of prestressed steel (Bertolini and Carsana, 2011; Blactot et al., 2007). Bertolini and Carsana (2011) proposed that low oxidizing conditions due to limited oxygen supply in crevice regions, and highly alkaline pore water conditions with pH greater than 14, would allow for stability of the $HFeO_2^-$ ion and allow for active corrosion conditions. Coincidently, high sulfate ion concentrations were consistently associated with segregated grout (Lau et al., 2013a; Carsana and Bertolini, 2015; Merrill, 2010). Hydrolysis reactions involving sulfate ions such as $Fe^{2+} + 2H_2O + 2SO_4^{2-} \rightarrow Fe(OH)_2 + 2H_2SO_4$ in crevice environments may allow for localized corrosion (Jones, 1996). Information from the technical literature also indicated that there could be conditions where enhanced sulfate ion concentrations may lead to corrosion development, but a uniform description of the corrosion activation processes of steel in relevant grout environments is lacking. Gouda (1970) showed that breakdown of steel passivity in saturated calcium hydroxide solution (pH $\sim$ 12.1) can occur at sodium sulfate concentrations greater than 0.2%. Acha et al. (1990) also indicated the role of potassium sulfate in inhibiting passive layer formation in steel in saturated calcium hydroxide solution. Al-Tayyib et al. (1988) also indicated an increased corrosion current for steel in calcium hydroxide solution with sodium sulfate presence. Gouda and Halaka (1970) furthermore investigated the role of sulfates (up to 8%) in the corrosion of steel in concrete. Reported test results showed no breakdown of steel passivity with the presence of sulfates, and the authors posed that alumina-containing cement phases react with the sulfate to form insoluble compounds. Al-Tayyib and Khan (1991) reported only a

modest increase in the corrosion rate of steel in concrete with up to 1.8 kg/m^3 sulfate by weight of concrete. Research on the role of sulfates in the corrosion of steel in deficient grout is ongoing.

Concerns about corrosion development in steel strands after repair of void spaces with dissimilar grout materials may be particularly relevant for tendon systems containing deficient grout materials. Corrosion failure of an external tendon in the Varina-Enon Bridge in Virginia in 2007 has often been cited, as the tendon failure occurred less than 4 years after repair of a void space (Hansen, 2007). In the absence of grout degradation and other tendon deficiencies, complete repair of the void space with dissimilar materials can be expected not to produce any significant corrosion development if both materials yield high-pH environments where the steel should maintain its passive behavior. Moderate levels of polarization in the anodic region due to coupling of the steel in the dissimilar grouts should not cause significant enhanced corrosion rates if the repair is made in such a way that it prevents moisture accumulation and external exposure. Voids created by bleed water and grout segregation could lead to localized grout deficiencies such as carbonation and enrichment of aggressive chemical species, where steel depassivation can occur and the condition can be aggravated by macrocell development. Laboratory testing of repair void spaces filled with repair grout in field-extracted external tendons containing some form of grout segregation indicated corrosion activity after placement of the repair material (Lau et al., 2013b,c; O'Reilly et al., 2012). Removal of deficient grout prior to repair remains a challenge.

3.4   Overview of corrosion failures and current corrosion problems

The corrosion failures of early posttensioned concrete bridges in the United Kingdom in 1967 and 1985 have often been referenced in written work regarding the corrosion durability of posttensioned concrete bridge systems (Hewson, 2003). The catastrophic failure of the Ynys-y-Gwas Bridge in 1985 occurred without warning as a result of ineffective corrosion protection from moisture and deicing salts of the prestressing steel at mortar-filled segment joints. In the United Kingdom, a moratorium on internal posttensioned tendons was placed in 1992 over concern about the corrosion durability of the prestressing steel located at joints (Hewson, 2003). Lessons learned from this bridge failure included the need for multilevel strand protection and detailing in order to provide corrosion durability.

In the United States, corrosion of external grouted posttensioned tendons occurred in several bridges in Florida (Niles Channel, Mid-Bay, Seven Mile, and Sunshine Skyway) (Powers, 1999; Corven Engineering, 2001; Hartt and Venugopalan, 2002) and Virginia (Varina-Enon) (Hansen, 2007) from the late 1990s to the mid of the first decade of the twenty-first century. Design of these bridges incorporated materials thought to provide corrosion durability, such as the use of HDPE duct and the sealing of anchors with coating materials. Although specific details vary from case to case,

corrosion of the prestressing steel in these cases was largely attributed to void forma-
tion in the tendon due to bleed water formation in the neat grout commonly used at the
time. The void spaces are generally formed at high point tendon anchors. In some of
the cases, recharging of moisture occurred as a result of inadequately sealed anchor
heads. Cases of cracked HDPE ducts were observed in Mid-Bay and Sunshine
Skyway, but were not directly attributed to corrosion initiation (Hartt and Venugopa-
lan, 2002). Following these events, strategies to improve the corrosion durability of
posttensioned systems were implemented. These included the use of prebagged thixo-
tropic grout materials to improve quality control and prevent bleed water formation,
the use of enhanced posttensioning system components, the detailing of multiple levels
of corrosion protection for the duct and anchors, and the sealing of joints and anchors
(Corven Engineering, 2002).

The Ringling Causeway Bridge is a posttensioned segmental bridge with internal
and external tendons spanning across intracoastal water in Florida. In 2011, corrosion
failures of two longitudinal external posttensioned tendons occurred after only approx-
imately 8 years of service (Lau et al., 2013a). Further inspection showed that greater
than 10% (17) of the external posttensioned tendons had to be replaced because of
corrosion. The corrosion was alarming not only because of the number and severity
of corroded tendons, but also because corrosion occurred in tendons containing a pre-
packaged thixotropic grout product conforming to updated specifications that were
introduced to minimize corrosion. The severe corrosion of the strand was not consis-
tently associated with grout voids as described for earlier cases, but occurred at loca-
tions with deficient grout. In the most severe manifestation of the deficient grout, the
grout remained unhardened (Figure 3.5) with a putty-like consistency, and became
friable upon drying. In nearby regions, the deficient grout had a white color and chalky
consistency. The deficient grout material contained as much as 80% moisture. Pore
water pH as determined by an ex situ leaching method was generally greater than 12,

Figure 3.5 Corrosion of a strand embedded in deficient grout. Pink color shows the pH indicator
(phenolphthalein) sprayed on the grout surface.

and the pH in the soft grout with nearby corrosion was sometimes greater than 13. No consistent indication of carbonation as the primary corrosion mechanism was observed. The total chloride content was low to moderate, but may be enhanced in deficient grout by capillary transport during the grout segregation process. There may be some occasion where chloride and pH conditions may exceed critical $[Cl^-]$/$[OH^-]$ concentrations, but in general these conditions may not have always been consistent in locations with severe corrosion. Severe corrosion and deficient grout was associated with high free sulfate concentrations (as high as $\sim$10,000 ppm). As seen in Figure 3.6, variation of grout consistency and chemical makeup was observed in stratified grout layers at a low point anchor cap. Corrosion of the strand and wedge plate was predominant in regions of severe grout deficiency that had enhanced moisture and sulfate ion presence.

As of 2014, five other bridges in Florida built with low-bleed water formation grouts had been identified as having analogous deficient grout, but the amount and severity varied significantly between bridges (Lau et al., 2014). One of the five had significant corrosion of the metal duct in internal tendons, with the thickness of the duct being fully penetrated as a result of corrosion (Figure 3.7). Fourteen tendons had deficient grout. Similar to the deficient grout found in the Ringling Causeway, the extracted deficient grout in that case had high sulfate ion concentrations (ranging from 1000 to 12,000 ppm) relative to extracted hardened grout (10−200 ppm). Studies on the corrosion behavior of steel in deficient grout are ongoing.

As further exacerbation of recent corrosion failures, the prepackaged grout product sometimes contained elevated chloride levels that well exceeded the specified limit. (Gee, 2011). Bridges identified as containing batches of the contaminated grout have recently been inspected in order to measure chloride content. Laboratory studies were conducted to further investigate the critical chloride threshold concentrations in prepackaged thixotropic grout materials. In an FHWA report (Lee and Zielske, 2014), corrosion risk was described to be low if the total chloride content is less than 0.4%, and high if the total chloride content is greater than 0.8%. These values are not applicable to grouts that have any other form of deficiencies. Further deliberation is needed on grout deficiencies associated with segregation, possible exposure, and negative interaction with chloride contamination, even below specification limits.

Methodologies to inspect and repair tendons with deficient grout can be difficult because of complexities associated with the geometry of internal and external draped tendons. Following the reports of corrosion of strand in deficient grout in Florida bridges, a guideline for sampling and assessment of deficient grout was published by FHWA (Theryo et al., 2013). Where tendon sections cannot be completely replaced, removal of the deficient grout may be needed. Water-jetting may be suitable to remove the deficient grout, but water must not be entrapped within the tendon after the procedure. Tendon drying and inhibitor impregnation techniques have recently been explored. Nondestructive testing to identify the corrosion of strands and deficient grouts in tendons is needed. Positive results were obtained in recent demonstrations of
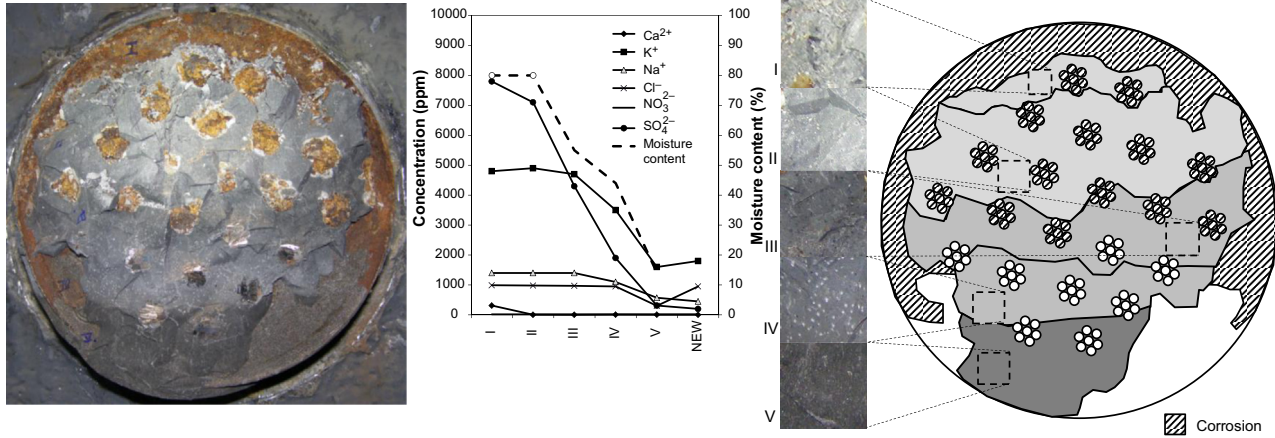
Figure 3.6 Visual and chemical makeup of stratified deficient grout at an anchor cap.

Figure 3.7 Corrosion of metal duct with deficient grout.
Photos courtesy of Florida Department of Transportation.

techniques such as magnetic main flux and magnetic flux leakage for detection of steel metal loss within external tendons and sonic/ultrasonic impact echo testing for detection of anomalies in the internal tendons of posttensioned girders. Also, acoustic emission monitoring devices may be implemented to identify wire breaks. The reader is referred to the technical literature for detailed description of nondestructive testing and evaluation techniques (Lee et al., 2014; DMJM Harris, 2003; Azizinamini and Gull, 2012). Studies to identify suitable nondestructive tests for posttensioned systems have been made, and others including the National Cooperative Highway Research Program's NCHRP 14−28 are ongoing.

As a result of recent corrosion failures of posttensioned tendons that incorporated a prepackaged thixotropic grout product, and the associated difficulties with its inspection and repair, there has been momentum in Florida for the specification of nonbonded posttensioned systems using flexible fillers such as waxes for continuity tendons, I beams, hammerhead piers, and straddle piers (Robertson, 2015; Hamilton and Rice, 2015). Top slab transverse and cantilever tendons still require bonded tendons. The arguments for the change are that wax materials should remain stable and inert, and good performance has been observed in the nuclear industry and in Europe; but if corrosion were to occur, failure would be progressive and the tendons can be replaced. Disadvantages for implementation of the technology in the United States include the need to develop material and structural specifications, increased material costs, specialized construction, limited material suppliers, and limited technological expertise among the workforce.

3.5 Cathodic protection

Cathodic protection (CP) systems have been implemented for prestressed concrete systems (notably for prestressed concrete cylinder pipes, but ongoing experience with prestressed bridge piles and beams continues). CP systems and their materials are diverse, but can be generally grouped as galvanic or impressed current systems. Their application in atmospheric, buried, or submerged environments can further

diversify CP systems and their materials. NACE International's state-of-the art-report on CP of prestressed concrete structures is available (NACE Int, 2002).

Limitations of using CP systems for prestressed concrete include possible adverse effects due to the enhanced formation of products from the cathodic reaction. Alkalinization of the pore water at the steel surface due to cathodic polarization may contribute to reduction of bond strength at the steel/cement interface (Eyre and Chess, 1998). At potentials more negative to the half-cell potential of reaction $H_2O + e^- \rightarrow H_{ads} + OH^-$, excessive atomic hydrogen dissolution into the steel atomic lattice can cause hydrogen embrittlement. The pore water chemistry and environment can affect the condition and rate at which hydrogen can form. Steel material makeup, properties, and surface conditions can also affect its susceptibility to hydrogen embrittlement, further complicating practical CP criteria (NACE Int, 2002; Eyre and Chess, 1998; Bennett and Schue, 1998). Generally, CP systems are maintained to prevent hydrogen formation. Other practical complications for CP of prestressed concrete include consideration of appropriate or inappropriate continuity of strand and other steel components, the requirement for uniform current distribution despite adverse geometry and mixed environments, and appropriate current shielding.

3.6 Closing remarks

Despite the sometimes pessimistic overtones used in discussions of the corrosion of prestressed concrete, pretensioned and posttensioned concrete remain viable building materials for highway bridges. As with any construction materials, consideration of the material performance in construction and service environments is vital when assessing long-term bridge durability. The design service life of bridges must exceed 75 years as required by owners. Corrosion durability problems encountered during the modern application of prestressed concrete highlight the need for the holistic consideration of manufacturing and building economics, structural design, materials performance and durability, construction practices, attainable construction quality, and maintenance tools to ensure the success of bridge construction and utility. This is necessary in order to maintain confidence among all relevant parties from materials providers and builders, to bridge designers and owners, and ultimately the public consumer. Product development, novel materials, changes in technology, improvements in manufacturing, structural design and detailing, and construction technology all provide function for innovation to further advance the building technology. Improved communication between government, industry, and academia (in sectors from highways to defense, and in disciplines from chemistry and materials science to engineering) should further advance the good use of building technology for its application in vital highway infrastructure. Innovations for corrosion control should be implemented in engineering practice only if there is confidence primarily in its safe use and performance, and secondly if it has economic rationale. The challenge remains to set forth a complete system that fulfills market needs for industry materials providers and builders, maintains quality engineering practices, and provides economic and safe infrastructure for public use.

References

ACI 318R, 2014. Building Code Requirements for Structural Concrete (ACI 318-14) and Commentary. Farmington Hills, MI.

ACI 222.2R, 2014. Report on Corrosion of Prestressing Steels (ACI222.2R-14). American Concrete Institute, Farmington Hills, MI.

ACI 440.4R, 2004. Prestressing Concrete Structures with FRP Tendons (ACI 440.4R-04). American Concrete Institute, Farmington Hills, MI.

Acha, M., Alonso, C., Andrade, C., 1990. Corrosión bajo tension de alambres de acero de pretensado en medios alcalinos, conteniendo sulfatos. Ref. Revista/Libro: Hormigón y Acero, 2 Trimestre, pp. 89−94.

Al-Tayyib, A.J., Somuah, S.K., Boah, J.K., Leblanc, P., Al-Mana, A.I., 1988. Cement and Concrete Research 18, 774−782.

Al-Tayyib, A.J., Khan, M.S., 1991. Effect of sulfate ions on the corrosion of rebars embedded in concrete. Cement and Concrete Composites 13, 123−127.

Azizinamini, A., Gull, J., June 2012. Improved Inspection Techniques for Steel Prestressing/ Post-Tensioning Strand, vol. 1. Final Report to Florida Department of Transportation. BDK80-977-13.

Bentur, A., Diamond, S., Berke, N.S., 1997. Steel Corrosion in Concrete. E&FN Spon, London.

Bertolini, L., Elsener, B., Pedeferri, P., Polder, R., 2004. Corrosion of Steel in Concrete: Prevention, Diagnosis, Repair. Wiley-VCH, Germany.

Bertolini, L., Carsana, M., 2011. High pH Corrosion of Prestressing Steel in Segregated Grout. In: Modeling of Corroding Concrete Structures. RILEM Bookseries, vol. 5. RILEM.

Blactot, E., Brunet-Vogel, C., Farcas, F., Gailet, L., Mabille, I., Chaussadent, T., Sutter, E., 2007. Electrochemical Behavior and Corrosion Sensitivity of Prestressed Steel in Cement Grout. In: WIT Transactions on Engineering Sciences, Simulation of Electrochemical Processes II, vol. 54, pp. 267−276.

Bennett, J., Schue, T.J., 1998. Cathodic Protection Field Trials on Prestressed Concrete Components. Final Report to FHWA. Report No. RD97-153.

Corven, J., Morenton, A., May 2013. Post-Tensioning Tendon Installation and Grouting Manual. Federal Highway Administration, U.S. Department of Transportation. FHWA-NI-13-026.

Corven Engineering, October 10, 2001. Mid-Bay Bridge Post-Tensioning Evaluation. Final Report to Florida Department of Transportation.

Carsana, M., Bertolini, L., 2015. Corrosion failure of post-tensioning tendons in alkaline and chloride-free segregated grout: a case study. Structure and Infrastructure Engineering: Maintenance, Management, Life-Cycle Design and Performance 11 (3), 402−411.

Corven Engineering, February 15, 2002. New Direction for Florida Post-Tensioned Bridges, vol. 1. Final Report to Florida Department of Transportation.

DMJM Harris, February 15, 2003. Test and Assessment of NDT Methods for Post-Tensioning Systems in Segmental Balanced Cantilever Concrete Bridges. Florida Department of Transportation.

ETAG 013, 2002. Guideline for European Technical Approval of Post-Tensioning Kits for Prestressing of Structures. EOTA, B-1040 Brussels.

Eyre, D., 1998. In: Chess, P.M. (Ed.), Cathodic Protection of Steel in Concrete. E&FN Spon, London.

Fernandez, J., Hutchison, M., Sagüés, A.A., Mullins, G., May 2014. Corrosion Characteristics of Unprotected Post-Tensioning Strands under Stress. Final Report to Florida Department of Transportation. BDK84-977-22.

Gee, K.W., November 23, 2011. Memorandum. Elevated Chloride Levels in SikaGrout 300PT Cementitious Grout. US Department of Transportation, Federal Highway Adminstration. Available online: https://www.fhwa.dot.gov/bridge/111123.pdf.

Gouda, V.K., 1970. Corrosion and corrosion inhibition of reinforcing steel: I. Immersed in alkaline solution. British Corrosion Journal 5, 198−203.

Gouda, V.K., Halaka, W.Y., 1970. Corrosion and corrosion inhibition of reinforcing steel: II. Embedded in concrete. British Corrosion Journal 5, 204−208.

Hewson, N.R., 2003. Prestressed Concrete Bridges: Design and Construction. Thomas Telford Publishing, London.

Hartt, W., Venugopalan, S., April 2002. Corrosion Evaluation of Post-Tensioned Tendons on the Mid Bay Bridge in Destin, Florida. Final Report to Florida Department of Transportation.

Hamilton, H.R., April 2014. Simulation of Prepackaged Grout Bleed under Field Conditions. Revised Draft Final Report to Florida Department of Transportation. BDK75-977-59.

Hamilton, H.R., Rice, J.A., January 2015. Replaceable Unbonded Tendons for Post-Tensioned Bridges. Interim Report to Florida Department of Transportation. Task 1. BDV31-977-15.

Hansen, B., 2007. Forensic engineering: tendon failure raises questions about grout in post-tensioned bridges. Civil Engineering News 17−18.

Jones, D.A., 1996. Principles and Prevention of Corrosion, second ed. Prentice Hall, Upper Saddle River.

Lau, K., Lasa, I., Paredes, M., 2013. Corrosion Failure of Post-Tensioned Tendons in Presence of Deficient Grout. Paper No. 2600. CORROSION/2013. NACE International, Houston, TX.

Lau, K., Sagüés, A.A., February 2009. Corrosion of Steel in Locally Deficient Concrete. Final Report to Florida Department of Transportation. BDV544-31.

Lau, K., Rafols, J., Lasa, I., Paredes, M., 2013. Laboratory Corrosion Assessment of Post-Tensioned Tendons Repaired with Dissimilar Grout. Paper No. 2602. CORROSION/2013. NACE International, Houston, TX.

Lau, K., Powers, R., Paredes, M., 2013. Corrosion Evaluation of Repair-Grouted Post-Tensioned Tendons in Presence of Bleed Water. NACE International, Houston, TX. Paper No. 2604. CORROSION/2013.

Lau, K., Lasa, I., Paredes, M., 2014. Update on Corrosion of Post-Tensioned Tendons with Deficient Grout in Florida. Paper No. 4225. CORROSION/2014. NACE International, Houston, TX.

Lee, S., Kalos, N., Shin, D.H., 2014. Non-destructive testing methods in the U.S. for bridge inspection and maintenance. KSCE Journal of Civil Engineering 18 (5), 1322−1331.

Lee, S.K., Zielske, J., May 2014. An FHWA Special Study: Post-Tensioning Tendon Grout Chloride Thresholds. FHWA-HRT-14e039. Department of Transportation, Federal Highway Administration, U.S.

Mullins, G., Sen, R., Sagüés, A.A., January 2014. Design and Construction of Precast Piles with Stainless Reinforcing Steel. Draft Final Report to Florida Department of Transportation. BDK84-977-07.

Moser, R.J., 2013. Preliminary Studies of High-Strength Stainless Prestressing Steels. ACI SP 291-6, Farmington Hills, MI, pp. 95−104.

Matsushima, I., 2011. Carbon steel- atmospheric corrosion. In: Revie, R.W. (Ed.), Uhlig's Corrosion Handbook, third ed. Wiley, Hoboken.

Merrill, B., September 14, 2010. Memorandum. Grout Testing and Analysis. Texas Department of Transportation.

Naaman, A.E., 2004. Prestressed Concrete Analysis and Design, second ed. Techno Press, Ann Arbor.

NACE Int, February 2002. State of the Art Report: Criteria for Cathodic Protection of Prestressed Concrete Structures. No. 24217.

O'Reilly, M., Darwin, D., Browning, J., April 2012. Corrosion Performance of Prestressing Strands in Contact with Dissimilar Grouts, SL Report 12-1. The University of Kansas Center for Research.

PCI, 2010. PCI Design Handbook: Precast and Prestressed Concrete (PCI MNL-120). Precast/Prestressed Concrete Institute, Chicago, IL.

PTI M55.1-12, 2012. Specification for Grouting of Post-Tensioned Structures (PTI M55.1-12). Post-Tensioning Institute, Farmington Hills, MI.

Parsons Brinckerhoff, July 2012. Unbonded Tendon System Practices for Bridges in Europe. Brief Report to Florida Department of Transportation.

Powers, R.G., 1999. Corrosion Evaluation of Post-Tensioned Tendons on the Niles Channel Bridge. Florida Department of Transportation.

Roddenberry, M., Mtenga, P., Joshi, K., April 2014. Investigation of Carbon Fiber Composite Cables in Prestressed Concrete Piles. Final Report to Florida Department of Transportation. BDK83-977-17.

Robertson, R., May 20, 2015. Structures Design Bulletin 15-03. Florida Department of Transportation. Available online: http://www.dot.state.fl.us/structures/Bulletins/2015/SDB15-03.pdf.

Reis, R.E., 2006. Corrosion Evaluation and Tensile Results of Selected Post-Tensioning Strands at the SFOBB Skyway Seismic Replacement Project. Phase I Report. Caltrans, Sacramento, CA.

Reis, R.E., 2007. Corrosion Evaluation and Tensile Results of Selected Post-Tensioning Strands at the SFOBB Skyway Seismic Replacement Project. Phase II Report. Caltrans, Sacramento, CA.

Reis, R.E., 2007. Corrosion Evaluation and Tensile Results of Selected Post-Tensioning Strands at the SFOBB Skyway Seismic Replacement Project. Phase III Report. Caltrans, Sacramento, CA.

Roberge, P.R., 2011. Atmospheric corrosion. In: Revie, R.W. (Ed.), Uhlig's Corrosion Handbook, third ed. Wiley, Hoboken.

Revie, R.W., Uhlig, H.H., 2008. Corrosion and Corrosion Control, fourth ed. Wiley, Hoboken.

Sason, A.S., 1992. Evaluation of degree of rusting on prestressed concrete strand. PCI Journal 37 (3), 25−30.

Sagüés, A.A., Karins, F.C., Lau, K., May 2011. Corrosion Characteristics of Post-Tensioning Strands in Ungrouted Ducts. Final Report to Florida Department of Transportation. BDK84-977-04.

Trejo, D., Hueste, M., Gardoni, P., Pillai, R., Reinschmidt, K., Im, S.B., Hurrlebaus, S., Gamble, M., Ngo, T.T., September 2009. Effect of Voids in Grouted, Post-Tensioned Concrete Bridge Construction, vol. 1. Technical Report to Texas Department of Transportation. FHWA/TX-09/0-4588-1.

Trejo, D., Hueste, M., Gardoni, P., Pillai, R., Reinschmidt, K., Im, S.B., Hurrlebaus, S., Gamble, M., Ngo, T.T., September 2009. Effect of Voids in Grouted, Post-Tensioned Concrete Bridge Construction, vol. 2. Technical Report to Texas Department of Transportation. FHWA/TX-09/0-4588-1.

Theryo, T., Hartt, W.H., Paczkowski, P., October 2013. Guidelines for Sampling, Assessing, and Restoring Defective Grout in Prestressed Concrete Bridge Post-Tensioning Ducts. FHWA-HRT-13-028. FHWA-HRT-14−039. U.S. Department of Transportation, Federal Highway Administration.

VSL, 2002. Grouting of Post-Tensioning Tendons. VSL Report Series 5. VSL International, Switzerland.

Wang, H., Sagüés, A.A., Powers, R., 2005. Corrosion of the Strand-Anchorage System in Post-Tensioned Grouted Assemblies. NACE International, Houston, TX. Paper No. 05266. CORROSION/2005.

Corrosion of stainless steel in concrete

4

C.M. Hansson

Mechanical and Mechatronics Engineering, University of Waterloo, Waterloo, ON, Canada

4.1 Rationale for the use of stainless alloys as reinforcing bars in chloride-contaminated environments

Although noncontaminated concrete provides an ideal passivating environment for carbon steel as described in Chapter 2, the ingress of chlorides from anti-icing and de-icing salts results in the breakdown of the passive film on the steel, the production of voluminous corrosion products, and finally cracking and spalling of the concrete. The application of rock salt, and more recently concentrated brines with chloride contents up to 23% to the roads and highways, has resulted in increasingly high deterioration rates of highway structures and parking garages. At the same time, national bridge codes are demanding increasing service lives − 75 years in Canada (CSA, 2006), with discussions underway to increase this to 100 years.

In order to meet these demands, owners of these structures are seeking more corrosion-resistant alloys, both as reinforcing bars (rebar) and in order to limit the need for frequent maintenance and associated traffic delays. Stainless steel is the obvious candidate.

Stainless steels are iron-based alloys with a minimum chromium (Cr) content of 11% (ASM, 1990). This limit is such that the oxide layer formed on alloys with >11% Cr is Cr_2O_3, whereas at lower levels of Cr content, an iron oxide is formed. Other alloying elements such as nickel (Ni), molybdenum (Mo), copper (Cu) and nitrogen (N) are added to achieve the desired mechanical, fabrication and corrosion-resistance characteristics.

Some advantages of stainless steel as rebar material are (Tullmin et al., 1998):

- Good ductility
- Homogeneity of microstructure
- Cut ends do not have to be protected
- Magnetic or nonmagnetic depending on alloy type
- Good weldability

Four types of stainless steel are commercially available and classified based on their microstructure: martensitic, ferritic, austenitic and duplex (ferritic−austenitic). The microstructure and properties of stainless steel are dependent on the type and concentrations of the different alloying elements. The corrosion resistance of martensitic

and ferritic stainless steels is not sufficient for their use as reinforcing steel, and therefore these stainless types are not cost-effective alternatives to carbon steel rebar (Knudsen et al., 1998) and are not considered further. Austenitic stainless steel contains 16−26% chromium and 6−22% nickel, while duplex steel contains 18−29% chromium and 4−9% nickel depending on specifications (Sedriks, 1996). Several grades also contain molybdenum, which increases pitting resistance. Cold-working of austenitic stainless steel results in increased yield and tensile strengths to meet the current values specified for reinforcing steel. A 10% cold working results in a tensile strength of 540 MPa and a yield strength of 400 MPa (McGurn, 1998; Nürnberger, 2005). Austenitic stainless steel is not ferromagnetic, but may become magnetic if cold-worked, whereas duplex steel is magnetic. More details of the mechanical and physical properties are given in the references (Concrete Society, 1998; Nürnberger, 2005).

Since reinforced concrete is a composite of concrete and steel, the coefficients of thermal expansion of the two materials should be considered. Concrete has a coefficient of thermal expansion of $1.1 \times 10^{-5}\,°C^{-1}$ (Nürnberger, 1996). Plain carbon steel and ferritic stainless steel have a thermal expansion coefficient of $1.2 \times 10^{-5}\,°C^{-1}$, which is very similar to that of concrete (Nürnberger, 2005). The thermal expansion coefficients of austenitic and duplex steels are $1.8 \times 10^{-5}\,°C^{-1}$ and $1.3 \times 10^{-5}\,°C^{-1}$, respectively (Concrete Society, 1998; Nürnberger, 1996). The somewhat higher coefficient for austenitic stainless steel suggests that thermal cycling could result in crack formation due to tensile stresses forming at the concrete/steel interface. However, there have not been any problems or reports of such cracking in the laboratory or in field applications (Nürnberger, 1996, 2005).

It is clear that the most commonly used grades, namely UNS31653 and UNS32205, would meet all the requirements for durable rebar. However, despite the significantly lower *lifetime* costs of a structure reinforced with these alloys, the greatest handicap to their use is their *initial* cost, which is expected to be only 5−15% of the total cost of the structure (Nürnberger, 1996). The variation in cost of the component metals of stainless steel over a decade, shown in Figure 4.1, illustrates both the uncertainty in overall cost and the influence of nickel and molybdenum contents Data courtesy of J. Mauro, ASW Inc. Welland Ontario.

To address this problem, steel companies have been developing stainless grades with less expensive alloying components than those of UNS31653 and UNS32205 by replacing some of the nickel with manganese and reducing or eliminating the molybdenum content. Understandably, however, authorities are reluctant to install untested alloys in structures intended to last for 75 years or more. A number of research groups in Europe and North America have been investigating the relative corrosion performance of the newer alloys in short-term laboratory tests. However, these tests use various methods to accelerate corrosion and typically consist of three to five years of exposure to salts at most, but sometimes the periods are as short as 3−4 days. Extrapolating the results of accelerated tests to real-world exposure for three-quarters of a century or more leaves many questions.
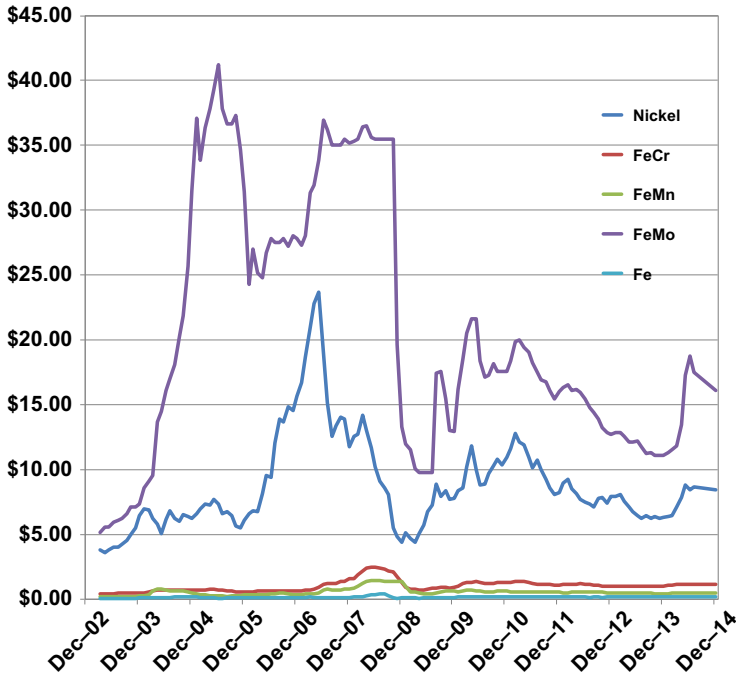
Figure 4.1 Monthly variation in market cost of the components of stainless steels over a 12-year period.
Data from the London Metal Exchange.

4.2 Experience to date with stainless rebar in the field

The application of stainless steel as a concrete reinforcement is gaining interest worldwide. Stainless-steel rebar has primarily been used in marine structures and climates that require the use of de-icing salts. The earliest application of stainless steel found in the literature was the use of a stainless steel with a chemistry similar to AISI 304 in a marine pier built from 1938 to 1941 in Progreso, Mexico (Knudsen et al., 1999). The hot, humid, salt-laden environment is one of the most corrosive exposures possible. Yet, a recent condition analysis (Castro-Borges, 2002) found that the pier built with stainless steel did not show any signs of reinforcement corrosion after 60 years of marine exposure, whereas a parallel pier built with black steel rebar had disintegrated. This difference in durability is well illustrated in Figure 4.2.

Another early application was the use of AISI 316 stainless-steel rebar for exterior precast cladding panels in Wellington, New Zealand in 1977 (MacGregor, 1998). An inspection of the panels in 1997 did not reveal any corrosion of the stainless-steel reinforcing, despite the use of a cover of only 20 mm. The atmospheric conditions for the building location were classified as marine or severe marine (MacGregor, 1998). For comparison, severe corrosion was observed in the same area for in-place concrete sections reinforced

Figure 4.2 The pier on the right was built with stainless-steel rebar in Progreso, Mexico between 1938 and 1941. The remains of a parallel pier built 30 years later with black steel rebar can be seen in the foreground.
Photograph courtesy the Nickel Institute.

with carbon steel. In 1983−84, a bridge deck was built using 20 metric tons of 304-clad reinforcement (McDonald et al., 1995). In the intervening three decades, an increasing number of structures have taken advantage of the greater corrosion resistance of the stainless-steel rebar grades, and in North America alone, between 20,000 and 30,000 tons are shipped annually (personal communication, Salit Steel).

4.3   Available grades of stainless rebar

The stainless steels available for rebar commonly fall into two types: austenitic − i.e. single-phase, face-centred cubic and nonferromagnetic − or duplex, an approximately equal mixture of austenitic and ferritic phases, the latter being body-centred cubic and ferromagnetic. From a structural viewpoint, the austenitic grades are highly ductile and work-hardenable, making them a choice material for structures where seismic activity must be considered. The duplex steels, on the other hand, are less ductile but stronger, potentially allowing the use of smaller-diameter bars, creating less congestion of bars and better compaction of the concrete. The composition and microstructure of several currently available grades are given in Table 4.1. To illustrate how significant is the variation in the *material* costs of these alloys (i.e. excluding processing costs), the compositions in Table 4.1 and the data in Figure 4.1 have been used to produce the graphs in Figure 4.3 (Whiting, 1981). The corrosion behaviour of several nonstandard alloys has been reported in the literature (e.g. Fajardo et al. (2011), Garcia-Alonzo et al. (2007a)), but are not covered in detail in this review.

4.4   Experimental corrosion tests for stainless rebar

The generally employed corrosion tests are described in detail in Part III, so this section will be confined to those tests specific to stainless-steel rebar. As for other types of

Table 4.1 **Specified ranges (in weight%) of constituent elements of some stainless-steel rebar (single figures represent the maximum allowable content)**

| Steel types			Alloying element								
UNS	AISI	EN	C	N	Cr	Ni	Mo	Mn	P	S	Si
S31653	316LN	1.4429/1.4403?	0.03	0.16	16.0−18.0	10.0−14.0	2.0−3.0	2.00	0.045	0.03	0.75
S30403	304L	1.4306/1.4307?	0.03	0.10	18.0−20.0	8.0−12.0	−	2.00	0.045	0.030	1.0
S24100	24100	XM28	0.15	0.2−0.45	16.5−19.5	0.5−2.5	−	11−14	0.06	0.03	1.0
S32205	2205	1.4462	0.03	0.14−0.20	22.0−23.0	4.5−6.5	3.0−3.5	2.00	0.03	0.02	1.0
S32304	2304	1.4362	0.03	0.05−0.2	21.5−24.5	3.0−5.5	0.05−0.6	2.5	0.04	0.03	1.0
S32101	2101	1.4162	0.03	0.22	21.5	1.5	0.3	5.0	0.04	−	1.0
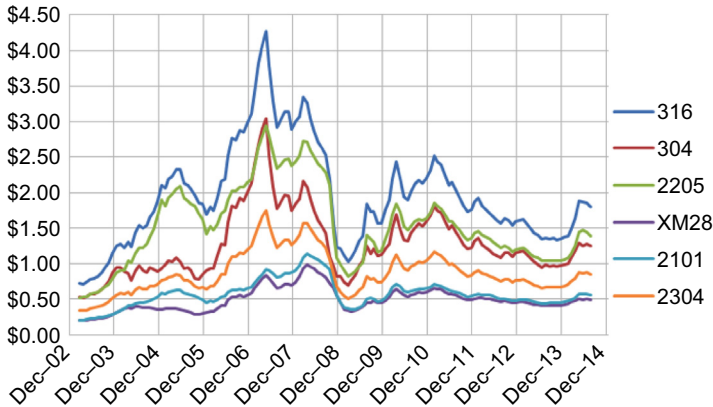
Figure 4.3 Effect of variations in the monthly market price of components on the material costs of stainless steel for rebar. Processing costs are not included (Van Niejenhuis, 2015).

rebar, it is important to conduct experiments on stainless-steel rebar in the condition in which it will be used in service. Using metallographically polished surfaces or employing cleaning/pickling methods will provide more 'scientific' results, but may not relate to the behaviour of the rebar in the field.

'Failure' of reinforced-concrete structures due to rebar corrosion is usually defined as the time when corrosion has progressed to the stage that corrosion products have created sufficient stresses in the concrete cover to cause cracking and spalling. Consequently, the major goals of corrosion testing of stainless-steel rebar include:

1. determining the critical chloride threshold level (CCTL) of the concrete necessary to initiate corrosion;
2. determining the critical pitting potential in different chloride-containing environments;
3. determining the active corrosion rate after initiation and the specific volume of the corrosion products in order to estimate the time before cracking and spalling of the concrete; and
4. evaluating the relative protection afforded by the different grades of stainless steel − i.e. ranking the different grades.

Most research attention has been on the first and fourth goals. However, the obvious problem with all of the goals is that realistic long-term tests are not possible, considering the anticipated 75−100 year lifetime of a structure reinforced with stainless bars. Consequently, all tests involve some form of acceleration, and all have disadvantages (Poursaee and Hansson, 2009). An example of the more minor forms of acceleration is the application of salt continuously at room temperature, compared with the field practice of intermittent application over the winter months at very low temperatures at which both diffusion through the concrete and corrosion rates are very low. The more aggressive tests include applying high anodic currents or potentials in order to induce corrosion and/or adding chlorides to the concrete mix.

For all types of rebar in concrete, however, the greatest obstacle in assessing corrosion behaviour is that concrete is not transparent, so the actual corroding area cannot be determined without destroying the concrete and removing the rebar. To overcome

this obstacle, many studies have been made of the corrosion of stainless-steel rebar immersed in either saturated $Ca(OH)_2$ with a pH of 12.6 or synthetic pore solution (pH ~ 13.5). The former is used as a measure of the environment in carbonated concrete in which all the excess KOH and NaOH has reacted, and the pH is buffered at 12.6 by the presence of a reservoir of solid $Ca(OH)_2$. The synthetic pore solution recommended by ASTM A955 is 1 L of solution containing 18.81 g KOH, 17.87 g NaOH and 974.8 g distilled water. Some researchers have used solutions based on the content of the major components of pore solution expressed from hardened concrete (Barneyback and Diamond, 1981). The pore solution compositions for an OPC concrete is given in Table 4.2 (Marcotte, 2001) The advantages of tests in solution are that chloride content can be accurately controlled and the corrosion can be observed visually.

The importance of pH of the synthetic pore solution on the corrosion behaviour of stainless steels is illustrated by its effect on the pitting potentials of 304 steel in Figure 4.4 (Elsener et al., 2011).

Table 4.2 The major components of pore solution expressed from 120-day-old cement paste w/cm ratio 0.45 and analysed using inductively coupled plasma and ion chromatography for the cations and anions respectively (Marcotte, 2001)

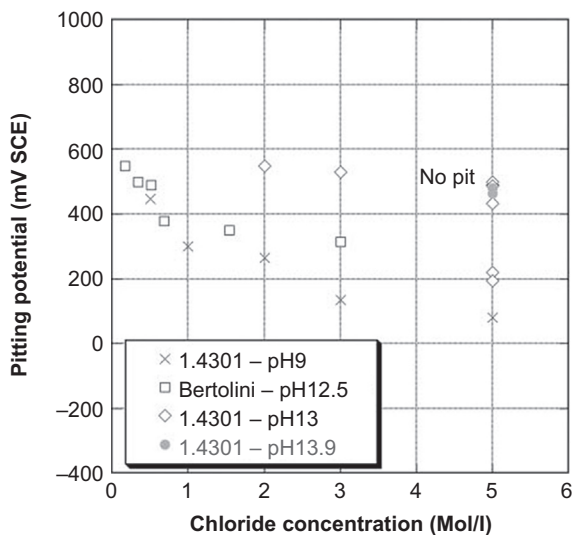| Species	B	Ca	Cl^-	K	Na	SO_4^{2-}
mm/L	2.69	2.55	0.22	319.7	130.9	3.24

Figure 4.4 The pitting potentials of polished specimens of 304 stainless steel tested in solutions of different pH and NaCl contents (Elsener et al., 2011).
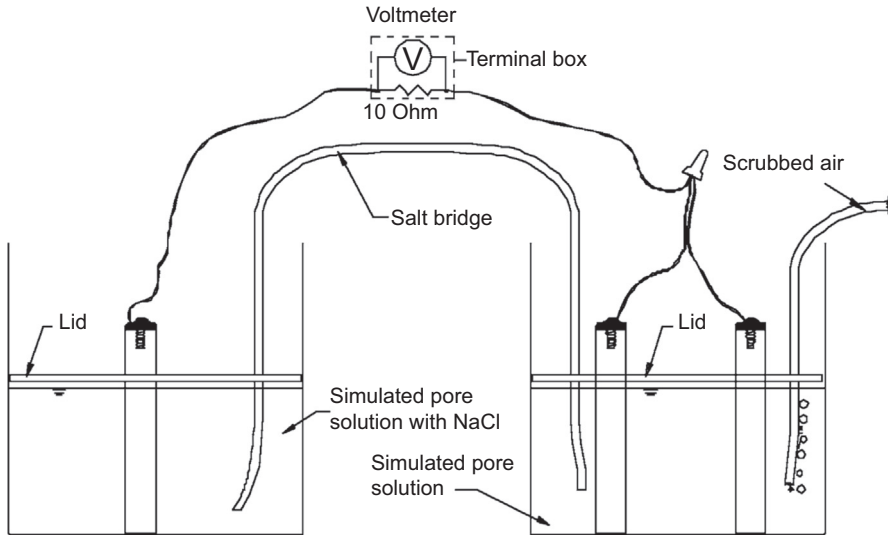
Figure 4.5 Experimental set-up for the ASTM A955 Rapid Macrocell Test (ASTM, 2010). Reprinted, with permission, from the ASTM A955/A955M-15 Standard Specification for Deformed and Plain Stainless-Steel Bars for Concrete Reinforcement, copyright ASTM International, 100 Barr Harbor Drive, West Conshohocken, PA 19428.

4.4.1 ASTM A955 standard specification for deformed and plain stainless-steel bars for concrete reinforcement (ASTM, 2010)

All stainless steels for reinforcing bars sold in North America are required to comply with this standard specification, which covers mechanical property requirements as well as corrosion resistance. The specific corrosion rate criteria are described briefly below.

- A.1 The corrosion resistance of the reinforcing steel, including the method of removing the mill scale, shall be evaluated based on either A1.2 or A1.3.
- 'A.2 Using a macrocell test of bare bars in a synthetic concrete pore solution with 15% sodium chloride over a 15-week period, as illustrated in Figure 4.5, the average corrosion rate for a minimum of five specimens shall at no time during the test exceed 0.25 μm/year, with no single specimen exceeding a corrosion rate of 0.50 μm/year' (ASTM, 2010; Ji et al., 2005).
- 'A.3 Using a cracked beam test over a 75-week period, as specified in Annex A3, the average corrosion rate for a minimum of five specimens shall at no time during the test exceed 0.20 μm/year, with no single specimen exceeding a corrosion rate of 0.50 μm/year' (ASTM, 2010).

In this test, a prism specimen, as illustrated in Figure 4.6, is cast with a 0.03 mm stainless-steel shim parallel to and above the top rebar to create a standard 'crack' after the shim is removed from the hardened concrete. Each week, the ponding well is filled with 15% NaCl for four days, and the potential drop across the 10 Ω standard resistor

Figure 4.6 Schematic representation of the prism for macrocell corrosion testing according to ASTM A955 (Islam et al., 2013).

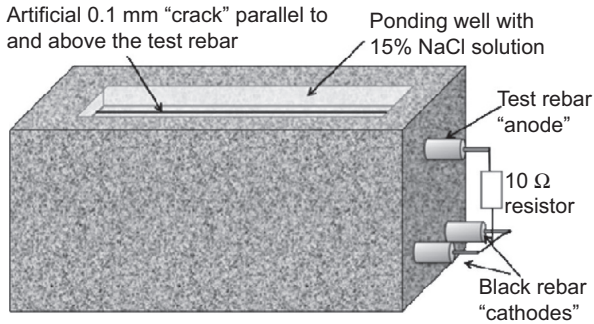recorded and converted by Ohm's law and the area of the top bar to corrosion rate in μm/year. The NaCl solution is then syphoned off and the prism held at 38 °C for three days. This procedure is continued for 12 weeks, followed by 12 weeks of continuous chloride exposure. The 12 week wet-dry cycle + 12 week continuous ponding is then repeated, to complete 72 weeks of testing, although the standard reports both 75 weeks and 96 weeks as 'common practice'.

Very few researchers appear to have used this specific test (Ji et al., 2005; Islam et al., 2013; Smith and Virmani, 2000), although a number have used a similar arrangement without the synthetic crack in the 'southern exposure test' (Hartt, 2009).

4.4.2 Modified EN 480-14 'rapid screening test'

The European standard EN 480-14 was designed to 'determine the effect of admixtures to concrete on the corrosion susceptibility of reinforcing steel by a potentiostatic electrochemical test'. It has been proposed (Schönning and Randström, 2011) that this test be modified to evaluate the relative corrosion resistance of different grades of stainless-steel rebar. The originally proposed test involves embedding a 100 mm length of stainless rebar in a standard mortar cylinder containing 4% NaCl by mass of cement added to the mixing water. The specimens are demoulded after 24 h and immersed in a saturated $Ca(OH)_2$ to prevent leaching. The corrosion potential (E_{corr}) is monitored for 24 h, after which a potential of +200 mV versus SCE is applied to the rebar and the resulting anodic current flowing between the rebar and a counter-electrode encircling the concrete cylinder is monitored for a minimum 84 h. The experimental set-up is shown in Figure 4.7.

The pass/fail criterion was set as a current density of 0.25 A/m^2 for at least 2 h. Thus, results can be obtained within six days. Subsequently, further modifications have been adopted (Schönning et al., 2013; Gastaldi et al., 2014) including (1) varying the chloride content of the mortar in order to determine a critical chloride content, (2) increasing the curing time and (3) decreasing the pass/fail limit to 0.080 A/m^2. In addition, it has been proposed that the mortar be replaced by the concrete of a mixture design to be used in practice, and it has been shown that the concrete
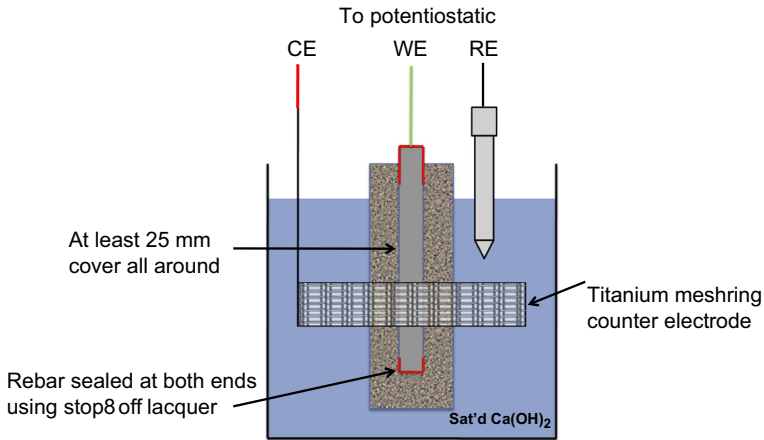
Figure 4.7 Experimental set-up for potentiostatic tests of stainless rebar embedded in concrete with admixed chlorides.

mix has a significant influence on the results of this test (Bandura et al., 2014). Also, the +200 mV SCE is an undesirable value for two reasons. First, it corresponds to the equilibrium potential for the oxygen/water reaction ($1/2\,O_2 + H_2 + 2e^- = 4(OH)^-$) at the typical pH in concrete. Second, it has been shown that the Cr_2O_3 component of the passive film is unstable, and the current density in cyclic polarization curves is at a maximum at potentials of around +200 mV SCE for all the stainless grades tested (Beverskog and Puigdomenech, 1999; Alvarez et al., 2011; Bandura et al., 2014; Garcia-Alonzo et al., 2007a) as illustrated in Figure 4.8. Consequently, it has been proposed (Bandura et al., 2014) that the potential should be no more positive than +100 mV SCE, and preferably that a set polarization level rather than a fixed applied potential be used because of the variation in corrosion potential of the different grades of stainless steel. Finally, it is understood that the passive film developed on stainless steels embedded in concrete differs from that formed in air (Serdar et al., 2013). Thus, the potentiostatic test described above, in which the steel with its air-formed film is placed directly in chloride-contaminated concrete, is a test of the corrosion resistance of the air-formed film and not of the film formed over a period in concrete.

4.4.3 Other nonstandard tests

The vast majority of investigations of the corrosion behaviour of stainless rebar have been conducted in either sound (uncracked) concrete or mortar, or in synthetic pore solution. However, structural concrete in the field is always cracked, so it is relevant to consider the rebar corrosion behaviour in such concrete. The ASTM A955 Procedure A3, described above is an attempt at that, but in order to create a 'reproducible crack', the shim actually produces a parallel-sided slot that allows direct access of the exposure solution to the rebar. Moreover, the sides of the slot are lined with Portlandite-rich cement paste. In contrast, a crack produced by loading follows a
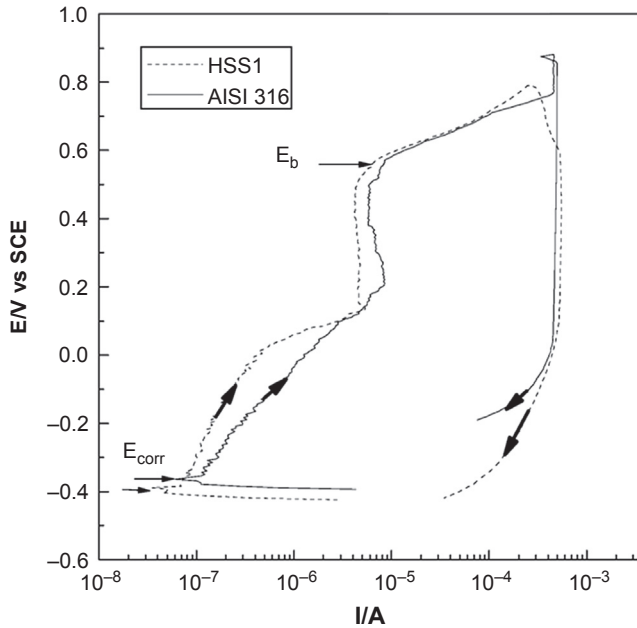
Figure 4.8 Anodic polarization curves of grades 316 and a low-nickel high-manganese stainless steel (approximately equivalent to XM28) in concrete with 4% admixed Cl⁻ by mass of cement (Garcia-Alonzo et al., 2007a).

much more tortuous path. It usually circumvents the coarse aggregate and propagates through the more porous interfacial zone between the paste and aggregate, and has varying widths and bottlenecks along its route. Tests involving specimens that are cracked after the concrete has hardened but before exposure thus require several replicate specimens to allow statistical analysis. Nevertheless, some research is now being conducted on steel embedded in cracked concrete (Nürnberger and Beul, 1999; Nürnberger, 2005; Ji et al., 2005; Van Niejenhuis et al., 2016).

4.5 Results to date on corrosion behaviour of stainless rebar

4.5.1 Critical chloride threshold level

The simplest method of testing the CCTL of highly corrosion-resistant steels is by measuring the corrosion current density of the steel in synthetic pore solution with increasing chloride additions. However, it should be noted these levels will always be significantly higher than those measured in mortar or concrete, because the chlorides are largely concentrated in the pore solution. While the proportion of chemically bound chlorides is significant relative to the CCTL of black steel, it is much less so for

stainless steels, with their much higher CCTL values. The actual concentration in the pore solution relative to the total chloride content will be affected by the w/cm ratio, the maturity and moisture content of the concrete and the concrete mixture design. This has been described by Anders et al. (2014).

Randström et al. (2010) used the potentiostatic test described above, but with bare steel rebar in synthetic pore solution in which air was bubbled to saturate the solution with oxygen. The bars were held at +200 mV versus SCE; chloride was added as NaCl every 12 h and the resulting current monitored. The authors concluded from these data that there is no significant difference in the corrosion resistance between 316L, LDX 2101 and 2304, with 304L being slightly lower. The CCTL, defined as the chloride content at which the current density rose above 10 A/m^2, showed significant scatter as indicated in Figure 4.9. A range of values is typical for corrosion of all rebar steels irrespective of whether the test is in pore solution, mortar or concrete. This is attributed to the stochastic nature of corrosion in general as well as the inhomogeneity both of a typical ribbed rebar surface and of concrete.

These authors also compared their results with those of Bertolini et al. (1996), Bertolini and Gastaldi (2009) and Hurley and Scully (2006), and indicated the importance of comparing the alloys in the same surface condition. Because of the variability, Gastaldi et al. (2014) propose a probability approach to defining the threshold.

The initial studies on the chloride threshold of 304 and 316 stainless-steel rebar were reported by Sørensen et al. in 1990 and by McDonald et al. in 1995 and 1998. These authors agreed that the threshold concentration for corrosion initiation in grade 316 was ∼5% Cl by mass of cement, and in 304 was somewhat lower.
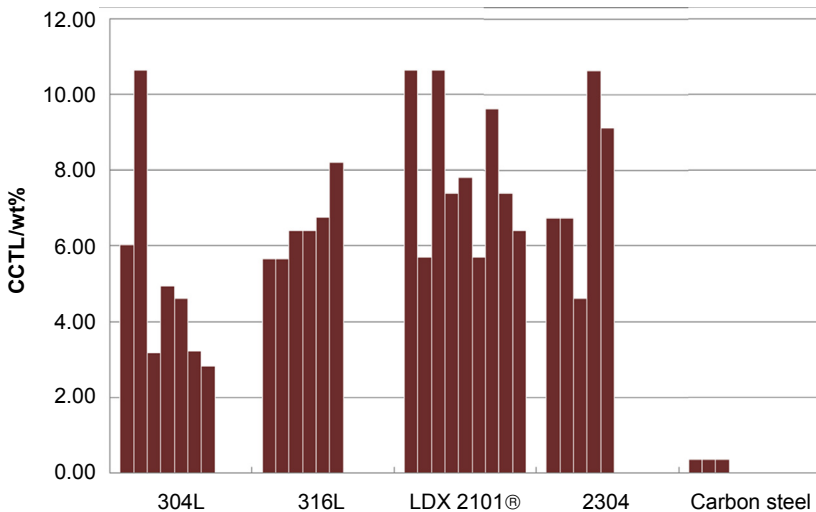

Figure 4.9 The critical chloride threshold levels (CCTLs) of different rebar grades (Randström et al., 2010).

Lollini et al. (2015) have recently presented a summary of the literature on CCTL values for 304 and 2205 grades, for both laboratory tests in concrete or mortar and in the field. For most tests, however, the CCTL is reported as 'greater than'; i.e. corrosion had not been initiated, in some cases with admixed chloride levels as high as 8% by mass of cementitious material. The tests in which corrosion was initiated were either under accelerated chloride transport and/or at elevated temperature (Gastaldi and Bertolini, 2014).

A summary of some threshold levels reported in the literature is provided in Table 4.3. It must be noted that the threshold obtained in pore solution is significantly higher than that measured in mortar or concrete, because the pores constitute a small proportion of the mixture.

4.5.2 Post-initiation corrosion behaviour and corrosion products

It is generally considered that once it is initiated, corrosion will propagate rapidly and cause distress in the concrete within a very short period (Luo et al., 2012; Lollini et al., 2015). However, this assumption is based almost exclusively on the experience with black steel rebar. A literature search has revealed very few studies of the post-initiation corrosion rates for stainless steel in concrete, obviously because it takes a very long time to initiate the corrosion. Nevertheless, several post-initiation factors should be considered as discussed below.

1. *The distribution and dimensions of any localized attack.* Once pits are initiated in a passive surface, the localization and any subsequent lateral growth of the pit determine the build-up of corrosion products (Scully and Hurley, 2007) and subsequent failure of the concrete. The acidification inside the pit will be greater for pits with a high aspect ratio, and this will affect the solubility of the corrosion products. Alvarez et al. (2011) reported that after polarization to the same current density in chloride-containing $Ca(OH)_2$ solution, large rounded pits were produced in austenitic 304L, whereas those in the duplex 2001 steel (20% Cr; 1.8% Ni; 4.1% Mn; 0.2% Mo) were smaller, angular and more numerous as illustrated in Figure 4.10. Also, there was some more generalized corrosion at the ribs in the 2001 steel, and the authors concluded that this is a 'less dangerous morphology'.

Studies have been conducted in pore solution with incremental additions of chlorides for the six different grades of stainless rebar listed in Table 4.1. In these tests, all the bars from one producer exhibited a dark line parallel to the length of the bar. It is postulated that it is an area of localized strain, but evidence of such strain has not been observed in metallographic examination of the cross-section through this location. Nevertheless, the effect on corrosion behaviour is pronounced, as illustrated in Figure 4.11, for S31653 (316LN).

In cyclic polarization tests of six different grades of steel in pore solution containing 16% chlorides, only 2205 did not show any pitting behaviour (Bandura, 2015). However, it is unlikely that steels will be subjected to the high anodic potentials required to induce corrosion while being exposed to such high chloride concentrations.

Table 4.3 **Chloride threshold values**

Alloy	Environment	Salt application	Exposure or test	CCTL % by wt. cement or solution	References
304 304LN 304L	Concrete	Admixed	Potentiostatic: +200 mV SCE	5−8	Sørensen et al. (1990)
	Pore solution		Polarization resistance	>3	McDonald et al. (1995)
	Pore solution		Pickled steel	>15	Kouril et al. (2010)
			Steel with mill scale	15	
	Mortar, admixed Cl		Polarization resistance	>5	Garcia-Alonzo et al. (2007b)
	Pore solution	Sand blasted surface	Potentiostatic: +200 mV SCE	2.8−10.6	Randström et al. (2010)
	Mortar	Admixed	Polarization resistance	>5	Garcia-Alonzo et al. (2007b)
	Ca(OH)$_2$ pH 12.6		Potentiostatic: +200 mV SCE	5−10	Bertolini et al. (1996)
	NaOH pH 13.9			>10	
	Ca(OH)$_2$		Potentiostatic: +200 mV SCE	6.5−10	Bertolini and Gastaldi (2009)
302	Concrete	Admixed	10 years outdoor exposure	3.2	Treadaway et al. (1989)
315	Concrete	Admixed	10 years outdoor exposure	>3.2	Treadaway et al. (1989)

316 316LN	Concrete	Admixed	Potentiostatic: +200 mV SCE	>8	Sørensen et al. (1990)
	Concrete	Admixed	10 years outdoor exposure	>3.2	Treadaway et al. (1989)
	Pore solution		Pickled	>15	Kouril et al. (2010)
			With mill scale	15	
	Mortar	Admixed	Polarization resistance	>5	Garcia-Alonzo et al. (2007b)
	Pore solution	Sand blasted surface	Potentiostatic: +200 mV SCE	5.7−6.8	Randström et al. (2010)
	Ca(OH)$_2$ pH 12.6		Potentiostatic: +200 mV SCE	>10	Bertolini et al., (1996)
	NaOH pH 13.9			>10	
	Ca(OH)$_2$		Potentiostatic: +200 mV SCE	>10	Bertolini and Gastaldi (2009)
	Ca(OH)$_2$	Pickled	Potentiostatic: +200 mV SCE	2.8−11.3	Hurley and Scully (2006)
24100	Mortar	Admixed	Polarization resistance	>5	Garcia-Alonzo et al. (2007b)
2205	Pore solution		Pickled	>15	Kouril et al. (2010)
			With mill scale	>15	
	Concrete	Ponding		3.5	Ji et al. (2005)

Continued

Table 4.3 Continued

Alloy	Environment	Salt application	Exposure or test	CCTL % by wt. cement or solution	References
2304	Pore solution	Sand blasted	Potentiostatic: +200 mV SCE	4.6−10.6	Schönning et al. (2013)
	Pore solution			7.9	Mahmoud et al. (2015)
	Ca(OH)$_2$ pH 12.5		Potentiostatic: +200 mV SCE	>10	Bertolini et al. 1996)
	NaOH pH 13.9			>10	
	Ca(OH)$_2$		Potentiostatic: +200 mV SCE	7.5−8	Bertolini and Gastaldi (2009)
2101	Pore solution pH 12.8−13.3		Potentiostatic: +200 mV SCE	5.7−10.6	Schönning et al. (2013)
	Ca(OH)$_2$		Potentiostatic: +200 mV SCE	3.5−6	Bertolini and Gastaldi (2009)
	Ca(OH)$_2$	Pickled in lab	Potentiostatic: +200 mV SCE	1.1−1.4	Hurley and Scully (2006)
2102	Concrete	Ponding		2.9	Ji et al. (2005)
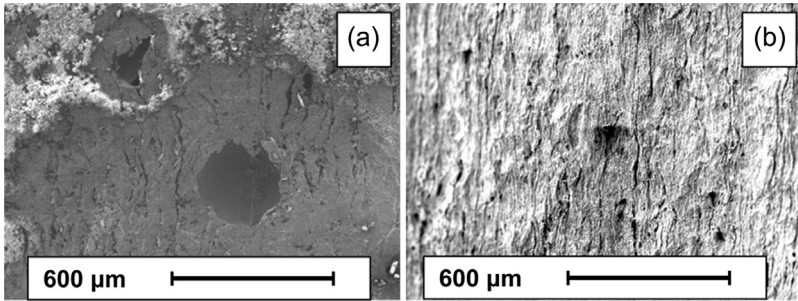
Figure 4.10 SEM micrographs of pits in rebar after polarization in chloride-containing synthetic pore solution. (a) austenitic 304L; (b) duplex 2001. (Alvarez et al., 2011).

Figure 4.11 Corrosion of 316LN along a processing defect: (a) as-received bar; (b) after exposure to pore solution with increasing chloride content up to 16%; and (c) after pickling in inhibited acid (Bandura, 2015).

2. *The ability of the noncorroding areas to act as a cathode* (Presuel-Moreno et al., 2010). Stainless steel has been shown to be less effective than carbon steel as a cathode, due to the exchange of current density for the oxygen reaction ($1/2\,O_2 + H_2 + 2e^- = 4(OH)^-$) being significantly lower on the surface of stainless steel than on carbon steel. One consequence of this is that once the passive film is broken down locally and anodic areas are formed, the pits will grow slowly because the surrounding steel surface is an inefficient cathode. A second consequence is that the galvanic interaction between black steel in chloride-contaminated areas and stainless steel in chloride-free areas is much less severe than if black steel were in both regions (Bertolini et al., 1998; Hope, 2000). Presuel-Moreno et al. (2010) attributed the low post-initiation corrosion rate of stainless rebar to small anodes and poor cathode efficiency.

3. *The composition, solubility and specific volume of the corrosion products*. Particularly in electrochemical impedance spectroscopy studies, specific parameters have been attributed to the characteristics of the corrosion product (Serdar et al., 2013). However, chemical identification of the products has not been specifically confirmed.

4. *The ability of the corrosion products to protect the underlying steel from very rapid corrosion rates*. When corrosion is initiated, the corrosion current density is very high, but it decreases over time. This may be attributed to lack of oxygen for the cathodic half-cell reaction or to the solid corrosion products creating a partial barrier to the transfer of ions. Cui and Sagüés measured corrosion activity at the defect sites in a stainless clad bar and found that corrosion moderated with time, which they attributed to progressively developing corrosion products.

5. *The ability of the corrosion products to block or partially block any pre-existing cracks*. Corrosion of stainless rebar has been observed at the intersection between structural cracks and the embedded rebar when the concrete has been exposed to anti-icing brine containing $21\%\ Cl^-$, one of the brines currently in use in Canada (Van Niejenhuis et al., 2016). Once the passive film has broken down, there is a rapid surge in corrosion current density followed by a slow decline, as illustrated for the austenitic S24100 (XM28) and the duplex S32304 (2304) in Figure 4.12. The curves in these figures represent the average current densities for five replicate specimens, each in sound (uncracked) concrete, in concrete specimens with a loading crack transverse to the bars and in concrete specimens with a loading crack longitudinal to the bar. Autopsying the specimens revealed corrosion *only* at the location of the cracks, and there was indication that the corrosion products were deposited within the crack.

In another study of the influence of loading cracks, Nürnberger (Nürnberger and Beul, 1999; Nürnberger, 2005) did not detect any 'serious corrosion' of 316LN or 2205 in concrete with cracks <1 mm after 2.5 years of outdoor exposure to wetting in salt solution and drying. Small shallow pits were observed along the border of the welding material in welded bars. Also, it was concluded that 'welded bars show distinctly poorer performance than unwelded bars' (Jaffer and Hansson, 2008; Nürnberger, 2005).

4.5.3 Ranking of alloy grades

One of the pressing questions posed by authorities proposing to incorporate stainless rebar in new structures exposed to de-icing salts or marine environments is 'What is the most appropriate grade to use?' Note this is not 'What is the best grade?' As Knudsen et al. (1998) have indicated, the 'best' grades (usually the most expensive) are not required in every situation, and the less expensive grades will be adequate in many cases. The rankings of different grades reported in the literature are given in Table 4.4, where the number 1 indicates the most corrosion resistant.

One factor that has received little attention is how differences in composition within the specified range, and/or processing details, can influence behaviour. For example, bars of S24100 (XM28) from different producers have varied carbon, nickel and molybdenum contents. An earlier batch of this alloy had a carbon content of 0.12% (i.e. less than the specified maximum of 0.15%) and had been coiled after heat treatment for shipping. The combination of fairly high carbon content and inadequate quenching
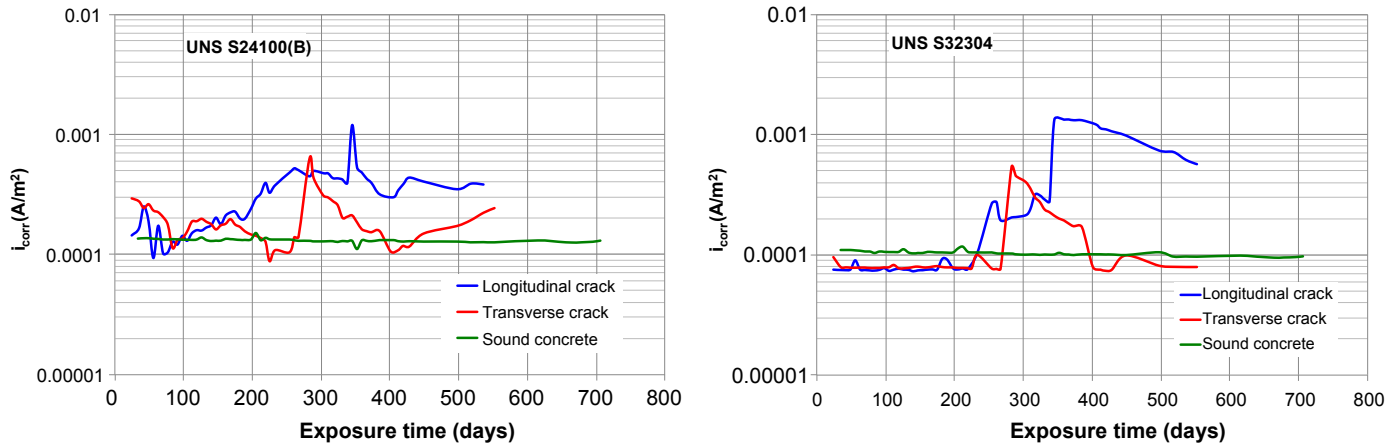
Figure 4.12 Average values of the corrosion current densities of the replicate specimens in sound, transversely cracked and longitudinally cracked concrete as a function of time of exposure to multi-chloride brine (Van Niejenhuis et al., 2016).

Table 4.4 **Ranking of the more common rebar alloys**

Alloy						
2205	316LN	2304	2101	304LN	XM28	References
—	1	2	3	1304 equivalent	—	Bertolini and Gastaldi (2011)
—	1	—	—	2	—	Castro et al. (2003)
—	—	—	—	—	High Mn, low Ni	Elsener et al. (2011)
—	2	3	1	—	—	Randström et al. (2010)
—	3 (316)	1	2	4 (304L)	—	Schönning and Randström (2011)
1 pre-cracked concrete	4 pre-cracked concrete	3 pre-cracked concrete	2 pre-cracked concrete	5 pre-cracked concrete	6 pre-cracked concrete	Van Niejenhuis et al. (2016)
2 as-rolled	1 clad, pickled	3 pickled	4 as-rolled	—	—	Hartt (2009)
1	—	2	—	3	—	Alvarez et al. (2011)
—	1 (316) no corrosion	1 no corrosion	3 (crevice corrosion at seal)	2 (304)	—	Serdar et al. (2013)
1	—	—	2	—	—	Ji et al. (2005)
—	1	—	2	—	—	Scully and Hurley (2007)

Table 4.5 Alloy composition from mill certificates provided by the producers

Steel	C	N	Cr	Ni	Mo	Mn	P	S	Si
24100-A	0.05	0.31	17.2	0.70	0.20	12.12	0.02	0.001	0.50
24100-B	0.04	0.34	18.04	2.28	–	12.31	0.03	0.001	0.44

during coiling resulted in sensitization − i.e. precipitation of chromium carbides at the grain boundaries, leaving the adjacent areas depleted in chromium and subject to reduced corrosion resistance. The producer solved the problem by reducing the carbon and shipping straight bar.

In the project mentioned above (Van Niejenhuis et al., 2016), a comparison was made of the corrosion behaviour of the same rebar grade (S24100) from the two different producers, the compositions of which are given in Table 4.5. The average corrosion rates of five replicate bars of each alloy embedded in sound, transversely cracked and longitudinally cracked concrete are shown in Figure 4.13. The low-nickel alloy bars in the cracked concrete exhibited very high corrosion rates immediately on exposure to the 21% Cl⁻ brine, indicating low corrosion resistance of the air-formed passive film. The corrosion rate decreased over time, which might be attributed to blocking of the crack and stifling of oxygen. A second factor could be the modification of the passive film to that in equilibrium at the high pH level.

4.5.4 Passive film investigations

The Cr_2O_3 oxide is generally considered as the passive film on stainless steels in neutral or acid solutions (Sedriks, 1996). However, the thermodynamically stable pH/potential range of this phase at high pH levels is very limited (Pourbaix, 1974). Instead, the potential/pH equilibrium plots developed by Beverskog and Puigdomenech (1999) indicate that the most likely stable phase at pH ∼ 13 is the spinel Fe_2NiO_4. It is generally agreed that the air-formed passive film existing on the steels when they are embedded in concrete changes over time to achieve equilibrium with the high-alkaline pore solution, and that the new equilibrium passive film is dependent on the pH of the pore solution (Luo et al., 2012; Blanco et al., 2006). A number of researchers have identified the percentages of each individual metal oxide in 304, 316, 2205 and a high-Mn low-Ni grade using X-ray photoelectron spectroscopy (Elsener et al., 2011; Addari et al., 2008; Abreu et al., 2004), energy-dispersive X-ray spectroscopy (Veleva et al., 2002, 2012) and secondary ion mass spectroscopy (Bandura et al., 2014). It is generally agreed that the inner layer of the passive film is chromium-rich, while the outer layer is iron-rich. However, the techniques used did not allow identification of spinels (mixed oxides) such as those identified by X-ray diffraction or Raman spectroscopy (Bergsma and Hansson, 2013). Therefore, it is not possible to calculate a theoretical specific volume of the films.
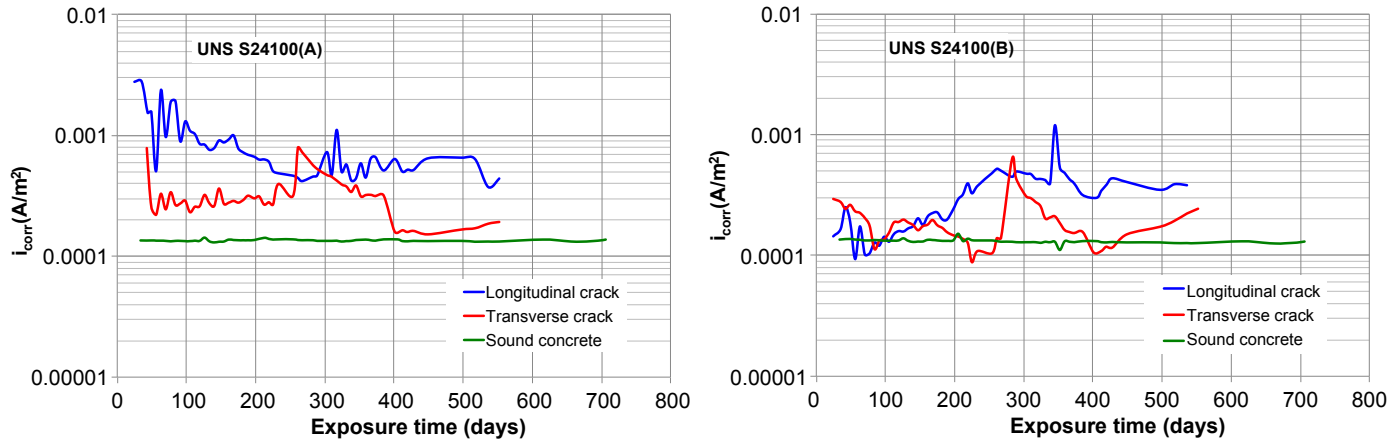
Figure 4.13 Average values of the corrosion current densities of 24100 bars from two different producers in sound, transversely cracked and longitudinally cracked concrete as a function of time of exposure to multi-chloride brine containing 21% Cl⁻ (Van Niejenhuis et al., 2016).

4.6 Conclusions

It is clear that all stainless-steel rebar grades discussed in this chapter, when embedded in sound concrete, would fulfil design service lives, if the processing procedure is controlled to eliminate any defects and prevent sensitization of the steel (Moser et al., 2012; Hansson and Bergsma, 2012).

However, all structural concrete contains cracks, and it is equally clear that in areas subject to heavy salt applications, corrosion can occur at the root of cracks. Consequently, a major goal of designers should be to eliminate or minimize the presence of cracks. This is of course a common goal for concrete structures with any metallic rebar. One major attribute of the high corrosion resistance of stainless steels is that the cover thickness could be reduced, because chloride diffusion through the concrete to the level of the bar in concentrations required to initiate corrosion is highly unlikely over the life of the structure. Reducing the cover would also reduce load-induced cracks and the crack widths of shrinkage cracks. A second possibility is to prestress the concrete, and work is ongoing on the development of high-strength stainless-steel strand for this purpose (Alonso et al., 2008, 2010; Recio et al., 2013; Nürnberger, 2008).

References

Abreu, C.M., Cristóbal, M.J., Losada, R., Nóvoa, X.R., Pena, G., Pérez, M.C., 2004. High frequency impedance spectroscopy study of passive films formed on AISI 316 stainless steel in alkaline medium. Journal of Electroanalytical Chemistry 572, 335−345.

Addari, D., Elsener, B., Rossi, A., 2008. Electrochemistry and surface chemistry of stainless steels in alkaline media simulating concrete pore solutions. Electrochimica Acta 53, 8078−8086.

Alonso, C., Sanchez, M., Mazario, E., Recio, F.J., Mahmoud, H., Hingorani, R., 2010. High strength stainless steel 14301 for prestressed concrete structures protection. In: Castro-Borges, P., Moreno, E.I., Sakai, K., Gjørv, O.E., Banthia, N. (Eds.), Concrete under Severe Conditions. CRC Press, Mérida, Mexico, pp. 1047−1054.

Alonso, M.C., Recio, F.J., Sanchez, M., 2008. High strength stainless steels for prestressed structures in marine environment. In: 1st International Conference on Construction Heritage in Coastal and Marine Environments. Damage, Diagnosis, Maintenance and Rehabilitation. Lisbon, Portugal.

Alvarez, S.M., Bautista, A., Velasco, F., 2011. Corrosion behaviour of corrugated lean duplex stainless steels in simulated concrete pore solutions. Corrosion Science 53, 1748−1755.

Anders, K.A., Bergsma, B.P., Hansson, C.M., 2014. Chloride concentration in the pore solution of Portland cement paste and Portland cement concrete. Cement and Concrete Research 63, 35−37.

ASM, 1990. Metals Handbook − Tenth Edition − Properties and Selection: Irons, Steels, and High-performance Alloys. Materials Park, ASM International.

ASTM, 2010. A955M-10a Standard Specification for Deformed and Plain Stainless Steel Bars for Concrete Reinforcement (Metric). American Society for Testing and Materials, Philadelphia, PA.

Bandura, T.W., 2015. Influence of Exposure to Anti-icing Brines on the Corrosion Resistance of Different Stainless Steel Rebar Grades in Concrete Simulated Pore Solution. M.A.Sc. University of Waterloo.

Bandura, T.W., Van Niejenhuis, C.B., Hansson, C.M., 2014. Evaluation of the Proposed European Rapid Screening Test for Stainless Steel Rebar. Submitted to NACE Corrosion, October 2015.

Barneyback, R., Diamond, S., 1981. Expression and analysis of pore fluids from hardened cement pastes and mortars. Cement and Concrete Research 11, 279.

Bergsma, B.P., Hansson, C.M., 2013. The formation and stability of the passive films formed on the new generation of stainless steel rebar alloys. In: Khan, M. (Ed.), Hope/Schupack Symposium. American Concrete Institute, Dallas TX, pp. 29−43.

Bertolini, L., Bolzoni, F., Pastore, T., Pedeferri, P., 1996. Behaviour of stainless steel in simulated concrete pore solution. British Corrosion Journal 31, 218−222.

Bertolini, L., Gastaldi, M., September 6−9, 2009. Corrosion resistance of austenitic and low-nickel duplex stainless steel bars. In: Eurocorr 2009. Nice, France.

Bertolini, L., Gastaldi, M., 2011. Corrosion resistance of low nickel-stainless steel rebars. Materials and Corrosion 62, 120−129.

Bertolini, L., Gastaldi, M., Pedeferri, M., Pedeferri, P., 1998. Effects of galvanic coupling between carbon steel and stainless steel reinforcement in concrete. In: International Conference on Corrosion and Rehabilitation of Reinforced Concrete Structures. FHWA, Orlando, FL.

Beverskog, B., Puigdomenech, I., 1999. Pourbaix diagrams for the ternary system of iron-chromium-nickel. Corrosion 55, 1077−1087.

Blanco, G., Bautista, A., Takenouti, H., 2006. EIS study of passivation of austenitic and duplex stainless steel reinforcements in simulated pore solution. Cement and Concrete Composites 28, 212−219.

Castro, H., Rodriguez, C., Belzunce, F.J., Canteli, A.F., 2003. Mechanical properties and corrosion behaviour of stainless steel reinforcing bars. Journal of Materials Processing and Technology 134−137, 143−144.

Castro-Borges, P., 2002. Performance of a 60-year old concrete pier with stainless steel reinforcement. Materials Performance 21, 50−55.

Concrete Society, 1998. Guidance on the Use of Stainless Steel Reinforcement. Concrete Society.

CSA, 2006. S6−06: Canadian Highway Bridge Design Code. Canadian Standards Association, Rexdale, Ontario, Canada.

Elsener, B., Addari, D., Coray, S., Rossi, A., 2011. Stainless steel reinforcing bars − reasons for their high pitting resistance. Materials and Corrosion 62, 111−119.

Fajardo, S., Bastidas, D.M., Criado, M., Romero, M., Bastidas, J.M., 2011. Corrosion behaviour of new low-nickel stainless steel in saturated calcium hydroxide solution. Construction and Building Materials 25, 4190−4196.

Garcia-Alonzo, M.C., Escudero, M.L., Miranda, J.M., Vega, M.I., Capilla, F., Correira, M.J., Salta, M., Bennani, A., Gonzalez, J.A., 2007a. Corrosion behaviour of new stainless steel reinforcing bars embedded in concrete. Cement and Concrete Research 37, 1463−1471.

Garcia-Alonzo, M.C., Gonzalez, J.A., Miranda, J.M., Escudero, M.L., Correira, M.J., Salta, M., Bennani, A., 2007b. Corrosion behaviour of innovative stainless steels in mortar. Cement and Concrete Research 37, 1562−1569.

Gastaldi, M., Bertolini, L., 2014. Effect of temperature on the corrosion behaviour of low-nickel duplex stainless steel bars in concrete. Cement and Concrete Research 56, 52−60.

Gastaldi, M., Lollini, F., Bertolini, L., 2014. Performance-based durability design of concrete structures reinforced with stainless steel bars. La Metallurgica Italiana 7−8, 17−21.

Hansson, C.M., Bergsma, B.P., 2012. Corrosion Behaviour of Sensitized and Non-sensitized XM28 (UNS S24100) Stainless Steel Reinforcing Bars. Alberta Transportation, Edmonton, Alberta.

Hartt, W.H., 2009. Comparison of corrosion resistant reinforcement performance from short term aqueous solution and concrete exposures. In: Corrosion 2009. National Association of Corrosion Engineers.

Hope, B.B., 2000. Corrosion Aspects of Stainless Steel Reinforcement in Concrete. Queen's University, Kingston, ON.

Hurley, M.F., Scully, J.R., 2006. Threshold chloride concentrations of selected corrosion-resistant rebar materials compared to carbon steels. Corrosion 62, 892−904.

Islam, M.A., Bergsma, B.P., Hansson, C.M., 2013. The chloride-induced corrosion behaviour of stainless steel and carbon steel reinforcing bars in sound and cracked concrete. Corrosion 69, 303−313.

Jaffer, S.J., Hansson, C.M., 2008. The influence of cracks on chloride-induced corrosion of steel in ordinary Portland cement and high performance concretes subjected to different loading conditions. Corrosion Science 50, 3343−3355.

Ji, J., Darwin, D., Browning, J.P., 2005. Corrosion Resistance of Duplex Stainless Steels and MMFX Microcomposite Steel for Reinfored Concrete Bridge Decks. The University of Kansas Centre for Research.

Knudsen, A., Jensen, F.M., Klinghoffer, O., Skovsgaard, T., 1998. Cost-effective enhancement of durability of concrete structures by intelligent use of stainless steel reinforcement. In: International Conference on Corrosion and Rehabilitation of Reinforced Concrete Structures. FHWA, Orlando, FL.

Knudsen, A., Klinghoffer, O., Skovsgaard, T., 1999. Pier in Progreso, Mexico. Inspection report. Arminox, Denmark.

Kouril, M., Novák, P., Bojko, M., 2010. Threshold chloride concentration for stainless steels activation in concrete pore solutions. Cement and Concrete Research 40, 431−436.

Lollini, F., Carsana, M., Gastaldi, M., Redaelli, E., Bertolini, L., 2015. The challenge of the performance-based approach for the design of reinforced concrete structures in chloride bearing environment. Construction and Building Materials 79, 245−254.

Luo, H., Dong, C.F., Li, X.G., Xiao, K., 2012. The electrochemical behaviour of 2205 duplex stainless steel in alkaline solutions with different pH in the presence of chloride. Electrochimica Acta 64, 211−220.

Macgregor, I.D., 1998. White Precast Stainless Reinforced Formwork: 20 Years on Structures and Buildings, ICE, vol. 128, pp. 211−218.

Mahmoud, H., Sanchez, M., Alonso, M.C., 2015. Ageing of the spontaneous passive state of 2304 duplex stainless steel in high-alkaline conditions with the presence of chloride. Journal of Solid State Electrochemistry 19 (10), 2961−2972.

Marcotte, T.D., 2001. Characterization of Chloride-induced Corrosion Products that Form in Steel-reinforced Cementitious Materials. Ph.D. University of Waterloo.

Mcdonald, D.B., Krauss, P.D., 1998. Corrosion-resistant reinforcing steel: results from 96 Weeks of in-concrete tests. In: Gjorv, O.E., Sakai, K., Banthia, N. (Eds.), Proceedings of the Second International Conference under Severe Conditions CONSEC '98. E & FN Spon, Tromsø, Norway, pp. 382−391.

Mcdonald, D.B., Sherman, M.R., Pfeifer, D.W., Virmani, Y.P., 1995. Stainless steel reinforcing as corrosion protection. Concrete International 65−70.

Mcgurn, J.F., 1998. Stainless steel reinforcing bars in concrete. In: International Conference on Corrosion and Rehabilitation of Reinforced Concrete Structures. FHWA, Orlando, FL.

Moser, R.D., Singh, P.M., Kahn, L.F., Kurtis, K.E., 2012. Chloride-induced corrosion resistance of high-strength stainless steels in simulated alkaline and carbonated concrete pore solutions. Corrosion Science 57, 241−253.

Nürnberger, U. (Ed.), 1996. Stainless Steel in Concrete − State of the Art Report. The Institute of Materials, London, UK.

Nürnberger, U., 2005. Stainless steel reinforcement - a survey. Otto-Graf-Journal 16, 111−138.

Nürnberger, U., 2008. Stainless steel in concrete structure and in the fastening techniques. Materials and Corrosion 59, 144−158.

Nürnberger, U., Beul, W., 1999. Corrosion of stainless steel reinforcement in cracked concrete. Otto-Graf Journal 10.

Pourbaix, M., 1974. Atlas of Electrochemical Equilibria in Aqueous Solutions. National Association of Corrosion Engineers, Paris, France.

Poursaee, A., Hansson, C.M., 2009. Potential pitfalls in assessing chlorid-induced corrosion of steel in concrete. Cement and Concrete Research 39, 391−400.

Presuel-Moreno, F., Scully, J.R., Sharp, S.R., 2010. Literature review of commercially available alloys that have potential as low-cost corrosion resistant concrete reinforcement. Corrosion 66. National Association of Corrosion Engineers.

Randström, S., Almén, M., Petersson, R., Adair, M., 2010. Reproducibility of Critical Chloride Threshold Levels for Stainless Steel Reinforcement. Structural Faults and Repair. Edinburgh, UK.

Recio, F.J., Wu, Y., Alonso, M.C., Nürnerberger, U., 2013. Hydrogen embrittlement risk in cold-drawn stainless steels. Materials Science and Engineering: A 564, 57−64.

Schönning, M., Randström, S., 2011. Adaptation of EN 480-14:2006 as a test method for determining a critical chloride threshold level for stainless steel rebar. Eurocorr. Paper 4903.

Schönning, M., Randström, S., Adair, M., 2013. Chloride tolerance of stainless steel reinforcement using an accelerated in-concrete method. In: Eurocorr 2013. Estoril, Portugal.

Scully, J.R., Hurley, M.F., 2007. Investigation of the Corrosion Propagation Characteristics of New Metallic Reinforcing Bars. Virginia Transportation Research Council.

Sedriks, A.J., 1996. Corrosion of Stainless Steels. John Wiley and Sons, Inc, New York, NY.

Serdar, M., Zulj, L.V., Bjegovic, D., 2013. Long-term corrosion behaviour of stainless reinforcing steel in mortar exposed to chloride environment. Corrosion Science 69, 149−157.

Smith, J.L., Virmani, Y.P., 2000. Materials and Methods for Corrosion Control of Reinforced and Prestressed Concrete Structures in New Construction. Federal Highway Administration.

Sørensen, B., Jensen, P.B., Maahn, E., 1990. The corrosion properties of stainless steel reinforcement. In: Page, C.L., Treadaway, K.W.J., Bamworth, P.B. (Eds.), Corrosion of Reinforcement in Concrete. Elsevier Applied Science, Wishaw, UK, pp. 601−610.

Treadaway, K.W.J., Cox, R.N., Brown, B.L., 1989. Durability of corrosion resisting steels in concrete. Proceedings of the Institution of Civil Engineers, Part 1 86, 305−331.

Tullmin, M., Smith, F.N., Gu, P., 1998. The inclusion of stainless steel rebars into a major highway − the information super highway. In: International Conference on Corrosion and Rehabilitation of Reinforced Concrete Structures. FHWA, Orlando, FL.

Van Niejenhuis, C.B., 2015. The Case for Stainless Steel Reinforcing Bars. M.A.Sc. University of Waterloo, Ontario, Canada.

Van Niejenhuis, C.B., Walbridge, S., Hansson, C.M., 2016. The performance of austenitic and duplex stainless steels in cracked concrete exposed to concentrated chloride brine. Journal of Materials Science 50 (1). http://dx.doi.org/10.1007/s10853-015-9387-0.

Veleva, L., Alpuche-Aviles, M.A., Graves-Brook, M.K., Wipf, D.O., 2002. Comparative cyclic voltammetry and surface analysis of passive films grown on stainless steel 316 in concrete pore model solutions. Journal of Electroanalytical Chemistry 537, 85−93.

Veleva, L., Tsaneva, B., Castro-Borges, P., Burova, M., 2012. Characterization of passive films formed on manganese nickel-free stainless steel exposed to simulated concrete pore environment. International Journal of Electrochemical Science 7, 4121−4132.

Whiting, D., 1981. Rapid Determination of the Chloride Permeability of Concrete. U.S. Federal Highway Administration, Washington DC, USA.

Corrosion of epoxy-coated steel in concrete

5

D.B. McDonald

Epoxy Interest Group of the Concrete Reinforcing Steel Institute, Schaumburg, IL, USA

5.1   Introduction

The highway system in the United States was principally built prior to the widespread use of deicing salts. The concrete structures were constructed using high-permeability concrete, with generally high water−cement ratios and low concrete cover of only 25 mm (1 in.) over the reinforcing steel. In the late 1960s, North America started using deicing salts to reduce vehicle accidents caused by snow and ice.

The introduction of deicing salts and resultant problems was summarized by Clifton et al. (1974) as follows:

"The premature deterioration of concrete bridge decks, in 5−10 years, has become a major problem during the past decade. The annual cost of such repairs on interstate highways has been estimated to be more than $70 M in 1972. Often this deterioration has been attributed to accelerated corrosion…induced by chloride ions from deicing materials. Use of the two most common deicing materials, CaCl and NaCl, has increased substantially since the early 1960s."

The Federal Highway Administration (FHWA) recognized the problem and approached the National Bureau of Standards (now National Institute of Standards and Technology) for assistance. In 1973, Clifton et al. concluded that fusion-bonded epoxy not only provided corrosion protection, but provided suitable robustness for reinforcing steel.

5.2   Use

Epoxy-coated reinforcing steel was first used in a bridge in Pennsylvania in West Conshohocken in 1973 on route I-476. Four spans of this 15-span steel multigirder and plate-structure bridge were constructed with epoxy-coated reinforcing steel. By 1987, at least 41 US state transportation departments were using epoxy-coated reinforcing steel as the corrosion-protection system in their concrete decks. Epoxy-coated reinforcing steel (or rebar) is also known as fusion-bonded epoxy-coated rebar or FBECR.

Over 550,000 tonnes (600,000 tons) of epoxy-coated reinforcing steel is produced every year in the United States and Canada, and according to the 2013 National Bridge Inventory, more than 80,000 of the 600,000 bridge decks in the United States use

epoxy-coated reinforcing steel covering greater than 83 million m^2 (900 million ft^2). Epoxy-coated reinforcing steel is also used in concrete substructures and superstructures, parking garages, and marine structures to protect the steel against corrosion-induced damage. Many of these structures are being designed with design lives of 75−100 years.

In 2004, departments of transportation within the United States were surveyed regarding corrosion-protection methods (Russell, 2004). That study found that over 80% of agencies used epoxy-coated reinforcing steel, and that this was the second most commonly favored method of protecting from corrosion of steel in concrete, closely following the increasing of the clear cover over the reinforcing steel.

Highlighted projects in North America include the Bay Bridge in California, opened in 2013, which is the most expensive bridge ever constructed in North America, Wacker Drive in downtown Chicago, completed in 2014, which has a design life of 100 years, the Dallas High-Five segmental ramps completed in 2004, and the Biloxi Bay Bridge in Mississippi, opened in 2007. Nonbridge structures include the Kona International Airport Air Traffic Control Tower opened in 2011, the award-winning Aqua Building in Chicago, opened in 2010, and the Denver Union Station Redevelopment, completed in 2014.

There are many international projects using epoxy-coated reinforcing steel. Some are outlined below:

Between 1988 and 1996, the 12 km-long Belt Tunnel between Sprogø and Zealand in Denmark was constructed with epoxy-coated reinforcement. In this application, reinforcing bars were prefabricated and coated using a fluidized bed process. The tunnel had a design life of 100 years.

Epoxy-coated reinforcing steel is extensively used in the Middle East to protect concrete structures against reinforcing steel damage in marine and salt-contaminated soils, and a similar amount of coated reinforcing steel to that being used in North America is being manufactured each year in that region. The Ministry of Defense building in Riyadh, Saudi Arabia, completed in 2003, and the Museum of Islamic Art in Doha, opened in 2008, utilize epoxy-coated reinforcing steel in their foundations. Epoxy-coated bar is being used in the Yanbu desalination plant, Saudi Arabia, due to be completed in 2016.

Epoxy-coated reinforcing steel is being used for major structures in India, including the 5.6 km (3.5 mile) Bandra−Worli Sea Link in Mumbai, opened in 2010. Epoxy-coated reinforcing steel is required to be used within 1 km (0.6 mile) of the coast in all bridges in Japan. The US embassy in the Philippines, opened in 2012, used epoxy-coated reinforcing steel.

In China, epoxy-coated reinforcing steel is being used for long-span bridges and to protect high-speed rail systems from stray-current-induced corrosion. For example, the Shijiazhuang−Wuhan passenger railway station in Henan, which is the largest interchange railway station in China, was opened in 2012 and extensively utilized epoxy-coated reinforcing steel.

In the United Kingdom, epoxy-coated reinforcing steel was used on a bridge on the Colwick Loop Road, a test section of the M18, and the Cardiff Peripheral Distribution. Additional projects at that time are reported by Read (Read, 1990). In 1991, the

Schießberg Road Bridge in Leverkusen, Germany was built using epoxy-coated reinforcing steel, and in 1988, a demonstration project was built in Spiez, Switzerland (Zintel et al., 2014).

5.3 Current specifications

Epoxy-coated reinforcing steel was initially used in 1973; however, it was not until 1981 that the first American Society for Testing and Materials (ASTM) specification for epoxy-coated reinforcing steel was introduced. Specifications used in North America include:

ASTM A775/A775M Standard Specification for Epoxy-Coated Steel Reinforcing Bars
ASTM A884/A884M Standard Specification for Epoxy-Coated Steel Wire and Welded Wire Fabric for Reinforcement
ASTM A934/A934M Standard Specification for Epoxy-Coated Prefabricated Steel Reinforcing Bars
ASTM A1078/A1078M Standard Specification for Epoxy-Coated Steel Dowels for Concrete Pavement
Concrete Reinforcing Steel Institute (CRSI) Standard for Epoxy Coating Plant: Straight Bar Lines
CRSI Standard for Epoxy-Coated Steel Reinforcing Bar Fabrication Facilities
ASTM D3963/D3963M Standard Specification for Fabrication and Jobsite Handling of Epoxy-Coated Steel Reinforcing Bars

Several American Association of State Highway and Transportation Officials (AASHTO) specifications were developed but subsequently withdrawn due to the widespread adoption of the ASTM specifications. These included:

AASHTO M 254: Standard Specification for Corrosion-Resistant Coated Dowel Bars
AASHTO M284M/M284 Standard Specification for Epoxy-Coated Reinforcing Bars: Materials and Coating Requirements
AASHTO M 317 Standard Specification for Epoxy-Coated Reinforcing Bars: Handling Requirements for Fabrication and Job Site

Other specifications include:

ISO 14654:1999 Epoxy-coated steel for the reinforcement of concrete (initially BS 7295: 1990)
ISO 14656:1999 Epoxy powder and sealing material for the coating of steel for the reinforcement of concrete
JG 3042-1997 Epoxy resin coated steel bars
JIS G 3112:2010 Steel bars for concrete reinforcement
NACE SP0395-2013 Fusion-Bonded Epoxy Coating of Steel Reinforcing Bars
OPSS 1442 Ontario Provincial Standard Specification for Epoxy Coated Reinforcing Steel in Concrete
SP0395-2013 (formerly RP0395) Fusion-Bonded Epoxy Coating of Steel Reinforcing Bars

In 1990, the German Institute for Building Technology published a guideline for the testing of reinforcing steels with epoxy resin coatings (Bautechnik, 1990), and in 1991,

the Swiss Federal Roads Authority published a guideline for the application of epoxy-coated reinforcing bars (Straßenbau, 1991). In 1992, the Center for Civil Engineering Research and Codes in the Netherlands published a recommendation for epoxy-coated reinforcing steel (Regelgeving, 1992).

5.4 Specification changes

ASTM A775/A775M is the most commonly used specification for epoxy-coated reinforcing steel in concrete, and this specification has undergone significant improvements during the past 30 years based upon ongoing research. Epoxy-coated reinforcing steel was initially used based upon the research and testing procedure developed by Clifton et al., and it was not until 1981 that an ASTM standard was developed.

Damage in coatings permits the passage of electrical current, and may be visible to the corrected and unaided vision, or very small. Small nonvisible damage locations are termed holidays. In 1981, ASTM A775/A775M required a coating thickness of 175 ± 50 μm (7 ± 2 mils) and allowed 6 holidays/m (2 holidays/ft). The specifications did not require patching for visible damage less than 65 mm^2 (0.1 in.^{2}) and permitted 2% damage on the steel surface. The specification also used a 120° bend to evaluate the coating performance and permitted 8 h between blasting and coating. Such criteria are now significantly more stringent.

In 1989, the maximum allowable average number of holidays in ASTM A775/A775M was reduced from 6 to 3/m (from 2 to 1/ft). Also in that year, the concept of anchor profile was introduced. The bar anchor profile is a measurement of the steel surface roughness prior to coating, and is specified to be between 40 and 100 μm (1.5 and 4.0 mils) when measured according to ASTM D4417 Standard Test Methods for Field Measurement of Surface Profile of Blast Cleaned Steel. The 1989 standard required all damage to be patched and permitted no more than 1% total repair area.

Based upon research conducted by Pfeifer et al., it was found that the 1980s specifications may result in low thickness coatings at the top of ribs, and that these may be subject to damage (Pfeifer et al., 1993). After 1993, the ASTM A775/A775M specification was changed from a required coating thickness of 175 ± 50 μm to $175-300$ μm (7 ± 2 mil to $2-12$ mil).

Prior to 1994, coatings would occasionally crack during fabrication. These cracks were required to be patched. In 1994, the severity-of-bending test was increased from a 120° bend within 60 s, to 180° within $15-45$ s. Bending bars to 180° will reveal several items of quality control including surface cleanliness, surface roughness, and coating cure. Passing the test requires all steps in the manufacturing process to be properly controlled. Bending to 180° is significantly more severe than bending to only 120° due to the increase in coating elongation.

In 1991, the cathodic disbondment test was introduced in ASTM A775/A775M along with requirements for outdoor storage of coated bars. The cathodic disbondment tests induce an electrical current to the bars while they are in a sodium chloride solution. This test is commonly used for pipelines, as they are frequently subjected to

cathodic protection; however, correlations between the test results and the performance of reinforcing bars in concrete have not been demonstrated.

In 1995, the ASTM A775/A775M specification reduced the time between blasting and coating application to 3 h, and also before visible oxidation of the steel surface occurred. An optional surface pretreatment was permitted in the 1995 specification; however, this treatment was used routinely only in Canada, and little data show that the chemical washing changed long-term corrosion performance of epoxy-coated reinforcing steel in concrete.

In 2004, the specification was modified to enable thicker permissible coatings for bars greater than 20 mm (3/4 in.), allowing them to be increased from 175 to 405 μm (7−16 mil). This change was introduced largely to assist with manufacturing issues, as it is difficult to maintain coating thicknesses on the larger diameter bars within the 175−300 μm (7−12 mil) range. Prior to adoption of these changes, tests were conducted to show that thicker coatings did not reduce the bond of the bars in concrete.

5.5 Manufacture

ASTM A775/A775M covers bars that are coated prior to fabrication, while ASTM A934/A934M covers bars that are coated after fabrication. The process for bars coated prior to fabrication will be described in detail; however, similar manufacturing methods are used for prefabricated bars.

The critical parts of the manufacturing process are the follows:

Blasting
Heating
Powder application
Quenching
Holiday inspection
Bar handling

Epoxy-coated bar plants may process up to 16 lengths of reinforcing steel at a time, running side by side in a continuous operation. Straight lengths of reinforcing steel, typically 20 m (60 ft) in length, are passed into the blasting machine where the steel surface is cleaned using grit. Coils of reinforcing steel may also be coated, but must first be somewhat straightened.

During the blast cleaning process, mill scale is removed. After blasting, any residual dust is blown from the steel surface to reduce the amount of backside contamination, as coatings applied over this contamination will possess reduced coating bond. It is also required that the surface roughness of the steel is appropriate and that sufficient steel surface area is available on the steel for coating bond.

After cleaning, the surfaces of the bars are heated to around 220 °C (425 °F) using either an electrical induction or a gas-fired heater. The surface temperature of the bars is measured using temperature-indicating crayons, as the surface temperature is a critical parameter in ensuring good coating cross-linking.

Figure 5.1 Epoxy powder being applied to cleaned and heated reinforcing steel.
From Western Coating Inc.

After heating, the bars are passed through a cloud of epoxy powder that has the consistency of fine flour (See Figure 5.1). The powder is ionized and attracted to the surface of the bars by electrostatic forces, evenly coating the reinforcing steel. As the powder heats up from the residual heat of the steel, the coating gels and cross-links. Epoxy coatings are generally made of an epoxy resin (usually bisphenol-A-epoxy resin) and a curing agent (Kahhaleh et al., 1993). The fusion-bonding process using powder coatings applies the coating in a more uniform manner, compared with wet coating systems.

After coating, the epoxy-coated bars are cooled using either water sprays or a water bath (See Figure 5.2). At this time the coating fuses, forming a thermosetting polymer. Quality control checks are typically made at this time using in-line holiday detectors that determine if electrical current can pass to the bar. The existence of too many holidays or damage sites will reduce the long-term performance of the bars in concrete. Bars are also selected for bend testing to ensure coating adhesion and coating flexibility, and coating thicknesses are checked (See Figure 5.3). The bars are then moved from the line and either shipped or fabricated. Prior to shipment, uncoated ends are coated using a two-part epoxy repair material.

Almost all epoxy-coated reinforcing steel in North America is produced under an independent quality control program that reviews manufacturing procedures to ensure that applicator plants have trained staff and are capable of producing quality epoxy-coated steel reinforcing steel in accordance with industry standards and recommendations. Evaluation is generally conducted according to CRSI Standard Practices (Concrete Reinforcing Steel Institute CRSI, 2014a,b,c).

In North America, epoxy-coated bars are generally made using over 97% recycled steel from primarily postconsumer sources (McDonald, 2011). They are coated using environmentally friendly coatings in safe operations. The embodied energy of
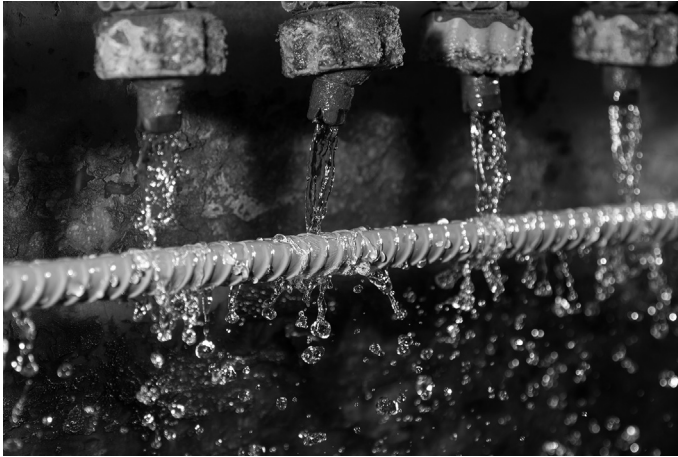
Figure 5.2 Quenching of the epoxy-coated reinforcing steel after powder coating. From Western Coating Inc.

Figure 5.3 Measuring epoxy coating thickness as part of quality control within manufacturing.

epoxy-coated bars during manufacture is lower than that of other corrosion-resistant reinforcing steels, and they are typically made from locally sourced materials available near most major cities.

5.6   Fabrication

ASTM D3963 or the CRSI Standard for Epoxy-Coated Steel Reinforcing Bar Fabrication Facilities may be used as the standard specifications for fabrication of epoxy-coated reinforcing steel. During bending and cutting, all materials in contact

with the epoxy-coated reinforcing steel are required to be padded to minimize coating damage. After bending, epoxy-coated coated reinforcing steel should be evaluated for cracking, and any cracking should be repaired.

Epoxy-coated reinforcing steel should be properly handled and stored to minimize damage. Bundling bands and strapping should be padded, and bars should not be dropped or dragged. Dunnage should be used when storing on ground and when stacking multiple bundles. Bar (mill heat) identification should be maintained during the process, and coated and uncoated reinforcing steel should be stored separately. Epoxy-coated reinforcing steel should also be protected against prolonged UV exposure.

5.7   Field handling

Field handling of epoxy-coated reinforcing steel should be conducted such that damage to the coatings is minimized. Additional information is provided in ASTM D3963 or ACI 301 Specifications for Structural Concrete.

Spreader bars or strong backs with multiple pickup points are recommended to minimize sagging of large bundles. Epoxy-coated reinforcing steel should be lifted using nylon or padded slings, not bare chains or cables. If outdoor storage is to exceed 30 days, the steel should be covered with a suitable material that will also minimize condensation. Coated reinforcing steel should be stored on timber cribbing and not stored directly on the ground. If jobsite bending is required, it should be done only with the permission of the licensed design professional. Bending should be conducted at ambient temperatures.

Epoxy-coated reinforcing steel should be placed on epoxy-coated or composite bar supports and tied using coated tie wire. If cutting is required, bars should be cut using power shears or a chop saw, and flame cutting should be avoided. After cutting, the ends should be coated using a two-part patch material. If bars are to be welded, this should be done only with the permission of the engineer.

Prior to concrete placement, the coated reinforcing steel should be inspected for damage, and any visible coating damage should be repaired using a two-part patch material. This patch material should be approved by the coating manufacturer and used according to the written directions.

The ASTM specifications permit bars to be rejected if any 0.3 m (1 ft) length shows greater than 2% damage or more than 5% patching material. This does not include bar ends.

During concrete placement, a rubber-headed vibrator should be used to consolidate concrete. Epoxy-coated bars should also be protected against damage that may be caused by hose couplers.

5.8   Corrosion research

Substantial research has been published on epoxy-coated reinforcing steel during the past 40 years, and it is not possible to discuss all the various reports. The most widely cited works will be presented below. It should be noted that almost all the laboratory

research includes some form of damage in the coated reinforcing steel, as through-coating damage is recognized as a potential weakness in the epoxy-coated reinforcing steel corrosion system.

Initial research on organic-coated reinforcing steel was conducted on 47 coating materials from 26 different manufacturers (Clifton et al., 1974), which included 15 epoxies. The research found that powder epoxies have better overall properties as barrier coatings than liquid epoxies do. They recommended an electrostatic spray gun method for application and proper curing, and discussed that the "success of epoxy coatings in protection the bars from corrosion will be governed by the application, fabrication and installation processes." They also suggested coating prefabricated bars to reduce coating damage. Many of the initial ASTM specifications were developed based upon tests presented by these researchers, and even prior to completion of this work, the first structures were being built using epoxy-coated reinforcing steel.

In the 1980s, work was conducted at the FHWA (Virmani et al., 1983) using 31 reinforced concrete slabs. Poor-quality concrete and nonspecification reinforcing bars were chosen. The bars were three years old, had greater than 80 holidays/m (25 holidays/ft), up to 0.8% damage, failed the bend test, and readily peeled from the bars. The top layers of bars were cast into concrete that contained 8.8 kg/m^3 (15 lb/yd^3) of chloride ions, which is about 10 times the amount of chloride required to initiate corrosion in uncoated reinforcing steel. Measured corrosion rates were 12−46 times less than uncoated bars cast in similar concrete. The researchers concluded that the electrical resistance of the epoxy-coated reinforcing steel provided substantial corrosion benefit. They also stated for slabs that contained both mats of epoxy-coated reinforcing steel that "macro-cathode polarization occurs due to the inability of the small cathodic areas to reduce sufficient oxygen, further minimizing the corrosion rate at bare areas in the salty concrete." Research conducted at that time by the same authors found that galvanized bars would provide inadequate protection (Clear et al., 1981).

In 1986, significant corrosion-induced spalling of concrete piers in bridges in the Florida Keys occurred just six years after construction (Powers, 1987). This corrosion occurred 0.6−2.4 m (2−8 ft) above the mean high-water mark (splash zone) on the substructures. Poor-quality concrete had been used, and several of the structures contained high initial salt content. Further, while 75 mm (3 in.) of concrete cover was specified, cover as low as 25 mm (1 in.) was found. Other significant problems with construction and design of the project were also reported (Bradley and Nohlgren, 1985).

Based upon private discussions with the manufacturers of the bars used in these particular bridges in Florida by the author of this chapter, it was determined that not only were construction and concrete materials poor, but also the manufacture of the coated bars was problematic, in that the industry did not understand the effects of coating chloride-contaminated bars or the effect of UV damage on bar performance. The bars used in the structure were not manufactured in a way that represents acceptable practice.

In 1980, the Oregon Department of Transportation (DOT) constructed several reinforcement concrete beams and lashed them to an existing bridge substructure in the

tidal zone of Yaquina Bay in Oregon. Nine years later, one of the piles was autopsied (Riemenschneider, 1989). Two of the longitudinal bars had light corrosion and disbondment; however, two of the bars did not show signs of distress and the coating was well adhered, even with chloride levels in excess of 11.9 kg/m^3 (22 lb/yd^3) (See Figure 5.4). The good-performing bars had a coating thickness of 225−300 μm (9−12 mils), compared with 100−150 μm (4−6 mils) for the distressed bars. Bars with the thin coating also showed inadequate blast cleaning and evidence that the bars had been salt contaminated prior to coating. This evaluation showed that poorly coated bars with low coating thicknesses would be susceptible to corrosion.

In 1992, results from a seven-year exposure site program conducted in Saudi Arabia were published (Rasheeduzzafar et al., 1992). The bars were cast in prismatic concrete specimens with admixed chloride. The uncoated bars suffered severe corrosion-related damage at 2.5 kg/m^3, while no corrosion or cracking for epoxy-coated reinforcing steel was observed with 2.5 and 5 kg/m^3 (4.2 and 8.5 lb/yd^3) of admixed chloride. The tests also concluded that while galvanized reinforcing bars reduced the onset of cracking, severe corrosion occurred in concrete containing 5 kg/m^3 (8.5 lb/yd^3) of admixed chloride.

In 1993, a research was presented that evaluated bent and straight epoxy-coated reinforcing bars from seven different suppliers (Pfeifer et al., 1993). After two years of laboratory evaluations, bars from two sources remained passive, while many bars from other sources started to corrode. This research concluded that the performance of epoxy-coated reinforcing steel was strongly dependent on the manufacturing processes, specifically holidays, and that plant quality had a significant effect. The research found that bars with holidays less than 3−7/meter (1−2.3/ft) performed well. The research also highlighted the need to repair visible damage to bars in order to improve performance. Research conducted in this study led to substantial changes in the ASTM specifications and the development of the CRSI Epoxy Plant Certification program.

In 1994, results from tests using precracked concrete specimens in a marine environment in Japan were reported (Sakai and Shinichi, 1994). After five years of exposure, the authors found that "…when epoxy-coated reinforcing bars were used,
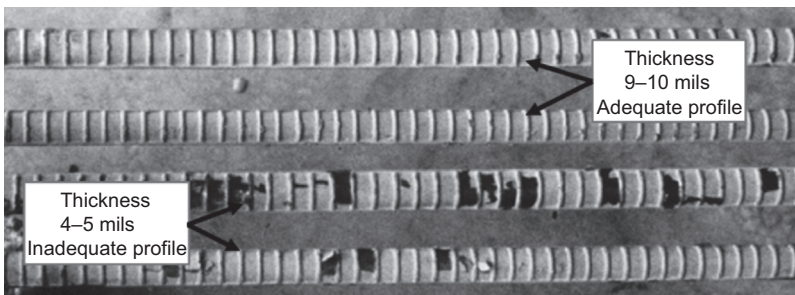

Figure 5.4 Bars extracted from concrete beams Yaquina Bay, Oregon. The top bars with suitable coating thickness show minimal corrosion, compared with the bottom bars that have poor coating thickness.

almost no corrosion or longitudinal cracks were found." After 10 years of exposure, there was evidence of corrosion in some epoxy-coated bars that the authors attributed to: "…inadequate hardening of the coating, bluing of the reinforcing bar, and partial lack of coating thickness, all of which reflected inadequate manufacturing technology for epoxy-coated reinforcing bars at the early stages of that industry in Japan."

In 1995, a study was conducted to evaluate the effects of steel anchor pattern and surface contaminations on the performance of epoxy-coated bars (Walzak, 1995). This work showed that both of these factors have a significant role in adhesion loss, and this study suggested use of an adhesion promoter. Changes were made to the ASTM specifications to address these concerns.

In 1996, a report was presented on epoxy-coated bars, summarizing findings of the Ministry of Transportation in Ontario (MTO) (Manning, 1996). Epoxy-coated reinforcing steel had been used by this agency in the top mat of bridge decks and in barrier walls in 1979, and by 1981, it was also specified for areas of substructure components exposed to deicing salts. Their studies found that the bars in 19 field structures evaluated had higher-than-allowed holidays, with a median of 20/m (8/ft). Underfilm contamination (backside contamination) ranged from 10% to 70%, with a median of 25%, and poor adhesion was observed.

The early specifications in Ontario permitted damage up to 2% of the surface area without touchup, unless the damage was greater than 25 mm^2 (1 in.^{2}). Based upon the poor performance of epoxy-coated reinforcing steel in barrier walls with poor concrete, and concerns about long-term adhesion, MTO changed its specifications to require covering of bars if they were stored for more than 30 days, rejection of bars with more than 1% surface area damage, repair of all coating damage, and the use of plastic-coated vibrators for consolidation of the concrete. The report also discussed that the performance of structures with epoxy-coated bars only in the upper mat would not perform as well as structures that contained epoxy-coated bars in both the upper and the lower mats.

In 1997, a report was published on the performance of epoxy-coated reinforcing bars in bridge decks and piles in Virginia (Weyers et al., 1997). Three bridge decks with an age of approximately 17 years and containing epoxy-coated bars in the top mat were selected, and samples were taken from areas in the lowest 12% of cover. Two of the bridges exhibited sections with carbonation depths of over 50 mm (2 in.), and one bridge exhibited bars with average coating thicknesses less than 125 μm (5 mil), indicative of poor concrete and coating quality. All three bars exhibited continuous holidays in most of the bar samples, and the highest adhesion loss correlated with the highest concrete moisture content. Three piles in brackish water were also selected. These piles contained 6.5 mm (0.25 in.) smooth tie bars, and cores were removed from within the tidal zone. Two of the samples exhibited incomplete coating, and one coating sample was blue. This coating has not been found in any other test reports within North America. These field studies concluded that disbondment of coatings occurs faster in poor-quality concrete, and may occur prior to the arrival of chloride.

In 1998, results from a five-year study on corrosion-resistant reinforcing steel was reported (McDonald et al., 1998). This work conducted extensive screening on 33 organic coatings, 14 ceramic, metallic, or inorganic clad bars, and 10 solid metallic

bars. After this screening process, 12 different bar types were selected for 96 weeks of in-concrete testing. The research supported continued use of epoxy-coated reinforcing steel and indicated that corrosion rates in all cases were less than those of uncoated bars. The data showed that substantially different corrosion performance of the epoxy-coated reinforcing steel was found when cathodic bars on the bottom mat were coated, compared with the use of uncoated bars in that location. When an uncoated bottom mat was used, the measured corrosion was less than 30% that of uncoated bars, while when a coated bottom mat was used, the corrosion rate for the coated bars was less than 2% that of the uncoated bars. Many of the earliest uses of epoxy-coated reinforcing steel in decks only used epoxy-coated bars on the top mat of the concrete decks, and the performance of the deck may be expected to be substantially less than it would be if two mats of epoxy-coated bars were utilized.

The research also concluded that "for the straight epoxy-coated bars tested in uncracked concrete with an epoxy-coated bottom mat, the macrocell currents were almost as low as that obtained for the stainless steel bars…" The research also determined that "the corrosion mechanism for epoxy-coated bars may be the inhibition of the cathodic reaction that requires electrons, oxygen and water to be present at the cathode surface." The research also recommended that bars be used in both top and bottom mats in decks.

The tests by McDonald et al. also evaluated galvanized bars, where it was found that the corrosion rates of these bars may substantially increase after bending, and that the corrosion rates of galvanized bars in uncracked concrete with a galvanized cathode were nine times greater than those of epoxy-coated bars with an epoxy-coated cathode.

In 1998, the performance of epoxy-coated reinforcing steel was evaluated in concrete with and without calcium nitrite (Berke and Hicks, 1998). These tests utilized bars with 3% damage, and tests were conducted over a period of either five or seven years. The tests found that the epoxy-coated reinforcing steel performed significantly better than uncoated bars, and those improvements occurred with the use of both epoxy-coated steel and calcium nitrite.

In 1998, results of tests conducted on epoxy-coated bars that were initiated in 1990 at the University of New Brunswick were reported (Kondratova et al., 1998). These tests included epoxy and black reinforcing steel in either cracked or uncracked concrete. The research evaluated the performance of bars with corrosion inhibitors. Field tests were conducted in a natural marine exposure site at Treat Island, Maine. Epoxy-coated bars were found to outperform black bars in uncracked and precracked concrete specimens in the accelerated testing chamber and at the natural marine exposure site, and the epoxy-coated bars outperformed black bars in the service tunnel/sidewalk. Combined use of epoxy-coated bars and corrosion inhibitors was found to provide the best corrosion protection in 0.6 w/c ratio concrete. It was also concluded that use of epoxy-coated reinforcement extends the service life of a structure by a factor of 8−10, and that the best corrosion protection for cracked specimens was achieved by using high-performance concrete plus epoxy-coated reinforcement.

In 1998, a paper presented data on the performance of black, galvanized, and epoxy-coated reinforcing bars that were subjected to stress (Swamy et al., 1988).

During 24 months of evaluation, the uncoated bars showed extensive corrosion, while the epoxy-coated reinforcing bars remained unaffected and retained all their original properties, even with low concrete cover. With a coating thickness of 200 µm (8 mil), the epoxy coating protected the substrate well against chloride attack and corrosion. The research also found that the corrosion rates of the epoxy-coated reinforcing steel were far less than that of galvanized reinforcing steel.

In 1999, research was conducted for the New York State and Pennsylvania DOTs (Sohanghpurwala and Scannell, 1999). A statistically based sampling plan was used for the 40 spans evaluated in New York and the 40 spans evaluated in Pennsylvania. From a total of 240 cores, 473 coated reinforcing bars were extracted in which:

86% (409) showed no evidence of corrosion;
13% (62) had a number of small, countable corrosion spots; and
0.4% (2), both in New York, exhibited significant visible corrosion.

Corrosion products were observed under the coating on approximately 7% of the bars tested. However, in most cases, corrosion products found under the coating were not the result of ongoing corrosion. The existing condition of epoxy-coated reinforcing bars was found to be very good from a corrosion point of view.

Coating adhesion reduction or loss was found to be more prevalent and extensive. It was found that:

47% of the bars tested had no reduction in adhesion;
40% had varying degrees of adhesion reduction;
greater than 13% exhibited a complete loss of adhesion.

The researchers concluded that although progressive corrosion must be accompanied by complete adhesion loss, coating adhesion alone was not a good predictor of corrosion condition in this study.

In 2000, a report was prepared on the Perley Bridge that spans the Ottawa River in Canada (Covino et al., 2000). Of the 34 spans, only span 17 contained epoxy-coated reinforcing steel.

In 1998, it was found that the two lanes (eastbound and westbound) had experienced vastly different corrosion behavior, although both contained epoxy-coated steel of apparently equal quality. It was found that the southbound span had half the cover of the northbound span, and that the northbound span required about 30% of its surface to be repaired. Specifications used for construction in 1979 permitted 2% of bare steel area. The coatings were also found to be electrically porous, indicative of poor coating materials or application processes.

In 2000, the performance of 18 bridges built between 1977 and 1983 in Virginia with epoxy-coated reinforcing steel was reported (Pyc et al., 2000). The visual condition of all decks was good, with no spalling and very little cracking. Four bridges contained a red-brown coating that was discontinued early in the history of epoxy-coated reinforcing steel. Two bridges revealed bars with large numbers of holidays, approximately 10−12 times that permissible by specifications. The research found a wide range of adhesion values, and in general, truss bars had significantly lower adhesion ratings than top bars. There did not appear to be a correlation between the age of

the decks and the adhesion ratings. Generally, the straight bars had damage of approximately 0.1%, while the truss bars had more damage of approximately 1.5%. One bridge evaluated as part of the study had coating thicknesses less than 65 μm (2.5 mil). The authors presented the theory that if coatings were debonded prior to the arrival of chloride ions, corrosion underneath the coating would develop rapidly. They suggested that a laboratory study be conducted to monitor the development and progress of chloride-induced corrosion.

In 2000, a report on the impact of deck cracking on durability was presented (Fanous et al., 2000). For each of the 81 bridges in Iowa, two core samples were obtained from uncracked concrete, and two cores were obtained from cracked concrete. Forty-one of the bridges had epoxy-coated reinforcing bars only in the top mat, while the remaining 40 bridges had epoxy coatings in both the top and the bottom mats. Statistical studies found that the age, geographic location, type of structure (concrete or steel), and average daily traffic volume have the most significant impact on the deck condition rating, and it was found that a large number of core samples had chloride concentrations greater than the corrosion threshold at the bar depth. It was concluded that a corrosive threshold range from 2.1 to 4.4 kg/m^3 (3.6−7.5 lb/yd^3) may be used to estimate the service life of a bridge deck. Coating adhesion was found to decrease as time increases, and moisture and high chloride concentration were among the factors that can weaken the coating adhesion. Using obtained field data, it was determined that a deck using epoxy-coated reinforcing steel will exhibit spalling after 65 years, compared with 20.5 years for decks with uncoated reinforcing steel.

In 2006, a report critical of the performance of epoxy-coated reinforcing steel was presented (Weyers et al., 2006). A deterioration mechanism for epoxy-coated reinforcing steel was proposed, whereby concrete pore water solution penetrates the coating and debonds the epoxy coating at weak adhesion areas, and the pH of the solution under the coating at that point is about 12. Chlorides arrive and initiate the corrosion process under the coating; the pH decreases to 5 as corrosion proceeds. The authors of this report believed that the epoxy coating on reinforcing steel debonds from the steel surface in as little as four years in bridge decks, long before chlorides arrive at the depth of the reinforcement. Field observations found that the number of holidays of in-place epoxy-coated reinforcing steel appeared to be excessive. The researchers concluded that observed microcracking in the surface of epoxy-coated reinforcing steel coatings is related to the epoxy coating moisture content after long-term exposure in concrete and a measurable change in glass transition temperature under testing, which indicates incomplete curing. The data presented by these researchers did not show that the electrical properties of the coating were affected, nor that the cracking did not penetrate the coating.

In 2006, a statistical analysis of data from 17,000 structures for the New York State DOT was presented (Agrawal et al., 2006). This research found that structural decks with epoxy-coated reinforcement perform significantly better than those with uncoated reinforcement, especially in later years.

In 2007, a field evaluation of four bridges in Georgia and North Carolina found no concrete distress induced by corrosion of epoxy-coated bars (Cui et al., 2007). In that study, it was found that coating adhesion was a poor indicator of bar performance,

even though most bars examined from these bridges had greater coating damage and lower coating thickness than admissible by current specifications governing the manufacture of epoxy-coated reinforcing steel. No epoxy-coated steel bar corrosion-induced distress in well-consolidated concrete was observed, and the epoxy-coated reinforcing steel was found to have resisted up to 0.079 wt% chloride even though it had thin, substandard coating thickness, often less than 125 μm (5 mils). Corrosion of epoxy-coated steel bars was observed on one epoxy-coated steel bar from the tidal zone that had significant coating damage (5%) and was exposed to a very high chloride concentration (0.251 wt%). Coating adhesion is not a good indicator of epoxy-coated steel bar performance. Many coatings had lost adhesion completely. However, bars with no coating damage were consistently in a corrosion-free condition despite the presence of high chloride concentrations that were well above the threshold for uncoated bars.

In 2008, an in-concrete research program was reported using coatings that had been deliberately debonded from the steel substrate (Lee, 2008). Test variables include artificial defect size, defect density, coating disbondment, clear cover, concrete quality, and bar type of the bottom mat. It was concluded that the corrosion performance of epoxy-coated reinforcing steel was mainly influenced by the number of defects and the bar type in the top and bottom mats. Coating disbondment did not create a noticeable negative impact on the corrosion performance of defective epoxy-coated reinforcing steels. In addition, electrochemical impedance spectroscopy data analysis using an equivalent circuit modeling technique confirmed that coating disbondment did not mean losing the epoxy coating's barrier function against steel corrosion inside concrete.

In 2008, studies were reported on four bridges containing epoxy-coated reinforcing bars built in Minnesota (Pincheira et al., 2008). The bridge decks were found to be in generally good condition, with few delaminated areas and only modest corrosion. While the researchers found no sign of increased corrosion activity in coated bars in the bridge with a lower mat of uncoated bars, rust stains on the bottom of the deck suggested corrosion activity in these bars. Minnesota DOT continues to use epoxy-coated bars in both mats for decks.

In 2009, the results of field evaluations of epoxy-coated reinforcing steel conducted during 2009 in West Virginia were reported (Lawler and Krauss, 2010). Alternate bridges on I-79 near Charleston had been constructed using either coated or uncoated reinforcing steel between 1974 and 1976. In 2009, all bridges using uncoated bars had been overlaid after only 17 years of use due to observed distress, and none of the bridges using epoxy-coated bars had been repaired. The field work evaluated six decks that were 34−36 years old. None of these decks exhibited corrosion-induced distress, even at cracked locations.

As part of the studies, Bridge No. 2930, which carries an arterial road in Clarksburg, WV, was specifically chosen for analysis, as deterioration of this deck containing epoxy-coated reinforcing steel had been reported by the West Virginia DOT. During the survey, it was found that most of the deck contained epoxy-coated bars; however, several spans contained uncoated bars. No distress was observed in the deck area containing epoxy-coated reinforcing steel; however, extensive distress was observed in the areas containing uncoated steel (See Figure 5.5).
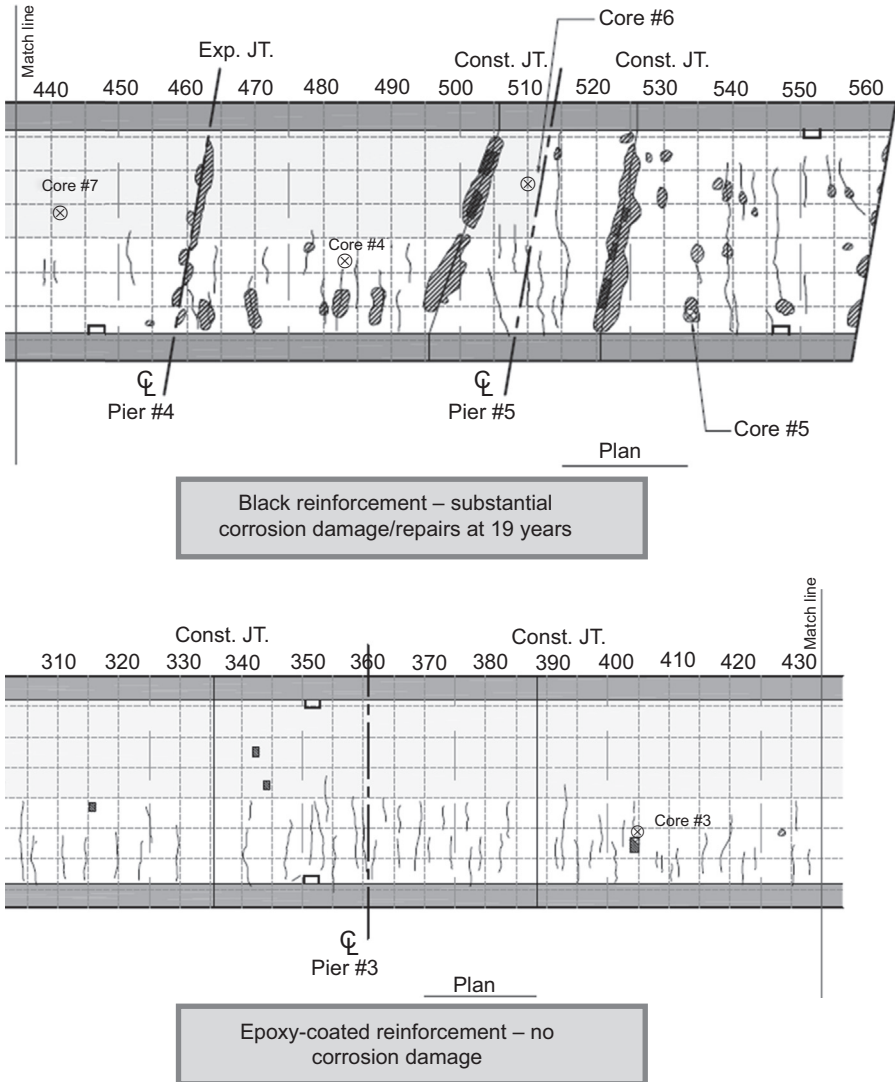
Figure 5.5 Deterioration maps of West Virginia Bridge 2930 after 34 years of service. This structure contains both uncoated and epoxy-coated bars. Top: Delamination and cracking in the bridge section containing the uncoated bars. Bottom: No delamination or cracking in the bride section containing epoxy-coated reinforcing steel.

In these field studies, the distribution of chloride values for epoxy-coated reinforcing steel segments was evaluated (Lawler and Krauss, 2010). For the coated bars, 22 epoxy-coated reinforcing steel segments without active corrosion had a chloride concentration of greater than 0.035% by weight of concrete. The chloride concentrations at the four actively corroding epoxy-coated reinforcing steel segments were

greater than 0.13% by weight of concrete, or about four times the black bar threshold. Furthermore, five other epoxy-coated reinforcing steel segments exposed to chloride concentrations greater than 0.13% by weight of concrete were not actively corroding, with the greatest at 0.263% by weight of concrete.

In 2010, the poor performance of bridge construction joints on I-81 that were reinforced with epoxy-coated reinforcing steel was reported (Sprinkel et al., 2010). Examination found corrosion on the fractured epoxy-coated reinforcing steel. Later examination found that the joints had vertical faces that did not provide any means for shear transfer across the joint, and that the joints were located under a wheel load path. This created atypical conditions where shear forces across the joint due to wheel loads were carried only by the reinforcing steel, and the stress range in the reinforcing steel was greatly magnified under this scenario, thereby making fatigue a possibility (Rivera et al., 2014). Failure of this joint is now believed to be related to unusual fatigue stresses that were later subjected to corrosion, rather than to a corrosion problem with the epoxy-coated reinforcing steel.

In 2010, statistical analyses of existing bridges in Michigan were conducted (Boatman, 2010). The analyses considered data from 1790 bridges, with 766 containing epoxy-coated reinforcing steel and 1024 containing uncoated reinforcing. The data showed that epoxy-coated bars are providing better performance than standard bridge decks containing uncoated reinforcing steel. The data indicated that the service life of bridge decks with uncoated bars is estimated to be 35 years, while the service life of a bridge deck containing epoxy-coated reinforcing steel is estimated to be approximately 70 years.

In 2010, a paper was published on the performance of the nearly 300 structures containing epoxy-coated bars in Florida (Sagüés et al., 2009). The work grouped the performance of the structures into three main groups. Only five were considered to be undergoing significant early-age distress, and only 4% showed distress after 30 years of service. The majority of bridges (290) were predicted to provide 100-year design lives with minimal damage (See Figure 5.6).

In 2011, results from a laboratory study of 12 different reinforcing bar types was presented (Lee, 2011). Bars were placed into large concrete specimens with various levels of damage ranging from 0.15% to 1.0%. Slabs were subjected to wetting and drying using a 15% NaCl solution. Results were presented that separated bars into four groups of performance ranging from poor, which included the uncoated black bars, to excellent, which included stainless steels and epoxy-coated bars. It was stated "It was reconfirmed that epoxy-coated bar… placed in both mats yielded excellent corrosion resistance similar to stainless steel bars." The performance of galvanized bars was regarded as less than that of epoxy-coated bars.

In 2011, the performance of various bar systems in of cracked and uncracked specimens was evaluated (O'Reilly et al., 2011). Specimens included epoxy-coated reinforcing steel and specimens with corrosion inhibitors. The research used southern exposure specimens, similar to those used by McDonald et al. (1998) (See Figure 5.7). The research found that conventional reinforcement exhibits the highest corrosion rates among all systems studied, and that epoxy coatings significantly reduce corrosion rates compared with conventional reinforcement. Corrosion inhibitors, in conjunction
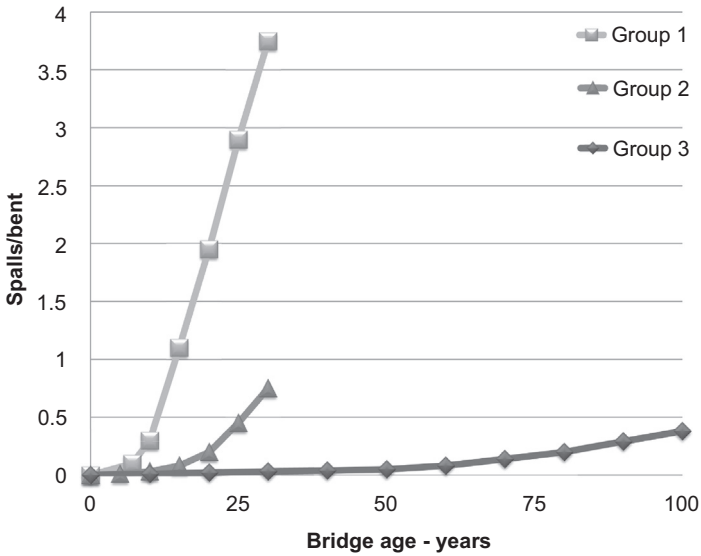
Figure 5.6 Predicted and measured spalls in Florida Bridges containing epoxy-coated reinforcing steel showing that the majority of these are predicted to perform for 100 years (after Sagüés et al., 2009). Group 1 consists of five bridges, Group 2 consists of four bridges and Group 3 consists of 290 bridges.
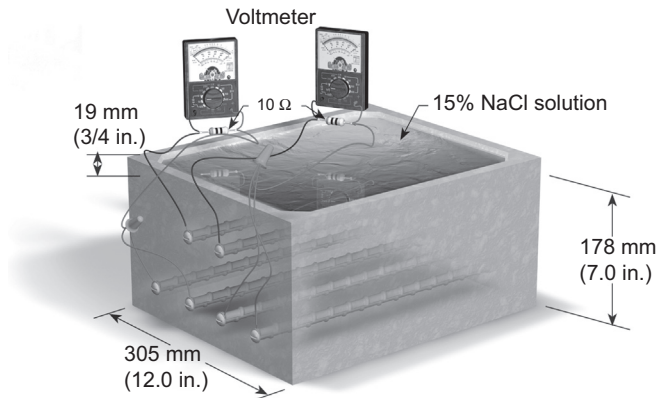

Figure 5.7 Southern exposure concrete specimens used to evaluate corrosion-resistant reinforcing bar systems.

with both epoxy-coated reinforcing steel and conventional reinforcement, reduce corrosion rates in uncracked concrete; however, corrosion inhibitors are significantly less effective in cracked concrete. For bare conventional steel reinforcing bars, the corrosion losses required to crack concrete are directly proportional to the clear concrete cover. For isolated regions of corrosion, such as occurs at damage sites on epoxy-coated reinforcing steel, the relationship changes to one that is directly

proportional to the square of the concrete cover as the exposed region on the bar decreases. An equation was developed to predict the corrosion losses required to crack concrete for both bare reinforcement and damaged epoxy-coated reinforcement.

Results of critical threshold coefficients for uncoated and epoxy-coated bars were presented. For the uncoated bars, a threshold of 0.93 kg/m^3 (1.58 lb/yd^3) was identified, compared with 4.3 kg/m^3 (7.28 lb/yd^3) for epoxy-coated reinforcing. This increase in threshold, based upon a large number of test samples, was attributed as follows: "The values for epoxy-coated reinforcing steel are significantly greater than that of conventional reinforcement. To initiate corrosion on a coated bar, the chloride threshold must be reached at a damage site, as opposed to uncoated bars, which initiate corrosion once the chloride threshold is reached anywhere on the bar surface. This results in an increase in average chloride content at the depth of the reinforcement for coated bars at corrosion initiation."

In 2012, results from deterministic and stochastic deterioration modeling was presented for existing bridges in Nebraska (Hatami and Morcous, 2012). Visual inspection data between 1998 and 2010 were collected from 1688 bridges that contained either uncoated or epoxy-coated reinforcing steel. They considered the impact of various parameters, and found that the service life of bridge decks with uncoated reinforcing steel and epoxy-coated reinforcing steel at fair condition (condition 5) are approximately 40 and 68 years, respectively (See Figure 5.8). If a distress rating of 4 is permitted, then the service lives increase to approximately 60 and 90 years, respectively. The bridge data analysis demonstrates that the use of epoxy-coated reinforcing steel will significantly extend the service lives of structures with epoxy-coated reinforcing steel.

In 2014, Zintel reported on solution tests using various chloride/hydroxide ratios and epoxy-coated reinforcing steel (Zintel et al., 2014). The research found that as the damage size decreased, the amount of chloride required to cause corrosion increased. When damage was 50 mm^2 (0.078 in.^{2}), the chloride threshold was at least 1.5 times greater than that for uncoated steel; however, if the damage was lower than 3.5 mm^2 (0.005 in.^{2}), the threshold increased to a critical Cl-/OH ratio two to three times greater than that of uncoated reinforcing steel.
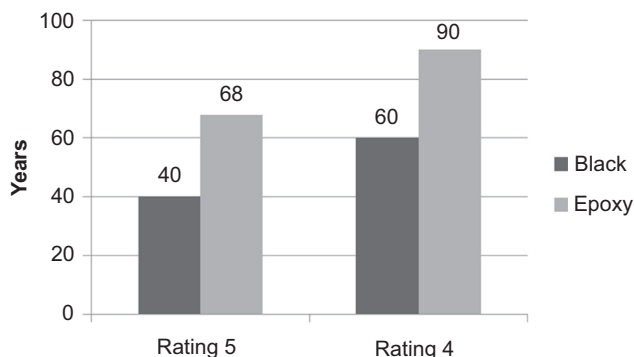

Figure 5.8 Predicted design lives obtained from modeling of Nebraska bridges. After Hatami and Morcous (2012).

In 2014, results from corrosion tests conducted on several types of reinforcing steel were reported (Sim, 2014). Prior to testing, the epoxy-coated bars were subjected to damage created by dropping a steel channel from a constant height using a load guillotine. The epoxy-coated reinforcing steel showed significantly lower visual corrosion in the cracked concrete specimens than that for the uncoated bars. The amount of corrosion was approximately 2.5% that of the amount observed in the uncoated bars. These bars also exhibited measured corrosion currents 95 times less than those of uncoated bars. The performance of the epoxy-coated reinforcing steel compared favorably with some stainless steels.

5.9 Changes in agency specification of epoxy-coated reinforcing steel

Several agencies in North America have recommended not using epoxy-coated reinforcing steel in their structures as discussed below.

The Florida DOT determined in the early 1990s that they would discontinue use of epoxy-coated reinforcing steel in their substructures based upon poor performance of structures containing epoxy-coated bars in the Florida Keys. It was stated that "Corrosion was determined to be resulting from the presence of coating production imperfections (within allowable limits at the time of construction) then aggravated by fabrication, handling, and a severe construction yard environment which promoted coating-metal disbondment (Lau et al., 2007)." As discussed earlier in this report, the coating technology used for these structures is no longer considered suitable practice. More recent field data have shown long lives for most of the structures containing epoxy-coated reinforcing steel in Florida (Sagüés et al., 2010). This agency has recently permitted the use of ASTM A1035 dual-coated reinforcing steel, which uses an epoxy coating over a zinc layer.

In 1998, the MTO placed a moratorium on the use of epoxy-coated reinforcing steel for its transportation structures, as deck corrosion is minimized by this agency through the use of waterproofing and a concrete cover of 70 ± 20 mm (2.75 ± 0.8 in.) (Pianca et al., 2005). Examples of poor performance are discussed earlier in this report, such as the Perley Bridge, where poor electrical properties of the coatings were found. In 2013, construction on the Province of Ontario−owned 65-km (40 mile) Highway 407 East extension was initiated, and this project utilizes epoxy-coated reinforcing steel in the bridges.

In 2010, the Virginia DOT moved to replace epoxy-coated reinforcing steel with alloyed reinforcing bar products, classifying three levels of protection with a required design life of 75 years. Classes 2 and 3 require the use of stainless steel reinforcing bars. Further, in 2002 it was reported that: "Less than 25% of all Virginia bridge decks built under specifications in place since 1981 is projected to corrode sufficiently to require rehabilitation within 100 years, regardless of bar type" and these structures fall under Class 1 (Brown, 2002).

The Virginia DOT reported poor performance of bridge construction joints on I-81 that were reinforced with epoxy-coated reinforcing steel (Sprinkel et al., 2010). Later

examination found that the joints in the I-81 deck had vertical joint faces that did not provide any means for shear transfer across the joint, and that the joints were located under a wheel load path (Rivera et al., 2014). This created atypical conditions where shear forces across the joint due to wheel loads were carried only by the reinforcing steel, and the stress range in the reinforcing steel was greatly magnified under this scenario, thereby making fatigue a possibility.

Despite these three agencies choosing not to specify epoxy-coated reinforcing steel, most other agencies continue to specify epoxy-coated reinforcing steel in 2014. These include basically all agencies throughout the Midwest and Northeast United States, and agencies in Texas and California.

5.10   Summary

Epoxy-coated reinforcing steel has been used for over 40 years and is the most commonly used corrosion-resistant reinforcement used in concrete. The first concrete deck was built in 1973, and currently over 550,000 tonnes (600,000 tons) of epoxy-coated reinforcing steel is produced every year in North America. There are also many international manufacturers and projects using epoxy-coated reinforcing steel.

The most commonly used specification is ASTM A775/A775M, and based upon field and laboratory findings, this specification has undergone significant improvements during the past 30 years, Revisions of coating thickness, bendability, and steel surface preparation have been made. The performance of epoxy-coated reinforcing steel is strongly dependent on the manufacturing processes, and plant quality has a significant effect. Independent certification programs, introduced in the 1990s, dramatically changed the quality of coated reinforcing steel.

Like any construction material, epoxy-coated reinforcing steel should be handled and stored appropriately to minimize damage. Prior to concrete placement, epoxy-coated reinforcing steel should be inspected for damage and any visible coating damage repaired.

Substantial research has been conducted on epoxy-coated reinforcing steel. Laboratory tests generally demonstrate the high performance of epoxy-coated reinforcing bars in protecting against corrosion.

Large statistical analyses of the performance of structures containing epoxy-coated reinforcing steel have been conducted for agencies including the Florida, New York State, Michigan, and Nebraska DOTs, and these have shown long lives for concrete structures containing epoxy-coated reinforcing steel. While several reports of poor performance in the field have been reported, these generally include outdated coating technologies, poor coating chemistries, low coating thickness, high holiday counts, and a high amount of damage to the coating. This distress is also found in poor-quality concretes and where coated bars have been used in only one mat of the concrete slab.

While long-term coating adhesion has been viewed as a concern, testing using debonded coatings has shown that the effect of coating adhesion is not important compared with the effects of coating damage.

Epoxy-coated reinforcing steel continues to remain the most commonly used corrosion-resisting reinforcing steel due to its use of existing reinforcing steel stocks, relatively simple manufacturing technology, and long-term performance in concrete structures. Future research will focus on design life, life cycle predictions, and coating robustness.

5.11   Sources of further information

Additional information on the use and performance of epoxy-coated reinforcing steel may be obtained from the Epoxy Interest Group of the Concrete Reinforcing Steel Institute, Schaumburg, IL (www.epoxyinterestgroup.org).

References

Agrawal, A.K., Qian, G., Kawaguchi, A., Lagace, S., Delisle, R., Kelly, B., Weykamp, P., Conway, T., Dubin, E., 2006. Deterioration Rates of Typical Bridge Elements in New York. Structures Congress 2006. American Society of Civil Engineers, St. Louis, MO.

Bautechnik, D.I.F., 1990. Richtlinie für Prüfungen an Betonstählen mit Epoxidharz-Beschichtung (Guideline for testing of reinforcing steel with epoxy coating). Kolonnenstraße 30, D-10829. Deutsches Institut für Bautechnik (German Institute for Building Technology (DIBt)), Berlin.

Berke, N., Hicks, M., 1998. Long-term corrosion performance of epoxy-coated steel and calcium nitrite. Corrosion 98. NACE International.

Boatman, B., 2010. Epoxy Coated Rebar Bridge Decks: Expected Service Life. Michigan Department of Transportation, Lansing, MI.

Bradley, B., Nohlgren, S., July 8, 1985. The Florida Keys: Costly Repair for New Bridge. St. Petersburg Times.

Brown, M., 2002. Corrosion Protection Service Life of Epoxy Coated Reinforcing Steel in Virginia Bridge Decks. Doctor of Philosophy. Virginia Polytechnic Institute and State University.

Clear, K.C., Virmani, Y.P., Jones, W., Jones, D., 1981. Time-to-Corrosion of Reinforcing Steel in Concrete. In: Galvanizing Reinforcing Steel, vol. 4. Federal Highway Administration, Washington, DC.

Clifton, J., Beeghly, H., Mathey, R., 1974. Nonmetallic Coatings for Concrete Reinforcing Bars. National Bureau of Standards, Washington, DC.

Concrete Reinforcing Steel Institute CRSI, 2014a. Standard Practice for Epoxy-coated Steel Reinforcing Bar Fabrication Facilities. CG2.1. Schaumburg, IL.

Concrete Reinforcing Steel Institute CRSI, 2014b. Standard Practice for Epoxy Coating Plant: Custom Lines. Schaumburg, IL.

Concrete Reinforcing Steel Institute CRSI, 2014c. Standard Practice for Epoxy Coating Plant: Straight Bar Lines. CG1.1. Schaumburg, IL.

Covino, B., Cramer, S., Holcomb, G.R., Russell, H.G., Bullard, S.J., Dahlen, E.P., 2000. Performance of Epoxy Coated Rebar in the Deck of the Perley Bridge. Albany Research Center, Albany, OR.

Cui, F., Lawler, J., Krauss, P., 2007. Corrosion performance of epoxy-coated reinforcing bars in a bridge substructure in a marine environment. In: Corrosion 2007. NACE, Nashville, TN, 30 pp. Paper No. 07286.

Fanous, F., Wu, H., Pape, J., 2000. Impact of Deck Cracking on Durability. Iowa State University. Iowa Department of Transportation, Ames, IA.

Hatami, A., Morcous, G., 2012. Developing Deterioration Models for Life Cycle Cost Analysis of Nebraska Bridges. TRB. Transportation Research Board, Washington, DC.

Kahhaleh, K., Chao, H., Jirsa, J., Carrasquillo, R., Wheat, H., 1993. Studies on Damage and Corrosion Performance of Fabricated Epoxy-coated Reinforcement. National Technical Information Service. Report No. FHWA/TX-93. Center for Transportation Research, University of Texas at Austin, Austin, TX.

Kondratova, I., Erdogdu, S., Bremner, T., 1998. Field and Laboratory Performance of Epoxy − Coated Reinforcement in Cracked and Uncracked Concrete. Transportation Research Board, Washington, DC.

Lau, K., Sagues, A.A., Powers, R., 2007. Long-term corrosion behavior of epoxy coated rebar in Florida bridges. In: Corrosion 2007. NACE International, Houston, TX, 10 pp. Paper No. 07306.

Lawler, J., Krauss, P.D., 2010. Condition Survey of Older West Virginia Bridge Decks Constructed with Epoxy-coated Reinforcing Bars. Wiss, Janney, Elstner Associates, Northbrook, IL.

Lee, S.K., 2008. Characterizing corrosion behavior of disbonded epoxy coated reinforcing steel − updated results. In: Corrosion 2008. NACE International, New Orleans, LA. Paper No. 08312.

Lee, S.K., 2011. Up-to-date Research Results of FHWA Coatings and Corrosion Laboratory. NACE Bridge Forum, Houston, TX.

Manning, D., 1996. Corrosion performance of epoxy-coated reinforcing steel: North American experience. Construction and Building Materials 10, 349−365.

McDonald, D.B., 2011. Cost-effective methods for improving the corrosion resistance of concrete. In: PCI and National 57th Annual Bridge Convention Conference, October 22−26, 2011, Salt Lake City, UT. Precast/Prestressed Concrete Institute, Chicago, IL.

McDonald, D.B., Pfeifer, D.W., Sherman, M.R., 1998. Corrosion Evaluation of Epoxy-coated, Metallic-clad and Solid Metallic Reinforcing Bars in Concrete. Federal Highway Administration, McLean, VA, 127.

O'reilly, M., Darwin, D., Browning, J., Locke Jr., C.E., 2011. Evaluation of Multiple Corrosion Protection Systems for Reinforced Concrete Bridge Decks. The University of Kansas Research Inc, Lawrence, KA.

Pfeifer, D., Landgren, R., Krauss, P., 1993. Performance of epoxy-coated rebars: a review of CRSI research studies. Transportation Research Circular 403.

Pianca, F., Schell, H., Cautillo, G., 2005. The performance of epoxy coated reinforcement: experience of the Ontario ministry of transportation. International Journal of Materials and Product Technology 23, 286−308.

Pincheira, J.A., Aramayo, A.A., Kim, K.S., Fratta, D., 2008. Corrosion Protection Performance of Epoxy-coated Reinforcing Bars. Department of Civil and Environmental Engineering: Minnesota Department of Transportation.

Powers, R.G., 1987. Corrosion Evaluation of Substructure − Long Key Bridge. Interim Report. Florida Department of Transportation, Gainesville, FL.

Pyc, W.A., Weyers, R.E., Sprinkel, M.M., Weyers, R.M., Mokarem, D.W., Dillard, J.G., 2000. Performance of epoxy-coated reinforcing steel. Concrete International 22, 6.

Rasheeduzzafar, F., Bader, M., Khan, M., 1992. Performance of corrosion-resisting steels in chloride-bearing Concrete. ACI Materials Journal 89.

Read, J.A., 1990. Rebar corrosion − FBECR: the fight to cure the problem. In: Harding, J.E., Gerard, P., Ryall, M. (Eds.), First International Conference on Bridge Management. University of Surrey. Taylor & Francis, Guildford, UK, pp. 231−248.

Regelgeving, C.C.U.R.E., 1992. Met Epoxy Bekleed Betonstaal (Epoxy Coated Rebar). AK
    Gouda. Civieltechnisch Centrum Uitvoering Research en Regelgeving (Centre for Civil
    Engineering Research and Codes), Netherlands.
Riemenschneider, J.A., 1989. Oregon Test Pile, Log 209 Rebar Evaluation for the Oregon
    Department of Transportation. 3M Laboratory, Minnesotta, MN.
Rivera, E., Abbas, E.K., Wright, W.J., Weyers, R.E., Roberts-Wollmann, C.L., 2014. Fatigue
    Assessment for the Failed Bridge Deck Closure Pour at Mile Marker 43 on I-81. Virginia
    Tech Transportation Institute, Blacksburg, VA.
Russell, H., 2004. Concrete bridge deck performance: a synthesis of highway practice. In:
    Program, N. C. R. Transportation Research Board, Washington, DC.
Sagues, A.A., Lau, K., Powers, R.G., Kessler, R.J., 2010. Corrosion of epoxy-coated rebar in
    marine bridges − Part 1: a 30-year perspective. Corrosion 66.
Sagüés, A.A., Lau, K., Powers, R.G., Kessler, R.J., 2009. Corrosion of epoxy-coated rebar in
    marine bridges − a 30 year perspective. In: International, N. (Ed.), 17th International
    Corrosion Congress. Las Vegas, NV.
Sakai, K., Shinichi, S., 1994. Ten-year exposure test of precracked reinforced concrete in a
    marine environment. In: 3rd International Conference on Durability of Concrete, Nice,
    France. American Concrete Institute, Farmington Hills, MI, pp. 353−369.
Sim, C., 2014. Structural and Corrosion Performance of Concrete Bridge Decks Reinforced with
    Corrosion-resistant Reinforcing Steel (Ph.D.). Purdue University.
Sohanghpurwala, A.A., Scannell, W.T., 1999. Condition and Performance of Epoxy-coated
    Rebars in Bridge Decks. Public Roads. Federal Highway Administration, Washington, DC.
Sprinkel, M., Weyers, R., Blevins, C., Ramniceanu, A., Weyers, S., 2010. Failure and Repair of
    Deck Closure Pour on Interstate 81. Transportation Research Board, DC.
Straßenbau, S.B.F., 1991. Richtlinien zur Anwendung von epoxidharzbeschichteten
    Betonstählen. (Guidelines for the application of the epoxy-coated reinforcing bars.). Swiss
    Federal Office of Road, Bern, Switzerland.
Swamy, R., Koyama, S., Arai, T., Mikami, N., 1988. Durability of steel reinforcement in marine
    environment. In: Malhotra, V.M. (Ed.), Concrete in Marine Environment. St. Andrews
    By-The-Sea. ACI International, Canada, pp. 147−162.
Virmani, Y.P., Clear, K.C., Pasko, T.J., 1983. Time-to-Corrosion of Reinforcing Steel in
    Concretes. In: Calcium Nitrite Admixture or Epoxy-coated Reinforcing Bars as Corrosion
    Protection Systems, vol. 5. Federal Highway Administration1983, Washington, DC.
Walzak, T., 1995. Adhesion loss mechanisms of epoxy coatings on rebar surfaces. In:
    Schaumburg, I.L. (Ed.), Surface Science Western. Concrete Reinforcing Steel Institute and
    the Ministry of Transportation, Ontario.
Weyers, R.E., Sprinkel, M.M., Brown, M.C., 2006. Summary Report on the Performance of
    Epoxy-coated Reinforcing Steel in Virginia. Virginia Transportation Research Council,
    Charlottesville, VA 22903.
Weyers, R.E., Sprinkel, M.M., Pyc, W., Zemajtis, J., Liu, Y., Mokarem, D., 1997. Field
    Investigation of the Corrosion Protection Performance of Bridge Decks and Piles Con-
    structed with Epoxy-coated Reinforcing Steel in Virginia. Virginia Polytechnic Institute
    and State University, Blacksburg, Virginia Transportation Research Council, Virginia
    Department of Transportation, Charlottesville, VA.
Zintel, M., Angst, U., Keßler, S., Gehlen, C., 2014. Epoxidharzbeschichtete Bewehrung Neue
    Erkenntnisse nach zwei Jahrzehnten Praxiserfahrung: Epoxy-coated reinforcement − New
    findings after two decades of practical experience.

Galvanized steel reinforcement

6

S.R. Yeomans

School of Engineering and Information Technology, University of New South Wales
at the Australian Defence Force Academy, Canberra, Australia

6.1 Introduction

The corrosion of steel reinforcement in concrete is a worldwide problem that impacts the long-term durability and serviceability of concrete construction. Should the reinforcement corrode, this may have serious consequences on the longevity of the component or structure that in turn affect the environmental sustainability of a project as well as its economic viability.

While the provision of good-quality concrete is fundamental to ensuring the adequate durability of concrete and primary protection of the reinforcement, the galvanizing of reinforcement (i.e. coating with zinc) provides additional corrosion protection to embedded steel in the event of a lack of durability of the concrete due to inappropriate materials choices and/or poor workmanship and site practices, and also where a long maintenance-free life is required. From its first reported use in the United States in the 1930s, galvanized reinforcement has been widely used, especially so over the last 40−50 years, in many types of concrete construction in a variety of mild, moderate and aggressive exposure conditions.

In this chapter, a review is presented of the nature, characteristics and performance of galvanized coatings for concrete reinforcement. This will focus on the hot-dip coating of steel reinforcement, sometimes called 'batch' galvanizing, for which there is an extensive published record of laboratory-based research and field studies of existing structures, some more than 35 years old. Detailed reviews of this topic have been published by ILZRO (1981) and CEB (1992), and more recently by Yeomans (2004a). Reference will be made to these reviews where appropriate, along with recent research.

To conclude, an emerging technology for the continuous coating of steel reinforcement will be discussed. As a simple and convenient in-line process, continuous coating can process straight bar or coil-to-coil product directly into galvanized bar and offers not only an ease, speed and economy of production compared with traditional hot-dip galvanizing (HDG), but is more energy-efficient and has less environmental impact.

6.2 Galvanized reinforcement

A number of technologies are available to coat steel with zinc − that is to galvanize − and each method results in a characteristic thickness and morphology of the zinc coating produced (Porter, 1994). For steel products greater than 5−6 mm thick

including reinforcement, for which a durable, robust and long-life coating is required, hot dipping is the preferred and most commonly used method. HDG, often called 'batch galvanizing', involves immersing clean and prefluxed steel in a kettle of molten zinc at about 450 °C. During the immersion time while the steel is heating to the temperature of the molten zinc, a metallurgical reaction occurs between the steel and the zinc.

Depending on the mass of the steel being galvanized, the immersion time varies from a few minutes for light sections to 20−30 min for heavy structural sections. As a consequence, the thickness of the HDG coating varies with the mass (primarily thickness) of the steel being coated. This is accounted for in all national and international galvanizing standards, including those specifically for reinforcing steel ([the International Standards Organization] ISO 14657 (2005), BS ISO14756, [American Society for Testing and Materials] ASTM A767), which all nominate a minimum specified thickness of galvanized coatings as 85−87 μm, equating to a coating mass of approximately 600−610 g/m^2 for ISO14657 Class A coatings and ASTM A767 Class II coatings. It is to be noted that the typical coating thickness for HDG reinforcing steel is usually 110−120 μm, though it may be as much as 150−180 μm depending on the size of the bar.

The reaction between steel and molten zinc produces a coating on the steel made up of a series of iron−zinc alloy layers (gamma, delta and zeta) that grow from the steel/zinc interface, with a layer of essentially pure zinc (eta) at the outer surface. The alloy layer structure of a typical (so-called 'bright') galvanized coating is shown in Figure 6.1. What distinguishes galvanizing from other types of coatings is that the galvanized layer is metallurgically bonded to the steel due to inter-alloying between the steel and the molten zinc.

As shown in Figure 6.1, the alloy layers in the coating are harder than the base steel, resulting in a coating that is not only firmly adhered to the steel, but also tough and abrasion resistant. This allows the galvanized article to be handled, transported and fabricated in much the same way as ordinary steel. Further, as is the case with the galvanizing of general engineering products, the zinc coating on reinforcement provides both barrier protection to the underlying steel as well as sacrificial cathodic protection of exposed steel in the event the coating is damaged.
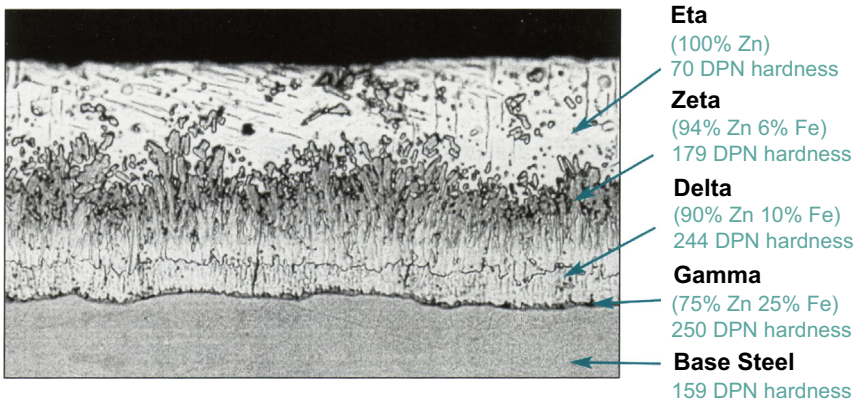

Eta
(100% Zn)
70 DPN hardness

Zeta
(94% Zn 6% Fe)
179 DPN hardness

Delta
(90% Zn 10% Fe)
244 DPN hardness

Gamma
(75% Zn 25% Fe)
250 DPN hardness

Base Steel
159 DPN hardness

Figure 6.1 Microstructure of hot-dip galvanized steel bar.
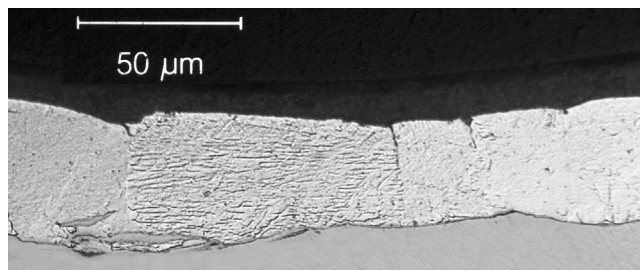
Figure 6.2 Microstructure of continuously galvanized bar.

A key feature of hot-dip coatings is that the outer eta layer, which is effectively pure zinc that remains on the surface of the product as it is withdrawn from the kettle, is generally about 40−50 μm thick. As will be discussed in the following, it is the presence of this eta layer that controls much of the behaviour of zinc when in contact with wet cement. It is to be noted, however, that not all galvanized coatings necessarily contain all of the alloy layers evident in a 'bright' coating.

Depending on the steel chemistry and processing conditions, the coating may contain only one or two of the alloy layers. For example, the microstructure of the coating on so-called 'reactive' steels, with a silicon content around a peak at 0.065% or above 0.3%, consists almost entirely of enlarged zeta crystals that grow in an uncontrolled manner and consume the outer pure zinc eta layer. Such coatings can be quite thick and have a dull grey surface appearance. Similarly, when galvanized steels are heated (i.e. annealed) above about 450 °C, the growth of the zeta phase is promoted at the expense of the pure zinc layer, which can also result in the disappearance of the eta layer at the surface.

A recent development has been continuous galvanizing of reinforcement (CGR). Continuous coating is an in-line (thus not batch dipping) process similar to the coating of sheet and pipe products, where blast cleaned and preheated bar is fed through a molten zinc bath at speeds higher than 10 m/min such that the bar remains in the zinc bath for no more than 1−2 s (Dallin, 2013), and the total time at temperature including the preheating stage is not more than 4−5 s.

By adding a small amount of aluminium (0.2%) to the zinc bath, a coating typically 50−60 μm thick is produced that is almost entirely pure zinc, with only a very thin layer (approximately 0.1 μm) of a ternary ($Fe_2Al_{5−x}Zn_x$) alloy at the zinc/steel interface. The typical microstructure of continuously coated bar is shown in Figure 6.2. Apart from the economy and speed of production with CGR, a key feature of this type of coating is the improved formability of the coated product. A pilot plant for CGR has recently been commissioned in Dubai.

6.3   Laboratory studies

Several extensive reviews of laboratory studies of galvanized steel in concrete have previously been compiled (ILZRO, 1981; Yeomans, 2004b). In much of the work undertaken, especially over the last 20−30 years, studies of galvanized steel have

used alkali solutions, simulated pore water solutions, cement pastes, and mortars and concretes as corrosion media. Comparison with black (i.e. uncoated) steel has commonly been used as a control. In some, other rebar types have been included, primarily epoxy-coated rebar, solid stainless steel rebar and/or stainless clad rebar. Being laboratory based, and in order to produce some corrosion reaction in a short period of time, most of the investigations have used a chloride-contaminated medium and accelerated testing protocols.

While the results from such a wide range and variety of laboratory investigations are sometimes difficult to compare, the results have clearly demonstrated a number of key features of galvanized steel in concrete. These include important issues such as the nature of the passivation reaction, the importance of the presence of a layer of pure zinc on the coating surface, the higher chloride tolerance of galvanized steel compared with black steel, and the resistance of galvanized steel to the carbonation of concrete. The effects of the differing morphology of the galvanized coating on its corrosion behaviour, the processes at work when the galvanized coating is actively corroding, and the migration of zinc corrosion products into the adjacent matrix interfacial zone have also been widely studied.

Though some contradictory results have been published, as well may be expected over such a long period, the vast majority of this extensive body of work has demonstrated the benefits of galvanizing as a long-term and robust corrosion-protection system for steel reinforcement (and other fittings) in concrete compared with black steel (Yeomans, 2004b). Some key aspects of this research follow.

6.3.1 Zinc in concrete

As is well known, when bare steel comes in contact with fresh concrete, it is passivated and thus protected from corrosion due to the high alkalinity of the concrete pore water, initially a saturated $Ca(OH)_2$ solution at a pH of about 12.2. As hydration proceeds, and depending on the alkali content of the cement, the pH rises to about 14 as other hydroxide forms (e.g. NaOH and KOH). The steel largely remains passivated through this transition.

A key feature of this change in pH that is relevant to the passivation of zinc in concrete is that as the pH rises, the concentration of Ca^{2+} ions in the pore solution steadily decreases. These and other effects impacting on the behaviour of zinc in concrete have been thoroughly reviewed by Andrade and Alonso (2004). Some detail of this follows.

6.3.2 Passivation of zinc

Zinc, as an amphoteric metal, reacts in both strong acids and strong bases but is relatively stable over the pH range from about 6 to 12.5. With relevance to the alkaline environment of wet cement and concrete, Macais and Andrade (1987a) indicated that while different zinc products form on the surface as corrosion proceeds, above pH 12.9 the main product is the soluble zincate ion (ZnO_2^{2-}). Over the pH range $12-13.2 \pm 0.1$, the galvanized coating corrodes at a relatively low rate and will passivate, while above this pH, dissolution of the coating occurs with no passivation.

The corrosion product that leads to the passivation of zinc in calcium-rich alkaline solutions is calcium hydroxyzincate (CaHZn), the morphology of which varies with the pH of the contact solution. For example, at a pH around 12.6, the zinc surface is totally covered with a dense and compact layer of CaHZn crystals. However, as the pH increases, the individual size and distribution of the CaHZn crystals also increase to a point where they cannot completely cover the surface.

Above pH 13.5, the crystals become quite coarse and isolated, and under these conditions, complete passivation of the surface is not possible and dissolution of the coating continues at a high corrosion rate (Macais and Andrade, 1987b). The reason for this change is that as the pH increases above 13.2, the reduced availability of calcium ions impedes the formation of CaHZn. As a consequence of this change, the dissolution of zinc as passivation proceeds is not retarded, so the galvanized coating may continue to dissolve.

What is generally observed with typical hot-dipped galvanized coatings in contact with wet cement is that about 10 μm of zinc from the outer layer of the coating is consumed by the passivation reaction. This process occurs through the initial set of the concrete (about 1−2 h), and while the initial reaction between zinc and the pore solution is quite vigorous, once the concrete has started to harden and mobility within the mix is restricted, the reaction at the surface diminishes as the passive film forms and blankets the zinc surface. Once the passive film has formed, it will remain intact even if the pH increases to about 13.6.

The effect of the surface condition of hot-dip galvanized rebar in ordinary Portland cement (OPC) concrete has been studied by Tan and Hansson (2008). This work showed that slight weathering of the bar resulting in the formation of zinc oxide and zinc carbonate on the surface increased the initial corrosion rate and passivation time compared with nonweathered bar. Further to this, galvanized coatings with iron−zinc intermetallic phases required longer to passivate than those with a pure zinc surface layer, thereby confirming the importance of the presence of pure zinc in the passivation reaction.

6.3.3 Hydrogen evolution

When galvanized steel comes in contact with wet cement (i.e. freshly placed concrete), the formation of the passivating film of CaHZn crystals is accompanied by the evolution of hydrogen gas. This reaction, in which only quite small quantities of hydrogen are produced, generally only lasts for a short period and effectively ceases once the cement starts to harden. An important consideration here is that the hydrogen evolved from a galvanized surface largely occurs where iron and zinc are in contact, but not on a pure zinc surface, suggesting that it is the zinc−iron alloy layers near the surface of the coating that initiate the formation of hydrogen. This being the case, it is to be expected that the evolution of hydrogen will not be a serious issue if the outer layer of the coating is predominantly pure zinc, which is the situation with both hot-dipped bright galvanized bars and continuously coated bars.

While the evolution of hydrogen from a galvanized surface is possible (as occasionally observed in precasting where galvanized steel forms are used), the practical effects

of this are often overemphasized. Concerns are sometimes expressed that the presence of hydrogen bubbles in and around the transition zone between the bar and the adjacent concrete will reduce the bond strength of galvanized bars in concrete. This matter has been the topic of extensive research that has almost universally demonstrated no reduction in bond strength for galvanized bars compared with equivalent black steel (Kayali, 2004).

It is to be noted that hydrogen evolution from the coating surface can effectively be eliminated if the coating is passivated by another means, the most effective of which is by treatment of the freshly galvanized steel with chromate salts. This is achieved by either quenching the freshly galvanized bars in an aqueous solution containing 0.2% sodium dichromate or by adding chromates to the concrete mix-water at a rate of 70 ppm, expressed as CrO_3 by mass of cement.

The advantage of the concrete mix-water addition approach (which has been widely used in the precasting industry) is that it ensures that the galvanized product is passivated at the actual time it is cast into concrete. However, for bar that is so-called 'quench passivated' as the final step in the galvanizing process, there can be no guarantee that the passive film remains on the bar surface at the time of the concrete pour. This is because the chromate passivating film naturally deteriorates over time, the speed and extent of which depends on both the nature of the storage conditions (in particular coastal or marine exposure) and the time of exposure prior to casting. For example, it is not uncommon that the chromate surface film would have been lost from galvanized product stored in moist chloride-containing conditions in just a few weeks.

Quite apart from this, however, there are serious occupation health and safety issues, and also environmental concerns, with the use of chromium salts. As such, the use of chromates in many parts of the world has been severely restricted, and stringent environmental regulations have been put in place.

In response to restrictions on the use of chromates for passivation, alternate conversion coatings and inhibitors for use with galvanized steel have been investigated. For example, Hernandez-Alvarado et al. (2012) studied the use of an organic inhibitor containing an alkanolamine salt of a polycarboxylic acid as a substitute for chromating and phosphating procedures in the protection of galvanized steel in a 0.5 M NaCl solution. The results indicated that a chromate-free organic inhibitor protects galvanized steel in this environment, though the protection afforded was less than that of a chromate conversion coating. While such results do not specifically relate to the concrete environment, they do point to viable alternatives to the use of chromates for the passivation of zinc.

6.3.4   Effect of carbonation

The carbonation of concrete, due to a reaction between the alkaline products in concrete and weak atmospheric acidic water, results in a progressive lowering of the pH of the cover concrete. This is a common cause of the corrosion of black steel reinforcement in concrete as the pH of the cover concrete drops to about pH 11.5, and as such is a primary durability consideration for conventional reinforced concrete construction.

The situation for galvanized steel is, however, quite different because of the increased corrosion resistance of zinc as the pH reduces below that for the depassivation of black steel (pH 11.5). As a result of this, it is to be expected that galvanized reinforcement would not be significantly affected by the carbonation of concrete. This observation, supported by both extensive laboratory studies and field observation, has clearly shown that carbonation does not significantly increase the corrosion of galvanized steel embedded in concrete, and in some circumstances may actually reduce the rate of corrosion (Andrade and Alonso, 2004).

6.3.5 Effect of chlorides

Chlorides are a common cause of corrosion of steel reinforcement in concrete. Chlorides find their way into concrete either by being mixed into the concrete through the raw materials used or by migration into the concrete in marine environments, in brackish water conditions or by the use of de-icing salts. A pH-dependent threshold concentration of chlorides is required to initiate corrosion. The effect of the chlorides is to disrupt the passive film on steel and prevent it from re-forming, resulting in a highly localized pitting-type attack that ultimately reduces the cross-section of the reinforcement. For steel, a chloride content of less than 0.2% by mass of cement is recommended for a low corrosion risk (ACI, 1994), while a chloride threshold of 0.4% by mass of cement is often cited.

For zinc in concrete, while there is some divergence of opinion on a precise chloride threshold, a conservative value of 1% chlorides by mass of cement is often used. What is clear from the extensive array of both laboratory and field studies is that a significantly higher chloride threshold is needed to initiate corrosion compared with that required with black steel. For example, comparative corrosion studies in calcium hydroxide solutions (Isikawa et al., 1969) with various chloride concentrations showed that zinc corrodes at a chloride concentration of approximately 0.45 M, while steel corrodes at 0.08 M. This represents about a $5\times$ higher threshold for zinc over black steel in solutions that simulate concrete pore water. While the situation is somewhat different in concrete, what has been observed in a range of laboratory tests and field studies is that the chloride threshold for galvanized bars is at least $2\times-2.5\times$ higher than that for black steel, and perhaps even higher (Yeomans, 1998).

Recent work by Darwin et al. (2007, 2009) showed that galvanized reinforcement had an average chloride corrosion threshold of 2.57 lb/yd^3, which is greater than conventional steel at 1.63 lb/yd^3. Galvanized reinforcement also exhibits a wider range of chloride corrosion initiation than conventional reinforcement, from values comparable to those for conventional steel to values $3\times-4\times$ higher. This work also compared test data obtained with chloride surveys on cracked bridge decks in Kansas. This indicated that galvanized steel increased the average time to corrosion initiation at crack locations from 2.3 years for conventional steel to 4.8 years, an increase in excess of $2\times$.

Presuel-Moreno and Rourke (2009) reported a nine-year study of chloride effects on black and galvanized rebar in a range of concretes. The results indicated that higher chloride levels at the depth of the bars (about 2% chlorides by weight of cement) for

the onset of attack on the zinc extended the service life of galvanized reinforcement. In a 14-year report on this study, Presuel-Moreno (2013) reported that in OPC concrete, galvanized bars outperformed black bars, while in concretes where fly ash and silica fume were added to restrict the chloride diffusivity, the performance difference was, as might be expected, marginal.

Maldonado (2009) investigated the chloride threshold and time to initiation of galvanized reinforcement in concretes exposed to the coastal conditions of the Mexican Caribbean. The results of this nine-year study indicated that galvanized reinforcement can resist chloride at levels $2.6\times-3\times$ higher than black steel even in poor quality concretes, and that the time to initiation for galvanized steel in these conditions was twice that for black steel reinforcement.

Srimahajariyaphong and Niltawach (2011) studied the chloride-induced corrosion of black and galvanized bars in concrete. Using half-cell potential mapping, they inferred the benefits of galvanizing for corrosion protection and recorded chloride levels as high as 0.38% by weight of concrete (about 2.3% by weight of cement) at 30 mm cover on galvanized bars, with no signs of corrosion.

In other work, Baltazar-Zamora et al. (2012) studied the corrosion of galvanized steel in concrete previously contaminated with NaCl (2%, 3% and 4%) and then exposed to a simulated marine environment. While this work indicated the benefit of galvanizing in noncontaminated concrete, in concretes heavily precontaminated with chlorides, the benefit was less apparent because of early disruption of the protective layers on the zinc surface. While actual chloride levels were not reported, the authors specifically noted that the chloride threshold to initiate attack on the galvanized bars was in all cases significantly higher than published chloride thresholds for zinc.

The issue of the extension of the life of galvanized coatings can be demonstrated by the Fick's law approximation of the time to corrosion of black steel and galvanized steel in similar exposure conditions (Broomfield, 2004). Assuming a marine concrete with 0.35% chloride concentration at the surface, a cover of 30 mm and $D = 1.4 \times 10^{-12}$ m²/s, an upper chloride threshold for black steel of 0.4% chloride (by mass of cement) and a higher threshold of 1.0% chloride for galvanized steel, the time to initiation of corrosion of black steel is 15 years, while for galvanized steel, corrosion initiates after 44 years. This indicates a $3\times$ theoretical extension of life for galvanized over black steel bar, which is in good agreement with both experimental and field observations.

6.3.6   Coating behaviour

Other important issues concern the behaviour of the zinc coating when in contact with concrete, in particular how the coating dissolves and what happens to the corrosion products so formed. What has been observed (and as previously noted) is that when the galvanized coating first comes in contact with wet cement and is initially passivated, about 10 µm of zinc is dissolved from the pure zinc outer layer of the coating. What has been widely observed in field structures is that the remainder of the galvanized coating (generally 100 µm or more) remains in its original condition for

extended periods of time provided the conditions in the concrete do not significantly change. In such circumstances, very little further metal loss will occur from the coating until active corrosion commences, usually due to the accumulation of threshold levels of chloride at the depth of the reinforcement.

Once this occurs, continued dissolution of remaining free zinc occurs in and around in the alloy layers, particularly so the delta phase, which comprises the bulk of a bright galvanized coating (Yeomans, 1998). Though the coating appears to be disintegrating at this stage, a dense layer of both the gamma and the delta phases remains intact at the bar surface, and this affords ongoing corrosion protection to the underlying steel. This effect is shown in Figure 6.3.

Sistonen et al. (2008) also studied the corrosion mechanisms of hot-dip galvanized reinforcement in cracked concrete. The work indicated a number of different mechanisms by which the galvanized coating dissolved, depending on the thickness and morphology of the coating. Primarily, local dissolution of the eta and zeta phases occurs as previously reported, though in coatings of nonuniform thickness, longitudinal and perpendicular cracking in the zinc layer may lead to separation of that layer. These results supported other observations that the thickness of the zinc coating influences the extent of corrosion.

Bellezze et al. (2006) compared the corrosion in concrete of traditionally galvanized steel with steels galvanized in zinc baths containing nickel and tin. Nickel additions reduce the zinc−iron reaction while maintaining coating thickness (Andrade and Alonso, 2004), as does tin, which is commonly used in combination with nickel. In comparison with pure zinc as a control, all galvanized bars showed higher corrosion rates due to the presence of alloying elements in the coating. Those from the Ni−Sn modified bath, while not suited to high-alkaline concrete, showed good corrosion behaviour in low-alkali chloride-contaminated concrete, where corrosion initiated
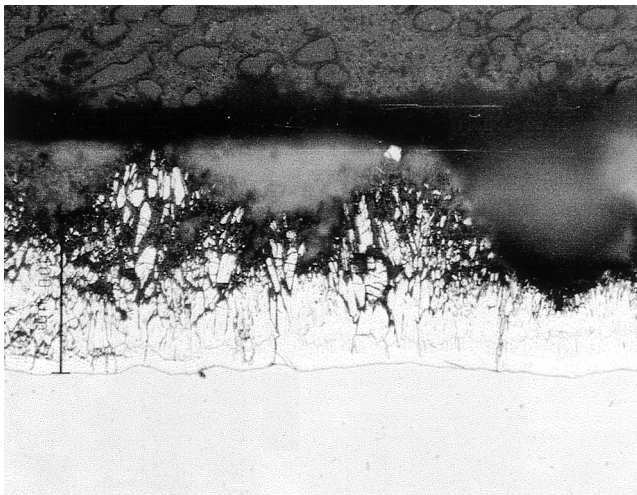
Figure 6.3 Dissolution of the galvanized coating in high-chloride environments.

at a chloride concentration of about 4% by mass of cement and was thus well above the chloride threshold for unprotected steel.

Manna et al. (2008) studied the corrosion of galvanized steel from traditional hot-dip and misch-metal modified baths. Misch-metal modifications create a thinner coating with the absence of Zn−Fe intermetallics, thus providing improved coating ductility. The results indicated that the coating from the misch-metal bath had 1.3×−5× better corrosion resistance in concrete pore solution and 2.5× better resistance to chlorides, compared with traditional hot-dip coating.

6.3.7 Zinc corrosion products

Some important questions are what happens to the zinc corrosion products so formed and what effects have these on the concrete mass. A number of minerals have been identified, primarily zinc oxide and zinc hydroxide, each of which is friable and less voluminous than bulky iron-rich corrosion products. It has also been observed that zinc corrosion products migrate away from the bar and into the adjacent concrete matrix where they fill voids and microcracks (Yeomans, 1998). This effect is shown in Figure 6.4, where the plume of zinc-rich corrosion products migrating away from the coating surface (at left) appears white against the grey calcium-rich cement matrix.

The key issue here is that in contrast to the situation when black steel corrodes in concrete, the zinc corrosion products cause very little physical disruption to the surrounding matrix, thereby maintaining the integrity of the cover concrete. There is also evidence that the filling of the pore space in the interfacial zone creates a barrier in the matrix of reduced permeability that not only increases the adhesion of the matrix to the bar but also reduces the transport of chlorides through the matrix to the coating surface.
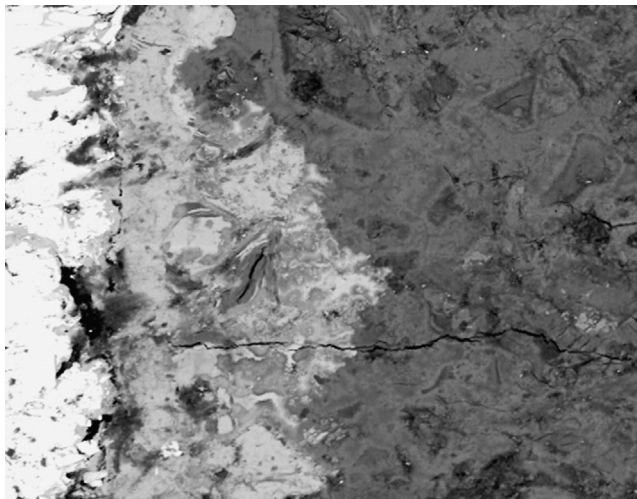
Figure 6.4 Migration of zinc corrosion products into the adjacent cement matrix.

6.4   Field studies

The corrosion protection afforded by the galvanizing of reinforcement is mainly due to the combination of the higher chloride threshold of zinc and its resistance to the effects of carbonation. The benefit is that the zinc coating not only delays the initiation of the corrosion process but continues to provide barrier protection during that period when the coating is reacting (i.e. dissolving) but remains intact. Supplementary sacrificial protection is also afforded where the underlying steel is exposed.

Evidence from numerous field applications has demonstrated that galvanizing extends the life of reinforcement in concrete and provides a safeguard against premature cracking and rust staining of the concrete. Considerable research has been done in the United States, in particular, investigating the use of galvanized reinforcement for concrete bridge and highway construction exposed to high levels of accumulated chlorides due to the application of de-icing salts or marine exposure. This has been extensively reviewed by ILZRO (1981), Yeomans (2004b) and Presuel-Moreno and Rourke (2009).

In the case of experimental bridge decks with top and bottom mat reinforcement when both top and bottom mat bars were galvanized, very low corrosion current densities resulted compared with black steel, and the extent of corrosion on the galvanized bars was significantly less, with no ferrous corrosion products apparent. It has been shown that when galvanized bars were used in the top mat only, with black steel bottom mats, significant corrosion of the zinc occurred, though with very much less red rust corrosion compared with black bars in equivalent conditions (Clear et al., 1981).

Further work in this area has indicated that for a 0.5 w/c concrete, galvanized bars performed better than black bars, though in a 0.4 w/c concrete there was similar behaviour for both black and galvanized bars after eight years of cyclic exposure, and meaningful comparisons could not be made. It was also noted that the worst-case corrosion occurred when top mat galvanized bars in high-chloride concrete were coupled to black steel bars in relatively chloride-free concrete at the bottom of the slab; the best case was when galvanized bars were used in both the top and the bottom mats.

Other data have also verified the enhanced field performance of galvanized reinforcement in both marine and bridge deck applications. Surveys of many structures at various ages of exposure with varying concrete quality (high w/c and low cover), and high-to-extreme chloride levels (up to $10\times$ recommended ACI levels) at the reinforcement, have consistently revealed that galvanized steel outperforms black steel where meaningful corrosion comparisons could be made.

In one long-term survey commenced in 1974, a number of bridges in Iowa, Florida and Pennsylvania were examined in order to compare the performance of galvanized and uncoated reinforcement in decks exposed year-round to humid marine conditions or de-icing salts in winter (Stejkal, 1992). After periods of up to 24 years of exposure, it was found that the galvanized bars had suffered only superficial corrosion in sound, uncracked concrete even when the chloride levels were high. Though the chloride levels had increased since a survey conducted in 1981, no major change in the galvanized bars was detected, and the average thickness of zinc remaining on the reinforcement had not significantly changed since 1981 and was still well in excess of that required by ASTM A767 for new galvanized reinforcement.

In 2002, a follow-up study of the long-term performance of galvanized steel in concrete bridge decks in Pennsylvania was again undertaken (Olsen and Nagi, 2002). Earlier surveys over the period 1974−1999 (previously noted) had examined bridges in Florida, Iowa, Pennsylvania and Vermont. This survey was of the Athens and Tioga Bridges in Pennsylvania, both galvanized reinforced bridges that had been previously examined in 1981 and 1991.

For the Athens Bridge (age 28 years), the average chloride level was $2.5\times$ higher than the threshold value for black steel, and the bars retained well in excess of the minimum 84 μm coating thickness. In the Tioga Bridge (age 27 years), the average chloride level was again more than $2.5\times$ higher than the black steel threshold value. There were no signs of corrosion on any of the galvanized bars, and the thickness of zinc remaining greatly exceeded the minimum specified thickness of 84 μm.

Similar data from Bermuda have also verified the long-term durability of galvanized reinforced concrete in marine environments (Allen, 2004). Commencing shortly after World War II (WWII) and still continuing, a number of docks, jetties and other infrastructure were constructed using a mix of galvanized and bare steel bars. As reported by Allen, a survey undertaken in 1991 showed that the galvanizing was providing continuing corrosion protection to reinforcement at chloride levels well in excess of threshold levels for bare steel corrosion. Follow-up examination confirmed these findings, and revealed that the galvanized bars maintained a residual zinc coating thickness at 42+ years, well in excess of the minimum requirement.

Examination of concrete cores from these structures confirmed the previously mentioned observations that the zinc corrosion products had migrated a considerable distance (300−500 μm) beyond the surface of the coating and into the adjacent concrete matrix with no visible effect on the concrete mass. Field data of this type provide practical evidence of the migration effects of the zinc corrosion products as shown in laboratory experiments (Yeomans, 1998).

6.5   Design and fabrication

6.5.1   Effect on steel properties

Verification testing has demonstrated that galvanizing does not adversely affect the yield and ultimate strength and ductility of traditional reinforcing steels (250 MPa yield), providing the steel has not been excessively cold-worked by bending and rebending (AGA, 2011). Where reinforcement has in earlier years been cold-twisted to raise its yield strength to about 410 MPa (this is no longer practiced), there is some evidence that such steels may be embrittled by galvanizing (Porter, 1991).

However, with the introduction of thermomechanically treated steels and microalloyed steels for high-strength bars (with minimum yield of 400 MPa), this problem has been effectively eliminated. More recently, higher strength reinforcement to 500 MPa yield has been introduced, and extensive testing has again verified that the mechanical properties of this material are not adversely affected by galvanizing. A summary of the effect of galvanizing on various grades of reinforcing steel is given in Table 6.1.

Table 6.1 Effect of galvanizing on grades of reinforcing steel

Type of steel	Considerations for galvanizing
Low strength grades −250 MPa yield strength	• No effect on mechanical properties provided the bar has not been excessively cold-worked during fabrication.
Cold-twisted steels (grade 410C) −410 MPa minimum yield	• Double-cold-worked material (i.e. to strengthen during manufacture plus fabrication by bending) may be embrittled by galvanizing; and so • requires expensive stress relief heat treatment.
Thermomechanically treated or micro-alloyed grades (grade 410Y) −410 MPa minimum yield	• Can be satisfactorily galvanized without need for any special requirements; and • no significant effect on strength or ductility.
New generation high-strength bars (grade 500N) −500 MPa minimum yield	• Superior mechanical properties are retained after hot-dip galvanizing; and • testing actually showed a slight improvement in yield and ultimate stress and also ductility.

6.5.2 Design considerations

The design and construction of galvanized reinforced concrete is, to all intents and purposes, the same as that used for conventional steel reinforced concrete. In particular, splice and lap lengths are the same as for black steel bar, as are bond and load transfer considerations, and as previously noted, the strength of galvanized bars is the same (for design purposes) as equivalent black bar. In effect, best practice when utilizing galvanized reinforcement is to use appropriately designed and placed concrete as would normally be used in general reinforced concrete construction (Swamy, 2004).

Significant research has been undertaken concerning the bond capacity of galvanized reinforcement, and this has been thoroughly reviewed by Kayali (2004). A key issue in much of this research has been whether there is any significant difference in the bond-slip behaviour and total bond capacity of galvanized bars compared with conventional black steel bars.

Kayali and Yeomans (1995) investigated the bond and slip of coated reinforcement in concrete. Beam samples reinforced with either black or galvanized steel bars were tested to failure in flexure. This work revealed that the ultimate capacity of beams with galvanized reinforcement was not statistically different to that of black steel reinforced beams, and further, the mean critical load at slip of 0.01 and 0.02 mm was also not statistically different for the black and galvanized steel.

Further work by Kayali and Yeomans (2000) investigated the bond of galvanized reinforcing steel in concrete using ASTM A944 beam-end test samples. The results confirmed that there was no adverse effect on bond with the use of galvanized steel. This work also identified the very strong adhesion between concrete and the galvanized coating, something that is almost lacking between black steel and concrete.

Further, due to the inhibiting effect of zinc on the early set of concrete, the time to develop full bond strength for galvanized bars may initially be longer than that for black steel, though this effect is usually overcome by 28 days curing. This work also indicated that the chromate treatment of galvanized bars was unnecessary, as there was no evidence of long-term reduction in bond due to the possible effects of hydrogen evolution resulting from the initial reaction between zinc and wet concrete.

Hamid and Mike (2005) investigated the bond strength of hot-dip galvanized reinforcement in normal-strength (28 MPa) concrete. By testing concrete beam specimens with tension lap splices in positive bending, it was found that the use of galvanized bars (compared with equivalent black steel) has a negligible effect on bond strength of reinforcement in this concrete. Further, Maldonado et al. (2010) examined the bond between galvanized steel and concrete at two different w/c ratios, 0.4 and 0.5. This work found that the average total bond strength of black steel and galvanized steel bars in concrete was very similar, with less than a 2% difference over the 28-day curing period, which would be considered within normal statistical variation.

As regards fabrication and construction, because of the robust nature of galvanized coatings, there are no special transportation and handling requirements except that appropriate bend radii (depending on the diameter of the bar) need to be used to minimize cracking of the coating. It is however recommended that galvanized or plastic-coated tie wires be used for fixing, and cut ends and areas of damage to the coating should be protected with a zinc-rich paint or zinc solder (Langill and Dugan, 2004; AGA, 2011). There are also no special precautions or work practices needed in the placement of the reinforcement, other than the use of ties as noted earlier, or in the pouring, compaction and finishing of the concrete. All practices are in effect the same as for the use of black steel reinforcement.

6.6   Applications of galvanized reinforcement

Over a period of some 50–60 years, hot-dip galvanized reinforcement and fittings including bolts, ties, anchors, dowels etc. have been successfully used in a range of reinforced concrete construction in many different environmental exposure conditions. The majority of such product is pregalvanized straight lengths of reinforcing bars and associated stirrups and ties. There is also a significant use of galvanized mesh, especially in lightweight and precast concrete construction and panels for building facades and tilt-up construction.

There is also an important use of galvanizing to provide corrosion protection to large prefabricated reinforcement cages and column reinforcement. The advantage of postfabrication galvanizing (i.e. after bending, cutting and welding) is that total protection is provided to the entire reinforcement structure, thereby eliminating the need for touch-up of cut ends, bends and welds in particular.

A detailed review of the worldwide application of galvanized reinforcement and other galvanized steel inserts in concrete construction has been compiled by Yeomans (2004a, Chapter 1). Of significant interest in this is an extensive listing compiled by the American Galvanizers Association (AGA) of galvanized reinforced structures,

extending to several thousand entries covering buildings, bridges and other transport infrastructure, marine structures, chemical and processing plants, power generation, and water treatment facilities.

In broad terms, the common uses of galvanized reinforcements, fittings and inserts have been in precast cladding and tilt-up elements, exposed building beams and columns, modular building units, and immersed or buried elements such as deep foundations, piles and tunnel linings. Galvanized reinforcement has also been used in a range of coastal and marine structures such as bridge abutments, beams and columns, seawalls, floating marinas, pontoons, docks, jetties and offshore platforms. In the area of transport infrastructure, it has been widely used in bridge decks, road pavements, crash barriers and parking structures. It has also found wide use in chemical and petrochemical processing, power generation, pulp and paper mills, and water and sewerage treatment works. Significantly, galvanized reinforcement has been used in expensive and prestige construction where very long life and the maintenance of appearance is vitally important, such as the Sydney Opera House, NZ, Australian Parliament buildings and the National Theatre, London.

6.7 Future trends

As previously noted, a recent development has been CGR. A key feature of this process is that it produces a coating that is almost entirely pure zinc without the underlying alloy layers typical of hot-dip processing. While affording an ease and economy of production, the nature of the coating also significantly improves the adhesion and formability of the galvanized bar.

Considering that the passivation of zinc requires the presence of pure zinc on the coating surface (noting that about 10 µm of zinc is consumed during passivation), it is to be expected that CGR would afford ongoing corrosion resistance in concrete due to the large reserve of pure zinc in the coating. While hot-dip coatings with thick pure zinc top layers do have good corrosion performance, the Zn$-$Fe alloy layers below may detract from formability and do not contribute significantly to the corrosion performance. CGR, with a much thicker pure zinc coating to about 50 µm, would thus provide ongoing corrosion protection over coatings with a thin or nonexistent pure zinc top layer, thereby using less zinc without compromising corrosion protection.

To this time, continuously galvanized reinforcement has been specified to ISO14657, since this standard caters for several classes of coatings, and a Class B coating with a minimum 300 g/m^2 of deposited zinc (i.e. 42 µm minimum thickness) is appropriate for continuously galvanized product. In this context, the ASTM has recently published a standard specification for continuous hot-dip galvanized steel bars for concrete reinforcement (ASTM A1094). This new standard, which is specific to CGR, specifies Coating Grade 50 as a minimum coating thickness of 50 µm and minimum coating mass of 360 g/m^2. In order to control alloy formation and promote adhesion of the zinc or zinc-alloy to the steel base, a small amount of aluminium (0.05$-$0.25%) is added to the molten bath. The coating process is identified as passing individual bars through a trough or tube of molten zinc and then immediately through

an air or steam wiping device to remove excess coating from the bars. It notes that the zinc coating shall be chromate treated unless waived by the purchaser. The specification also sets requirement for the finish and adhesion of the coating.

Another interesting development has been the duplex coating of reinforcing steel, involving powder coating over a galvanized base. This provides a synergy of corrosion protection actions to the underlying steel, with the galvanized coating itself being over-coated and further protected by the powder coating. Corrosion is delayed by the dual action of the two coatings working together, such that the total life of the duplex coating is more than the sum total of the two individual coatings combined — the synergic effect. Known commercially as ZBAR and specified to ASTM A1055 (ASTM A1055, 2008), this product consists of an inner metalized (i.e. sprayed) zinc layer that provides cathodic protection and an outer polymer membrane that serves to maintain anode to steel continuity during fabrication, shipment, installation and concrete curing. An opportunity here would be to use continuous coating rather than metalizing of the bar as the primary zinc coating process.

Recent work in this area by Dong et al. (2012) examined the corrosion behaviour of epoxy/zinc duplex-coated rebar embedded in concrete exposed for up to 43 months in an ocean environment by comparison with individual black steel, galvanized steel and epoxy-coated bars. Where the black steel corroded at a relatively short time of 6 months, the epoxy coating was able to provide good protection to the bar provided there was no obvious damage to the coating. While the individual galvanized coating provided cathodic protection to the bar but was limited in strongly alkali conditions, the epoxy/zinc duplex coating was able to provide the advantages of both coating systems.

As the authors noted, the galvanized coating provided a barrier layer and galvanic protection where the epoxy coating was damaged, and the epoxy coating, while acting as an external barrier to corrosive elements, assisted in prolonging the protection afforded by the galvanizing. It is anticipated that further commercial development of duplex-coated galvanized reinforcement will follow in coming years.

6.8 Summary

In 1992, the Comite Euro-International du Beton published a state-of-the-art report on coating protection for reinforcement. This seminal report, compiled by an expert panel including key concrete researchers and agencies, reviewed the performance of a number of coating systems for reinforcement, including galvanizing. In its summary, the report stated, inter alia, that:

- proper galvanizing procedures have no significant effect on the mechanical properties of the steel reinforcement;
- zinc coating furnishes local cathodic protection to the steel, as long as the coating has not been consumed;
- galvanized reinforcement provides protection to the steel during storage and construction prior to placing the concrete;

- corrosion of galvanized steel in concrete is less intense and less extensive for a substantial period of time than that of black steel;
- galvanized steel in concrete tolerates higher chloride concentration than black steel before corrosion starts;
- galvanized reinforcement delays the onset of cracking, and spalling of concrete is less likely to occur or is delayed;
- lightweight and porous concretes can be used with the same cover as for normal concretes;
- poor workmanship resulting in variable concrete quality (poor compaction, high water/ cement ratio) can easily be tolerated;
- accidentally reduced cover is less dangerous than with black steel; and
- galvanized reinforcement ensures a clean appearance of the finished concrete with no trouble arising at cracks either from spalling or rust staining.

Though this report is now dated, the context in which it was set and the conclusions reached remain current, as evidenced by the extensive body of ongoing research and field studies of the characteristics and use of galvanized reinforcement. What this points to is that galvanizing provides protection to steel reinforcement and other fittings in concrete well beyond that of black steel in equivalent concrete and exposure conditions. Key features of this protection are the higher chloride tolerance of zinc in concrete, the resistance to the effects of carbonation, the ongoing protection afforded by the thickness of the zinc coating, and a reduction in disruption of the adjacent concrete should the coating corrode.

6.9   Further information

A wide range of technical information is freely available on galvanized reinforcement. Most countries have general galvanizing standards that can (and are) used for the coating of reinforcement, and as noted earlier, there are a number of standards specifically related to galvanized reinforcement from (for example) the ASTM (ASTM A767 (2009), A1094 (2015)), the ISO (ISO 14657), the United Kingdom (BS ISO 14657 (2005)), France (NF A35-025), Italy (UNI 10622) and India (IS 12594). There are also a number of technical specifications from US and Canadian government agencies such as state/province departments of transport and other instrumentalities.

Technical information on galvanized reinforcement is also available from associations such as the International Zinc Association; American Galvanizers Association; the Australian, New Zealand and South African Galvanizing Associations; the Indian Lead and Zinc Development Association and the European General Galvanizing Association. All of these associations have a range of freely available web-based resources on galvanized reinforcement.

References

ACI, 1994. Committee 20, Guide to Durable Concrete. American Concrete Institute (Chapter 4).

AGA, 2011. Hot-Dip Galvanized Reinforcing Steel: A Specifiers Guide. American Galvanizing Association Centennial, CO, USA.

Allan, N., 2004. The Bermuda experience: leading the way on galvanized reinforcement. In: Yeomans, S. (Ed.), Galvanized Steel Reinforcement in Concrete. Elsevier, Oxford (Chapter 7).

Andrade, C., Alonso, C., 2004. Electrochemical aspects of galvanized reinforcement corrosion. In: Yeomans, S. (Ed.), Galvanized Steel Reinforcement in Concrete. Elsevier, Oxford (Chapter 5).

ASTM A767/A767M, 2009. Zinc-Coated (Galvanized) Steel Bars for Concrete Reinforcement. American Society for Testing and Materials.

ASTM A1055/A1055M, 2008. Standard Specification for Zinc and Epoxy Dual-Coated Steel Reinforcing Bars. American Society for Testing and Materials.

ASTM A1094/A1094M, 2015. Standard Specification for Continuous Hot-Dip Galvanized Steel Bars for Concrete Reinforcement. American Society for Testing and Materials.

Baltazar-Zamora, M., et al., 2012. Efficiency of galvanized steel embedded in concrete previously contaminated with 2, 3 and 4% NaCl. International Journal of Electrochemical Society 7, 2997−3007.

Bellezze, T., et al., 2006. Corrosion behaviour in concrete of three differently galvanized steel bars. Cement and Concrete Composites 28, 246−255.

Broomfield, J., 2004. Galvanized steel reinforcement in concrete: a consultant's perspective. In: Yeomans, S. (Ed.), Galvanized Steel Reinforcement in Concrete. Elsevier, Oxford (Chapter 9).

BS ISO 14657, 2005. Zinc Coated Steel for the Reinforcement of Concrete. British Standards Institution.

CEB, 1992. Committee Euro-International du Beton, Coating Protection for Reinforcement: State of the Art Report. CEB Bulletin d'Information No. 211, Chapters 2 and 5 (also published by Thomas Telford Services, London 1995).

Clear, K., et al., 1981. Time-to-Corrosion of Reinforcing Steels in Concrete: Vol. 4 Galvanized Reinforcing Steel. FHWA Report No FHWA/RD-82/028. Federal Highway Administration, McLean, VA, USA.

Dallin, G., 2013. Continuously Coated Galvanized Steel Reinforcing Bar, Literature Review of the Advantages of Zinc Coatings versus Zinc/Zinc-Iron Coatings. GalvInfo Centre, International Zinc Association, Brussels, Belgium.

Darwin, D., et al., December 2007. Critical Chloride Threshold for Galvanized Reinforcing Bars. ILZRO Project ZC-24-2. University of Kansas Centre for Research, Structural Engineering and Engineering Materials SL Report 07−2.

Darwin, D., et al., 2009. Critical chloride threshold for galvanized reinforcing bars. ACI Materials Journal 106, 176−183.

Dong, S.G., et al., 2012. Corrosion behavior of epoxy/zinc duplex coated rebar embedded in concrete in ocean environment. Construction and Building Materials 28, 72−78.

Hamad, B., Mike, J., 2005. Bond strength of hot-dip galvanized reinforcement in normal strength concrete structures. Construction and Building Materials 19, 275−283.

Hernandez-Alvarado, L., et al., 2012. Evaluation of corrosion behavior of galvanized steel treated with conventional conversion coatings and a chromate-free organic inhibitor. International Journal of Corrosion 2012. Article ID: 368130, 8 pp.

Isikawa, T., et al., 1969. Electrochemical study of the corrosion behaviour of galvanized steel in concrete. Fourth International Congress on Metallic Corrosion, (ICMC), Netherlands, pp. 136−138.

ILZRO, 1981. Galvanized Reinforcement for Concrete − II. International Lead Zinc Research Organization, NC, USA.

ISO 14657, 2005. Zinc-Coated Steel for the Reinforcement of Concrete. International Standards Organization.

Kayali, O., 2004. Bond of steel in concrete and the effect of galvanizing. In: Yeomans, S. (Ed.), Galvanized Steel Reinforcement in Concrete. Elsevier, Oxford (Chapter 8).

Kayali, O., Yeomans, S., 1995. Bond and slip of coated reinforcement in concrete. Construction and Building Materials 9 (4), 219−226.

Kayali, O., Yeomans, S., 2000. Bond of ribbed galvanized reinforcing steel in concrete. Cement and Concrete Composites 22, 459−467.

Langill, T., Dugan, B., 2004. Zinc Materials for Use in Concrete. In: Yeomans, S. (Ed.), Galvanized Steel Reinforcement in Concrete. Elsevier, Oxford (Chapter 4).

Macais, A., Andrade, C., 1987a. Corrosion of galvanized steel reinforcements in alkaline solutions, part I − electrochemical results. British Corrosion Journal 22, 113−118.

Macais, A., Andrade, C., 1987b. Corrosion of galvanized steel reinforcements in alkaline solutions, part II − SEM study and identification of the corrosion products. British Corrosion Journal 22, 119−129.

Maldonado, L., 2009. Chloride threshold for corrosion of galvanized reinforcement in concrete exposed in the Mexican Caribbean. Materials and Corrosion 60, 536−539.

Maldonado, L., et al., 2010. Bond between galvanized steel and concretes prepared with limestone aggregates. Anti-Corrosion Methods and Materials 57 (6), 305−313.

Manna, M., et al., 2008. Characterisation of coating on rebar surface using hot-dip Zn and Zn-4.9%Al-0.1% misch metal bath. Surface and Coatings Technology 202, 1510−1516.

Olsen, C., Nagi, M., 2002. Evaluation of the Performance of Galvanized Steel in Concrete Bridge Decks. ILZRO Project ZC-10. Construction Technology Laboratories, Skokie, IL, USA.

Porter, F., 1991. Zinc Handbook: Properties, Processing and Use in Design. Marcel Dekker, New York.

Porter, F., 1994. Corrosion Resistance of Zinc and Zinc Alloys. Marcel Dekker, New York.

Presuel-Moreno, F., Rourke, D., 2009. Review of Galvanized Rebar Performance on G-109 Specimens after 9 Years. NACE Corrosion 2009, Paper No 09209. National Association of Corrosion Engineers, Houston, TX, USA.

Presuel-Moreno, F., 2013. Achieving the 100 Year Bridge Using Galvanized Rebar, Performance of Galvanized Rebar up to 14 Years: G-109 Reinforced Concrete Specimens. ILZRO Project ZC-3. Florida Atlantic University, Florida. December 2013.

Sistonen, E., et al., 2008. Corrosion of hot-dip galvanized reinforcement bar in cracked concrete. Corrosion Science 50, 3416−3428.

Stejkal, B., 1992. Evaluation of the Performance of Galvanized Steel Reinforcement in Concrete Bridge Decks. CTL Project 050324. Construction Technology Laboratories, Skokie, IL, USA.

Srimahajariyaphong, Y., Niltawach, S., 2011. Corrosion prevention of rebar in concrete due to chloride. Journal of Metals, Materials and Minerals 21 (1), 57−66.

Swamy, R., 2004. Design for durability with galvanized reinforcement. In: Yeomans, S. (Ed.), Galvanized Steel Reinforcement in Concrete. Elsevier, Oxford (Chapter 2).

Tan, Z., Hansson, C., 2008. Effect of surface condition on the initial corrosion of galvanized reinforcing steel embedded in concrete. Corrosion Science 50, 2512−2522.

Yeomans, S., 1998. Corrosion of the Zinc Alloy Coating in Galvanized Reinforced Concrete. NACE Corrosion 1998, Paper 98653. National Association of Corrosion Engineers, Houston, TX, USA.

Yeomans, S. (Ed.), 2004a. Galvanized Steel Reinforcement in Concrete. Elsevier, Oxford.

Yeomans, S., 2004b. Laboratory and field performance of galvanized steel in concrete. In: Yeomans, S. (Ed.), Galvanized Steel Reinforcement in Concrete. Elsevier, Oxford (Chapter 6).

Effect of different concrete materials on the corrosion of the embedded reinforcing steel

7

R.B. Holland [1], *K.E. Kurtis* [2], *L.F. Kahn* [2]
[1]Simpson Gumpertz & Heger, Waltham, MA, USA; [2]Georgia Institute of Technology, Atlanta, GA, USA

7.1   Introduction

Repair and rehabilitation of concrete structures in the United States has been estimated at \$20 billion annually; approximately 40% of that cost is due to corrosion of embedded steel reinforcement (ICRI, 2006; Koch et al., 2008), with much of the corrosion damage occurring in bridges. In the United States, about \$4 billion is spent annually to maintain and replace corroded bridge structures (Koch et al., 2008).

As detailed in Chapter 2, for corrosion (an electrochemical reaction) to occur, five components are necessary: (1) an anodic oxidation site (e.g., $Fe \rightarrow Fe^{2+} + 2e^-$), (2) a cathodic reduction site (e.g., $2H_2O + O_2 + 4e^- \rightarrow 4OH^-$), (3) an electrical connection between the anode and cathode to transfer electrons, (4) an electrolytic environment to transfer ions and complete the circuit, and (5) the availability of reactants at the site of corrosion such as O_2, Cl^-, and H_2O. In concrete, due to the high pH environment it provides, steel exists in a passive state, and a sixth requirement—the depassivation of the steel—is also necessary for corrosion to occur at a meaningful rate. Depassivation can occur commonly through carbonation, via interaction of cement hydration products with environmental sources of carbon dioxide, which decreases the concrete pH, or through localized depassivation when the chloride ion concentration at the steel surface exceeds the threshold required to initiate corrosion.

Both chloride ingress and carbonation at the level of the internal reinforcing steel are delayed by the concrete cover—the distance between the exterior of the concrete member and the nearest position of a reinforcing bar or embedded structural steel shape. The goal of a good concrete mix design is to enhance the concrete material in that cover to mitigate corrosion while simultaneously providing adequate strength at minimal cost.

This chapter reviews the influence of the water-to-cementitious-materials (w/cm) ratio, curing methods, supplementary cementitious materials (SCMs), and other admixtures on the corrosion of embedded steel reinforcement in concrete structures. Commonly available SCMs include fly ash, slag, silica fume (SF), and metakaolin; they are considered in both binary and ternary blends. Each of these parameters affects the ingress of chlorides as well as the natural carbonation of the concrete.

Emerging trends in concrete technology to further extend the service lives of reinforced concrete structures are discussed.

7.2   Chloride ingress resistance

7.2.1   Sources of chlorides

Chlorides can be introduced into concrete from internal or external sources. Internal sources of chlorides include the use of seawater for mixing water, dredged aggregate, aggregate washed with seawater, and chloride-containing admixtures (Bertolini et al., 2004). External chlorides typically occur from environmental factors. Typical external sources are from the ingress of seawater in marine environments and from the use of deicing salts containing chlorides in colder climates (Bertolini et al., 2004). Additionally, concrete may be exposed to chlorides if used in industrial applications where chemicals may contain chlorides, such as dry-cleaning facilities, paper mills, and aquariums (Bertolini et al., 2004).

7.2.2   Effects of mix design on chloride durability

Alterations to concrete mix design can significantly affect chloride ingress. The resistance of concrete to chloride ingress is primarily driven by the transport properties of the concrete, including its permeability, diffusivity, and absorptivity. When good-quality aggregate is used, these properties are related to the microstructure of the hydrated cement paste. The pore structure of the hardened cement paste is the primary influence in the durability of concrete exposed to external chlorides. However, the chemistry of the hydrated cement paste influences the concrete's ability to chemically bind chlorides, which prevents them from interacting with embedded reinforcing steel.

For the long-term performance of concrete structures exposed to external chlorides, diffusion is typically the main form of transport for chlorides to the depth of the reinforcing steel. The primary parameters of concrete mix design that have large effects on the concrete's diffusion coefficient are the w/cm ratio and the maturity of the concrete at the time of first chloride exposure, and the addition of SCMs such as fly ash and ground granulated blast-furnace slag (slag).

7.2.2.1   w/cm ratio

The w/cm ratio directly influences the pore structure of the hydrated cement paste. At high w/cm ratios, the pore structure of the concrete is highly interconnected, allowing for more rapid transport through the microstructure. However, as the w/cm ratio decreases, the pore structure becomes more refined and the microstructure denser. The diffusion coefficient of concrete can vary by over an order of magnitude for a concrete using the same relative proportions and materials, simply as a result of varying the w/cm ratio (Luping, 1995). Figure 7.1 shows the results of research studies investigating the variation of diffusion coefficients of concrete with a varying w/cm ratio. The large spread of values on the graph for the same w/cm
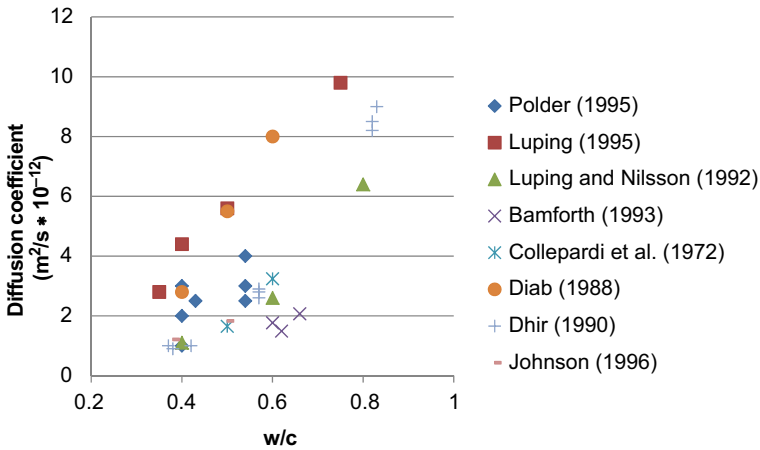
Figure 7.1 Effect of water-to-cement (w/c) ratio on diffusion coefficient in plain portland cement concrete.

ratio is due to differences in mix designs, including aggregate type and content, type of cement used, and maturity before exposure.

7.2.2.2   Age at exposure

The age of concrete when exposed to chlorides, or more specifically the concrete's maturity, greatly influences the transport properties of the concrete. Like the compressive strength of concrete, the transport properties change over time. At young ages, the concrete microstructure is more porous and will transport chlorides at a faster rate. As concrete matures, hydration reactions continue and the microstructure becomes more refined, resulting in a denser microstructure that is more resistant to chloride ingress. Research studies investigating the diffusion coefficient of concrete have demonstrated that the diffusion coefficient can vary by orders of magnitude for the same concrete at different ages, as shown in Figure 7.2.

Similarly large changes in the diffusion coefficient with time are related to the composition of the binder. The use of SCMs, especially pozzolanic materials that require longer durations to react, can influence the extent and rate of the relative decrease in the diffusion coefficient over time.

Research into changes in transport properties as concrete matures has led to the development of estimation techniques. A simple relationship was developed by Stanish and Thomas (2003) to predict the diffusion coefficient of concrete at any age given that it is known through testing for at least one age, as shown below in Eqn (7.1). The coefficient, m, for mix designs can be determined experimentally using bulk diffusion tests:

$$D_{avg} = D_{ref}(t_{ref}/t_{eff})^m \tag{7.1}$$
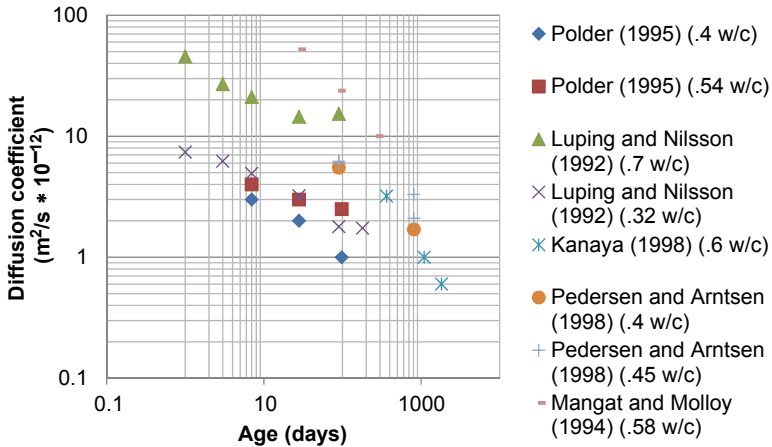
Figure 7.2 Effect of age at exposure on diffusion coefficient in plain portland cement concrete.

where

D_{avg} = average diffusion coefficient at t_{eff}
D_{ref} = diffusion coefficient at the reference age
t_{ref} = reference age of concrete
t_{eff} = effective age of concrete
m = coefficient based upon mix parameters
  = 0.32 for portland cement and 0.66 for 25% fly ash replacement

Figure 7.3 shows Stanish's estimator equation plotted with the experimental results for diffusion coefficients of plain portland cement concrete mixes. The research data demonstrate a similar trend to the estimator equation, with the diffusion coefficient
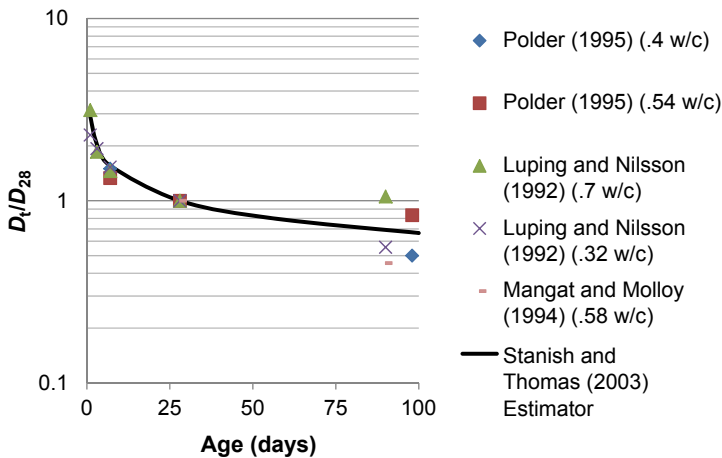
Figure 7.3 Comparison of normalized time-dependent diffusion coefficients with the Stanish and Thomas (2003) estimator equation.

decreasing as the age at exposure increases. The trend of the testing exemplifies that longer curing periods will lead to decreased rates of chloride ingress for the same concrete.

7.2.2.3   Curing

Curing refers to the temperature and relative humidity to which concrete is exposed during the time the cement and SCMs react to form hydration products. While hydration occurs over many months, most of the hydration process occurs within 1 month, and the critical curing duration is about one week. During that time, the internal temperature in the concrete should be between 5 and 70 °C. For hydration to occur, the internal relative humidity must be above 80% (Mindess et al., 2003). Because water is drawn from the capillary pores into the $C-S-H$ product, water generally must be drawn from excess water in the concrete mixture and from externally supplied moisture. For such moisture to be available, the concrete surface must be moist-cured either by submerging, ponding, or sprinkling the surface; or by inhibiting any moisture from escaping the surface by coating the surface with a polymer film (curing agent) or a plastic sheet over wet burlap or cotton batting. Appropriate curing assures the development of a well-hydrated and dense structure. Improper curing results in a concrete with large voids, capillaries, and cracks, all of which lead to greater permeability and the ability for chlorides to rapidly move through the concrete to the reinforcement. Further, improper curing can lead to plastic shrinkage cracks due to early evaporation of surface water, and cracks can provide a "fast path" for aggressive ion ingress.

7.2.2.4   Supplementary cementitious materials

The addition of SCMs to concrete can substantially increase the concrete's resistance to chloride ingress. The SCMs most commonly used in concrete exposed to chlorides are fly ash, slag, SF, and metakaolin. The use of SCMs can improve concrete's durability, resistance to degradation due to multiple mechanisms, and strength gain behavior.

SCMs have two primary forms of reaction that influence the properties of the concrete. The hydration and chemical reactivities of SCMs are functions of their compositions, with many SCMs showing varying ranges of each type of reactivity.

- **Latent Hydraulic Reactivity:** The material will react with water to form strength-bearing phases, with or without the presence of portland cement. SCMs of this form typically will contain both calcium and reactive silicates.
- **Pozzolanic Reactivity:** The SCMs will react chemically with water and the hydrated cement paste to form additional strength-bearing phases and cause a densification of the microstructure. Pozzolanic materials are typically siliceous in nature and need not contain lime-bearing phases.

The reaction rates of SCMs impact their influence on the pore structure, and as a result the rate of diffusion of aggressive species through concrete. In general, SCMs that react quickly and at early ages during the cement hydration process will result in a lower rate of diffusion, even at early ages. For SCMs that react slowly, the

diffusion rates at early ages may be similar to or higher than those of a plain portland cement concrete, but as the concrete matures, they will decrease more than they do for a plain portland cement concrete. Often, the decrease in diffusion rates for concretes with slow-reacting SCMs will result in a concrete that is more resistant than a plain portland cement concrete at ages greater than 56 days.

Fly ash

Fly ash is a by-product of coal combustion and composed primarily of silicon dioxide (SiO_2) and calcium oxide (CaO). When added to concrete, fly ash reacts with the hydrated cement paste in a primarily pozzolanic reaction; the result is a denser microstructure over time. Research has shown that fly ash does not decrease the diffusion coefficient of concrete at early ages compared with plain portland cement concrete (Basheer et al., 2002; Mangat and Molloy, 1994; Papadakis, 2000; Thomas and Bamforth, 1999; Thomas and Matthews, 2004; and Thomas et al., 1999). However, at later ages, the addition of fly ash does result in a lower diffusion coefficient. Class F fly ash (low CaO content) leads to a marginally lower diffusion coefficient than does a Class C fly ash (high CaO) at later ages (Papadakis, 2000). Typical fly ash replacement levels for portland cement range from 15% to 35%. The compressive strength of concrete with these replacement levels of fly ash is about the same as that achieved using plain portland cement after 90 days when adequate curing is provided, but strength at earlier times may be less. Resistance to other concrete deterioration mechanisms, such as sulfate attack and alkali—silica reaction, generally is improved with the addition of low calcium or Class F fly ash in particular.

Slag

Ground granulated blast-furnace slag, more commonly referred to as slag or slag cement, is a by-product of steel production. Slag is primarily composed of CaO, SiO_2, aluminum oxide (Al_2O_3), and magnesium oxide (MgO). When used as part of a portland cement concrete, slag reacts with both the water (latent hydraulic reaction) and the hydrated cement paste (pozzolanic reaction), resulting in a more refined microstructure than that of a plain portland cement. At early exposure ages, concrete containing slag will have a similar to slightly higher diffusion coefficient than in plain portland cement concrete, but at ages greater than 90 days, it will have a lower diffusion coefficient. Research has shown that slag replacement levels of 40% or higher result in large reductions in the diffusion coefficient at later ages (Basheer et al., 2002; Bleszynski et al., 2002; Luo et al., 2003; Mangat and Molloy, 1994; Saleem et al., 2010; Thomas and Bamforth, 1999; Thomas et al., 1999, 2008). Typical replacement levels for slag in concrete range from 40% to 80%.

Silica fume

SF is a by-product from silicon alloy production in electric arc furnaces. SF is an ultrafine powder approximately $100\times$ finer than cement grains, and it is almost pure silicon dioxide (SiO_2). The addition of SF to concrete greatly decreases the permeability and diffusion coefficient of the concrete compared with those of plain portland cement
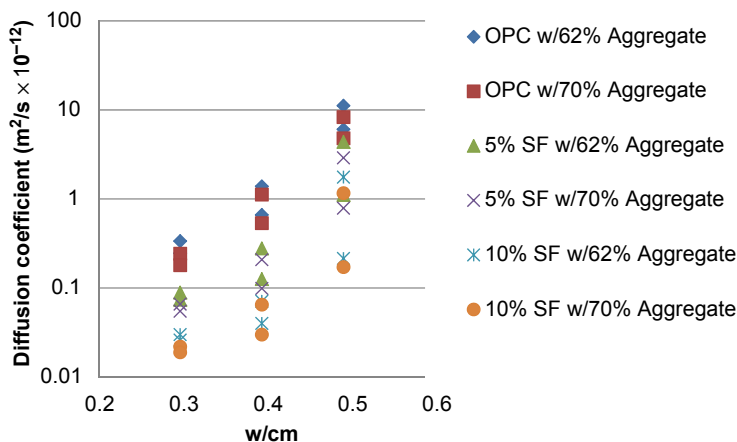
Figure 7.4 Effect of SF content on diffusion coefficient (Bentz, 2000). OPC is ordinary portland cement. SF contents of 0%, 5%, and 10% replacement.

concrete. Due to the high surface area and small particle size of SF, it reacts quickly and results in a decrease in the diffusion coefficient at all ages compared with those of plain portland cement concrete (Bentz, 2000; Bleszynski et al., 2002; Mangat and Molloy, 1994; Papadakis, 2000; Saleem et al., 2010; Smith, 2001; and Thomas et al., 1999). Figure 7.4 shows the results of a study by Bentz (2000), where the decrease in diffusion coefficient is plotted for various replacement levels of SF. SF is typically used at replacement levels between 3% and 10% of weight of cement. Replacement levels above 10% can lead to further durability improvements, but the workability and finishability of the concrete can be problematic.

Metakaolin

Metakaolin is a dehydroxylated form of the clay mineral kaolinite. Metakaolin is commonly used in the production of ceramics, but is also used as cement replacement in concrete. Metakaolin has a smaller particle size ($\sim 1-2$ μm) and higher surface area compared with portland cement, but a larger particle size than SF. When used in concrete, metakaolin undergoes a pozzolanic reaction and refines the microstructure of the hydrated cement paste. Due to the small particle size and high surface area, metakaolin reacts quickly and reduces the diffusion coefficient compared with plain portland cement (Basheer et al., 2002; Batis et al., 2005; Gruber et al., 2001; and Saleem et al., 2010). Research suggests that SF and metakaolin have similar influences on the chloride ingress resistance of concrete. Typical replacement levels for metakaolin range from 5% to 10%.

Binary and ternary blends

The use of binary blends (portland cement plus one SCM) and ternary blends (portland cement plus two SCMs) can substantially improve the performance of concrete exposed to chlorides. Research has shown that the use of SCMs can lower the

apparent diffusion coefficient and reduce permeability significantly, as shown in Figures 7.5 and 7.6, respectively. The type of SCM used depends on the application. For applications that will have early age exposures, the use of fly ash or slag alone may not be appropriate; the use of SF or metakaolin may be preferable due to their faster reaction rates. However, for concretes that will not be exposed to chlorides until later ages, fly ash or slag can be an effective solution to improve the durability.
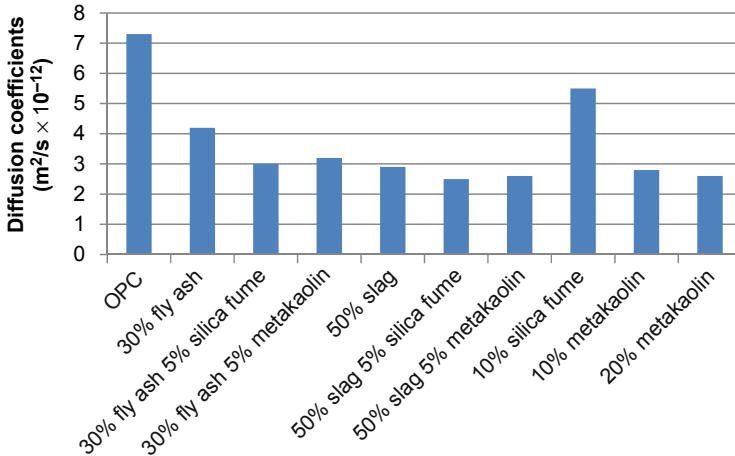
Figure 7.5 Effect of SCMs on diffusion coefficient for concretes exposed for 1 year after curing for 30 days.
Based upon Basheer et al. (2002).
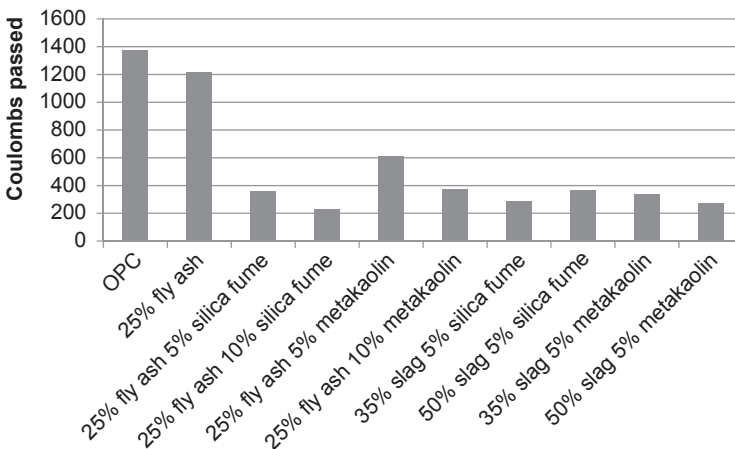
Figure 7.6 Rapid chloride permeability test results for binary and ternary blend concretes tested at an age of 56 days.
Based upon Holland (2012).

When ternary blends are used, the concrete will generally exhibit the properties of both SCMs. Research has shown that ternary blends result in superior chloride ingress resistance compared with binary blends of similar replacement levels and plain portland cement concretes (Thomas et al., 1999). Frequently, ternary blends will contain a slow-reacting SCM and a fast-reacting SCM, which results in improved chloride ingress resistance at both early and late ages compared with a binary blend (Holland, 2012; Saleem et al., 2010; Basheer et al., 2002).

7.3   Carbonation resistance

Carbonation of concrete can occur due to the diffusion of carbon dioxide from the environment through the pores of concrete. Carbonation of concrete consumes slightly soluble calcium hydroxide and produces insoluble calcium carbonate, which causes the decrease in pore solution pH. As pH decreases, the stability of hydration products, including calcium silicate hydrate (C−S−H), the primary strength-giving component of hydrated cement paste, can be compromised (Neville, 1997). Additionally, carbonation shrinkage can occur, altering the surface properties and causing cracking near the exposed surface of a structural element (Mindess et al., 2003).

In addition to leading to strength loss, carbonation of concrete can initiate corrosion of reinforcing steel due to the decreased pH (Papadakis et al., 1991). A decrease in pH at the depth of reinforcing steel can cause the passive film on the surface of the steel to become unstable, and carbonation-induced corrosion will occur (Broomfield, 2007).

Carbonation is a time-dependent process. A simple model for the depth of carbonation is given below in Eqn (7.2).

$$D_{\text{carbonation}} = k * t^{1/2} \tag{7.2}$$

where

$D_{\text{carbonation}}$ = depth of carbonation front
k = carbonation constant
t = duration of exposure

The carbonation constant for a given concrete is greatly affected by environmental factors such as humidity, temperature, and CO_2 concentration. The carbonation constant is dependent upon the concrete mix design and maturity. Figure 7.7 shows the depth of the carbonation front (as indicated by phenolphthalein indicator solution) for concrete with increasing exposure durations to an accelerated test.

7.3.1   Concrete mix design

Both the chemistry and transport properties, as influenced by the concrete mix design, can have a large influence on the rate of carbonation. The two primary mix design parameters that influence the carbonation rate are the w/cm ratio and the amount and type of SCMs.
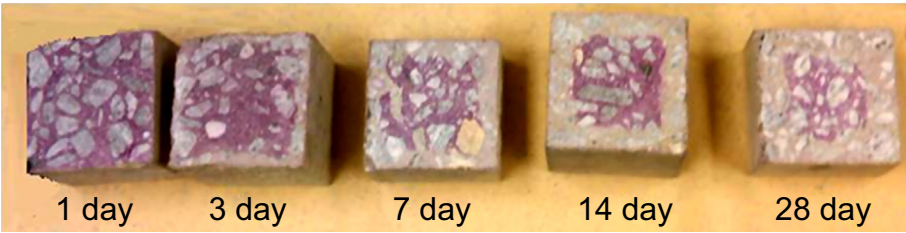
Figure 7.7 Accelerated carbonation test samples with increasing carbonation depth (Holland, 2012). The purple phenolphthalein shows a high pH where there is no carbonation; carbonation occurred to a depth of 19 mm after 28 days.
Ref. Chang and Chen (2006).
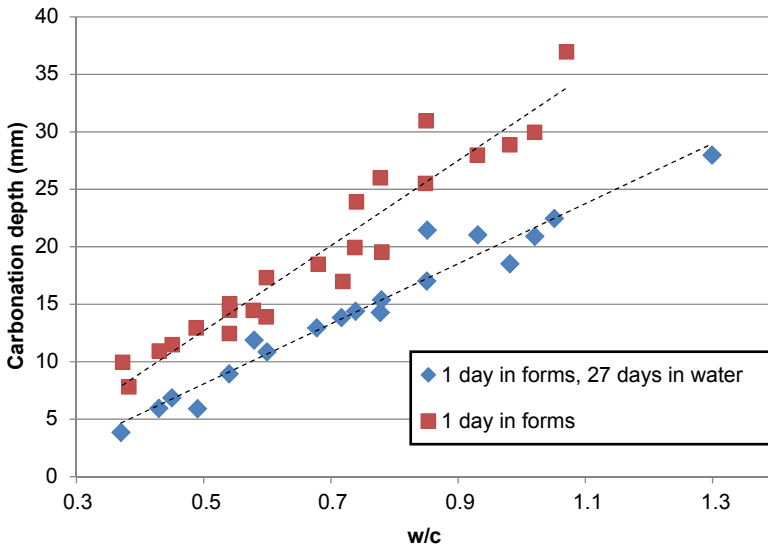
Figure 7.8 Effect of w/c ratio and water curing on carbonation depth.
Based upon Page (1992).

7.3.1.1   w/cm ratio

The permeability and diffusivity of concrete has a large influence on the rate of carbonation. Decreasing the w/c ratio can cause the transport properties of concrete to vary by orders of magnitude for carbonation, similarly to chloride ingress (Papadakis et al., 1991). The influence of a lower w/c ratio is shown in Figure 7.8.

Research by Sulapha et al. (2003) investigated the pore structure of mix designs and found that keeping the binder composition and quantity the same but decreasing the w/c ratio led to a decrease in the carbonation constant. This was linked to a reduction in the maximum size of the pores. Those results demonstrate the importance of microstructural refinement to the carbonation resistance of concrete.

7.3.1.2 *Supplementary cementitious materials*

The binder composition has a large influence on the carbonation resistance. The use of SCMs may decrease the initial pH of the concrete through consumption of calcium hydroxide, but SCMs also decrease permeability by refinement of the pore structure and the creation of secondary C−S−H (Bertolini et al., 2004). Research by Holland (2012) demonstrated that at low w/cm ratio, the decreased permeability of the microstructure resulted in a slower rate of carbonation than in plain portland cement concrete. Therefore, the effect of the decrease in the initial $Ca(OH)_2$ content due to SCMs did not control the carbonation rate. Studies on higher w/cm ratio by Papadakis (2000) demonstrated that if the microstructure is more permeable, the depletion of the $Ca(OH)_2$ caused concrete with SCMs to exhibit higher rates of carbonation. Sideris et al. (2006) found that the carbonation rate was lower at later ages for mix designs containing SCMs. This suggests that the decreased pH initially due to $Ca(OH)_2$ consumption in the formation of secondary C−S−H may be offset in the long term by the decreased rate of ingress due to the formation of a denser matrix with smaller pores with the use of SCMs.

Concretes utilizing fly ash replacement for cement showed that the carbonation depth at early ages increased with increasing replacement levels, but that the rate of ingress is decreased in mixes containing fly ash and with a low w/cm ratio (Atis, 2003; Maslehuddin et al., 1996; Papadakis, 2000; Sideris et al., 2006; Sulapha et al., 2003; and Holland, 2012). Additionally, Papadakis (2000) demonstrated that the CaO content of fly ash had a negligible effect on the carbonation rate. Slag replacement has been shown to have a similar effect on the carbonation depth and rate (Maslehuddin et al., 1996; Sulapha et al., 2003).

The replacement of cement with SF was shown to increase the carbonation depth (as defined by the color change of a phenolphthalein solution) at all ages by Papadakis (2000) and by Sulapha et al. (2003). However, research on low w/cm mixes containing SF have shown that the addition of 5%−10% SF decreases the carbonation rate compared with a plain portland cement concrete (Maslehuddin et al., 1996; Sulapha et al., 2003). Sulapha et al. (2003) found that 10% SF replacement performed better than fly ash replacement (20%−50%) and slag replacement (65%).

Research using ternary blends suggests that they may offer lower rates of carbonation than those of binary mix designs. Figure 7.9 shows the results of a study that investigated the use of binary and ternary blends, which indicated that the carbonation rate was decreased by the use of ternary blends.

Research by Sulapha et al. (2003) investigated the pore structure of binary and ternary mix designs with a 0.50 w/cm ratio. That study reported that fly ash and SF mix designs offered the best refinement of the pore structure but still resulted in slightly higher carbonation constants than cement-only samples. They concluded that a reduction in cement content resulted in a decrease of carbonatable materials that could not be compensated for by pore structure refinement. However, the age or maturity of the concrete at the time of carbonation exposure could have affected the results.

More recently, research by Holland (2012) showed that when the w/cm ratio was lowered to 0.30, ternary blends offered superior carbonation resistance compared
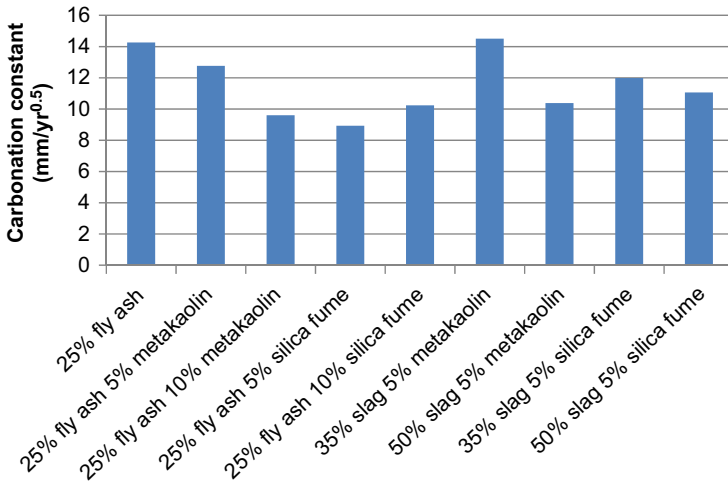
Figure 7.9 Carbonation constants for mix designs containing SCMs (Holland, 2012). Ref. Bertolini et al. (2004).

with plain portland cement concrete and binary mixes. Ternary mix designs containing fly ash, metakaolin, or SF had the highest silica and alumina contents, which would likely result in a larger depletion of calcium hydroxide—but those mixes demonstrated lower carbonation rates. This suggests that the use of SCMs at a low w/cm ratio results in a more refined microstructure that resists carbonation. These findings agree with the findings of Sulapha et al. (2003) when comparing concretes with varying w/c ratios. These results further demonstrate that at very low w/cm ratios, chemical composition plays a smaller role than transport rates in determining carbonation resistance.

7.3.2 Curing and maturity

The maturity of concrete prior to exposure to carbon dioxide−rich environments greatly improves the carbonation resistance properties. Maturity gains obtained by extending the duration of wet-curing can reduce the depth of carbonation during exposure by over 50%, as shown in Figure 7.10. Similar to chloride ingress resistance, wet-curing allows the concrete to continue to hydrate and develop a more refined and dense microstructure. For mix designs containing SCMs like slag or fly ash, longer wet-cure durations allow for the majority of the pozzolanic reactions to occur, resulting in concrete with superior resistance to carbonation.

7.4 Future trends

Clearly, because the issues of corrosion damage to reinforced concrete infrastructure continues to be of importance, innovations that have the potential to extend service
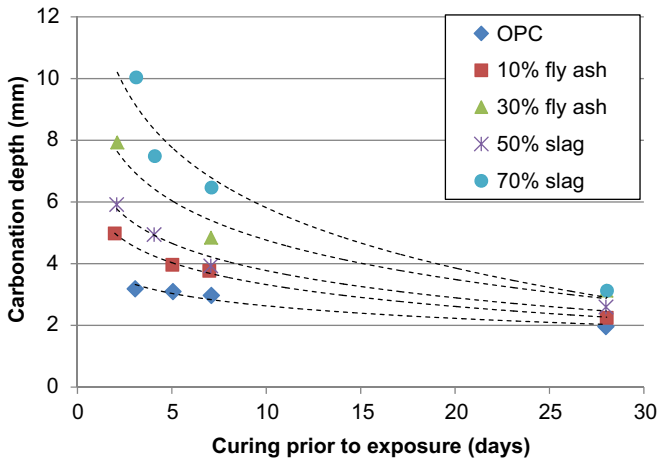
Figure 7.10 Effect of binder composition on carbonation depth.
Based upon Page (1992).

life are of interest. A few emerging topics of relevance to extending the service life of reinforced concrete subject to chloride-laden environments or carbonation are briefly presented here.

7.4.1 Self-healing concrete

Corrosion in cracked concrete often occurs as a direct result of increased rates of transport of aggressive agents at or near the site of cracking, and the corrosion initiation time is reduced compared with uncracked concrete under similar conditions (Holland, 2012). Yet, cracks in concrete can self-heal and reduce the penetrability of chlorides into the section by (1) the formation of calcium carbonate or calcium hydroxide, (2) sedimentation of particles, and (3) continued hydration and swelling of the cement matrix. Lauer and Slate (1955) and Heide (2005) found that the following environmental conditions must be present for self-healing to occur: the presence of water, stability of the crack, and liquid that will not lead to a leaching or dissolution reaction. For corrosion to be mitigated, the healing must occur prior to the concrete being exposed to chlorides. Holland (2012) found that cracks up 0.10 mm wide in concrete mixtures with fly ash replacement of 25% and those with a combination of fly ash and slag totaling 50% self-cured and helped to mitigate chloride intrusion.

7.4.2 Ultra-high-performance concrete

Ultra-high-performance-concrete (UHPC) is generally defined as concrete with a compressive strength greater than 150 MPa. UHPC typically is made with high-strength steel fibers, fine sand, cement, fly ash, a large volume of SF, and a low amount of water (a w/cm ratio less than 0.20). Graybeal (2006) has found that the chloride permeability as measured by ASTM C 1202-12 was less than 100

coulombs, a very low permeability. Structural beams cracked in flexure showed chloride penetration into a 5-μm-wide crack of only 5 mm. Such small cracking is typical of even highly stressed UHPC; therefore, its resistance to both chloride penetration and carbonation is high. While considerably more expensive than conventional concrete, UHPC is highly durable and provides excellent protection of embedded steel reinforcement.

7.4.3   Alternative binders

Alternatives to portland cement are increasingly of interest. Mineral-based alternative binder systems include calcium sulfoaluminate cements, calcium aluminate cements, magnesium-based cements, alkali-activated systems, and blends of these. Some of these binders possess rapid setting and/or strength gain, making them attractive for repair or rapid construction. Some compositions are deemed to contribute to sustainability by offering properties similar to portland cement concrete, but with reductions in measures such as embodied energy or embodied CO_2. In such systems, the pH must be high enough to ensure the corrosion resistance of embedded steel, due to passivation. In addition, the influence of carbonation on the structure and composition of the binder is also important to ensure corrosion resistance. Threshold chloride contents, where corrosion is expected, may also have to be established. While attractive from a performance, economic, or sustainability perspective, greater understanding of these cementitious systems, their chemistry and structure, and their interaction with the environment are needed to ensure satisfactory corrosion resistance when reinforced.

7.4.4   Noncorrosive reinforcement

An alternative to using improved concrete for protection of the steel reinforcement is the use of noncorroding reinforcement, especially stainless steels. Stainless steel reinforcement has been used for many years to provide excellent durability of bridge decks and members. Typically, austenitic stainless steel alloys like UNS S30400 and UNS S31600 (ASTM A276) have been used for non-prestressed reinforcement. For prestressing of wires and strands, the US Navy has used an austenitic grade for special marine piles since the late 1960s. New research has indicated that UNS S31803 (also known in the industry as Type 2205) shows promise as a higher-strength low-cost duplex stainless steel prestressing reinforcement (Moser et al., 2012).

7.5   Conclusions

In this chapter, the influence of the concrete mixture is shown to have important effects on the resistance to corrosion of embedded reinforcing steel. Creating a concrete mixture with a dense, impermeable microstructure will maximize corrosion resistance. In general, the use of a low w/cm mix design containing SCMs will provide a more dense, more corrosion resistant concrete compared with a plain portland cement

concrete. Additionally, providing curing conditions to increase maturity prior to exposure will increase corrosion resistance. There is not a single mix design that will result in the best performance for all applications; however, the particular application should be considered in order to develop a concrete mix design that will provide the necessary durability for a project.

References

Atis, C.D., 2003. Accelerated carbonation and testing of concrete made with fly ash. Construction and Building Materials 17, 147–152.

Bamforth, P., 1993. Concrete classification for R.C. structures exposed to marine and other salt-laden environments. In: Structural Faults and Repair Conference, Edinburgh, UK.

Basheer, L., Kropp, J., Cleland, D., 2002. Assessment of the durability of concrete from its permeation properties: a review. Construction and Building Materials 15, 93–103.

Batis, G., Pantazopoulou, P., Tsivilis, S., Badogiannis, E., 2005. The effect of metakaolin on the corrosion behavior of cement mortars. Cement and Concrete Composties 27, 125–130.

Bentz, D.P., 2000. Influence of silica fume on diffusivity in cement-based materials II. Multi-scale modeling of concrete diffusivity. Cement and Concrete Research 30, 1121–1129.

Bertolini, L., Elsener, B., Pedeferri, P., Polder, R., 2004. Corrosion of Steel in Concrete: Prevention Diagnosis, Repair. Wiley-VCH, p. 392.

Bleszynski, R., Hooten, R., Thomas, M., Rogers, C., 2002. Durability of ternary blend concrete with silica fume and blast-furnace slag: laboratory and outdoor exposure site studies. ACI Materials Journal 99, 499–508.

Broomfield, J.P., 2007. Corrosion of Steel in Concrete. Taylor and Francis Group, New York, NY.

Chang, C.F., Chen, J.W., 2006. The experimental investigation of concrete carbonation depth. Cement and Concrete Research 36 (9), 1760–1767.

Collepardi, M., Marcialis, A., Turriziani, R., 1972. Penetration of chloride ions into cement pastes and concrete. Journal of the American Ceramic Society 55, 534–535.

Dhir, R.K., Jones, M., Ahmed, H., Seneviratne, A., 1990. Rapid estimation of chloride diffusion coefficient in concrete. Magazine of Concrete Research 42, 177–185.

Diab, H., Bentur, A., Heitner-Wirguin, C., Ben-Dor, L., 1988. The diffusion of Cl^- ions through Portland cement and Portland cement-polymer pastes. Cement and Concrete Research 18, 715–722.

Graybeal, B.A., 2006. Material Property Characterization of Ultra-high Performance Concrete. Report No. FHWA-HRT-06-103. Federal Highway Administration, McLean, VA.

Gruber, K.A., Ramlochan, T., Boddy, A., Hooton, R., Thomas, M., 2001. Increasing concrete durability with high-reactivity metakaolin. Cement and Concrete Composites 23, 479–484.

Heide, N., 2005. Crack Healing in Hydrating Concrete. Masters thesis. Delft University of Technology p.128.

Holland, R., 2012. Durability of Precast Prestressed Concrete Piles in Marine Environements (Ph.D. Dissertation). Georgia Institute of Technology, USA.

ICRI, 2006. Vision 2020–a Vision for the Concrete Repair, Protection and Strengthening Industry. International Concrete Repair Institute, Chicago, IL.

Johnson, D., Miltenberger, M., Almy, S., 1996. Determining chloride diffusion coefficients for concrete using accelerated test methods. In: Proceedings on Performance of Concrete in a Marine Environment, New Brunswick, Canada, pp. 95–114.

Kanaya, M., Masuda, Y., Abe, M., Nishiyama, N., 1998. Diffusion of chloride ions in concrete exposed in the coastal area. In: Concrete Under Severe Conditions 2: Environment and Loading. E & FN Spon, pp. 242−249.

Koch, G.H., Brongers, M., Thompson, N., Virmani, Y., Payer, J., 2008. Corrosion Costs and Preventive Strategies in the United States. National Association of Corrosion Engineers, Houston, TX.

Lauer, K., Slate, F.O., June 1955. Autogenous healing of cement paste. Journal of the American Concrete Institute 41, 1083−1097.

Luo, R., Cai, Y., Wang, C., Huang, X., 2003. Study of chloride binding and diffusion in GGBS concrete. Cement and Concrete Research 33, 1−7.

Luping, T., 1995. On chloride diffusion coefficients obtained by using the electrically accelerated methods. In: RILEM International Conference, Paris, France.

Luping, T., Nilsson, L.O., 1992. Chloride diffusivity in high strength concrete at different ages. Nordic Concrete Research 11, 162−171.

Mangat, P.S., Molloy, B.T., 1994. Prediction of long term chloride concentration in concrete. Materials and Structures 27, 338−346.

Maslehuddin, M., Page, C., Rasheeduzzafar, 1996. Effect of temperature and salt contamination on carbonation of cements. Journal of Materials in Civil Engineering 63, 63−69.

Mindess, S., Young, J., Darwin, D., 2003. Concrete, second ed. Prentice Hall Publishers, Upper Saddle River, NJ.

Moser, R.D., Preet, M.S., Lawrence, F.K., Kimberly, E.K., 2012. Durability of Precast Prestressed Concrete Piles in Marine Environment, Volume 2: Stainless Steel Prestressing Strand & Wire. GDOT Research Project Report No. 10-26. Georgia Institute of Technology, Atlanta, Georgia, pp. 342. http://www.dot.ga.gov/doingbusiness/research/projects/Pages/Reports.aspx.

Neville, A.M., 1997. Properties of Concrete, fourth ed. John Wiley and Sons, New York, NY, pp. 844.

Page, C.L., 1992. Nature and properties of concrete in relation to reinforcement corrosion. Corrosion of Steel in Concrete. Conference Precedings, Aachen.

Papadakis, V.G., 2000. Effect of supplementary cementing materials on concrete resistance against carbonation and chloride ingress. Cement and Concrete Research 30, 291−299.

Papadakis, V.G., Vayenas, C., Fardis, M., 1991. Fundamental modeling and experimental investigation of concrete carbonation. ACI Materials Journal 88, 363−373.

Pedersen, V., Arntsen, B., 1998. Effect of early-age curing on penetration of chloride ions into concrete in the Tidal Zone. In: Concrete under Severe Conditions 2: Environment and Loading. E & FN Spon, pp. 468−477.

Polder, R.B., 1995. Chloride diffusion and resistivity testing of five concrete mixes for marine environment. In: RILEM International Conference, Paris, France.

Saleem, H., et al., 2010. Durability and strength evaluation of high-performance concrete in marine structures. Construction and Building Materials 24, 878−884.

Sideris, K.K., Savva, A., Papayianni, J., 2006. Sulfate resistance and carbonation of plain and blended cements. Cement and Concrete Composites 28, 47−56.

Smith, B.G., 2001. Durability of silica fume concrete exposed to chloride in hot climates. Journal of Materials in Civil Engineering 13, 41−48.

Stanish, K.D., Thomas, M., 2003. The use of bulk diffusion tests to establish time-dependent concrete chloride diffusion coefficients. Cement and Concrete Research 33, 55−62.

Sulapha, P., Wong, S., Wee, T., Swaddiwudhipong, S., 2003. Carbonation of concrete containing mineral admixtures. Journal of Materials in Civil Engineering 15, 134−143.

Thomas, M., Bamforth, P., 1999. Modelling chloride diffusion in concrete: effect of fly ash and slag. Cement and Concrete Research 29, 487−495.

Thomas, M.D.A., Matthews, J.D., 2004. Performance of PFA concrete in a marine environment−10-year results. Cement and Concrete Composites 26, 5−20.

Thomas, M.D.A., Shehata, M., Shashiprakash, S., Hopkins, D., Cail, K., 1999. Use of ternary cementitious systems containing silica fume and fly ash in concrete. Cement and Concrete Research 29, 1207−1214.

Thomas, M.D.A., Scott, A., Bremner, T., Bilodeau, A., Day, D., 2008. Performance of slag concrete in marine environment. ACI Materials Journal 105, 628−634.

Effect of using recycled materials in concrete on the corrosion of the steel bars

8

G. Moriconi
Università Politecnica delle Marche, Italy

8.1   Recycled materials in concrete

History teaches that the evolution of construction technology has continued upward since its beginnings, often accompanied by more or less innovative and successful operations that utilize the recycling and reuse of waste materials. Emblematic examples are represented by the use of finely ground clay pottery as "pozzolanic" additions to binders used by Phoenicians as early as the tenth century BC, and the use of scraps from amphorae, likely from the production of wine containers, as lightweight aggregates in the concrete used by Romans in the third century BC for the construction of the piers in the port of Cosa, an important ancient Roman colony for fishing activities.

Rapid industrialization and population growth in recent decades have resulted in the consumption of enormous amounts of the earth's resources and energy, causing unprecedented environmental changes on a global scale. This unsustainable trend, fostered by growing needs for energy, transportation, and manufactured products, as well as those of the construction industry, has induced a growing awareness of and movement toward sustainability concepts. The goal of more sustainable design and planning has encouraged researchers to explore new recycling opportunities in the fields of construction materials and technologies. These studies have long since proved the feasibility of advantageously incorporating industrial by-products, such as coal-combustion fly ash or silica fume,[1] in concrete (Berry and Malhotra, 1986; Mehta, 1989; Naik and Ramme, 1989; Malhotra and Mehta, 2002). Moreover, the feasibility of producing concrete for structural use by partially replacing natural aggregates with recycled concrete aggregates from the demolition of buildings at the end of their service lives has also been proved (Malhotra, 1978; Hansen, 1992a; Naik and Moriconi, 2005; Malešev et al., 2010; Ho et al., 2013). Obviously, recycled aggregates are used after processing in suitable recycling plants.

---

[1] Many by-products beyond fly ash and silica fume—for instance, finely ground blast-furnace slag—are generally used as supplementary cementing materials to produce blended cements. However, even if the use of different types of cement can induce different conditions affecting steel corrosion in concrete, in this chapter only the effect of recycled materials added to the concrete mixture on the corrosion of embedded steel bars is considered.

Fly ash (Malhotra and Mehta, 2002), generally accepted as coal-combustion fly ash, is a by-product of coal combustion in thermal power plants, constituted by a spherical shape and smooth surface particles with a particle size distribution similar to that of cement. It is classified as a supplementary cementing material with a filler effect and pozzolanic activity, since it reacts with the hydrolysis lime from cement hydration to produce further calcium silicate hydrates, thus contributing to strength development of the cementitious matrix through denser microstructure and finer pores. Fly ash in concrete favorably affects the rheological behavior of fresh concrete mixtures and the strength and durability of hardened concrete. Concrete containing relatively high amounts of fly ash not only is characterized by very low permeability and fewer cracks due to thermal and drying shrinkage effects (thus providing high resistance to chloride ion penetration[2]), but also provides effective and efficient protection against expansive reactions such as sulfate attack and the alkali—silica reaction.

A critical aspect of fly ash, like every pozzolanic material, is the low early strength developed by concrete containing it, in spite of satisfactory long-term strength that is generally higher than that of pure portland concrete. However, the low Young's modulus of elasticity at an early age of concrete containing fly ash can be an advantage, if not a need, when control of thermal cracking is a matter of concern because of very high heat of hydration.

Another critical aspect of fly ash could be the small amounts of leachable toxic metals that may be present in it. However, incorporation of fly ash into concrete solves this problem, because hydration products of portland or blended cements form complexes that permanently tie up the metal cations released by fly ash, making their presence in the leachate considerably below prescribed limits.

Fly ash to be used in concrete as a mineral addition has to comply with chemical and physical requirements (ASTM C618-12a in the United States or EN 450-1:2012 in Europe). In most countries where fly ash is allowed to produce blended cements like pozzolanic cement, the related specifications and concrete construction codes prescribe a maximum permissible limit of the blending material such as, for instance, 40% by mass in ASTM C595/C595M-14 (US), or 55% by mass in EN 197-1:2011 (Europe).

Silica fume (Holland, 2005) is "*very fine non-crystalline silica produced in electric arc furnaces as a by-product of the production of elemental silicon or alloys containing silicon*" (ACI 116R-00). Silica fume is a highly reactive pozzolanic material in concrete because of its amorphous nature, with more than 95% of the particles less than 1 μm, causing a very large surface area about 50 times that of fly ash or cement (about 20,000 against about 400 m^2/kg). Because of its extremely small particles, silica fume is able to fill in the spaces between cement grains (microfiller effect), contributing to significant improvement in concrete performance as a consequence of microstructure densification independently of the pozzolanic reaction.

---

[2] Indeed, when the concrete contains fly ash, chloride binding by the cement matrix significantly increases, as compared with reference concrete made without fly ash (Collepardi et al., 1972).

A major critical aspect of the use of silica fume in concrete is the high water demand caused by its very high fineness, so it is necessary to use silica fume in combination with a high-range water-reducing admixture or a superplasticizer in order to preserve concrete mixture proportions, in particular the water-to-cement ratio. However, this combined use allows for enhanced mechanical properties of concrete, especially compressive strength, that are unattainable through ordinary concrete technology. Furthermore, the resulting reduced permeability of the concrete is an important factor that slows down the penetration of aggressive agents and thus contributes to the significant extension of the structural service life.

Silica fume to be used in concrete has to comply with requirements in ASTM C1240-14 and AASHTO M307-13 (*Standard Specification for Silica Fume Used in Cementitious Mixtures*). The use of silica fume in concrete is also covered by ACI 234R-06 (*Guide for the Use of Silica Fume in Concrete*), reapproved in 2012.

8.1.1 Other potentially recyclable materials in concrete

Many other by-products, like ground granulated blast-furnace slag (GGBFS) from steel plants, biomass ashes from bioenergy production plants, calcareous powders from mud venting in marble and natural stone processing, ground waste glass and scraps from fiberglass processing, foundry sands, paper mill ashes, and so on can be profitably used in concrete technology. Some of these by-products are standardized, while others have yet to be, in spite of their potential for use in concrete technology.

GGBFS is a ferrous slag produced during iron processing in steel plants as a result of removing impurities from iron ore. Rapid quenching of molten slag yields glassy, granular product. If finely ground and mixed with free lime, GGBFS can be used as cement replacement, or if less finely ground, as concrete aggregate.

Biomass ashes can be strongly different chemically and morphologically because of heterogeneous materials defined as biomass, as well as different combustion technology. These differences can cause unexpected effects on the behavior of concrete in which the biomass ashes are incorporated, so their potential use is strongly dependent on their origin—this must be well known in addition to their chemical and physical characterizations. Generally, wood ashes from tree plantations show the best performance and prove safer than other biomass ashes.

Calcareous powder, improperly so-called since it can contain relevant amounts of powdered natural silicates from natural stones beyond marble processing, is generally used as a filler. Sometimes it is used as fines addition to produce self-compacting concrete, even if it does not seem very effective and competitive with other fillers in improving the concrete mixture rheology, at the same time avoiding segregation and bleeding.

Waste glass can be used provided that the risk of alkali−silica reaction between the alkalis of cement and the silica of the waste glass is avoided, since this expansive reaction can cause diffuse cracking phenomena, and consequently it can be extremely deleterious for concrete durability. However, data reported in the literature (Shao et al., 2000; Corinaldesi et al., 2005) show that if the waste glass is finely ground, under 100 µm, this reaction does not occur and concrete durability is

guaranteed. In this case, the waste glass powder acts as fly ash does when it is added to concrete mixtures in order to counteract the effect of alkali content exceeding 0.5% of the cement weight. Therefore, waste glass powder can be advantageously incorporated into concrete mixtures to replace cement without harmful effects. Furthermore, these mixtures perform satisfactorily with respect to drying shrinkage, and there are indications that glass powder reduces the chloride ion penetrability of concrete, thereby reducing the risk of chloride-induced corrosion of the steel reinforcement in concrete (Shayan and Xu, 2006; Niang et al., 2014). Conversely, recycling waste glass as sand replacement in concrete requires the use of suppressors to mitigate the potential risk of alkali—silica reaction, such as GGBFS, metakaolin, or lithium nitrate (Taha and Nounu, 2009).

Fiberglass, a glass fiber reinforced plastic composite material (Tittarelli and Moriconi, 2010), is widely used in several fields from building to furniture to boats, producing three main types of by-products: bars from faulty products, small pieces from finishing, and fine powder from cutting and polishing. This fine powder has proved suitable for reuse as a filler in self compacting concrete (SCC) manufacturing, causing a significant reduction of capillary water absorption and drying shrinkage in spite of a slight decrease in compressive strength.

Foundry sands, for a long time unemployed in spite of their potentiality, because of the presence of metal particles, actually show an improved quality due to sand thermal regeneration as a consequence of economy and sustainability issues. They can replace up to 40% of the natural sand in concrete technology without relevant mechanical strength loss, which in any case is recoverable by adding fly ash. Furthermore, the mechanical penalization, if any, proportional to the sand replacement rate, is detectable only at early ages and vanishes at later ages.

Paper mill ashes, obtained from mud burning for heat recovery in paper mills, are attractive for their pozzolanic properties. Under certain burning conditions, paper mill ashes can be converted to metakaolin with an increased added value.

8.1.2 Recycled aggregates for concrete from construction and demolition waste

Recycled materials from demolished buildings are suitably selected, ground, cleaned, and sieved in appropriate industrial crushing plants to produce recycled aggregates that can be qualified and certified as with natural aggregates. In many countries, only coarse aggregates made of recycled concrete coming from demolition only of concrete and reinforced concrete are authorized for use in structural concrete, both ready-mix and precast, with maximum replacement rates depending on the concrete strength class.

Recycled material coming from overall building demolition (concrete rubble that is not "clean" because it contains brick and low amounts of glass as well as asphalt rubble) can be used, but not in structural concrete (up to a concrete strength class of 10 MPa)—such as for subfoundations or in roadbeds—despite some codes that allow for structural use by adopting correcting factors for certain amounts of brick and glass rubble.

Recycled concrete aggregates show lower density (generally higher than 2.2 g/cm^3) and higher water absorption (up to 7%−8%), while all the other chemical and physical properties comply with the standard limits, including alkali reactivity and freezing resistance. However, the main characteristic of recycled concrete aggregates is mortar adhered to their surface, which is responsible for the mechanical behavioral change in addition to the strength loss of the recycled-aggregate concrete compared with ordinary natural-aggregate concrete. The mechanical penalization can be recovered through a reduction of the water-to-cement ratio by using a high-range water-reducing admixture in order to limit the cement dosage. An alternative or complementary way of recovering the strength loss is the use of fly ash, silica fume, and/or metakaolin as supplementary cementitious materials (Kou et al., 2011). On the other hand, the higher surface roughness (due to mortar adhered) of the recycled concrete aggregates is responsible for a better interfacial transition zone, is less prone to initiate cracks, and has a more pronounced aggregate interlock along the cracks (crucial in shear transfer), with higher bond strength to the cement matrix (Letelier Gonzaléz and Moriconi, 2014). At the same time, their high water absorption seems to be responsible for lower drying shrinkage of recycled-aggregate concrete (Corinaldesi and Moriconi, 2010a), thanks to the induced internal curing effect, just as for lightweight aggregates.

Based on the results of the great number of papers devoted to this topic in the international literature, a comparison can be made of the performance of recycled-aggregate concrete with respect to ordinary concrete of the same strength class. In particular, at equal compressive strength, recycled-aggregate concrete shows (Corinaldesi and Moriconi, 2010b):

- lower tensile strength (about 10%);
- lower elastic modulus (about 20%);
- equivalent bond strength with reinforcing steel bars;
- similar susceptibility to cracking due to shrinkage;
- at least equivalent durability in terms of resistance to freeze−thaw cycles, sulfate attachment, and penetration of aggressive agents for steel reinforcement;
- no leaching issues (Sani et al., 2005).

8.2   Effect of recycled materials in concrete on reinforcing steel corrosion

Reinforcing steel bars in concrete are considered to be protected by the formation of an adherent and passive oxide film in the high alkalinity conditions created by cement hydration. However, every action that causes a reduction in the free lime content of the aqueous solution in concrete pores, as in the case of concrete carbonation by air carbon dioxide, can reduce concrete's effectiveness as a protecting medium of the reinforcing steel bars, and thus could promote steel reinforcement corrosion. In the same way, one could think that the addition to concrete of any by-product showing pozzolanic activity—fly ash for instance—can specifically

reduce iron protection from corrosion promoted by pH reduction, owing to the pozzolanic reaction with hydrolysis lime.

On the other hand, by-product addition of fly ash to concrete, particularly without any cement reduction, improves concrete durability because of the filling effect due to the production of further calcium silicate and calcium aluminate hydrates caused by the pozzolanic reaction, which reduces concrete porosity and therefore its permeability to aggressive agents that induce corrosion, such as carbon dioxide. As a matter of fact, one should consider that in good-quality concrete, properly consolidated and cured, corrosion may not be a problem. Only in poor-quality porous concretes, or in the presence of low thickness concrete cover, is corrosion likely to become a problem.

Therefore, in order to evaluate the influence of pozzolanic by-product additions on steel reinforcement corrosion phenomena, let us consider the changes induced by the addition of fly ash on the concrete carbonation process (Branca et al., 1992) as a corrosion indicator.

It may be stated that permeability to carbon dioxide increases with increase in the water/cement ratio—that is, by increasing concrete porosity—so that when fly ash is used to replace cement, a quicker carbonation process could result. This is due to a greater initial porosity in the fly ash concretes caused by a higher actual water/cement ratio and a lower amount of available hydrolysis lime (Gonzales et al., 1983). On the contrary, when fly ash is added without any cement reduction, a decrease in the carbon dioxide penetration rate can be observed owing to the pozzolanic reaction and filling effect that lead to porosity reduction.

Electrochemical measurements indicate that every process that can reduce concrete alkalinity, such as the carbonation process or the pozzolanic reaction due to the presence of fly ash, is a necessary but not sufficient condition to promote corrosion in reinforced concrete. For instance, rebar corrosion seems to be strongly affected by concrete permeability, and then by concrete porosity. As a result, some corrosion risk can occur only when fly ash is added to replace cement at relatively high water/cement ratio. In this case, fly ash additions make concrete, particularly at an early age, more permeable and porous than corresponding portland cement concrete.

Furthermore, when by-products without any pozzolanic activity are added to the concrete mixture as filler or fine aggregate replacement, no change occurs in the passivity conditions of the steel reinforcement, since their addition does not modify the alkaline environment in concrete, while making its microstructure denser and then less permeable to the penetration of aggressive agents.

Cracks induced by loading, shrinkage, creep, and thermal stress, or in precast concrete by mechanical shock or flexural stress during transportation and mounting, decrease the service life of reinforced concrete structures when exposed to chloride aggression, such as in marine environments or frosty climates requiring deicing salt treatment (Francois et al., 1998).

In these cases, galvanized steel reinforcement can be used as a preventive method to slow steel corrosion and prolong the service lives of structures, mostly as a result of the formation of a dense passive layer resistant to chloride attack at higher concentration levels than in the case of bare steel (Swamy, 1990; Yeomans, 1994;

Fratesi et al., 1996). The formation of a dense protective passive layer on galvanized steel reinforcement seems to be favored by less alkaline conditions in the concrete pore solution (Andrade et al., 1983; Macias and Andrade, 1983, 1987a; Andrade and Macias, 1988), and this occurrence can be achieved by fly ash additions to concrete as either fine aggregate or cement replacement, because of its pozzolanic activity.

Therefore, the effect of fly ash on the corrosion behavior of galvanized steel reinforcements in cracked concrete specimens exposed to wet−dry cycles in an aqueous chloride solution was also monitored by electrochemical measurements (Fratesi et al., 2002). In this investigation, concrete specimens were reinforced by means of steel plates instead of bars for twofold reasons: the plate allows for control of concrete specimen cracking by stopping the crack propagation and allowing crack width modulation, and it significantly accelerates the corrosion process due to a much higher ratio of the cathodic to anodic area. The main results of this study are reported in Figures 8.1 and 8.2.

The data reported in Figure 8.1 clearly show that the use of fly ash as partial replacement of either cement or aggregate improves the corrosion resistance of galvanized steel reinforcements in cracked concrete exposed to aggressive environments. In particular, the pozzolanic addition of fly ash, even in the presence of concrete cracks, decreases the corrosion rate monitored in very porous concretes, such as those manufactured with $w/c = 0.80$, to values comparable with those obtained in good-quality concretes, such as those manufactured with $w/c = 0.45$, for which the beneficial effect
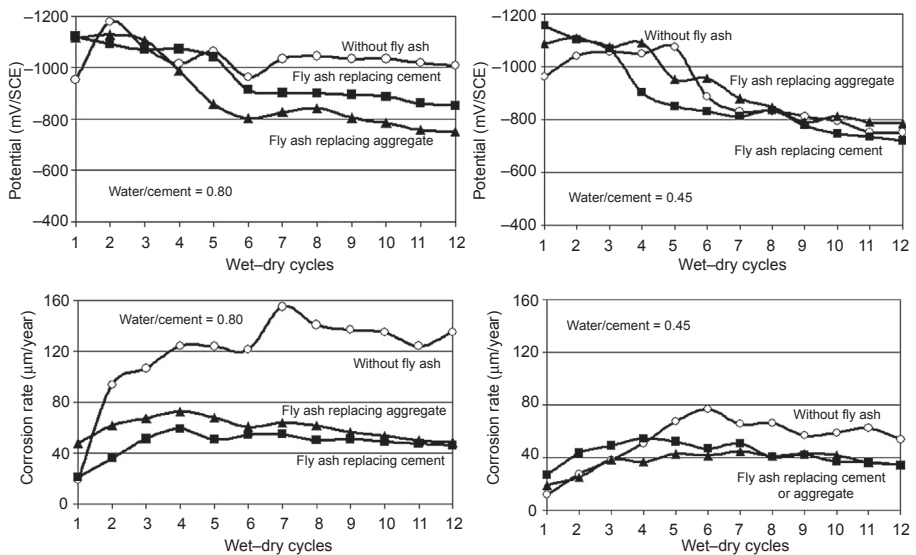
Figure 8.1 The influence of fly ash addition on free corrosion potential (upper) and corrosion rate (lower) of galvanized steel embedded in cracked concrete with different water/cement ratios (higher, 0.80, left; and lower, 0.45, right) as a function of the number of wet−dry cycles in 10% NaCl aqueous solution.
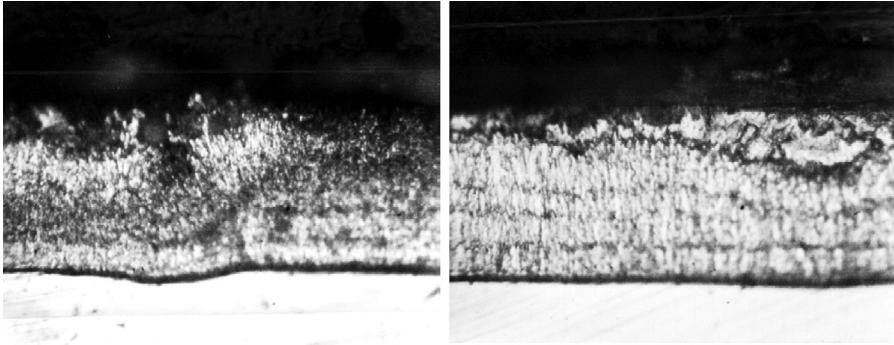
Figure 8.2 Metallographic aspect of the cross section of galvanized steel embedded in cracked concrete with w/c = 0.80 after exposure to the aggressive wet−dry cycles, in the absence (left) and in the presence (right) of fly ash.

appears hidden. In other words, fly ash cancels the detrimental effect, at least from a corrosion point of view, of great porosity of the cement matrix.

Moreover, Figure 8.2 shows that the use of galvanized steel reinforcement in fly ash concrete not only assures the concurrence of the technical and environmental benefits derived from the use of both steel galvanization and fly ash addition to concrete, but could further provide a useful synergic effect because of pozzolanic activity favoring the formation of a dense protective passive layer on the galvanized reinforcement that remains stable even in the presence of concrete cracks.

8.3   Effect of recycled aggregates in concrete on reinforcing steel corrosion

The manufacture of durable concrete for buildings can contribute to sustainable development construction (Mehta, 1997) based on principles, techniques, and materials that preserve natural resources and improve environmental quality by the use of recycling in concrete. Therefore, the concept of sustainable development includes, first and foremost, the judicious use of natural resources that are rapidly being depleted. One example is the use of industrial by-products, thereby reducing materials waste and carbon dioxide gas emissions due to cement production when used as supplementary cementing materials in partial cement replacement.

However, the use of other nonrenewable resources, such as natural aggregates, also needs to be reduced. This can be achieved by recycling rubble from demolished buildings that are no longer in service. The rubble can be processed in such a way that it can be used again in the original application as recycled aggregate (O'Brien, 1998). Replacing natural with recycled aggregate in concrete reduces the consumption of natural resources and protects natural site features. This also avoids the environmental impact resulting from quarries and allows a reduction in the volume of materials disposed in landfills (Desai, 1998; Hendriks and Pietersen, 1998; Uchikawa, 2000).

Experiments (Corinaldesi and Moriconi, 2001) allowed comparison between the structural properties of recycled-aggregate concrete, particularly when fly ash is added, and those of ordinary concrete for current applications. Moreover, structural service-ability in terms of corrosion tests on reinforced concrete (Hansen, 1992b), especially in the presence of cracks that generally affect all real concrete structures, with the only difference being crack width (Coleman, 2013), was also investigated (Moriconi, 2005). As a matter of fact, at the same concrete strength level, recycled instead of natural aggregate is not as important to the corrosion behavior of steel in concrete as is the pozzolanic action of fly ash by modifying the concrete environment in which steel reinforcement is embedded. However, when fly ash is added to recycled-aggregate concrete, the pore structure is improved, and particularly the volume of macropores is reduced, causing benefits in terms of mechanical performance such as compressive, tensile, and bond strengths (Corinaldesi et al., 2002). Similar performances are achieved using an ordinary concrete prepared with natural aggregate, the only difference being somewhat less stiffness of recycled-aggregate concrete containing fly ash; this aspect should be taken into account during structural designing.

According to the concept of sustainable development, the environmental load of a building must be evaluated throughout its life cycle—that is, from design to construction, maintenance and repair, demolition, and rubble disposal (Van Loo, 1998). Therefore, from a holistic point of view, sustainable construction means designing a reinforced concrete structure with appropriate durability during a specified service life. Overdesigned structures should be avoided because they represent energy and resource waste; on the other hand, underdesigned structures can cause excessive repair costs and environmental loads. To reduce maintenance costs of reinforced concrete structures, concrete cracking and the corrosion of steel reinforcement should be counteracted in particular. This can be achieved by, for instance, correctly designing concrete mixture proportions, adequate protection to the steel reinforcement, and structural detailing.

Additional reinforcement protection such as galvanization (Yeomans, 1994; Fratesi et al., 1996) can be used to reduce repair costs and environmental loads. Since galvanization protection seems to be favored by the alkalinity reduction (Andrade et al., 1983) of the concrete pore solution, which can be achieved by fly ash addition because of its pozzolanic activity, the corrosion resistance of galvanized steel in a so-called sustainable cracked concrete containing fly ash and/or recycled aggregate should be also considered.

The results and considerations that follow, regarding the influence of using fly ash and/or recycled aggregate on the corrosion behavior of cracked reinforced concrete, derive from a wide investigation (Moriconi, 2005) carried out through corrosion tests on well-cured concrete specimens reinforced with either bare or galvanized steel in the presence of concrete cracks reaching the reinforcement. Also in this investigation, steel plates were used as reinforcement instead of bars in order to modulate concrete specimen cracking and to significantly accelerate the corrosion process due to a much higher ratio of cathodic to anodic area. The corrosion process was monitored through free corrosion potential values of steel and polarization resistance measurements during specimen exposition to weekly wet−dry cycles (2 days dry followed by 5 days wet) in a 10% NaCl solution simulating a particularly aggressive environment such
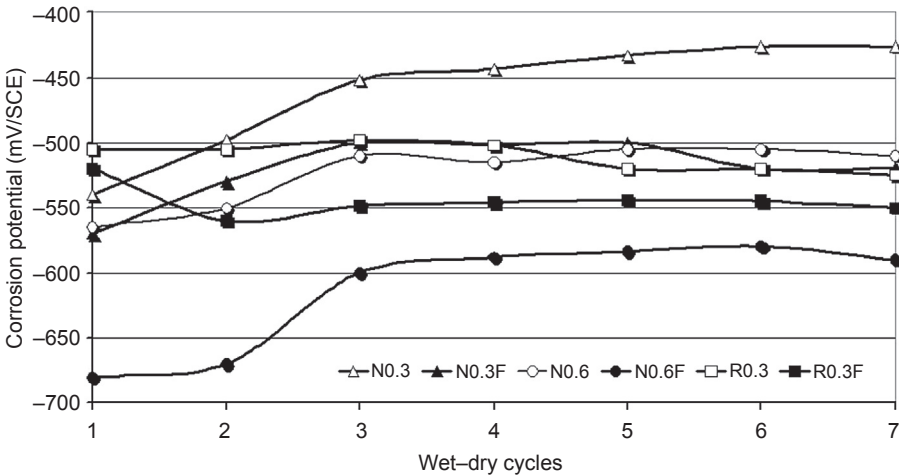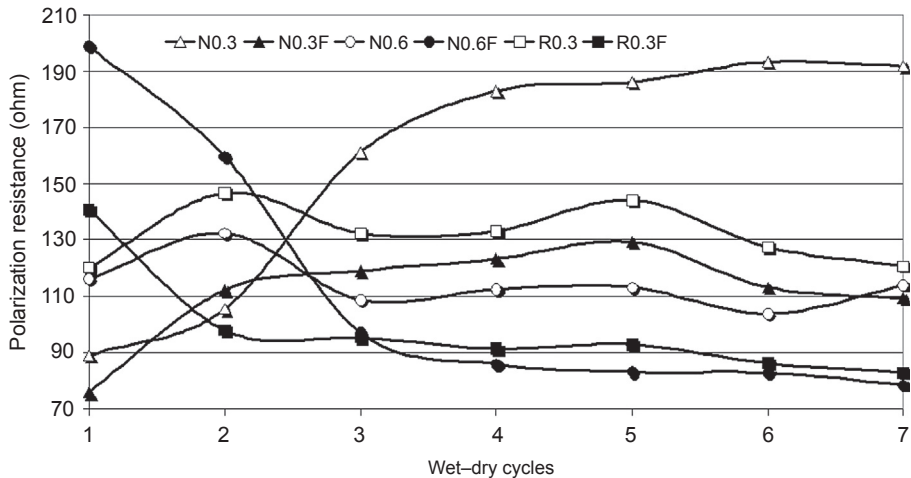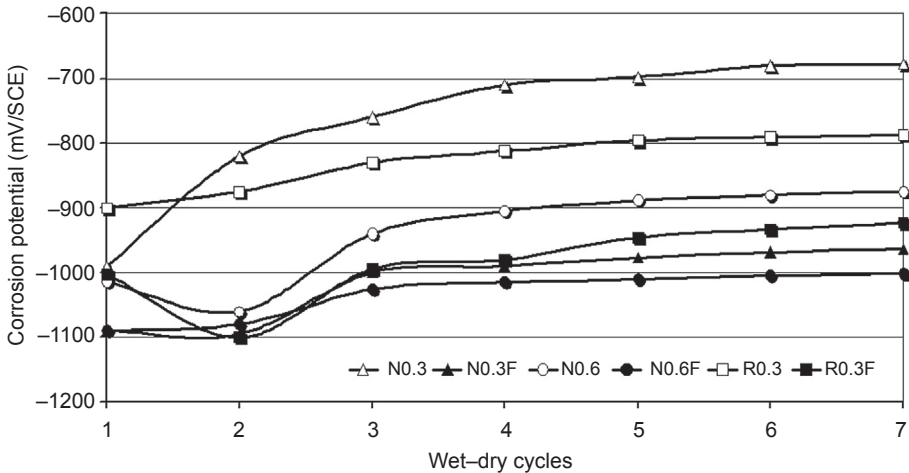
Figure 8.3 The influence of recycled aggregates (R) and/or fly ash addition (F) on the free corrosion potential of bare steel embedded in cracked concrete as a function of wet−dry cycles in 10% NaCl aqueous solution.

as deicing salt treatment. Finally, different concrete mixtures (identified through the aggregate type, N for natural and R for recycled; the water/cement ratio, 0.3 or 0.6; and fly ash addition, F when added) were deliberately chosen in order to classify the manufactured concretes into three different strength grades,[3] respectively equal to 50−60 MPa, 30−40 MPa, and 10−20 MPa.

Figures 8.3 and 8.4 show the free corrosion potential values and polarization resistance measurements, respectively, of bare steel embedded in cracked concrete (with natural as well as recycled aggregates and/or fly ash addition) as a function of wet−dry cycles.

The data reported in these figures indicate that replacing natural with recycled aggregate and/or adding high-fly-ash volume to the concrete mixture does not seem to negatively affect the corrosion behavior of the embedded steel reinforcements as far as the same strength class is concerned.

Indeed, it can be observed that just after exposure to the chloride environment, the steel assumes activation values lower than −500 mV/SCE regardless of the cement matrix type, reflecting a generally high corrosion risk. However, after a few wet−dry cycles, the steel embedded in the most porous concretes (N0.6F and R0.3F) show the highest corrosion risk with the lowest corrosion potential values. On the contrary, the steel embedded in the reference high-quality concrete (0.3N) shows the lowest

---

[3] N0.3 concrete belongs to the highest strength class as a reference high-quality concrete. Ordinary concretes generally used with compressive strength of about 30−40 MPa are represented by N0.6 concrete. N0.3F and R0.3 concretes belong to this strength class, because in the presence of fly ash or recycled aggregate, the water-to-cementitious-material ratio has to be lowered to 0.3 in order to achieve the same strength class value. Finally, poor-quality concretes with compressive strengths of about 10−20 MPa are represented by R0.3F and N0.6 concretes.

Figure 8.4 The influence of recycled aggregates (R) and/or fly ash addition (F) on the polarization resistance of bare steel embedded in cracked concrete as a function of wet−dry cycles in 10% NaCl aqueous solution.

corrosion risk. Finally, the steel embedded in other concrete mixtures belonging to the ordinary class strength (30−40 MPa) assumes corrosion potential values converging toward intermediate corrosion risk.

The corrosion behavior described by the corrosion potential measurements is completely confirmed by the polarization resistance measurements. Also, the corrosion resistance of the steel reinforcement seems to depend mainly on the mechanical strength of the cracked concrete regardless of the cementitious matrix type. In this case, obviously the higher the concrete strength class, the higher the corresponding polarization resistance. As a matter of fact, in ordinary concrete with compressive strength of about 30 MPa, recycled-aggregate concretes and high-fly-ash-volume concretes show higher polarization resistances. Moreover, the results obtained could dispel any doubt about the uncertain corrosion behavior of steel in high-fly-ash-volume concrete due to the concrete pore solution alkalinity reduction caused by fly ash pozzolanic activity, at least in the presence of cracks in concrete.

However, the electrochemical tests represent a partial feature of the reinforcement corrosion behavior, since instantaneous measurements can only be carried out during the wet period and there is no chance to estimate the metal surface area effectively corroding. Therefore, after seven wet−dry cycles, all the specimens were split in order to visually evaluate the corroded area and assess the weight loss of the bare steel after pickling (Figure 8.5).

All the reinforcements are characterized by a strong corrosive attack in the crack area that can be justified by the high chloride concentration detected on the reinforcement surface (2%−5% by cement weight), significantly greater than the concentration threshold (0.4% by cement weight) generally reported as the critical value capable of inducing the corrosion process in bare steel.

Figure 8.5 Visual observation of the corrosive attack on bare steel plates embedded in reference natural-aggregate concrete N0.3 (left), in recycled-aggregate concrete R0.3 (middle), and high-fly-ash-volume concrete N0.3F (right).

However, from a morphological point of view (Figure 8.5), in the presence of recycled aggregate, and particularly fly ash, the corrosive attack appears more diffuse and less penetrating with respect to that detected on the steel plate embedded in the reference concrete, where a more localized corrosive attack could also induce the steel plate blanking in spite of the very low water/cement ratio.

Figures 8.6 and 8.7 show the free corrosion potential values and the polarization resistance measurements, respectively, of galvanized steel embedded in cracked concrete as a function of wet−dry cycles.

It can be observed in Figure 8.6 that just after exposure to the aggressive environment, the corrosion potential of the galvanized steel plates assumes initial active values of about −1000 mV/SCE regardless of concrete type. During the wet−dry cycles, also in the case of galvanized steel reinforcement, a higher corrosion risk represented by low potential values is recorded for poor-quality concrete (N0.6F and R0.3F). The reference high-quality concrete (0.3N) assumes the highest potential values, and the

Figure 8.6 The influence of recycled aggregates (R) and/or fly ash addition (F) on the free corrosion potential of galvanized steel embedded in cracked concrete as a function of wet−dry cycles in 10% NaCl aqueous solution.
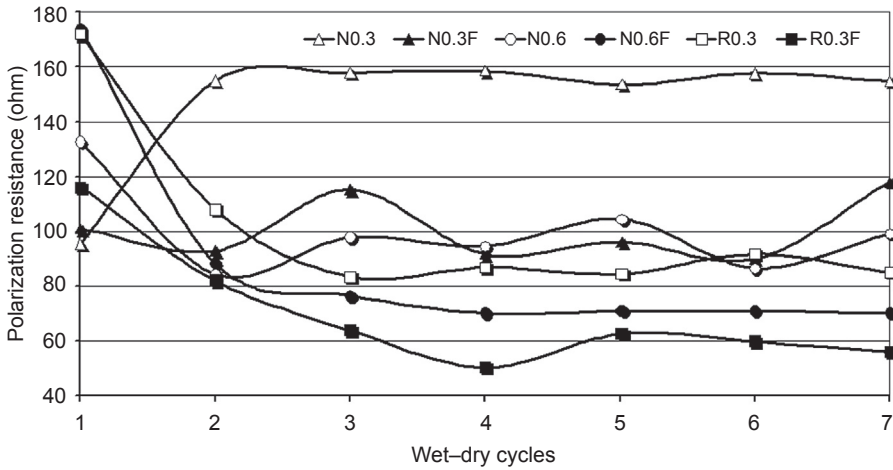
Figure 8.7 The influence of recycled aggregates (R) and/or fly ash addition (F) on the polarization resistance of galvanized steel embedded in cracked concrete as a function of wet−dry cycles in 10% NaCl aqueous solution.

ordinary concretes (R0.3, N0.6 N0.3F) showed intermediate values, indicating the lowest and intermediate corrosion risk, respectively.

The polarization resistance measurements carried out on galvanized steel reinforcements (Figure 8.7) again exhibit good agreement with the potential values for bare steel, by confirming the already stated hierarchy related to the concrete strength class.

However, the inspection carried out on the steel plates extracted from concrete specimens in this case (Figures 8.8−8.10) reveals additional unexpected information with respect to that obtained by the electrochemical measurements.

As a matter of fact, in the reference high-quality concrete (0.3N), where the reinforcement polarization resistance is high, the corrosive attack appears to be very localized at the crack apex and also very deep, even showing easily recognizable iron corrosion products (Figure 8.8(a)). Moreover, far from the crack apex, Fe−Zn alloy appears on the plate surface, meaning that total consumption of the pure zinc layer
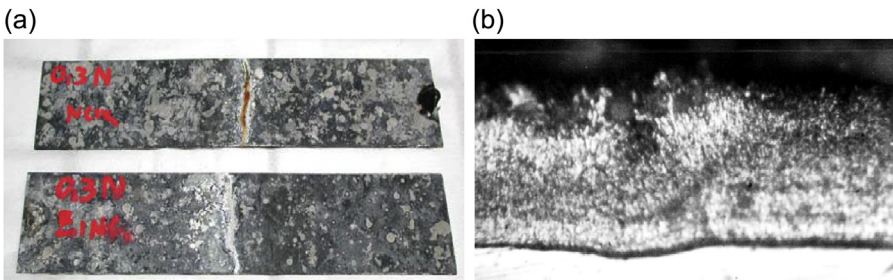
Figure 8.8 Visual observation (a) and metallographic cross section (b) of galvanized steel plates embedded in reference concrete (0.3N).

(a)   (b)
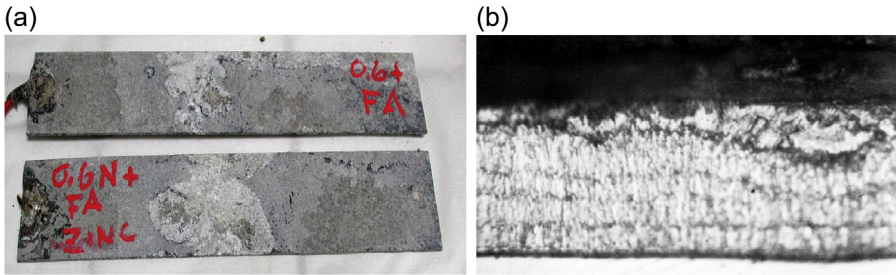
Figure 8.9 Visual observation (a) and metallographic cross section (b) of galvanized steel plates embedded in high-fly-ash-volume concrete (0.6NF).

(a)   (b)
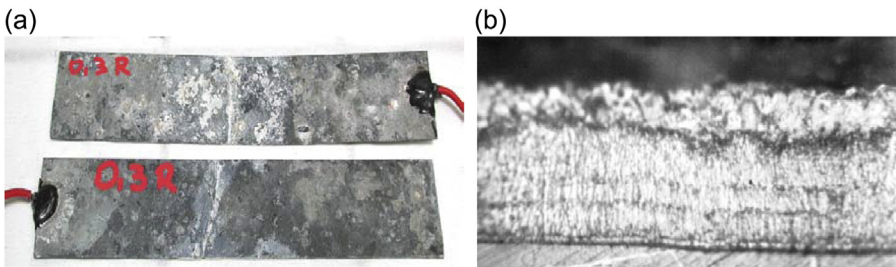
Figure 8.10 Visual observation (a) and metallographic cross section (b) of galvanized steel plates embedded in recycled-aggregate concrete (0.3R).

due to the corrosive attack occurred, as later confirmed by metallographic analysis (Figure 8.8(b)).

On the other hand, the galvanized steel plates extracted from concrete with a high volume of fly ash showed a surface coating made of zinc corrosion products (Figure 8.9(a)), later identified by X-ray diffraction as calcium hydroxyzincate. Calcium hydroxyzincate is a well-passivating zinc corrosion product (Duval and Arliguie, 1974; Macias and Andrade, 1987b) whose formation seems to be effectively favored by the low alkalinity of the concrete pore solution (Andrade et al., 1983), as achieved when a high volume of fly ash is added because of its pozzolanic activity. Once formed, calcium hydroxyzincate protects the underlying pure zinc layer from further corrosion, as later metallographic analysis on the cross section of the galvanized plates embedded in high-fly-ash-volume concrete put well into evidence (Figure 8.9(b)).

Unexpectedly, the galvanized steel plates extracted from the cracked recycled-aggregate concrete specimens show the lowest corrosive attack. Zinc grains are still highly visible on the galvanized plate surface after the aggressive exposure (Figure 8.10(a)), and metallographic observation reveals a continuously thick pure zinc layer still present on the reinforcements (Figure 8.10(b)).

Results previously obtained concerning the effect of fly ash on the corrosion behavior of galvanized steel reinforcement (Corinaldesi et al., 2002) must be underlined and are consistent with the results reported here. Those results showed that the

presence of fly ash always improves the corrosion resistance of galvanized steel reinforcement. In particular, the addition of fly ash as replacement of fine aggregate, even in the presence of concrete cracks, decreases the corrosion rate values in very porous concrete (such as for w/c = 0.80) to those obtained in good-quality concrete (such as for w/c = 0.45). In other words, the addition of fly ash can remove the detrimental effect of the high porosity of a cement matrix on the induction and propagation of corrosion. This beneficial effect can be attributed to the pozzolanic action of fly ash, mainly by lowering the pore solution alkalinity to cause better zinc passivation rather than reducing concrete porosity, which is at any rate a welcome effect to counteract reinforcement corrosion.

8.4 Concluding remarks

In conclusion, we can state that:

- using a high volume of fly ash and/or recycled aggregate in concrete has no deleterious effect on the corrosion behavior of bare steel reinforcements for similar concrete strength classes; indeed, especially when fly ash is added, the morphology of the corrosive attack turns more diffuse and less penetrating;
- the use of a high volume of fly ash in concrete significantly affects the corrosion behavior of galvanized reinforcement embedded in cracked concrete by generally improving its corrosion resistance; this is also true in very aggressive chloride environments and in the presence of cracks in concrete.

However, the most important conclusion that can be drawn from the experience described in this chapter is that the addition of fly ash to the concrete mixture, even at very high volume fractions, has no side effects as far as steel reinforcement corrosion is concerned. In fact, if on the one hand fly ash addition reduces concrete pore solution alkalinity by altering the passivity conditions of steel reinforcement, on the other hand it improves significantly the concrete microstructure, by making more and more difficult the penetration of aggressive agents and the onset of corrosion, hindered even when galvanized steel reinforcement is used.

References

Andrade, C., Macias, A., 1988. Galvanized reinforcements in concrete. In: Wilson, A.D., Nicholson, J.W., Prosser, H.J. (Eds.), Surface Coatings-2. Elsevier Applied Science, New York, USA, pp. 137−182.

Andrade, C., Molina, A., Huete, F., Gonzalez, J.A., 1983. Relation between the alkali content of cements and the corrosion rates of the galvanized reinforcements. In: Crane, A.P. (Ed.), Corrosion of Reinforcements in Concrete Constructions. The Society of Chemical Industry, London, UK, pp. 343−355.

Berry, E.E., Malhotra, V.M., 1986. Fly Ash in Concrete. Dept. of Energy, Mines and Resources, Ottawa, Canada.

Branca, C., Fratesi, R., Moriconi, G., Simoncini, S., 1992. Influence of Fly Ash on Concrete Carbonation and Rebar Corrosion, in Malhotra VM, Fly Ash, Silica Fume, Slag and Natural Pozzolans in Concrete. American Concrete Institute, Detroit, USA, pp. 245−255. SP-132.

Coleman, J.W., 2013. Cracking… defect or normal? Concrete International 35 (9), 35−38.

Collepardi, M., Marcialis, A., Turriziani, R., 1972. Penetration of chloride ions into cement pastes and concretes. Journal of American Ceramic Society 53, 534−535.

Corinaldesi, V., Gnappi, G., Moriconi, G., Montenero, A., 2005. Reuse of ground waste glass as aggregate for mortars. Waste Management 25, 197−201.

Corinaldesi, V., Moriconi, G., 2001. Role of Chemical and Mineral Admixtures on Performance and Economics of Recycled Aggregate Concrete, in Malhotra VM, Fly Ash, Silica Fume, Slag and Natural Pozzolans in Concrete. American Concrete Institute, Farmington Hills, USA, pp. 869−884. SP 199.

Corinaldesi, V., Moriconi, G., 2010a. Recycling of rubble from building demolition for low-shrinkage concretes. Waste Management 30 (4), 655−659.

Corinaldesi, V., Moriconi, G., 2010b. Characterization of mechanical and elastic behaviour of concretes made of recycled-concrete aggregates. In: Nzihou, A., Liu, H. (Eds.), Engineering for Waste and Biomass Valorisation (WasteEng10). Ecole des Mines d'Albi-Carmaux, Albi, France. 048-C.

Corinaldesi, V., Moriconi, G., Tittarelli, F., 2002. Sustainable and Durable Reinforced Concrete Construction, in Malhotra VM, Innovations in Design with Emphasis on Seismic, Wind and Environmental Loading, Quality Control and Innovations in Materials/Hot-Weather Concreting. American Concrete Institute, Farmington Hills, USA, pp. 169−186. SP-209.

Desai, S.B., 1998. Sustainable Development and Recycling of Concrete Aggregate, in Dhir RK, Henderson NA, Limbachiya MC, Use of Recycled Concrete Aggregate. Thomas Telford Publishing, London, UK, pp. 381−388.

Duval, R., Arliguie, G., 1974. Passivation du zinc dans l'hydroxyde de calcium, eu regard au comportement de l'acier galvanisè dans le beton. Memoires Scientifiques Review Metal-lurgy LXXXI (11), 719−727.

Francois, R., Arliguie, G., Castel, A., 1998. Influence of service cracking on service life of reinforced concrete. In: Gjørv, O.E., Sakai, K., Banthia, N. (Eds.), Concrete under Severe Conditions (CONSEC '98). E & FN Spon, London, UK, pp. 143−152.

Fratesi, R., Moriconi, G., Coppola, L., 1996. The influence of steel galvanization on rebars behaviour in concrete. In: Page, C.L., Bamforth, P.B., Figg, J.W. (Eds.), Corrosion of Reinforcement in Concrete Construction. SCI Special Publication No. 183, London, UK, pp. 630−641.

Fratesi, R., Moriconi, G., Tittarelli, F., 2002. Corrosion protection by galvanised reinforcement in cracked concrete structures containing fly ash. In: Dhir, R.K., Hewlett, P.C., Csetenyi, L.J. (Eds.), Innovations and Developments in Concrete Materials and Con-struction. Thomas Telford, London, UK, pp. 383−390.

Gonzales, J.A., Alonso, C., Andrade, C., 1983. Corrosion rate of reinforcements during accelerated carbonation of mortars made with different types of cement. In: Crane, A.P. (Ed.), Corrosion of Reinforcements in Concrete Construction. Ellis Horwood, Chichester, UK, pp. 159−174.

Hansen, T.C., 1992a. Recycling of Demolished Concrete and Masonry, Report of Technical Committee 37-DRC. RILEM Report 6. E & FN Spon, London, UK.

Hansen, T.C., 1992b. Recycled Aggregates and Recycled Aggregate Concrete, in Hansen TC, Recycling of Demolished Concrete and Masonry. E & FN Spon/Chapman & Hall, London, UK, pp. 92−94.

Hendriks, C.F., Pietersen, H.S., 1998. Concrete: durable but also sustainable? In: Dhir, R.K., Henderson, N.A., Limbachiya, M.C. (Eds.), Use of Recycled Concrete Aggregate. Thomas Telford Publishing, London, UK, pp. 1−17.

Ho, N., Lee, Y., Lim, W., Zayed, T., Chew, K., Low, G., Ting, S., 2013. Efficient utilization of recycled concrete aggregate in structural concrete. Journal of Materials in Civil Engineering 25 (3), 318−327.

Holland, T.C., 2005. Silica Fume User's Manual. Silica Fume Association, Lovettsville, USA.

Kou, S., Poon, C., Agrela, F., 2011. Comparisons of natural and recycled aggregate concretes prepared with the addition of different mineral admixtures. Cement and Concrete Composites 33 (8), 788−795.

Letelier González, V.C., Moriconi, G., 2014. The influence of recycled concrete aggregates on the behavior of beam−column joints under cyclic loading. Engineering Structures 60, 148−154.

Macias, A., Andrade, C., 1983. Corrosion rate of galvanized steel immersed in saturated solutions of $Ca(OH)_2$ in the pH range 12−13.8. British Corrosion Journal 18 (2), 82−87.

Macias, A., Andrade, C., 1987a. Corrosion of galvanized steel reinforcements in alkaline solutions. British Corrosion Journal 22 (2), 113−118.

Macias, A., Andrade, C., 1987b. Corrosion of galvanized steel in dilute $Ca(OH)_2$ solutions pH 11.1−12.6. British Corrosion Journal 22 (3), 162−171.

Malešev, M., Radonjanin, V., Marinković, S., 2010. Recycled concrete as aggregate for structural concrete production. Sustainability 2 (5), 1204−1225.

Malhotra, V.M., 1978. Use of Recycled Concrete as New Aggregate. CANMET, Ottawa, Canada, pp. 4−16. Report No. 76-8.

Malhotra, V.M., Mehta, P.K., 2002. High-Performance, High-Volume Fly Ash Concrete: Materials, Mixture Proportioning, Properties, Construction Practice, and Case Histories. Supplementary Cementing Materials for Sustainable Development Inc., Ottawa, Canada.

Mehta, P.K., 1989. Pozzolanic and Cementitious By-Products in Concrete − Another Look, in Malhotra VM, Use of Fly Ash, Silica Fume, Slag, and Natural Pozzolans in Concrete. American Concrete Institute, Detroit, USA, pp. 1−43.

Mehta, P.K., 1997. Bringing the Concrete Industry into a New Era of Sustainable Development, in Mehta PK, Advances in Concrete Science and Technology. American Concrete Institute, Farmington Hills, USA, pp. 49−67.

Moriconi, G., 2005. Reinforcement corrosion experience with concrete mixtures containing fly ash. In: Bhanumathidas, N., Kalidas, N. (Eds.), Concrete Technology for Sustainable Development with Emphasis on Infrastructure, Hyderabad, India, pp. 69−81.

Naik, T.R., Moriconi, G., 2005. Environmental-friendly durable concrete made with recycled materials for sustainable concrete construction. In: Malhotra, V.M., Sakai, K. (Eds.), Sustainable Development of Cement, Concrete and Concrete Structures, Toronto, Canada, pp. 485−505.

Naik, T.R., Ramme, B.W., 1989. High strength concrete containing large quantities of fly ash. ACI Materials Journal 86 (2), 111−117.

Niang, A., Roy, N., Tagnit-Hamou, A., 2014. Structural behavior of concrete incorporating glass powder used in reinforced concrete columns. Journal of Structural Engineering, 10.1061/(ASCE)ST.1943-541X.0000986.

O'Brien, K., 1998. Using recycled aggregate concrete as part of an overall approach to sustainable construction. In: Dhir, R.K., Henderson, N.A., Limbachiya, M.C. (Eds.), Use of Recycled Concrete Aggregate. Thomas Telford Publishing, London, UK, pp. 459−470.

Sani, D., Moriconi, G., Fava, G., Corinaldesi, V., 2005. Leaching and mechanical behaviour of concrete manufactured with recycled aggregates. Waste Management 25 (2), 177−182.

Shao, Y., Lefort, T., Moras, S., Rodriguez, D., 2000. Studies on concrete containing ground waste glass. Cement and Concrete Research 30 (1), 91−100.

Shayan, A., Xu, A., 2006. Performance of glass powder as a pozzolanic material in concrete: a field trial on concrete slabs. Cement and Concrete Research 36, 457−468.

Swamy, R.N., 1990. Resistance to chlorides of galvanized rebars. In: Page, C.L., Tradway, K.W.J., Bamforth, P.B. (Eds.), Corrosion of Reinforcement in Concrete. The Society of Chemical Industry, London, UK, pp. 586−600.

Taha, B., Nounu, G., 2009. Utilizing waste recycled glass as sand/cement replacement in concrete. Journal of Materials in Civil Engineering 21 (12), 709−721.

Tittarelli, F., Moriconi, G., 2010. Use of GRP industrial by-products in cement based composites. Cement & Concrete Composites 32 (3), 219−225.

Uchikawa, H., 2000. Approaches to ecologically benign system in cement and concrete industry. Journal of Materials in Civil Engineering 12 (4), 320−329.

Van Loo, W., 1998. Closing the concrete loop—from reuse to recycling. In: Dhir, R.K., Henderson, N.A., Limbachiya, M.C. (Eds.), Use of Recycled Concrete Aggregate. Thomas Telford Publishing, London, UK, pp. 83−97.

Yeomans, S.R., 1994. Performance of black, galvanized, and epoxy-coated reinforcing steels in chloride-contaminated concrete. Corrosion 50 (1), 72−81.

Corrosion measurement and evaluation techniques of steel in concrete structures

9

Amir Poursaee
Clemson University, Clemson, SC, USA

9.1 Introduction

Corrosion consists of electrochemical reactions at the interface between the metal and an electrolyte solution. During the anodic reaction, a metal is oxidized and releases electrons. These electrons are consumed by the cathodic reaction in which the reduction occurs. By equating these two reactions, a corrosion current, I_{corr}, which is the corrosion rate and half-cell potential (also called corrosion potential or open circuit potential), E_{corr}, which is the probability of corrosion, can be found.

E_{corr} is equivalent to the voltage of a cell or battery versus a reference electrode under no-load conditions and can be measured with a high impedance voltmeter or potentiometer (Elsener et al., 2003; Corrosion Doctors, 2005). I_{corr} cannot be measured directly but it can be estimated by using electrochemical techniques while E_{corr} must be determined as the potential difference between that of the metal/electrolyte interface and a reference electrode, as described in Chapter 1.

As mentioned, corrosion of steel in concrete occurs via electrochemical reactions. Therefore, electrochemical techniques are ideal for the study of the corrosion processes. Usually, in electrochemical measurements, a cell consists of a working electrode (the corroding metal), a counter electrode, a reference electrode and electrolyte. All of the electrodes are connected to a potentiostat which allows the potential of the metal to be changed in a controlled manner and the resultant current flow to be measured as a function of potential. This changing of the potential is called "polarization." When the polarization is done potentiostatically (controlled by potential), the current is measured, and when it is done galvanostatically (controlled by current), the potential is measured (Fontana, 1987; Jones, 1992; Gamry Instruments, 2005a).

9.2 Half-cell potential technique

The half-cell potential technique is the most widely used technique to evaluate the corrosion of the steel reinforcing bars (rebars) in concrete. It was introduced in the 1950s by Richard F. Stratfull in North America and by the Danish Corrosion Center in Europe (Stratfull, 1954; Gronvold and Arup, 1979). In 1980, the test was approved as a standard by the ASTM (2009). This technique is based on measuring the

electrochemical potential of the steel rebar with respect to a standard reference electrode (copper/copper sulfate electrode (CSE) is suggested by the ASTM-C876) placed on the surface of the concrete, and can provide an indication of the corrosion risk of the steel. Figure 9.1 shows the basics of half-cell potential measurement.

According to the ASTM C876 recommended guidelines for interpreting the results, if the measured potential is more negative than -350 mV versus the CSE, the probability of active corrosion is more than 90%. If the measured potential is more positive than -200 mV versus the CSE, the probability of the rebar being passive is 90% and between -200 mV and -350 mV is the uncertainty region. The most common way of presenting the half-cell potential data is plotting the potential distribution or potential contour mapping. It should be emphasized that since half-cell potential value is defined as the thermodynamic measure of the ease of removing electrons from the metal in steady state condition, it cannot be used as measurement of corrosion rate. A simple comparison of the half-cell potential data with the ASTM guidelines on steel reinforcement corrosion probability could cause mistakes in the evaluation of the structure. Although it is generally accepted by the practitioners that a more negative reading of potential means a higher probability of corrosion, this general rule may not always be correct. Some precautions are necessary in interpreting the data from half-cell potential measurements because many factors can affect the magnitude of the potentials (Poursaee and Hansson, 2009).
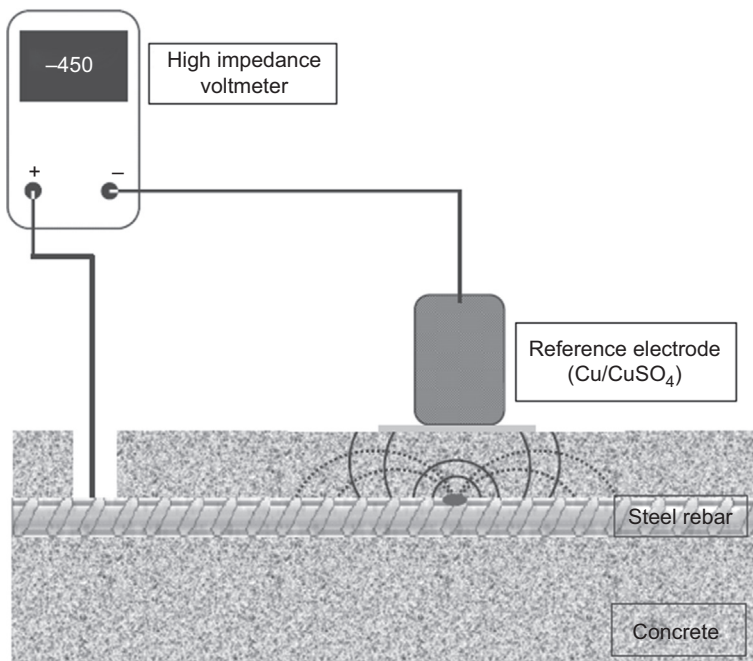
Figure 9.1 Apparatus for half-cell potential method described in ASTM C876 to measure surface potential associated with corrosion current.

9.3 Linear polarization resistance (LPR)

Figure 9.2 shows a schematic plot of the relationship between potential and current in the region of the open circuit potential. The curve plots the applied potential versus measured current or vice versa. As shown in Figure 9.2, there is an approximately linear region around the open circuit potential. The LPR measurements are performed by applying a potential in the range of ±10 mV about the E_{corr}, either as a constant pulse (potentiostatic) or a potential sweep (potentiodynamic), and measuring the current response. Alternatively, a current pulse (galvanostatic) or a current sweep (galvanodynamic) can be applied, and potential response is measured. Polarization resistance (R_p) is the resistance of the specimen to oxidation while an external potential is applied and the corrosion current which is inversely related to the R_p can be calculated from it.

R_p is determined by calculating the slope of this linear region:

$$R_p = \frac{\Delta E}{\Delta I} \tag{9.1}$$

where, ΔE = change in potential and ΔI = change in current. The Stern−Geary equation relates corrosion current to R_p (Stern and Geary, 1957):

$$I_{corr} = \frac{B}{R_p} \tag{9.2}$$

$$B = \frac{\beta_a \beta_c}{2.3(\beta_a + \beta_c)} \tag{9.3}$$
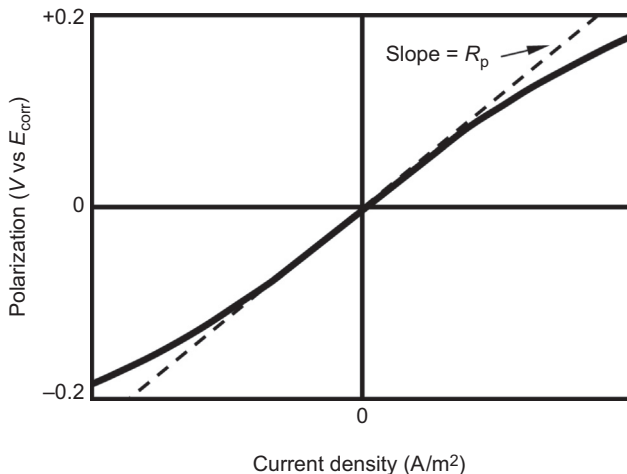
Figure 9.2 Schematic illustration of the linear polarization curve.

The corrosion current density, i_{corr}, can be calculated by dividing the corrosion current (I_{corr}) by the surface area of the polarized area (A):

$$i_{corr} = \frac{B}{R_p A} \tag{9.4}$$

B is Stern−Geary constant and β_a and β_c are anodic and cathodic Tafel constants, respectively. The value of B should be determined, empirically. However, for most cases, it is assumed to be 0.026 V for active and 0.052 V for passive corrosion of steel in concrete (Andrade and González, 1978; Andrade et al., 1990).

The resistance measured by the LPR actually is the sum of the polarization resistance, R_p, and the electrolyte resistance, R_Ω. If $R_p \gg R_\Omega$, the resistance which is measured by the LPR is close enough to the polarization resistance that can be used as the actual value. However, in some environments, such as concrete, the R_Ω is significant and should be considered (Jones, 1992).

According to some researchers, corrosion current densities over $\sim 1\ \mu A/cm^2$ are identified as the level of high corrosion risk and corrosion current density below $0.1\ \mu A/cm^2$ are characterized as passive corrosion in the system (Gonzalez et al., 1995; Alonso et al., 2000; Polder and Peelen, 2002). However, it seems that the equipment used by these researchers generally gives lower values than the other commercial equipment (Gepraegs, 2002). Therefore, applying such definitions may over- or underestimate the corrosion rate and cause errors in evaluations and life predictions. Interpreting the corrosion current density values of embedded steel bars in concrete, obtained from the LPR technique is difficult in large part because determining the actual corroding area of steel is almost impossible and usually causes underestimation of the actual corrosion current density in the areas of active corrosion. The LPR has some advantages over the other measurement techniques which make it popular in the evaluation of the corrosion rate in reinforced concrete: it is a nondestructive technique; it is a simple method and it usually needs only a few minutes for corrosion rate determination. Because of its rapidity, it can effectively be used in kinetic studies of corrosion monitoring (Jones, 1992).

9.3.1 Potentiostatic LPR (potentiostatic transient technique)

In the potentiostatic LPR technique, a constant potential signal (usually ± 10 mV or, for steel embedded in concrete ± 20 mV) in the form of square wave between the working electrode (steel bar in concrete) and reference electrode and the response current is measured. The period of application of the potential is determined by time for current to reach steady state, by using Eqn (9.1), the R_p and hence, the corrosion current density and corrosion rate can be calculated. Figure 9.3 schematically shows the applied potential and current response during potentiostatic transient measurement.

This technique can also be used to directly determine the corrosion current density of steel rebars without using Stern−Geary constant (B value) (Poursaee, 2010).
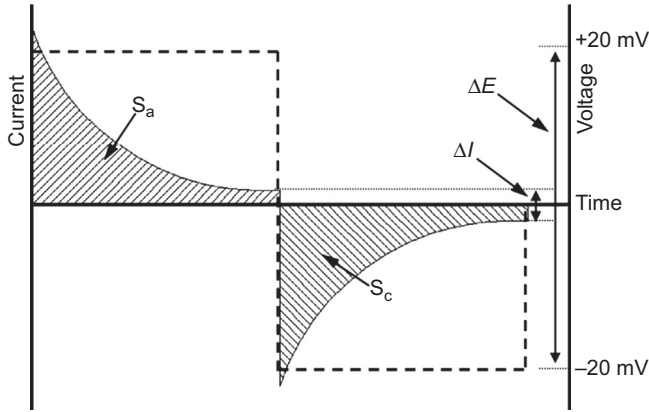
Figure 9.3 Applied potential and current response during potentiostatic LPR measurement.

When steel is polarized, the charge consumed from time $t = 0$ to t can be written as follows:

$$q_{total} = \int_0^t I \mathrm{d}t \tag{9.5}$$

where q_{total} is the consumed charge in coulomb, t is the time (s) and I is current (A). Therefore, the area under the current−time curves ($S_a + S_c$ in Figure 9.3) can be used to determine the consumed charge during the polarization process. It is imperative to note that this is the total consumed charge in both the interfacial corrosion process and the double layer capacitance. Therefore, the effect of capacitance should be considered in the calculations. The charge used by the double layer capacitance can be determined using Eqn (9.6):

$$q_{dl} = C_{dl} \times V \tag{9.6}$$

where C_{dl} is the double layer capacitance (F) and V is the potential (V). The value of the capacitance can be determined using electrochemical impedance spectroscopy or galvanostatic pulse technique. By deducting q_{dl} from q_{total}, the consumed charge during the corrosion processes can be calculated:

$$q_{corr} = \Delta q_{total} - q_{dl} \tag{9.7}$$

q_{corr} represents both charges obtained from anodic polarization and cathodic polarization with considering the effect of double layer capacitance. The mass loss during the polarization time can then be calculated by applying the Faraday's law as following:

$$m = \frac{q_{corr} \times M}{n \times F} \tag{9.8}$$

where m (g) is the mass loss during the polarization time, M is the atomic weight of steel (~ 55.845 g/mol for iron), n is the number of equivalent exchanged electrons (in this case considered 2) and F is Faraday's constant (96,500 C/mol). The amount of mass loss can be then determined per year and the penetration depth can be calculated as:

$$d = \frac{m_y}{n \times F} \tag{9.9}$$

where d is the penetration depth (μm/year), m_y is the mass loss per year (g) and A is the corroding area (cm^2). For iron, $M = 55.845$ g/mol, $\rho = 7.875$ g/cm^3, and $n = 2$, therefore:

$$i_{corr}\left(A/m^2\right) = \frac{\text{Corrosion rate } (\mu m/year)}{0.116} \tag{9.10}$$

9.4 Galvanostatic pulse technique

The galvanostatic pulse technique was introduced for field application in 1988 (Newton and Sykes, 1988). This method is a rapid nondestructive polarization technique. A short-time anodic current pulse is applied galvanostatically between a counter electrode placed on the concrete surface and the rebar. The applied current is usually in the range of $10-100$ μA and the typical pulse duration is between 5 and 30 s. The reinforcement is anodically polarized and the resulting change of the electrochemical potential of the reinforcement is measured with respect to a reference electrode and recorded as a function of polarization time (Klinghoffer, 1995; Elsener et al., 1997). A typical potential response for a corroding reinforcement is shown in the Figure 9.4.
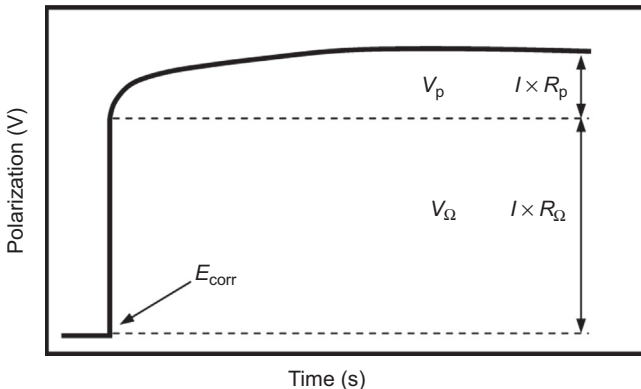
Figure 9.4 Schematic illustration of galvanostatic pulse results.
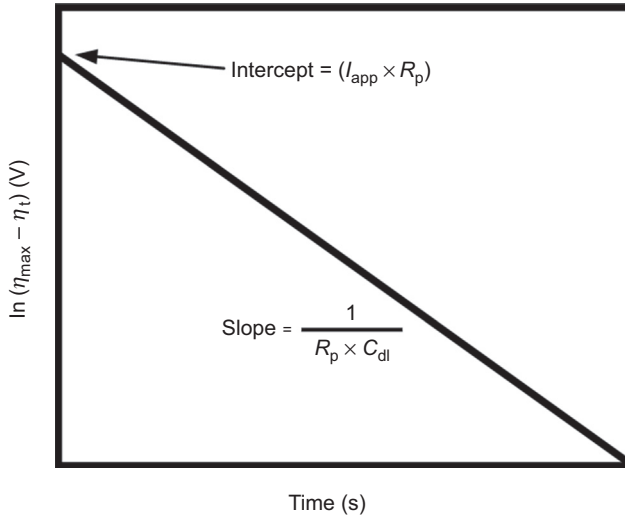
Figure 9.5 Schematic illustration of Eqn (9.12).

When the constant current, I_{app}, is applied to the rebar, the polarization of the rebar, η_t, at given time t can be expressed as (Jones and Greene, 1966):

$$\eta_t = I_{app} \times \left[R_p \times \left[1 - e^{\left(\frac{-t}{R_p C_{dl}}\right)} \right] + R_\Omega \right] \tag{9.11}$$

where: R_p = polarization resistance, C_{dl} = double layer capacitance and R_Ω = ohmic resistance of the concrete cover.

By transferring Eqn (9.11) to logarithmic form, the values of R_p and C_{dl}, can be calculated as following (Newton and Sykes, 1988):

$$\ln(\eta_{max} - \eta_t) = \ln(I_{app} \times R_p) - \left(\frac{t}{R_p C_{dl}}\right) \tag{9.12}$$

where η_{max} is the final steady state potential value. Figure 9.5 plots Eqn (9.12).

If the line through the data points is extrapolated to $t = 0$, it will give an intercept of $I_{app} \times R_p$ and the slope of the line in $1/R_p C_{dl}$. The remaining overpotential corresponds to $I_{app} \times R_\Omega$ which is the ohmic voltage drop across the concrete cover. After determining the polarization resistance (R_p) by using the above method, the corrosion current I_{corr} can be calculated from the Stern−Geary equation (Stern and Geary, 1957; Newton and Sykes, 1988), Eqn (9.2).

9.4.1 Equipment with the guard ring

An auxiliary counter electrode, referred to as a guard ring electrode, can be used to confine the polarization to a known length of reinforcing bar. The counter electrode
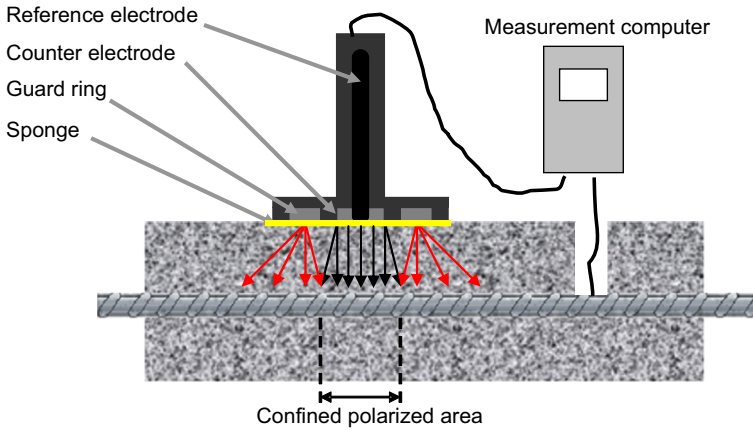
Figure 9.6 Schematic plan of the GalvaPulse™ with guarding to limit the polarized area while performing the corrosion measurement.

and the guard ring are typically arranged as annular metal rings with a reference electrode in the center. The potential or current applied from the guard ring is intended to repel the signals from the central counter electrode and confines them to an area of the structure located approximately under the counter electrode, as schematically shown in Figure 9.6.

There are two well-known commercially available instruments based on the galvanostatic pulse technique:

1. The GECOR is considered a galvanostatic pulse technique instrument although it is often referred to as an LPR device (Broomfield, 1996; Feliu et al., 1996; Newhouse and Weyers, 1996). The electrode assembly has a total of three reference electrodes, one located in the center and two located between the counter electrode and guard ring. The latter are used to adjust the guard electrode current to maintain the potential difference between the two reference electrodes constant during the polarization procedure.
2. The GalvaPulse is a galvanostatic pulse instrument developed by the FORCE Institute in Denmark. Signal confinement is over a 70-mm length of bar, and measurements can be made with or without the guard ring electrode. The measuring cell has an Ag/AgCl reference electrode at the center with a zinc counter electrode and a zinc guard ring.

9.5 Electrochemical impedance spectroscopy (EIS)

The EIS studies the system response to the application of a small amplitude alternating potential or current signal at different frequencies. The popularity of the EIS methods for reinforced concrete has increased remarkably in recent years, because analysis of the system response provides information about the double-layer capacitance, interface, structure, reactions which are taking place, corrosion rate and electrolyte (environment) resistance (Silverman, 1990; Jones, 1992; Lasia, 1999).

An electrochemical process can be considered as an electrical circuit with basic elements such as resistors, capacitors and inductors. Therefore, in interpreting the response to an alternating current, the AC circuit theory can be used successfully to demonstrate a corrosion process and also it may be used to understand the corrosion behavior and to predict the corrosion rates.

In direct current, Ohm's law is given as:

$$V = IR \tag{9.13}$$

where $V =$ Potential, $I =$ Direct current and $R =$ Actual resistor

In the AC condition, Ohm's law becomes:

$$V = IZ \tag{9.14}$$

where $V =$ Potential, $I =$ Amplitude of the alternating current and $Z =$ Impedance

Direct current can be viewed as alternating current at zero frequency. In this case, the resistance is composed of only one or more actual resistors. When the frequency is not zero, all circuit elements that can affect the flow of current, e.g., resistors, capacitors and inductors, cause the impedance. The created resistance by capacitors and inductors depends on frequency while that created by a resistor is not dependent on frequency (Silverman, 1986). A sinusoidal current or voltage can be represented as a rotating vector as shown in Figure 9.7. In the left-hand diagram of this figure, the x component shows the observed current so it becomes the real component of the rotating vector while the y component is a contribution that is not observed; therefore, it is named the imaginary component of the rotating vector.

The mathematical descriptions of the two components are as following:

$$\text{Real current} = I_x = |I| \cos(\omega t) \tag{9.15}$$

$$\text{Imaginary current} = I_y = |I| \sin(\omega t) \tag{9.16}$$

where $t =$ time and $\omega =$ frequency in radians per second $= 2\pi f$ ($f =$ frequency in hertz)
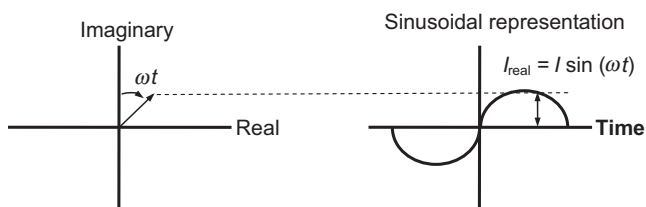
Figure 9.7 Relationship between sinusoidal alternating current and rotating vector representation.

To separate the real (x) and imaginary (y) components, the magnitude of the imaginary part should be multiplied by $j = \sqrt{-1}$[1] and then the real and imaginary values can be reported separately. The equations for AC impedance become:

$$E_{total} = E_{real} + E_{imaginary} = E' + jE'' \tag{9.17}$$

$$I_{total} = I_{real} + I_{imaginary} = I' + jI'' \tag{9.18}$$

$$Z_{total} = Z' + Z'' = \frac{E' + jE''}{I' + jI''} \tag{9.19}$$

Absolute amplitude, $|Z|$, of the impedance (that is the length of the vector) and the phase angle, θ, are defined by (Princeton Applied Research, 2000):

$$|Z| = \sqrt{Z'^2 + Z''^2} \tag{9.20}$$

$$\tan \theta = \frac{Z''}{Z'} \tag{9.21}$$

The goal of AC impedance is to measure the impedance Z as Z' and Z'', and then model the response by using an equivalent simple circuit (Silverman, 1986).

9.5.1 Data presentation

There are different ways to illustrate the response of an electrochemical system to an applied AC potential or current. The most common plots are the Nyquist plot and Bode plots. If, at each excitation frequency, the real part is plotted on the x-axis and the imaginary part is plotted on the y-axis of a chart, a "Nyquist plot" is formed. A simple corroding system can be assumed as: solution resistance, in series with a combination of a resistor and a capacitor, which represent the polarization resistance and double layer capacitance, respectively. This simple representation is called a Randles circuit and is shown in Figure 9.8.

Figure 9.9 schematically illustrates the Nyquist plot for a simple electrochemical system corresponding to the analogue circuit in Figure 9.8. It should be noted that each point on the Nyquist plot is the impedance at one frequency. On the Nyquist plot, the impedance can be represented as a vector of length $|Z|$ and the angle between this vector and the x-axis, is the phase angle "θ" (Princeton Applied Research, 2000; Gamry Instruments, 2006). At high frequencies, at the leftmost end of the semicircle, where the semicircle intersects the x-axis, the impedance of the Randles cell is entirely produced by the ohmic resistance, R_Ω. The frequency reaches its low limit at the

---

[1] Mathematicians use i to stand for $\sqrt{-1}$, but electrochemists use j to avoid confusion with i, the symbol for current.
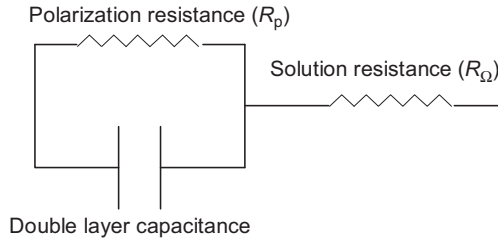
Figure 9.8 Equivalent circuit for a simple electrochemical system.
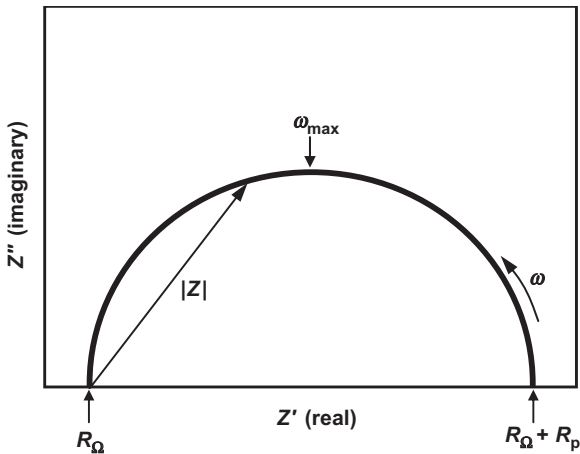
Figure 9.9 Nyquist plot for a simple electrochemical system.

rightmost end of the semicircle. At this frequency, the Randles cell also approximates a pure resistance, but now the value is $(R_\Omega + R_p)$ (Princeton Applied Research, 2000).

The Nyquist plot has some limitations (Princeton Applied Research, 2000):

1. The frequency is not clearly shown on the plot and it is not possible to determine, for a specific point, the frequency used to the record that point;
2. The ohmic and polarization resistances can be directly determined from the plot but the electrode capacitance can be only calculated if the frequency information is known, using Eqn (9.22):

$$C = \frac{1}{\omega_{max} \times R_p} \tag{9.22}$$

3. If there are high and low impedance components in the circuit, the larger impedance controls plot scaling and distinguishing the low impedance semicircle would probably be impossible.

Bode plots are another popular presentation method for the impedance data. In the Bode plot, the data are plotted with log of frequency on the abscissa and both the log of absolute value of the impedance ($|Z|$) and phase-shift (θ) on the ordinate
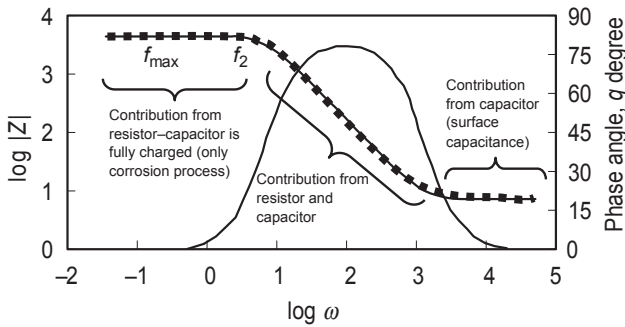
Figure 9.10 Bode plots of the frequency response (dotted line) and phase angle (solid line) for the an electrochemical system with $R_\Omega = 10\Omega$, $R_p = 1000\ \Omega$ and $C_{dl} = 93.8\ \mu F$. Adapted from Silverman (1998).

(Gamry Instruments, 2005b). Figure 9.10 shows a typical Bode plot for the same system as shown in Figure 9.8. Since the frequency appears as one of the axes in the Bode plot, it is easy to understand the dependence of impedance to the frequency from the plot. The log $|Z|$ versus log ω curve can be used to determine the values of R_p and R_Ω. At very high and very low frequencies, $|Z|$ becomes independent of frequency. At the highest frequencies the ohmic resistance controls the impedance and log (R_Ω) can be read from the high frequency horizontal level. On the other hand, at the lowest frequencies, log $(R_p + R_\Omega)$ can be read from the low frequency horizontal portion.

The Bode format is advantageous when data scatter prevents satisfactory fitting of the Nyquist semicircle. In general, the Bode plot provides a more understandable description of the frequency-dependent behavior of electrochemical system than does the Nyquist plot, in which frequency values are not clear (Princeton Applied Research, 2000).

9.6 Cyclic polarization

The cyclic potentiodynamic polarization technique is a relatively nondestructive measurement that can provide information about the corrosion rate, corrosion potential, susceptibility to pitting corrosion of the metal and concentration limitation of the electrolyte in the system. The technique is built on the idea that predictions of the behavior of a metal in an environment can be made by forcing the material from its steady state condition and monitoring how it responds to an increasing force and as the force is removed at a constant rate and the system is reversed to its original steady state condition. An applied potential is the force and is increased at a continuous, often slow, rate by using a potentiostat (Silverman). This rate is called polarization scan rate and is an experimental parameter. As the potential of the specimen is changed continuously, the resulting current is monitored and then the applied potential is plotted versus the logarithm of the resulting current density. The conductivity of the

electrolyte (environment) is a very important factor that should be considered in all electrochemical experiments, especially in cyclic polarization technique. The electrolyte resistance causes a potential drop between the working electrode and reference electrode and can cause errors. This effect has important impact on the interpretation, and should be compensated.

9.6.1 Scan rate

It is imperative that an appropriate cyclic polarization scan rate for the specific system under study be used; otherwise the results do not accurately reflect the corrosion behavior. To ascertain that the current/voltage relationship reflects only the interfacial corrosion process at every potential of the polarization scan, the effect of capacitance should be minimized. For this purpose, the capacitor should remain fully charged; otherwise, some of the current generated would reflect charging of the surface capacitance in addition to the polarization resistance and the measured current would then be greater than the current actually produced by the corrosion reactions. To reduce the effect of the capacitance, the scan rate should be slow enough to keep the capacitance fully charged during the experiment. In this case, the current-potential relationship just reflects the polarization resistance (interfacial corrosion process) at every potential of the polarization scan (Silverman, 1998).

Because, the capacitance and resistance are functions of the material, environment and the applied potential, choosing the appropriate scan rate is not an easy decision. An outline of an approach to determine the maximum scan rate is given by Mansfeld (Mansfeld and Kendig, 1981). The principle of the method is based on the Bode plot, Figure 9.9, represented by Randles circuit (Figure 9.7). At low frequencies, $|Z| = R_\Omega + R_p$; therefore, in order to determine the polarization resistance accurately, the frequency characterization of the scan rate should be less than the f_{max} in the low frequency portion of the Bode plot.

$\omega = 2\pi f$, where f is the frequency of the applied sine wave, and E can be calculated by using Eqn (9.23).

$$E = E_o \sin(\omega t) = 1/2 \, \Delta E e^{j2\pi ft} \qquad (9.23)$$

ΔE is the peak to peak amplitude and is equal to $2E_o$. ΔE is usually taken ~ 10 mV. This assures the linear response of the system to the applied potential (Stern and Geary, 1957). The rate of change of potential can be calculated by taking derivative of Eqn (9.23):

$$dE/dt = 1/2\Delta E \times (j2\pi ft) \times \left(e^{j2\pi ft}\right) \qquad (9.24)$$

and, the maximum rate of change would be:

$$\Delta E_{max} = \pi f \Delta E \qquad (9.25)$$

This maximum rate of change corresponds to scan rate, S, and by using f_{max} in Eqn (9.18) the maximum scan rate, S_{max}, can be calculated as following:

$$S_{max} = \pi \times \Delta E \times f_{max} < \frac{\pi \times \Delta E \times f_2}{10} \tag{9.26}$$

The value of f_{max} can be found from Bode plot as shown in Figure 9.10 as one decade slower than the lower cut-off frequency (break point),[2] f_2.

For example, in Figure 9.10, f_2 is ~ 0.63 Hz, and consequently:

$$S_{max} = \pi \times \Delta E \times f_{max} < \frac{\pi \times \Delta E \times f_2}{10} = 1.97 \text{mV/S}$$

To ascertain obtaining right frequency in the horizontal portion of the Bode plot, f_2 is divided by 10. Therefore, for a system shown in Figure 9.10, a scan rate lower than 1.97 mV/s has to be used for an accurate result.

In the aforementioned example, which shows a typical electrochemical system in liquid state with relatively low ohmic resistance, the measurement frequency range was between 10^5 and 0.01 Hz and the required time to perform the whole test would be relatively short (in this case it is about 2 min). However, due to the complexity of the concrete, to obtain the value of f_2, the experiment needs to be run in wider range of frequencies which would be very time-consuming (e.g., 10^6 Hz to 10^{-5} Hz).

It is also possible to determine the value of f_2, and consequently the appropriate scan rate in a very short time, using the galvanostatic pulse technique. When the constant current, $I_{app,}$ is applied to the rebar, the polarization of the rebar at given time t can be expressed as shown with Eqn (9.11) and by transferring Eqn (9.11) to logarithmic form, the values of R_p and C_{dl}, can be calculated using Eqn (9.12). As can be seen from Figure 9.4, the slope of the line of Eqn (9.12) is $1/R_p C_{dl}$. At cut-off frequency, the capacitive reactance is equal to the resistance value, $X_c = R$. Therefore, in an RC circuit (similar to Figure 9.8) the value of f_2 can be derived as following (Herrick, 1996):

$$X_c = \frac{1}{\omega C} = \frac{1}{2\pi f C} = R \tag{9.27}$$

$$S_{max} < \frac{\text{Slope} \times \Delta E}{20} \tag{9.28}$$

Since the cut-off frequency in this technique is obtained by using the galvanostatic pulse technique, ΔE in Eqn (9.22) would be equal to the V_p in Figure 9.3.

---

[2] Cut-off frequency is the point where low frequency behavior starts to change to high frequency behavior and vice versa.

9.7   Cyclic voltammetry (CV)

Cyclic voltammetry is a popular electrochemical measurement which was first introduced by Kemula (Kemula and Kublik, 1958), and widely applied later on solid electrodes, with the purpose of investigating the anodic oxidations (Adams, 1968). CV is one type of potentiodynamic electrochemical measurement in which a cyclic waveform potential is applied to the working electrode, the potential is in a triangle shape and changes linearly with time, as illustrated in Figure 9.11. The slope (V/s) is the scan rate; one cycle is completed after it scans from starting potential to terminating potential. The results of CV measurement can be plotted in a current versus potential curve that is often used to estimate the reversibility of electrode reaction and predict formation of intermediate product or new phase (Bard and Faulkner, 1980).

CV can be used to study the redox reactions and corrosion products on the surface of steel in concrete environment. As an example, Zhang and Poursaee (2015) used CV to estimate the reversibility of an electrode reaction and to observe the formation of intermediate products or new phases during oxidation and reduction reactions on steel specimens under stress in concrete pore solution. In that study, the working electrode potential continuously cycled from -1.4 V to $+0.4$ V with the scan rate of 50 mV/s, and repeated 10 times. This scan rate was applied in previous studies (Foulkes and McGrath, 1999; Pastore et al., 2011; Cabrini et al., 2014) and adapted in this work as well. Figure 9.12a−c shows the results of the CV test on one of the specimens under stress (compressive and tensile) at approximately 110% of its yield strength. After 72 h immersion in chloride-free pore solution, 5% wt NaCl was added to the pore solution. Measurements were performed 72 h after exposure to chloride-free pore solution and 24 and 120 h after addition of the NaCl to the solution.

As seen in Figure 9.12a, the voltammogram of the specimens in chloride-free pore solution showed two anodic peaks (a_1 and a_2) and two cathodic peaks (c_1 and H). Peak a_1 can be attributed to the formation of a film of $Fe(OH)_2$ and FeO, peak a_2 can be attributed to the transformation of Fe^{2+} to Fe^{3+}. Peak c_1 was considered to be the reduction reactions corresponding to the anodic reactions at peak a_2, and peak H
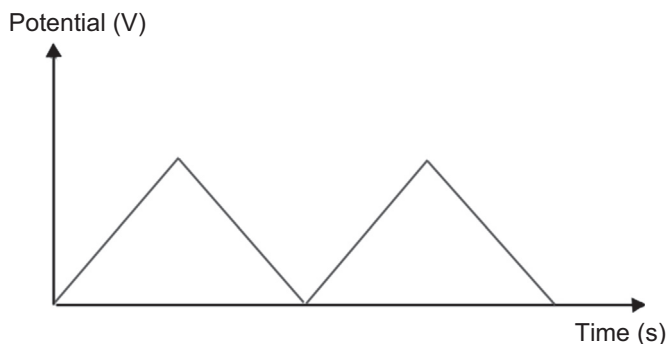
Figure 9.11 Cyclic voltammetry potential waveform.
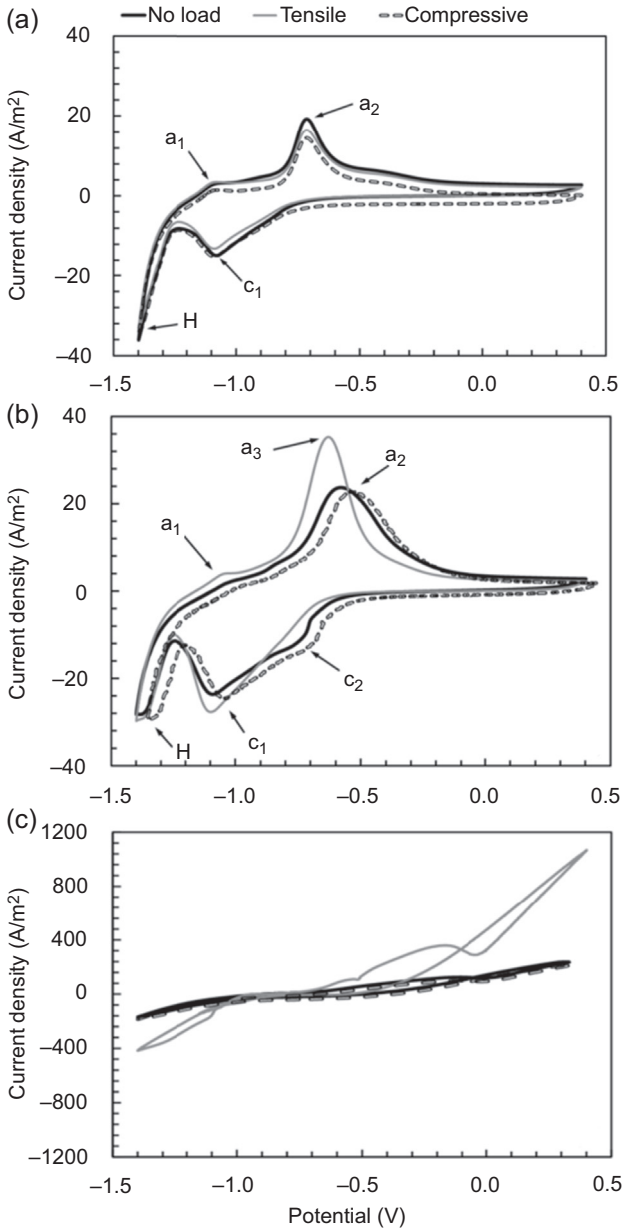
Figure 9.12 One-cycle voltammogram for one of the control specimens (no-load), one of the specimens under tensile stress, and one of the specimens under compressive stress (a) 72 h in chloride-free pore solution; (b) 24 h in chloride-contaminated pore solution; (c) 120 h in chloride-contaminated pore solution.

was associated with the hydrogen evolution (Burke and Murphy, 1980; Burke and Lyons, 1986; Mateo et al., 1990). Specimen under tensile stress and no stress showed higher current density values for peaks a_1 and a_2 compared to the specimen under compressive stress. This was an indication of more oxidation reactions due to passivation process when specimen was under tensile stress and no stress. The differences in peaks a_1 and a_2 for specimens under tensile stress and no stress were insignificant. Twenty-four hours after addition of the chloride ions to the solution (Figure 9.12b), all specimens showed higher current density values in their anodic peaks (peaks a_1 and a_2). However, in specimen under tensile stress, two peaks, a_3 and c_2, appeared on the anodic and cathodic portions of the voltammogram, respectively. Peak a_3 can be attributed to an oxidation within the compact passive layer, involving formation of the Fe_2O_3, Fe_3O_4 and FeOOH; and, peak c_2 was considered to be the result of the reduction reactions for peak a_3 (Burke and Murphy, 1980; Burke and Lyons, 1986). Results from the XRD test revealed that the corrosion products in both specimens were mainly consisted of α-FeOOH (goethite), γ-FeOOH (lepidocrocite), γ-Fe_2O_3 (maghemite) and Fe_3O_4 (magnetite). However, stronger peaks for both FeOOH compounds can be seen for corrosion products on the specimen under tensile stress. This observation confirmed the results from the CV test (peak a_3). This observation revealed the significance of tensile stress on the composition of the corrosion products formed on the surface of steel exposed to chloride ions. One hundred twenty hours after exposure to the chloride-contaminated pore solution (Figure 9.12c), extensive depassivation was observed with the voltammogram being extremely disordered with very large current flowing throughout (note the different current density scale for this figure).

9.8 Corrosion sensors for field monitoring

Application of sensors to monitor the corrosion activity of steel in concrete and to measure the corrosion rate of steel has been of great attraction. The embeddable corrosion sensors can provide early warning of conditions that damage steel reinforcement, leading to cracking and deterioration of concrete structures. In addition, lost cost, no or minimum need for trained personnel and maintenance make the application of sensors even more attractive.

9.8.1 Corrosion potential and corrosion current density sensors

Most of the sensors for this purpose are basically an embeddable reference electrode which are inert and stable in high alkaline environment in concrete, such as: Mn/MnO_2 (Arup et al., 1997) and Ti/TiO_2 (Muralidharan et al., 2007; Duffó and Farina, 2009; Dong et al., 2011), to perform half-cell potential measurement. The other category of sensors is designed to measure the corrosion current density as well as the half-cell potential, and, consequently, corrosion rate. These sensors are based on utilizing three electrodes (reference, counter or auxiliary and working

electrodes) which are usually being used in conventional electrochemical measuring systems. Most of the sensors in this category usually use the metal−metal oxide (MMO) as reference electrodes, such as Mn/MnO_2 and Ti/TiO_2, stainless steel as counter electrode and the reinforcing bar as the working electrode (Andrade and Martinez, 2009; Duffó and Farina, 2009; Dong et al., 2011). In the sensor developed by Poursaee, graphite rods are used as both reference and counter electrodes. The stability of graphite in high pH was evaluated and it was concluded that the potential of the graphite is stable enough during the period of measurements (approximately 1 h) and the potentiostatic LPR can be performed successfully, using this configuration (Poursaee, 2009). However, graphite cannot be used as the permanent reference electrode, unless it undergoes special treatment (Swette et al., 1999). The sensors with the three electrochemical components can be used to perform all the techniques such as the LPR, galvanostatic pulse, cyclic polarization, and the EIS.

9.8.2 Other sensors

The onset of corrosion in steel reinforced concrete can also be detected by different methods. The inductively coupled magnetic fields, with the core typically made of a simple LC resonator, have been used by researchers to sense the initiation of corrosion (Carkhuff and Cain, 2003; Andringa et al., 2005; Bhadra et al., 2010). Corrosion of the iron wire will change the inductance or the capacitance of the LC circuit. The resonant frequency of the whole LC circuit, schematically shown in Figure 9.13, is given by Thomson formula:

$$f = \frac{1}{2\pi\sqrt{LC}} \tag{9.29}$$

where L is the total inductance of the circuit and C is the total capacitance of the circuit.
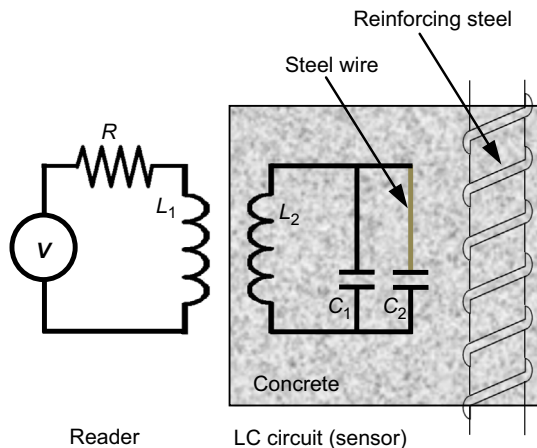
Figure 9.13 Circuit diagram for a corrosion sensor, based on inductance.

According to Eqn (9.29), the change of the inductance or the capacitance of the circuit will change the resonant frequency. As can be seen in Figure 9.11, the resonant frequency of the circuit depends on the state of the steel wire. When the steel wire is not broken, the total capacitance of the circuit is equal to the sum of the two capacitances ($C = C_1 + C_2$). However, when the steel wire is broken due to corrosion, the total capacitance of the circuit becomes C_1. The diameter of the steel wire is usually much smaller than that for the reinforcing steel and the steel wire will corrode before considerable corrosion damage has occurred in the reinforcement.

Eddy currents have also been used to detect the corrosion on the embedded steel bars in concrete (Gaydecki and Burdekin, 1994; Miller et al., 2003; Kumar et al., 2006). Eddy currents are generated in a conductive material by a changing magnetic field. In this technique, the magnetic field in a coil induces eddy currents in the rebar. This eddy current generates a magnetic field of its own that interferes with the main magnetic field. The change in inductance of the coil is then measured using the meter.

Sensors based on the application of fiber optics to detect corrosion have also been developed. An optical fiber consists of a glass core surrounded by a glass cladding which differs in index of refraction. The glass fiber is then coated during the manufacturing process with a protective polymer layer (Merzbachery et al., 1996). The direct spectroscopy of corroded versus uncorroded materials is the basis of this method. Spectrally broadband light is coupled into an optical fiber and then illuminates the region under measurement. The presence of corrosion is determined using color modulation of the broadband input signal (Fuhr and Huston, 1998).

The principle of light reflection has also been used to develop fiber optic sensors to detect corrosion of steel in concrete. The sensor consists of an optical fiber reflection sensor, a sacrificial metallic film, joined to a steel tube. One side of the film is finely polished and is isolated from the environment while the other side is exposed to the corrosive environment. The corrosion pits initiated at the exposed film surface slowly penetrate the sacrificial film as the exposure time increases. The corrosion pits that reach the polished surface reduce the surface reflectivity of the polished surface. This decrease in reflectivity can be detected by the optical fiber reflectivity sensor (Wang and Huang, 2011).

The fiber Bragg grating (FBG) is used for the corrosion detection purpose as well (Lo and Xiao, 1998; Yang et al., 2006; Gaon et al., 2011). Normal optical fibers are uniform along their lengths. In a simple FBG, the refractive index of the fiber core varies periodically along the length of the fiber. The FBG reflects particular wavelengths of light and transmits all others and therefore can be used as an inline optical filter to block certain wavelengths, or as a wavelength-specific reflector. The difference between the reflection of corrosion products and that of the steel rebar can be used to detect the corrosion activity on the surface of the rebar.

Acoustic emission monitoring of concrete is the other technique that has been used to detect rebar corrosion (Zdunek et al., 1995; Yoon et al., 2000; Golaski et al., 2002; Idrissia and Limam, 2003; Reis et al., 2003; Assouli et al., 2005; Fariduddin et al., 2007). Acoustic emission energy is released when a crack propagates. Since corrosion products are expansive (Lide, 1999), they cause multiple microfractures, which ultimately lead to macrocracks. This activity can be detected by acoustic emission

sensors. As the result, the initiation of corrosion, location of the zone containing intense corrosion products, crack formation mechanism, and the loss of bond strength due to corrosion between reinforcing steel and the surrounding concrete can be investigated, using this method. However, at this time, expensive equipment and the need for highly trained personnel limit the application of acoustic emission technique mainly to laboratory investigations.

References

Adams, R.N., 1968. Electrochemistry at Solid Electrodes. Marcel Dekker Inc.

Alonso, C., Andrade, C., Castellote, M., Castro, P., 2000. Chloride threshold values to depassivated reinforcing bars embedded in a standardised OPC mortar. Cement and Concrete Research 30, 1047−1055.

Andrade, C., Martinez, I., 2009. Embedded sensors for the monitoring of corrosion parameters in concrete structures. In: NDTCE'09, Non-destructive Testing in Civil Engineering, Nantes, France.

Andrade, C., González, J.A., 1978. Quantitative measurements of corrosion rate of reinforcing steels embedded in concrete using polarization resistance measurements. Werkstoffe und Korrosion 29, 515−519.

Andrade, C., Marcias, A., Feliu, S., Escudero, M.L., Gonzalez, J.A., 1990. Quantitative measurement of the corrosion rate using a small counter electrode in the boundary of passive and corroded zones of a long concrete beam. In: Berke, N.S., Chaker, V., Whiting, D. (Eds.), Corrosion Rates of Steel in Concrete, ASTM STP 1065. ASTM, Philadelphia, PA.

Andringa, M.M., Neikirk, D.P., Dickerson, N.P., Wood, S.L., 2005. Unpowered wireless corrosion sensor for steel reinforced concrete. In: 4th IEEE Conferemce on Sensors, Irvine, California, USA.

Arup, H., Klinghoffer, O., Mietz, J., 1997. Long term performance of MnO_2 reference electrodes in concrete. In: Corrosion 97. NACE.

Assouli, B., Simescu, F., Debicki, G., Idrissi, H., 2005. Detection and identification of concrete cracking during corrosion of reinforced concrete by acoustic emission coupled to the electrochemical techniques. NDT & E International 38, 682−689.

ASTM, 2009. C876-09: Standard Test Method for Half-cell Potentials of Uncoated Reinforcing Steel in Concrete, 03.02, pp. 446−451.

Bard, A.J., Faulkner, L.R., 1980. Electrochemical Methods: Fundamentals and Applications. John Wiley & Sons.

Bhadra, S., Bridges, G.E., Thomson, D.J., 2010. Coupled coil sensor for detecting surface corrosion on steel reinforcement. In: 14th International Symposium on Antenna Technology and Applied Electromagnetics [ANTEM] and the American Electromagnetics Conference [AMEREM]. Fairmont Chateau Laurier, Ontario, Canada.

Broomfield, J.P., 1996. Field Measurement of the Corrosion Rate of Steel in Concrete Using a Microprocessor Controlled Unit with a Monitored Guard Ring for Signal Confinement. ASTM International.

Burke, L.D., Lyons, M.E.G., 1986. The formation and stability of hydrous oxide films on iron under potential cycling conditions in aqueous solution at high pH. Journal of Electroanalytical Chemistry and Interfacial Electrochemistry 198 (2), 347−368.

Burke, L.D., Murphy, O.J., 1980. Growth of an electrochromic film on iron in base under potential cycling conditions. Journal of Electroanalytical Chemistry and Interfacial Electrochemistry 109 (1−3), 379−383.

Cabrini, M., Lorenzi, S., Pastore, T., 2014. Cyclic voltammetry evaluation of inhibitors for localised corrosion in alkaline solutions. Electrochimica Acta 124, 156−164.

Carkhuff, B., Cain, R., 2003. Corrosion sensors for concrete bridges. IEEE Instrumentation & Measurement Magazine 19−24.

Corrosion Doctors, 2005. http://www.corrosion-doctors.org.

Dong, S., Lin, C., Hu, R., Li, L., Du, R., 2011. Effective monitoring of corrosion in reinforcing steel in concrete constructions by a multifunctional sensor. Electrochimica Acta 56, 1881−1888.

Duffó, G.S., Farina, S.B., 2009. Development of an embeddable sensor to monitor the corrosion process of new and existing reinforced concrete structures. Construction and Building Materials 23, 2746−2751.

Elsener, B., Gulikers, J., Polder, R., Raupach, M., 2003. Half-cell potential measurements − potential mapping on reinforced concrete structures. Materials and Structures 36.

Elsener, B., Klinghoffer, O., Frolund, T., Rislund, E., Schiegg, Y., Böhni, H., 1997. Assessment of reinforcement corrosion by means of galvanostatic pulse technique. In: Blankvoll, A. (Ed.), Repair of Concrete Structures. Svolvær, Norway, pp. 391−400.

Fariduddin, A.K.M., Ohtsu, M., Hossain, K.M.A., Lachemi, M., 2007. Simulation of reinforcement-corrosion-induced crack propagation in concrete by acoustic emission technique and boundry element method analysis. Canadian Journal of Civil Engineering 34, 1197−1207.

Feliu, S., Gonzalez, J.A., Andrade, C., 1996. Electrochemical methods for on-site determination of corrosion rates of rebars. In: Berke, N.S., Escalante, E., Nmai, C., Whiting, D. (Eds.), Techniques to Assess Corrosion Activity of Steel Reinforced Concrete Structures, ASTM STP 1276. ASTM, pp. 107−118.

Fontana, M.G., 1987. Corrosion Engineering. McGraw-Hill.

Foulkes, F.R., McGrath, P., 1999. A rapid cyclic voltammetric method for studying cement factors affecting the corrosion of reinforced concrete. Cement and Concrete Research 29, 873−883.

Fuhr, P.L., Huston, D.R., 1998. Corrosion detection in reinforced concrete roadways and bridges via embedded fiber optic sensors. Smart Materials and Structures 7, 217−228.

Gamry Instruments, 2005a. DC Corrosion Techniques. Application Notes. http://www.gamry.com/App_Notes/DC_Corrosion/GettingStartedWithEchemCorrMeasurements.htm.

Gamry Instruments, 2005b. Electrochemical Impedance Spectroscopy Primer. Application Notes. http://www.gamry.com/App_Notes/EIS_Primer/EIS_Primer.htm.

Gamry Instruments, 2006. Basics of Electrochemical Impedance Spectroscopy. Gamry Instruments. http://www.gamry.com/App_Notes/EIS_Primer/EIS%20Primer%202006.pdf.

Gaon, J., Wu, J., Li, J., Zhao, X., 2011. Monitoring of corrosion in reinforced concrete structure using Bragg grating sensing. NDT & E International 44, 202−205.

Gaydecki, P.A., Burdekin, F.M., 1994. An inductive scanning system for two-dimensional imaging of reinforcing components in concrete structures. Measurement Science and Technology 5, 1272−1280.

Gepraegs, O.K., 2002. Comparison and Evaluation of Electrochemical Techniques and Monitoring Instruments to Determine the Corrosion Rate of Steel in Concrete (MA.Sc). University of Waterloo.

Golaski, L., Gebski, P., Ono, K., 2002. Diagnostic of reinforced concrete bridges by acoustic emission. Journal of Acoustic Emission 20, 83−98.

Gonzalez, J.A., Andrade, C., Alonso, C., Feliu, S., 1995. Comparison of rates of general corrosion and maximum pitting penetration on concrete embedded steel reinforcement. Cement and Concrete Research 25, 257−264.

Gronvold, F., Arup, H., 1979. Localization of corroding reinforcement by electrochemical potential surveys. In: RILEM Symposium on Quality Control of Concrete Structures, Sweden.

Herrick, C., 1996. Basic Electronics Math (Newnes).

Idrissia, H., Limam, A., 2003. Study and characterization by acoustic emission and electrochemical measurements of concrete deterioration caused by reinforcement steel corrosion. NDT & E International 36, 563−569.

Jones, D.A., 1992. Principles and Prevention of Corrosion. Macmillan Publishing Company.

Jones, D.A., Greene, N.D., 1966. Electrochemical measurement of low corrosion rates. Corrosion 22, 198−204.

Kemula, W., Kublik, Z., 1958. Application of the hanging mercury drop electrode to an investigation of intermetallic compounds in mercury. Nature 182, 1228−1229.

Klinghoffer, O., 1995. In situ monitoring of the reinforcement corrosion by means of electrochemical methods. Nordic Concrete Research 16.

Kumar, K., Muralidharan, S., Manjula, T., Karthikeyan, M.S., Palaniswamy, N., 2006. Sensor systems for corrosion monitoring in concrete structures. Sensors & Transducers Magazine 67 (5), 553−560.

Lasia, A., 1999. Electrochemical impedance spectroscopy and its applications. In: Conway, B.E., Bockris, J., White, R.E. (Eds.), Modern Aspects of Electrochemistry, vol. 32. Kluwer Academic/Plenum Publishers, New York, pp. 143−248.

Lide, D.R., 1999. CRC Handbook of Chemistry and Physics. CRC Press, New York, NY.

Lo, Y., Xiao, F., 1998. Measurement of corrosion and temperature using a single-pitch Bragg grating fiber sensor. Journal of Intelligent Material Systems and Structures 9 (10), 800−807.

Mansfeld, F., Kendig, M., 1981. Concerning the choice of scan rate in polarization measurements. Corrosion 37 (9), 545−546.

Mateo, M.L., Otero, T.F., Schiffrin, D.J., 1990. Mechanism of enhancement of the corrosion of steel by alternating currents and electrocatalytic properties of cycled steel surfaces. Journal of Applied Electrochemistry 20 (1), 26−31.

Merzbachery, C.I., Kersey, A.D., Friebele, E.J., 1996. Fiber optic sensors in concrete structures: a review. Smart Materials and Structures 5, 196−208.

Miller, G., Gaydecki, P., Quek, S., Fernandes, B.T., Zaid, M., 2003. Detection and imaging of surface corrosion on steel reinforcing bars using a phase-sensitive inductive sensor intended for use with concrete. NDT&E International 36 (1), 19−26.

Muralidharan, S., Ha, T.H., Bae, J.H., Ha, Y.C., Lee, H.G., Kim, D.K., 2007. A promising potential embeddable sensor for corrosion monitoring application in concrete structures. Measurement 600−606.

Newhouse, C.D., Weyers, R.E., 1996. Modeling the measured time to corrosion cracking. In: Escalante, E., Berke, N.S., Nmai, C.K., Whiting, D. (Eds.), STP 1276-Techniques to Assess the Corrosion Activity of Steel Reinforced Concrete Structures. ASTM International, West Conshohocken, PA.

Newton, C.J., Sykes, J.M., 1988. A galvanostatic pulse technique for investigation of steel corrosion in concrete. Corrosion Science 28 (11), 1051−1074.

Pastore, T., Cabrini, M., Coppola, L., Lorenzi, S., Marcassoli, P., Buoso, A., 2011. Evaluation of the corrosion inhibition of salts of organic acids in alkaline solutions and chloride contaminated concrete. Materials and Corrosion 62 (2), 187−195.

Polder, R.B., Peelen, W.H.A., 2002. Characterisation of chloride transport and reinforcement corrosion in concrete under cyclic wetting and drying electrical resistivity. Cement & Concrete Composites 24, 427−435.

Poursaee, A., 2009. Automatic system for monitoring corrosion of steel in concrete. Advances in Engineering Software 40 (11), 1179−1182.

Poursaee, A., 2010. Potentiostatic transient technique, a simple approach to estimate the corrosion current density and Stern−Geary constant of reinforcing steel in concrete. Cement and Concrete Research 40, 1451−1458.

Poursaee, A., Hansson, C.M., 2009. Potential pitfalls in assessing chloride-induced corrosion of steel in concrete. Cement and Concrete Research 39 (5), 391−400.

Princeton Applied Research, 2000. Basics of Electrochemical Impedance Spectroscopy. Application Note AC-1. http://new.ametek.com/content-manager/files/PAR/078.pdf.

Reis, H.L.M.d., Ervin, B., Kuchma, D.A., Bemhard, J.T., 2003. Evaluation of corrosion damage in steel reinforced concrete. In: International Workshop on Structural Health Monitoring, Stanford, CA, USA.

Silverman, D.C. Tutorial on POLEXPERT and the Cyclic Potentiodynamic Polarization Technique, Argentum Solutions Inc., http://www.argentumsolutions.com:80/tutorials/polexpert_tutorialpg1.html.

Silverman, D.C., 1986. Primer on the AC impedance technique. In: Baboian, R. (Ed.), Electrochemical Techniques for Corrosion Engineering. NACE.

Silverman, D.C., 1990. Simple models/practical answers using the electrochemical impedance technique. In: Baboian, R., Dean, W. (Eds.), Corrosion Testing and Evaluation. Silver Anniversary Volume, ASTM.

Silverman, D.C., 1998. Tutorial on cyclic potentiodynamic polarization technique. In: Corrosion 98. NACE International, San Diego, CA.

Stern, M., Geary, A.L., 1957. Electrochemical polarisation: I. A theoretical analysis of the shape of polarisation curves. Journal of the Electrochemical Society 104 (1), 56−63.

Stratfull, R.F., 1954. The corrosion of steel in a reinforced concrete bridge." Corrosion 13, 173−178.

Swette, L.L., Manoukian, M., Hamdan, M., LaConti, A., Sohanghpurwala, A., Scannell, W.T., 1999. Reference Electrode for Monitoring Steel-in-Concrete Potential. U.S. Patent. USA. 5964992.

Wang, Y., Huang, H., 2011. Optical fiber corrosion sensor based on laser light reflection. Smart Materials and Structures 20, 1−7.

Yang, S., Cai, H.W., Geng, J.X., 2006. Advanced fiber grating corrosion sensors for structural health monitoring. In: Ou, J.P., Li, H., Duan, Z.D. (Eds.), The Second International Conference on Structural Health Monitoring of Intelligent Infrastructure. Shenzhen, China, pp. 441−443.

Yoon, D., Weiss, W.J., Shah, S.P., March 2000. Assessing damage in corroded reinforced concrete using acoustic emission. Journal of Engineering Mechanics 1−11.

Zdunek, A.D., Prine, D., Li, Z., Landis, E., Shah, S.P., 1995. Early detection of steel rebar corrosion by acoustic emission monitoring. In: Corrosion 95. The NACE International, Baltimore, Maryland, USA.

Zhang, Y., Poursaee, A., 2015. Study the semi-conductive behavior of the passive film on carbon steel in simulated concrete pore solution under stress. Anti-Corrosion Methods and Materials 62 (6).

Acoustic emission monitoring for corrosion damage detection and classification

10

P. Ziehl [1], M. ElBatanouny [2]
[1]University of South Carolina, Columbia, SC, USA; [2]Wiss, Janney, Elstner Associates, Inc., Northbrook, IL, USA

10.1   Overview of the acoustic emission technique

Acoustic emission (AE) is the term used to define transient stress waves emitted from sudden release energy (ASTM E1316-13c, 2013) due to a deformation in the monitored material, such as crack formation or growth (Pollock, 1986; Ziehl, 2008). AE is a passive nondestructive evaluation/structural health monitoring (NDE/SHM) technique that does not need excitation or human intervention after the sensors are connected to the data acquisition system. The waveform of each AE signal (AE hit) can be used to calculate different parameters such as amplitude, duration, counts, rise time, absolute energy, and signal strength along with different frequency parameters as shown in Figure 10.1.

AE has the ability to locate cracks using triangulation. The location of each AE source event (AE signals that are detected by at least two sensors) can be determined using the arrival times of the compression waves. Assuming that the source lies in the (x, y) plane, the arrival time at the mth transducer is given by:

$$t_m = |d_m - d|/v \tag{10.1}$$
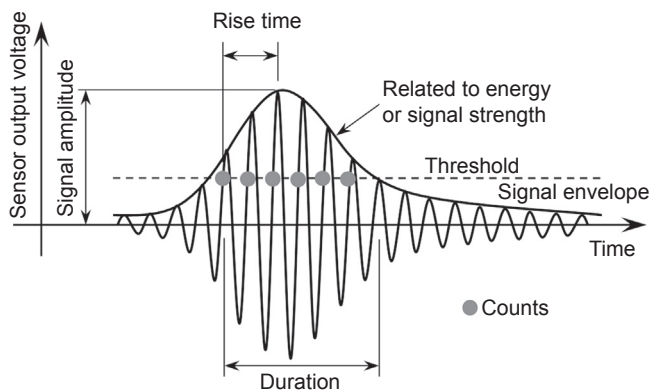
Figure 10.1 Schematic of acoustic emission waveform (ElBatanouny et al., 2014d).

$$t_m = \left[(x_m - x)^2 + (y_m - y)^2\right]^{1/2} \Big/ v \qquad\qquad (10.2)$$

$$\Delta t_{km} = (|d_k - d| - |d_m - d|)/v \qquad\qquad (10.3)$$

where v is the compression wave speed, $d = (x,y)$ is the source location, and $d_m = (x_m, y_m)$ is the location of the mth transducer. Because the absolute time of the source event is unknown, only time differences can be measured. Equations of this form are nonlinear and difficult to solve analytically, and numerical methods are generally implemented. While at least three transducers are required in order to measure two time differences and hence deduce the two unknowns x, y (Scruby et al., 1985), using more sensors improves source location accuracy (Miller and Mclntire, 1987). Nonlinear least-squares methods can be used to solve the equations for x and y (Scruby et al., 1985; Maji et al., 1990), and iterative procedures have been proposed by Enoki and Kishi (1988) and Ohtsu (1987), who also took into account the anisotropy of the compression wave speed in reinforced concrete (RC). The accuracy of source location in RC structures using AE has also been investigated (Grosse and Ohtsu, 2008; Shokri and Nanni, 2014). Well-established source location algorithms are usually embedded in AE data acquisition systems.

Due to the extreme sensitivity of the method, data filtering is a crucial step in AE analysis. The main source of noise in the AE data in laboratory testing is wave reflections. Duration-amplitude (D-A) filters, also known as Swansong II filters (Fowler et al., 1989), and rise time−amplitude (R-A) filters (ElBatanouny et al., 2014a) are widely used for rejection of wave reflections from AE data. These filters are usually developed through visual inspection of waveforms related to noise, and determining the relation between AE parameters for these hits. Literature indicates that crack maps can be produced with high reliability if proper data filters were used (Abdelrahman et al., 2014; ElBatanouny et al., 2014a,b).

Quantitative waveform analyses, such as source characterization (Wadley and Scrubby 1983; Kim and Sachse 1984) and moment tensor analysis (Ohtsu 1991, 1995), provide size, orientation, movement, and mode of AE sources, in addition to source location of AE events. Quantitative analyses are based on the generalized theory of AE (Ohtsu and Ono, 1984), which is based on the representation theorem of seismic sources (Aki and Richards, 1980) and models AE sources using a seismic moment tensor (Enoki and Kishi, 1988).

A simplified AE moment tensor analysis was introduced by Ohtsu (1991) using the simplified Green's function for moment tensor analysis (SiGMA) code, which has proven to be effective for analyzing fracture processes (Yuyama 2005; Ohno and Ohtsu 2010). Quantitative analyses have been applied to field geometries, such as a large concrete block or column, the corner of a rigid frame, a dam, and so forth (Yuyama, 2005). Moment tensor analysis has recently been implemented at the University of South Carolina during fatigue tests on compact tension specimens, enabling detection of crack locations and orientations. Source characterization was likewise performed to discriminate between ductile and brittle cracking mechanisms, and the results were confirmed through SEM micrographs (Hossain et al., 2012). When the

first compressive wave amplitudes are detectable and discernible at more than six observation points (AE sensors) an accurate three-dimensional source location is possible. If the specimen is comparable to a thin plate, a two-dimensional sensor placement with four sensors can be applied (Shigeishi and Ohtsu, 1992).

Moment tensor analysis is applicable even if there is access only to the outside of the structure (i.e., if all AE sensors must be placed on the outside plane). Murakami et al. (1993) reported that the analysis was successfully made in a large concrete block with all six sensors placed on the top plane. While the moment tensor approach can provide information related to damage sources, the primary limitation of this approach is the relatively dense sensor grid that must be used to obtain this information. Therefore, trade-offs exist between implementation costs and the results desired, and these must be taken into consideration for field applications.

Successful field applications of AE monitoring have been developed based on waveform analysis combined with damage rates that are based on parameters of the received waveform such as signal strength and energy. Much of the earlier work in AE was based on empirical observations of damage and large datasets, and trend analysis was utilized to track and quantify trends in AE data rates. This approach was highly successful in the fiber-reinforced polymer pressure vessel industry and also for qualification of railroad tank cars (Fowler et al., 1989). More recently, formalized pattern recognition techniques have been introduced to characterize the structure and to determine natural "signatures" in AE datasets (Marec et al., 2008; Gutkin et al., 2011; Li et al., 2012; Sause et al., 2012). Such techniques have evolved toward machine learning and data mining, which have been used for classification, regression, and prediction. Current investigations are implementing data mining tools for hypothesis searching, rule extraction, and decision making (e.g., Bhat et al., 2003; Olivera and Marques 2008; Qian et al., 2009; Omkar and Karanth 2008). Recently, Mejia (2012) addressed a common and important pattern recognition problem in AE: the presence of unwanted signals (or "noise") in AE datasets. The study designed and implemented a data mining scheme that enhanced the quality of AE datasets. The scheme was able to produce characterization rules for both unwanted and meaningful signals, showing that rule extraction using this technique could lead to the finding of general AE "signatures" for particular damage mechanisms.

10.2   Mechanism of corrosion detection using AE

Corrosion of reinforcement is a major cause for deterioration of RC structures in coastal areas or areas where deicing salts are used. In spite of the natural protection concrete provides for the steel reinforcement to resist corrosion due to formation of protecting passive oxide film around the steel as a result of the high alkalinity of concrete; however, chlorides can infiltrate through concrete cracks to break the passive film and initiate corrosion in reinforcing steel.

Chloride-induced corrosion reduces the mechanical strength of steel reinforcement and corrosion product exerts stress into the concrete structure that produces cracks that deteriorate the steel−concrete bond, which directly affects serviceability performance.

| Before corrosion | Build-up of corrosion products | Further corrosion Surface cracks Stains | Eventual spalling Corroded bar Exposed |
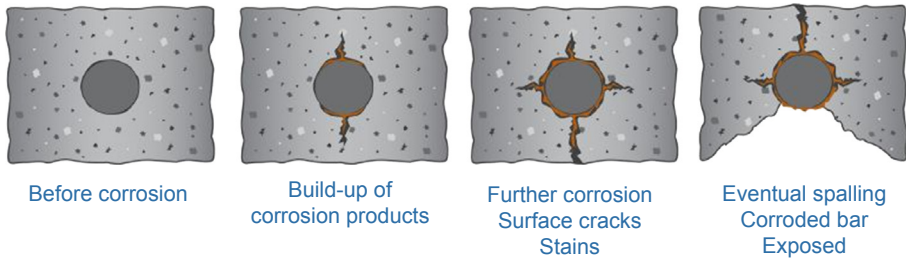
Figure 10.2 Corrosion process in concrete (http://concrete-forum.com/).

When steel starts to corrode, a gradual decrease of its diameter is produced, together with the generation of an oxide with a volume 6 to 10 times higher than that of steel (Li et al., 1998). The corrosion process is then accelerated by the presence of cracks, which increases the rate of chloride infiltration. Corrosion affects the durability of concrete structures and decreases its service life by: (1) reducing the cross-sectional area of the steel strands minimizing their ductility and increasing stress concentrations at the reinforcement interface (Yoon et al., 2000) and (2) degrading the integrity of the surrounding concrete (Jaffer and Hanson, 2009). Figure 10.2 shows a schematic of the corrosion process in concrete.

The mechanisms that enable correlation between AE data and corrosion intensity are: (1) accumulation of chlorides and breakdown of the passive film (Perrin et al., 2010; Prateepasen and Jirarungsatian, 2011) and (2) the microcracking of the concrete that occurs due to the expansive nature of the corrosion products (ElBatanouny et al., 2011, 2014c; Mangual et al., 2013a,b). The primary advantage of AE monitoring is its unique ability to detect and quantify the microcracking process as it occurs, making it an extremely sensitive monitoring method. Later stages of corrosion damage, such as visible surface cracking, are also easily detected and quantified.

10.3   Case studies for corrosion detection using AE

The use of AE to detect corrosion damage in RC started in the 1980s (Weng et al. 1982; Abdelrahman, 2013). However, most of the studies focused only on passively reinforced rather than prestressed concrete (PC). The main focus of earlier studies was to investigate the ability of AE to detect corrosion initiation. Literature indicates that AE parameters such as number of AE hits and/or events have the ability to detect corrosion as well as changes in the rate of the corrosion process (Li et al., 1998; Zdunek et al., 1995; Idrissi and Limam, 2003).

Figure 10.3 shows the results of AE events and current versus time (Li et al., 1998). This figure indicates the ability of AE to detect microcracking associated with corrosion damage. In addition, AE activity increased prior to the increase in galvanic current, which illustrates the ability of AE to detect corrosion damage earlier than can be achieved using electrochemical measurements.
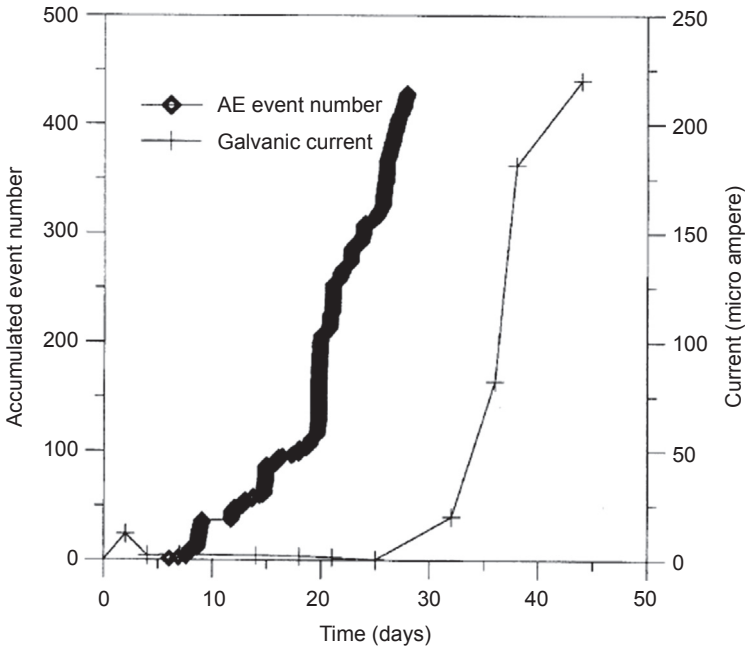
Figure 10.3 AE versus galvanic current readings (Li et al., 1998).

Recent studies also have investigated the use of AE-based condition assessments such as SiGMA, R-A value, and *b*-value (Farid Uddin et al., 2004; Ohtsu and Tomoda, 2008). Figure 10.4 shows the results of *b*-value versus time during an accelerated corrosion test using wet/dry cycles on a small scale specimen (Ohtsu and Tomoda, 2008). During this test, half-cell potential (HCP) measurements started decreasing at
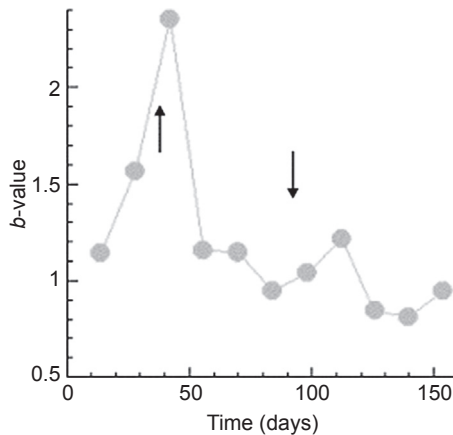
Figure 10.4 Variation of *b*-values in cyclic wet/dry test (Ohtsu and Tomoda, 2008).

approximately 100 days. A drop in the *b*-value was observed at the same time, indicating that corrosion damage is occurring. The rise in the *b*-value at approximately 40 days of testing was attributed to corrosion initiation, as the chloride concentration exceeded the threshold at this time.

10.4   Corrosion classification using AE

Most of the earlier studies focused on RC specimens and showed that AE can detect corrosion damage, but they did not directly relate AE activity to the rate of corrosion and in determining the extent of corrosion. Although the mechanism of corrosion activity in RC and PC is similar, the manufacturing process and shape of prestressing strands facilitates corrosion initiation at a lower chloride concentration as compared with steel rebars (Moser et al., 2011). This section summarizes recent efforts at the University of South Carolina for corrosion detection and classification of prestressing strands in PC and post-tensioned concrete (PT) specimens with different scales and durations of corrosion exposure. In these studies, 1/2 in. (12.7 mm) seven-wire low-relaxation prestressing strands were used in all specimens. AE R6i sensors (peak resonance at approximately 55 kHz, with integral 40 dB_{AE} (referred to as dB for simplicity) preamplification) were used to monitor corrosion in all the studies. It is noted that all the AE data shown is filtered. The main filters used are D-A filters, which are based on inspection of AE signals to differentiate noise from genuine AE data. The limits used in the D-A filters from ElBatanouny et al. (2014c) are shown in Table 10.1. For more information regarding the filtration techniques, please refer to the referenced manuscripts (ElBatanouny et al., 2014c; Mangual et al., 2013a,b).

10.4.1   Small-scale specimens

A total of 20 specimens were tested under an accelerated corrosion test setup. The specimens were reinforced with an embedded 1/2-inch-diameter prestressing strand;

Table 10.1 AE duration-amplitude data filter (ElBatanouny et al., 2014c)

Rejection limits		Rejection limits		Rejection limits	
Amp (dB)	Dur (µs)	Amp (dB)	Dur (µs)	Amp (dB)	Dur (µs)
40−42	>400	50−52	>1500	60−65	>4500
42−44	>600	52−54	>2000	65−70	>6500
44−46	>800	54−56	>2500	70−75	>7500
46−48	>1000	56−58	>3000	75−80	>9000
48−50	>1200	58−60	>3500	90−100	>10,000

dimensions of each specimen were 4.5 in. × 4.5 in. × 20 in. (114 mm × 114 mm × 1270 mm). The test matrix included 11 precracked specimens and 9 pristine specimens to evaluate the effect of cracks on AE attenuation. Specimens were immersed in a tank filled with a 3% NaCl solution at room temperature to a level 0.25 in. (7 mm) below the reinforcing strand. A copper plate with the same length of the specimens was placed below each specimen to serve as the cathode.

Accelerating the corrosion process was established by forming a galvanic cell using a rectifier to impress a direct external current to the specimens. The current that flows between the dissimilar metals controls the degree of corrosion activity in the cell. The rectifier was connected between the copper plate (cathode) and the prestressing strand (anode). Figure 10.5 shows a diagram of the corrosion cell for a single cracked specimen placed in the test vessel (Mangual et al., 2013a).

The results showed that stresses induced by volume expansion resulted in dense AE that was correlated to the onset of corrosion and nucleation of cracks as shown in Figure 10.6. Comparing AE data with electrochemical HCP measurements showed that the cumulative signal strength (CSS) relates well with potential variations as
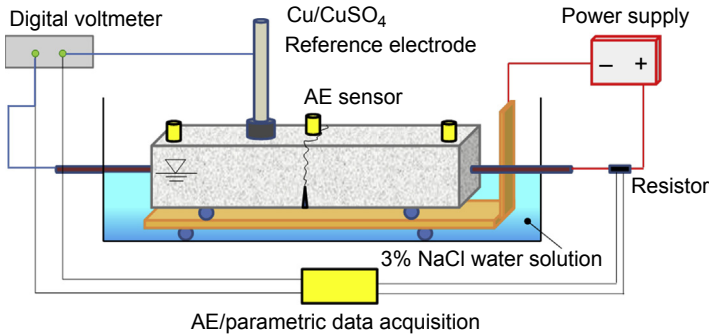
Figure 10.5 Schematic of the accelerated corrosion setup (Mangual et al., 2013a).
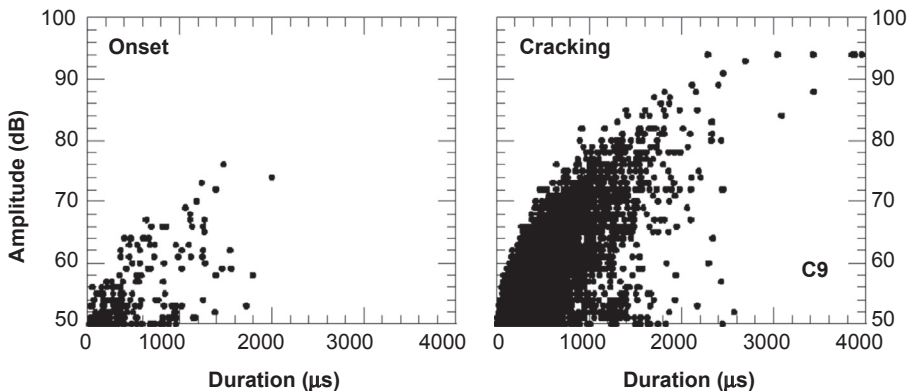
Figure 10.6 Amplitude (dB) versus duration (μs) plot (Mangual et al., 2013a).

shown in Figure 10.7. It also allowed discrimination between different corrosion stages. The magnitude of the slope in the CSS versus time curve was able to portray the depassivation process and onset of corrosion as corroborated by HCP. This shows that AE is capable of detecting and discriminating between early corrosion stages while mimicking the behavior of resistivity changes in the concrete.

Source location based on AE data enabled the accurate detection of events as a result of passivity breakdown along the reinforcement and debonding (Mangual et al., 2013a). Figure 10.8 shows the source location results for a precracked specimen. As seen in the figure, most of the AE activity concentrated near to the crack where corrosion is predicted to take place as a result of chloride accessibility in this region (no AE activity was detected at the exact crack location, as it is already formed). At the conclusion of the test, the specimens were taken apart, and the strand was removed for visual inspection of corrosion. The strand was then cleaned and reweighed to measure the steel mass loss as detailed in Mangual et al., (2013a). As shown in Figure 10.9, heavy corrosion damage, in terms of formation of longitudinal and tangential cracks, was observed in some specimens.
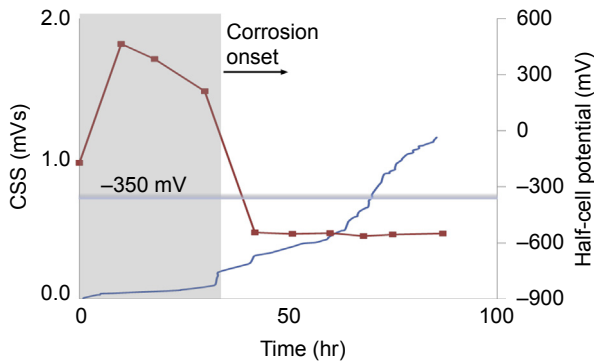
Figure 10.7 CSS and HCP versus time.
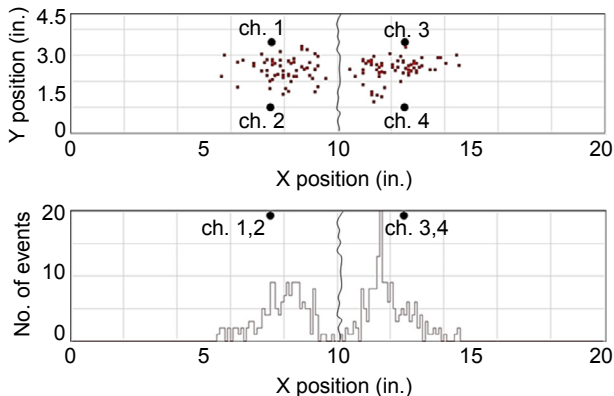
Figure 10.8 Source location and number of events for a precracked specimen.
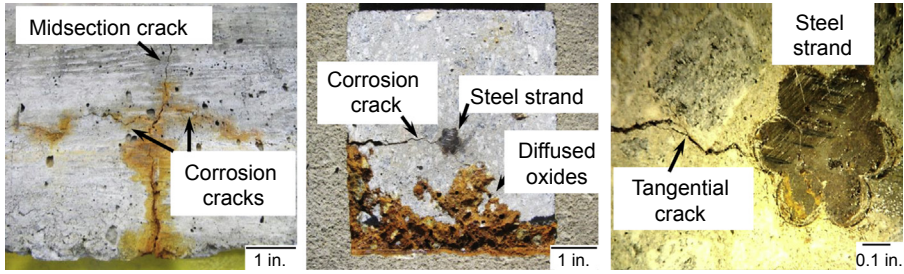
Figure 10.9 Corrosion damage in steel and concrete.

ElBatanouny et al. (2011) proposed that AE intensity analysis can be used to classify corrosion damage. The method was first proposed by Fowler et al. (1989) to quantify damage in fiber reinforced polymers (FRP) vessels and tanks by calculating two parameters: historic index, $H(t)$, and severity, S_r. Historic index is a form of trend analysis that measures the rate of change in the CSS, while severity is the average of a certain number of hits (50 hits) with the highest signal strength. The increase in these parameters can be related to accumulation of damage. Historic index and severity can be calculated using Eqns (10.4) and (10.5), where N is number of hits up to a time (t), S_{oi} is the signal strength of the ith event, and K is an empirically derived factor that varies with the number of hits. In this study, the value of K was selected to be: (a) N/A if $N \leq 50$; (b) $K = N - 30$ if $51 \leq N \leq 200$; (c) $K = 0.85N$ if $201 \leq N \leq 500$; and (d) $K = N - 75$ if $N \geq 501$.

$$H(t) = \frac{N}{N - K} \frac{\sum_{i=k+1}^{N} S_{oi}}{\sum_{i=1}^{N} S_{oi}} \tag{10.4}$$

$$S_r = \frac{1}{50} \sum_{i=1}^{i=50} S_{oi} \tag{10.5}$$

Intensity analysis results were correlated with HCP measurements and measured sectional mass loss, yielding two AE-based corrosion classification charts for precracked and uncracked specimens as shown in Figure 10.10. For precracked specimens, the chart divides the corrosion damage into four categories as illustrated in Mangual et al. (2013a) as follows: (1) No damage: at this level the steel is still in the passive condition and no corrosion damage occurred, (2) Depassivation: at this level corrosion has just initiated with sectional mass loss less than 15%, (3) Cracking: refers to the level at which cracks due to corrosion started to form and the sectional mass loss is less than 21%, and (4) Severe damage: more cracks form and the sectional mass loss exceeds 21%. For pristine specimens, specimens in which depassivation was absent laid in region A of the intensity analysis grading chart, whereas depassivated specimens lay in the B region (Mangual et al., 2013b). These charts enable early detection of corrosion and classification of corrosion damage. Such charts also could extend
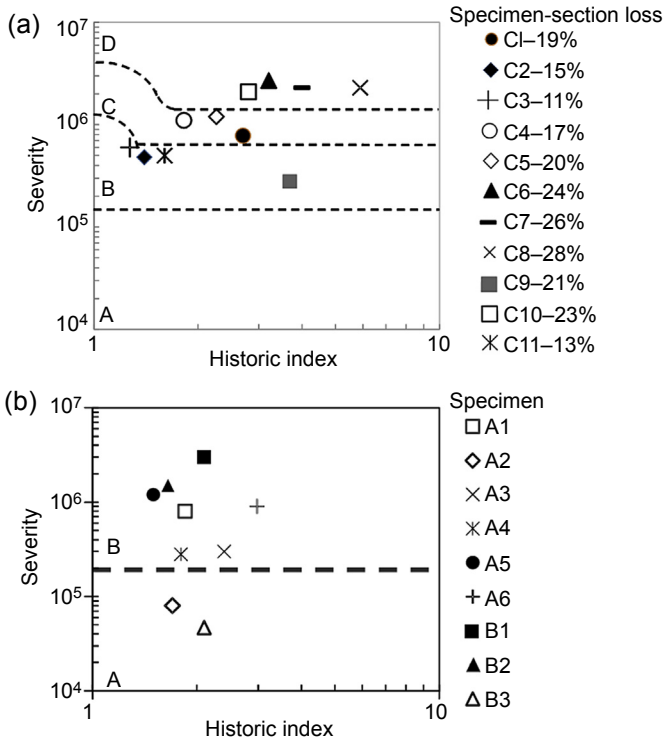
Figure 10.10 AE-based corrosion classification charts for: (a) precracked specimens and (b) pristine specimens (Mangual et al., 2013a,b).

the use of AE to personnel who are less acquainted with methods of performing damage evaluation, without the need to send the collected data to an AE specialist. It is noted that these figures include uncertainties associated with AE monitoring that should be studied and quantified in future studies.

10.4.2　Medium-scale specimens

Long-term corrosion tests were performed on medium-scale PC beams to provide better representation of actual environments for corrosion. The corrosion was accelerated using three-day-wet/four-day-dry cycles with a 3% NaCl solution as shown in Figure 10.11. Each beam was reinforced with two 1/2 in. (12.7 mm) prestressing strands located in the compression zone and measured 16 ft 4 in. in length (4.98 m). The beams were T-shaped with a total height of 15 in. (380 mm), a web thickness of 6 in. (150 mm), and a flange width and depth of 24 in. (610 mm) and 3 in. (75 mm), respectively. The test included three specimens, where two were precracked to 0.016 in. (0.4 mm), specimen CC-0.4; and 0.032 in. (0.8 mm), specimen CC-0.8; while the last specimen was pristine. The specimens were continuously monitored by AE for 140 days. No corrosion damage was detected in the pristine specimen
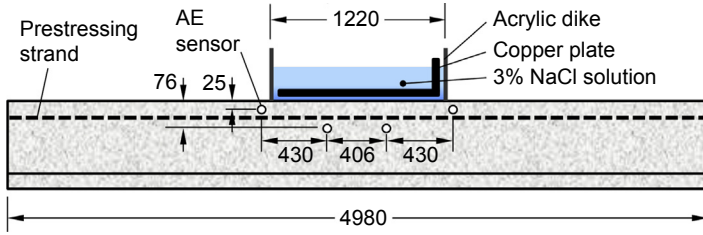
Figure 10.11 Corrosion test setup and AE sensor layout (in mm; 1 in. = 25.4 mm) (ElBatanouny et al., 2014c).

from any method due to the limited ability of chlorides to penetrate through concrete subjected to prestressing force.

The results of the precracked specimens showed that the AE parameter CSS is able to detect corrosion with a higher sensitivity than HCP. As shown in Figure 10.12, HCP for specimen CC-0.8 showed that corrosion initiated within the first week of testing agreed with CSS results that showed a high rate of corrosion activity. For specimen CC-0.4, HCP results only approached the corrosion threshold toward the
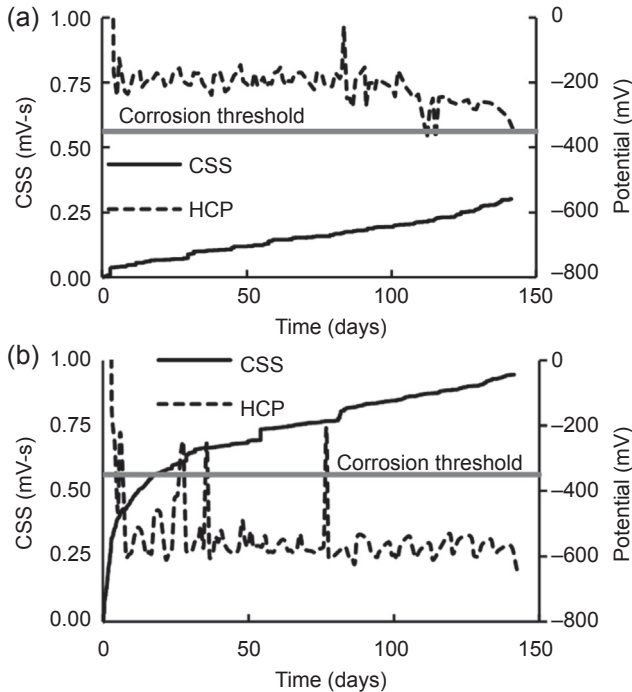
Figure 10.12 CSS and HCP versus time. (a) Specimen precracked crack width (a) 0.016 in. (0.4 mm), specimen CC-0.4 and (b) 0.032 in. (0.8 mm), specimen CC-0.8 (ElBatanouny et al., 2014c).

end of the test while AE was showing a steady increase in the AE activity, illustrating that corrosion is occurring. To further investigate the corrosion activity, linear polarization resistance (LPR) measurements were also taken to calculate the corrosion rate. Based on Andrade et al. (1990) classification, LPR results showed that CC-0.4 had a moderate corrosion rate, while CC-0.8 had a high corrosion rate. This agrees with the AE results, where the rate of AE activity for CC-0.8 was higher than that of CC-0.4. Visual inspection of damaged prestressing strands showed clear evidence of pitting (localized) corrosion in both specimens as shown in Figure 10.13. This corrosion type leads to a significant reduction in the residual capacity of the specimens. Crack width is a significant factor in the formation and intensity of pitting in terms of pit depth. Load testing of the beams at the conclusion of the test showed a reduction in the capacity of the beams where corrosion was detected by AE, as compared with the pristine specimen where no corrosion was detected. This indicated that AE has the ability to detect corrosion before a reduction in the strength of the structure occurs. Therefore, adapting this method for real-time corrosion monitoring can reduce, if not eliminate, the risk of sudden failure as a result of corrosion damage (ElBatanouny et al., 2014c).

Intensity analysis was performed on the cracked specimens using the limits set in the small-scale specimens study as shown in Figure 10.14. The results showed that AE intensity analysis can enable the detection and classification of corrosion damage. This is true for small- and medium-scale specimens, illustrating that the method may be independent of specimen size and duration of exposure. These results were also compared with LPR results and had a good agreement.
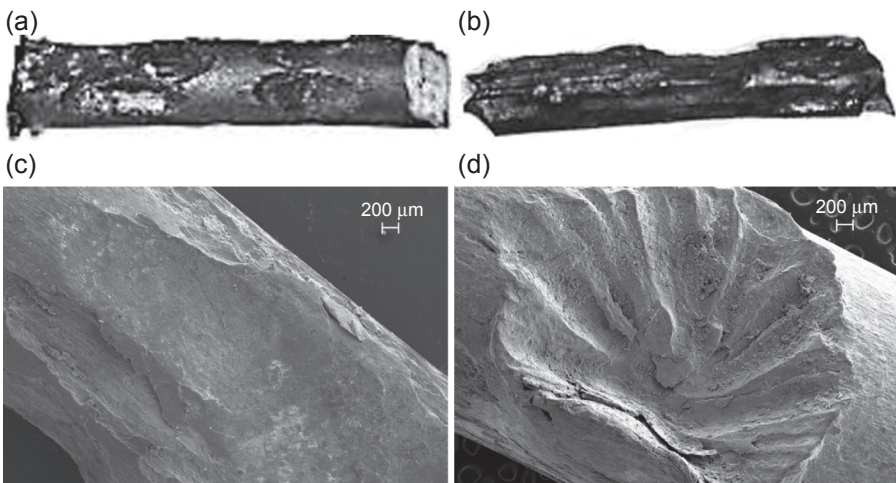
Figure 10.13 Photographs showing pitting corrosion: (a, b) specimens CC-0.4 and CC-0.8, respectively, and (c, d) SEM micrographs of specimens CC-0.4 and CC-0.8, respectively (1 in. = 25.4 mm) (ElBatanouny et al., 2014c).
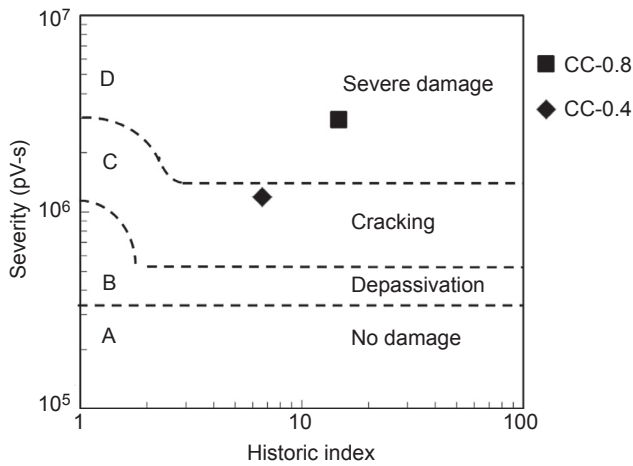
Figure 10.14 Corrosion intensity analysis results for cracked specimens (ElBatanouny et al., 2014c).

10.5 Special considerations and potential applications in the field

AE is a nonintrusive method that has the ability to detect damaged areas through source triangulation. The high sensitivity of the method enables it to perform global assessment of the structure. However, effective filtering protocols are needed for field applications to reject noise related to environmental containments such as rain, hail, and wind with debris.

The method is currently deployable in elements such as piles and foundations. For superstructures, a method to separate AE data from corrosion and that from other sources such as service loading should be developed. More studies should be conducted on the applicability of the developed charts for field applications. Uncertainties related to noise rejection, AE wave speed, and signal attenuation in the field should also be investigated (ElBatanouny et al., 2014d).

10.6 Special considerations for wireless sensing

AE systems have been steadily developing over the past decades to become affordable and deployable. Currently, a self-powered wireless AE system is commercially available in the United States through Mistras Group, Inc. This makes AE suitable for remote/real-time/rapid inspection of massive structures using a minimal number of sensors. The authors of this chapter successfully implemented AE wireless systems in a previous project with the Savannah River National Laboratory, where

AE sensors were embedded in a mesoscale test bed to monitor cracks in grout used for in situ decommissioning of nuclear structures (Ziehl et al., 2012; ElBatanouny et al., 2012).

The wireless AE system "smart node" reduces the data transferred wirelessly by sending the waveform parameters without including the waveforms. The waveforms are saved on an SD card that is attached to the node for more detailed signal processing. This data-reduction technique enables the system to process and send data wirelessly in real-time and reduces the possibility of data loss due to insufficient buffer. However, the capacity of data collection of the wireless system is less than that of wired systems. Therefore, future efforts should focus on comparing AE data collected from wireless AE systems with those of wired AE systems. Since all damage-evaluation techniques proposed are based on wired systems, a probabilistic analysis should be conducted to evaluate and modify damage assessment limits for wireless systems.

10.7   Summary

The feasibility of AE to detect corrosion was evaluated by comparing AE results with electrochemical methods, sectional mass loss, and visual evidence of corrosion damage. AE parameters such as cumulated events and signal strength were found to detect the initiation of corrosion prior to electrochemical measurements. The method can be effectively used in places where there is no provision for electrochemical measurements. AE-based intensity analysis charts can enable the detection and classification of corrosion damage using empirical limits for corrosion levels. This chart classifies corrosion damage in specimens with different sizes and exposure times showing that it may be independent of size and duration.

Unlike some electrochemical techniques, the proposed AE corrosion classification charts have the ability to detect and quantify corrosion damage at early stages. This enables the development of AE into a damage quantification tool for maintenance prioritization because significant damage (such as macrocracking and spalling) is not required for detection. The proposed chart can also be used to estimate safe remaining service life as it is linked to cross-sectional mass loss results. However, the uncertainties associated with the relation between AE and mass loss should be quantified prior to full implementation.

Acknowledgments

References

Abdelrahman, M., 2013. Assessment of Damage in Concrete Structures Using Acoustic Emission. Master thesis. University of South Carolina, p. 146.

Abdelrahman, M., ElBatanouny, M.K., Ziehl, P., 2014. Acoustic emission based damage assessment method for prestressed concrete structures: modified index of damage. Engineering Structures 60, 258−264.

Aki, K., Richards, P.G., 1980. Quantitative Seismology, Theory and Methods, vol. 1. W. H. Freeman and Company, New York, N.Y.

Andrade, C., Alonso, M.C., Gonzalez, J.A., 1990. An initial effort to use the corrosion rate measurements for estimating rebar durability. Corrosion Rates of Steel in Concrete, ASTM STP 1065, 29−37.

ASTM E1316-13c, 2013. Standard terminology for nondestructive examinations. American Standard for Testing and Materials 1−38.

Bhat, C., Bhat, M.R., Murthy, C.R.L., 2003. Acoustic emission characterization of failure modes in composites with ANN. Composite Structures 61, 213−220.

ElBatanouny, M., Mangual, J., Ziehl, P., Matta, F., 2011. Corrosion intensity classification in prestressed Concrete using acoustic emission technique. In: Proc. American Society for Nondestructive Testing (ASNT) Fall Conference and Quality Testing Show 2011, Palm Springs, CA, p. 8.

ElBatanouny, M., Larosche, A., Ziehl, P., Yu, L., 2012. Wireless monitoring of in situ decommissioning of nuclear structures using acoustic emission. In: 8th International Conference on Nuclear Plant Instrumentation, Control, and Human-machine Interface Technologies 2012 (NPIC & HMIT), San Diego, CA, July 22−26.

ElBatanouny, M., Ziehl, P., Larosche, A., Mangual, J., Matta, F., Nanni, A., 2014a. Acoustic emission monitoring for assessment of prestressed concrete beams. Construction and Building Materials 58, 46−53.

ElBatanouny, M., Larosche, A., Mazzoleni, P., Ziehl, P., Matta, F., Zappa, M., 2014b. Identification of cracking mechanisms in scaled FRP reinforced concrete beams using acoustic emission. Experimental Mechanics 54 (1), 69−82.

ElBatanouny, M., Mangual, J., Ziehl, P., Matta, F., 2014c. Early corrosion detection in prestressed concrete girders using acoustic emission. Journal of Materials in Civil Engineering 26 (3), 504−511.

ElBatanouny, M., Abdelrahman, M., Ziehl, P., 2014d. Review of acoustic emission corrosion monitoring of prestressed Concrete bridges. In: PCI Convention and National Bridge Conference, Washington, DC, September 6−9, 2014.

Enoki, M., Kishi, T., 1988. Theory and analysis of deformation moment tensor due to microcracking. International Journal of Fracture 38 (4), 295−310.

Farid Uddin, A.K.M., Numata, K., Shimasaki, J., Shigeishi, M., Ohtsu, M., 2004. Mechanisms of crack propagation due to corrosion of reinforcement in concrete by AE-SiGMA and BEM. Construction and Building Materials 18 (3), 181−188.

Fowler, T., Blessing, J., Conlisk, P., Swanson, T.L., 1989. The MONPAC system. Journal of Acoustic Emission 8 (3), 1−8.

Grosse, C.U., Ohtsu, M., 2008. Acoustic Emission Testing. Springer, Berlin, Germany.

Gutkin, R., Green, C.J., Vangrattanachai, S., Pinho, S.T., Robinson, P., Curtis, P.T., 2011. On acoustic emission for failure investigation in CFRP: pattern recognition and peak frequency analyses. Mechanical Systems and Signal Processing 25 (4), 1393−1407.

Hossain, M., Ziehl, P., Yu, J., 2012. Source characterization of acoustic emission during fatigue crack growth in steel bridge material. In: NDE/NDT for Highways and Bridges: Structural Materials Technology (SMT) Topical Conference, August 21−24, NY.

Idrissi, H., Limam, A., 2003. Study and characterization by acoustic emission and electrochemical measurements of concrete deterioration caused by reinforcement steel corrosion. NDT & E International 36 (8), 563−569.

Jaffer, S., Hansson, C., 2009. Chloride-induced corrosion products of steel in cracked-concrete subjected to different loading conditions. Cement and Concrete Research 39, 116−125.

Kim, K.Y., Sachse, W., 1984. Characteristics of AE signals from indentation cracks in glass. In: Progress in Acoustic Emission II (JSNDI), Proceedings of the 7th International AE Symposium, Zao, Japan, pp. 163−172.

Li, J., Du, G., Jiang, C., Jin, S., 2012. The classification of acoustic emission signals of 304 stainless steel during stress corrosion process based on K-means clustering. Anti-Corrosion Methods and Materials 59 (2), 76−80.

Li, Z., Li, F., Zdunek, A., Landis, E., Shah, S.P., 1998. Application of acoustic emission technique to detection of reinforcing steel corrosion in concrete. ACI Materials Journal 95 (1), 68−76.

Maji, A.K., Ouyang, C., Shah, S.P., 1990. Fracture mechanism of quasibrittle materials based on acoustic emission. Material Research 5 (1), 206−217.

Mangual, J., ElBatanouny, M.K., Ziehl, P., Matta, F., 2013a. Acoustic-emission-based characterization of corrosion damage in cracked concrete with prestressing strand. ACI Materials Journal 110 (1), 89−98.

Mangual, J., ElBatanouny, M.K., Ziehl, P., Matta, F., 2013b. Corrosion damage quantification of prestressing strands using acoustic emission. Journal of Materials in Civil Engineering 25 (9), 1326−1334.

Marec, A., Thomas, J.-H., El Guerjouma, R., 2008. Damage characterization of polymer-based composite materials: multivariable analysis and wavelet transform for clustering acoustic emission data. Mechanical Systems and Signal Processing 22 (6), 1441−1464.

Mejia, F., 2012. Advanced Computing Methods for Knowledge Discovery and Prognosis in Acoustic Emission Monitoring. Dissertation. University of Miami, Coral Gables, FL.

Miller, R.K., McIntire, P., 1987. Non-destructive Testing Handbook. In: Acoustic Emission Testing, vol. 5. American Society for Nondestructive Testing, Columbus, OH.

Moser, R.D., Singh, P.M., Kahn, L.F., Kurtis, K.E., 2011. Chloride-induced corrosion of prestressing steels considering crevice effects and surface imperfections. Corrosion 67 (6), 065001-1−065001-14.

Murakami, Y., Yuyama, S., Shimizu, T., Kouyama, H., Matsushima, M., 1993. Deformation behavior and AE characteristics for anchorage pulling tests on the foundations of power transmission Pylons (Part II, moment tensor analysis). In: Proceedings of the 9th National AE Conference (JSNDI), Okinawa, Japan, pp. 143−150.

Ohno, K., Ohtsu, M., 2010. Crack classification in concrete based on acoustic emission. Construction and Building Materials 24 (12), 2339−2346.

Ohtsu, M., 1987. Acoustic emission characteristics in concrete and diagnostic applications. Journal of Acoustic Emission 6 (2), 99−108.

Ohtsu, M., 1991. Simplified moment tensor analysis and unified decomposition of acoustic emission source: application to in-situ hydrofracturing test. Journal of Geophysics Research 96 (B4), 6211−6221.

Ohtsu, M., 1995. Acoustic emission theory for moment tensor analysis. Research in Nondestructive Evaluation 6 (3), 169−184.

Ohtsu, M., Ono, K., 1984. A generalized theory of acoustic emission and Green's functions in a half space. Journal of Acoustic Emission 3 (1), 27−40.

Ohtsu, M., Tomoda, Y., March 2008. Phenomenological model of corrosion process in reinforced Concrete Identified by acoustic emission. ACI Materials Journal 105 (2), 194−199.

Oliveira, R.d., Marques, A.T., 2008. Health monitoring of FRP using acoustic emission and artificial neural networks. Computers and Structures 86 (3−5), 367−373.

Omkar, S.N., Karanth, R., 2008. Rule extraction for classification of acoustic emission signals using Ant Colony Optimisation. Engineering Applications of Artificial Intelligence 21 (8), 1381−1388.

Perrin, M., Gaillet, L., Tessier, C., Idrissi, H., 2010. Hydrogen embrittlement of prestressing cables. Corrosion Science 52, 1915−1926.

Pollock, A.A., 1986. Classical wave theory in practical AE testing. In: Progress in AE III, Proceedings of the 8th International AE Symposium. Japanese Society for Nondestructive Testing, pp. 708−721.

Prateepasen, A., Jirarungsatian, C., 2011. Implementation of acoustic emission source recognition for corrosion severity prediction. Corrosion 67 (5), 11.

Qian, W., Xie, L., Huang, D., Yin, X., 2009. Pattern recognition of fatigue damage acoustic emission signal. In: IEEE International Conference: Mechatronics and Automation (IEEE-ICMA), Changchun, China, pp. 4371−4375.

Sause, M.G.R., Gribov, A., Unwin, A.R., Horn, S., 2012. Pattern recognition approach to identify natural clusters of acoustic emission signals. Pattern Recognition Letters 33 (1), 17−23.

Scruby, C.B., Baldwin, G.R., Stacey, K.A., 1985. Characterization of fatigue crack extension by quantitative acoustic emission. International Journal of Fracture 28 (4), 201−222.

Shigeishi, M., Ohtsu, M., 1992. A sigma analysis of the 2-dimensional PMMA model. In: Progress in Acoustic Emission VI (JSNDI), Proceedings of the 11th International AE Symposium, Fukuoka, Japan, pp. 211−217.

Shokri, T., Nanni, A., 2014. Crack source location by acoustic emission monitoring method in RC strips during in-situ load test. Smart Structures and Systems 13 (1), 155−171.

Wadley, H.N.G., Scrubby, D.B., 1983. Elastic wave radiation from cleavage crack extension. International Journal of Fracture 23 (2), 111−128.

Weng, M.S., Dunn, S.E., Hartt, W.H., Brown, R.P., 1982. Application of acoustic emission to detection of reinforcing steel corrosion in concrete. Corrosion 38 (1), 9−14.

Yoon, D., Weiss, W., Shah, S., 2000. Assessing damage in corroded reinforced concrete using acoustic emission. Journal of Engineering Mechanics 126 (3), 273−283.

Yuyama, S., 2005. Acoustic emission for fracture studies using moment tensor analysis. The Journal of Strain Analysis for Engineering Design 40 (1), 33−44.

Zdunek, A.D., Prine, D.W., Li, Z., Landis, E., Shah, S., 1995. Early detection of steel rebar corrosion by acoustic emission monitoring. In: Paper No. 547 Presented at CORROSION95, the NACE International Annual Conference and Corrosion, p. 9.

Ziehl, P., 2008. Applications of acoustic emission evaluation for civil infrastructure. In: SPIE Proc., SPIE Smart Structures NDE, San Diego, CA, p. 9.

Ziehl, P., Yu, L., ElBatanouny, M., Larosche, A., 2012. Sensor System Phase Two Test Report: In-situ Decommissioning Sensor Network, Meso-scale Test Bed prepared for DOE/SRNL, Final Report−Phase II, 25 pp.

Assessing a concrete's resistance to chloride ion ingress using the formation factor

11

R. Spragg [1], C. Qiao [1,2], T. Barrett [1], J. Weiss [3]
[1]Purdue University, West Lafayette, IN, USA; [2]University of Science and Technology Beijing, Beijing, China; [3]Oregon State University, Corvallis, OR, USA

11.1   Introduction

Assessing concrete quality, specifically to determine its resistance to ion ingress, has gained increasing interest in recent decades. One particular method that has been receiving increased interest is the use of electrical resistivity or conductivity to assess the transport properties of concrete. Numerous studies have correlated resistivity to diffusion coefficients and other transport coefficients (including Andrade, 1993; Tumidajski et al., 1996; Hall et al., 1997; McGrath and Hooton, 1999; McCarter et al., 2000; Castellote and Andrade, 2006; Nokken and Hooton, 2007; Radlinski et al., 2010; Rupnow and Icenogle, 2011; De La Varga et al., 2014; Bu and Weiss, 2014; Barrett, 2015). While these correlations have shown reasonable agreement, this chapter will highlight why, when assessing concrete quality, the formation factor may be preferred to resistivity alone. This chapter will begin by describing the background of electrical property measurement—that is, resistivity and conductivity—in cementitious materials and will define the formation factor. The formation factor, a microstructural material property that describes the pore network, can then be related to the diffusion coefficients of different ionic species. This chapter provides a review of the experimental techniques needed to determine the formation factor, specifically connectivity, pore volume, and pore solution resistivity, and discusses the role of the degree of saturation. The procedure used recently to determine the formation factor at different degrees of saturation will be presented. An illustration of the formation factor measured on portland cement concretes saturated with different concentrations of pore solution will be presented, along with formation factors measured for variations in portland cement concretes with moderate water-to-cementitious materials (w/c) ratios. Lastly, the process of developing performance ranges will be discussed. An approximation utilizes the surface concentration, reinforcement cover depth, and formation factor to approximate a time to corrosion initiation. The remainder of the chapter will discuss future research needs in advancing the use of the formation factor in specifying durable concrete materials.

11.2   Background

11.2.1   Electrical tests in porous materials

Electrical measurements in saturated porous materials with a nonconducting solid structure can be described using the modified parallel law (Forde et al., 1981; Garboczi, 1990; Torquato and Haslach, 2002), shown here in Eqn (11.1):

$$\rho_T = \rho_o \cdot \frac{1}{\phi \beta} \tag{11.1}$$

where ρ_T is the total resistivity (or the resistivity of the total bulk sample), ρ_o is the resistivity of the pore solution as a function of the ionic composition and concentration in solution, ϕ is the porosity of the system that is fluid filled, and β is the connectivity of the pores in the system (Dullien, 1992; Xie et al., 1992; Olson et al., 1995; Rajabipour, 2006).

It is often difficult to separate the fluid-filled pore volume and connectivity, so literature often presents the product of these two terms together, whose inverse has been termed the formation factor, shown as F in Eqn (11.2), (Snyder, 2001):

$$\phi \beta = \frac{1}{F} \tag{11.2}$$

The formation factor is a *material property* independent of specimen size or shape, but dependent on mixture characteristics such as the w/c ratio, volume of paste, and degree of hydration (Forde et al., 1981; Gu et al., 1992; Christensen et al., 1994). These can change as the system hydrates (ages), often by several orders of magnitude in typical cementitious systems (Rajabipour, 2006).

11.2.2   Nernst−Einstein relationship

The formation factor is typically referred to as a transport property, because it can be used to describe the diffusion of ionic species in porous materials. Diffusion is the process by which ions move through the pore solution due to a concentration gradient, and is often considered a primary transport mechanism for chloride ions through cement-based materials.

The formation factor is related to the diffusion coefficient by what is known as the Nernst−Einstein relationship (Snyder, 2001). This is presented in Eqn (11.3):

$$\frac{\rho_T}{\rho_o} = F = \frac{D_o}{D} \tag{11.3}$$

where ρ_T is the total resistivity, ρ_o is the resistivity of the pore solution, F is the formation factor (this is classically defined at complete saturation), D_o is the self-diffusion coefficient describing how different ionic species move through water,

and D is the effective diffusion coefficient. The self-diffusion coefficient, D_o, has been determined for different ionic species and is shown in Table 11.1 for particular ions that might be of interest.

11.2.3 Electrical tests in cementitious materials

While electrical resistivity tests are easily conducted, analyses of test results and the implications of these values can prove challenging. Most notably, the microstructure and pore solution change significantly over the lifetime of the material (Hammond and Robson, 1955; McCarter et al., 1981; Rajabipour, 2006; Sant et al., 2006).

Curing conditions can also influence measurements. Sealed curing versus water curing can lead to a significantly different extent of reaction (degree of hydration), which will affect both the microstructure and the pore solution properties (Weiss et al., 2013; Spragg et al., 2013b). Additionally, storage conditions can lead to different levels of drying that impact the volume of pore fluid, its connectivity, its pore solution resistivity and correspondingly the measured resistivity (Rajabipour and Weiss, 2007). For example, Presuel-Moreno et al. (2010) have shown that storage in limewater versus storage in a 100% relative humidity chamber can lead to differences in electrical measurements (Presuel-Moreno et al., 2009). There is a dependence of the measured electrical properties on moisture content, which can be accounted for with a correction (Weiss et al., 1999, 2013; Schiessel et al., 2000; Barrett, 2015).

Further, if samples are stored in a fluid there are additional complications. First, storage in a fluid does not necessarily mean that samples will be completely saturated (Rajabipour, 2006; Bu et al., 2014). The concrete sample can also leach alkali species from the pore solution into the surrounding storage solution, thereby changing the pore solution resistivity (Thomas et al., 2006; Spragg, 2013; Spragg et al., 2013b). Leaching of alkalis can influence the microstructure that forms (Bu and Weiss, 2014).

Table 11.1 Values of self-diffusion coefficient

Ionic species	Self-diffusion coefficient, D_o 10^{-10} m^2/s		
	0 °C	18 °C	25 °C
Na$^+$	6.3	11.3	13.3
K$^+$	9.9	16.7	19.6
Mg^{2+}	3.6	5.9	7.1
OH$^-$	25.6	44.9	52.7
Cl$^-$	10.1	17.1	20.3
SO$_4{}^{2-}$	5.0	8.9	10.7

From Yuan-Hui and Gregory (1974).

Two separate correction factors have been used to account for temperature; the first accounts for rate effects associated with hydration (e.g., an equivalent age), while the second accounts for changes in conduction with testing temperature (Sant et al., 2008). However, a general equation has been proposed to account for the effects of all of these factors on electrical resistivity measurements at an equivalent age (Spragg et al., 2013a), as shown in Eqn (11.4):

$$\rho_{T_{ref}} = \rho_o^* \cdot F \cdot f(S) \cdot f(T_{test}) \cdot f(\text{Leach}) \tag{11.4}$$

where $\rho_{T_{ref}}$ is the resistivity at a reference temperature at an equivalent age of t_{eq}, ρ_o^* is the resistivity of the pore solution at saturation, F is the formation factor, $f(S)$ is a saturation function that has typically been used for comparison with vacuum-saturated concretes, $f(T_{test})$ describes the effect of testing temperature on resistivity measurements, and $f(\text{Leach})$ is a leaching function. The equivalent age t_{eq} is a function of the time and temperature history—that is, maturity or degree of hydration.

Most importantly, it can be concluded that the formation factor is a microstructural property, while resistivity is a related parameter that has many outside influences.

11.2.4 Differing levels of saturation

Powers's gel space ratio theory provides a conceptual idea of the relative volumetric proportions of a hydrating cement paste (Powers and Brownyard, 1946). The series of papers dealing with the model provided a quantification of the reaction between cement and water. The major tenets of Powers's model are:

- Initially, the system is composed of cement and water. The free water is termed capillary water. The volume ratio of initial capillary water is given by the term initial porosity, $p = (\text{w/c})/(\text{w/c} + \rho_w/\rho_c)$, where w/c is the water-to-cementitious mass ratio, ρ_w is the density of water, and ρ_c is the density of cement.
- The amount of reacted cement is termed the degree of hydration, α, where 0.0 means no cement is reacted and 1.0 means all of the cement has reacted.
- The reaction between cement and water results in a reduction of volume termed chemical shrinkage, which is approximately 6.4 mL/100 g reacted cement.
- Hydration products are classified as gel solids and gel water, with the latter approximately 28% of the volume of the reacted products.

A graphical representation of Powers's model is shown in Figure 11.1 for a 0.42 w/c ratio paste (after Jensen and Hansen, 2001). Initially, the volume fraction of capillary water is characterized by the term initial porosity described above, with the remainder of the volume representing cement. As the degree of hydration progresses, the formation of gel solids and gel water takes place, with a reduction in the volume of capillary water and un-hydrated cement.

It should be noted that while both capillary water and gel water represent porosity—that is, water-filled voids in the system—they represent very different size scales. Capillary pores are on the order of 10 µm to 10 nm (Mindess et al., 2003). Capillary water behaves as bulk water, and pores of this large size and connectedness are a major
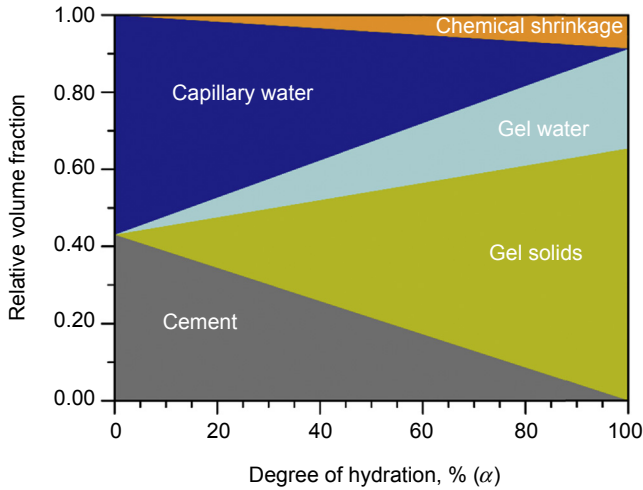
Figure 11.1 Graphical illustration of Powers's model for a 0.42 w/c ratio paste.

contributor to the mass transport that occurs through the matrix. Gel pores are smaller, on the order of 10 to 2 nm, and are a porosity inherent in the hydration process of cement (Mindess et al., 2003). Since the gel pores are much smaller, they do not contribute much to the mass transport (Sant et al., 2011; Barrett, 2015).

Additionally, due to reduction in volume between reactants and products, the formation of chemical shrinkage occurs. Chemical shrinkage consists of vapor-filled voids in a sealed sample, as contrasted with gel and capillary pores, which are typically viewed as fluid-filled porosities.

As Powers's model was designed to describe cement paste, its application to concrete can be achieved by considering that concrete is typically only 25−32% paste. As an example, Figure 11.2 shows a 28% paste concrete with a 0.42 w/c ratio. The paste portion is similar to that shown in Figure 11.1; however, it only occupies 28% of the volume. Concrete typically also contains entrained air voids, usually on the order of 6−8% by total volume; in this example, an air content of 6.5% is used. The remainder of the volume is composed of aggregates (Barrett, 2015; Todak, 2015).

Air voids typically are air bubbles that are stabilized during the mixing process. As such, they are often vapor-filled pores (and correspondingly nearly non-conductive) ranging in size from 0.05 to 1 mm (Lamond and Pielert, 2006; Lucero, 2015).

To assess paste properties with electrical tests and formation factor calculations, it is important to understand which pores are filled with fluid. One way to describe the pore space filled with fluid is to evaluate the de*gree* of saturation. This is defined in Eqn (11.5):

$$S = \frac{\text{Fluid in specimen}}{\text{Fluid in specimen at complete saturation}} = \frac{m_{\text{at moisture state}} - m_{\text{OD}}}{m_{\text{SSD}} - m_{\text{OD}}} \quad (11.5)$$
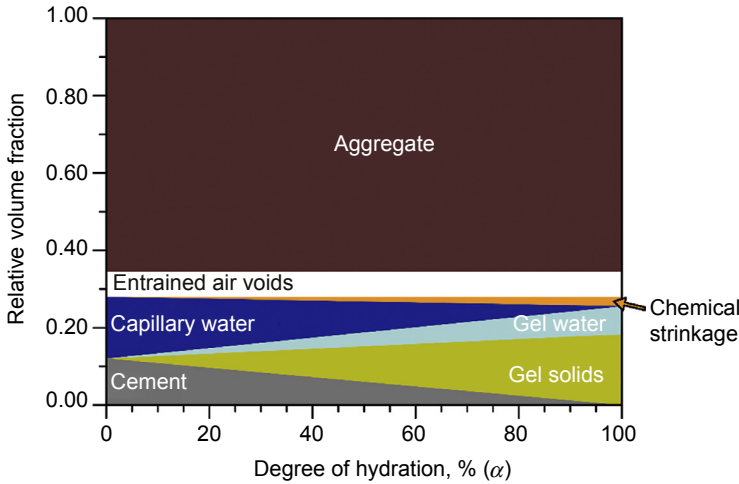
Figure 11.2 Graphical illustration of Powers's model for a 0.42 w/c ratio concrete having a 28% paste volume and 6.5% air content.

where $m_{at\ moisture\ state}$ is the specimen mass at the moisture state in question, m_{OD} is the oven dry mass of the specimen, and m_{SSD} is the saturated-surface dry mass of the specimen after vacuum saturation at an absolute pressure of 6 Torr (Bu et al., 2014). This parameter describes the fraction of the porosity that is filled with fluid at a given moisture state.

The degree of saturation in a sealed sample can be calculated based upon Powers's model (Barrett, 2015; Todak, 2015). In a paste system, the gel pores and capillary pores remain fluid filled. The vapor-filled space of chemical shrinkage represents the only reduction in degree of saturation (in a non-air-entrained system). As such, the sealed degree of saturation can be calculated as simply the volume of the gel and capillary pores divided by the sum of the volume of gel pores, capillary pores, and chemical shrinkage. In the paste system, if the chemical shrinkage is filled, the degree of saturation should be 100%. Figure 11.3(a) shows the reduction
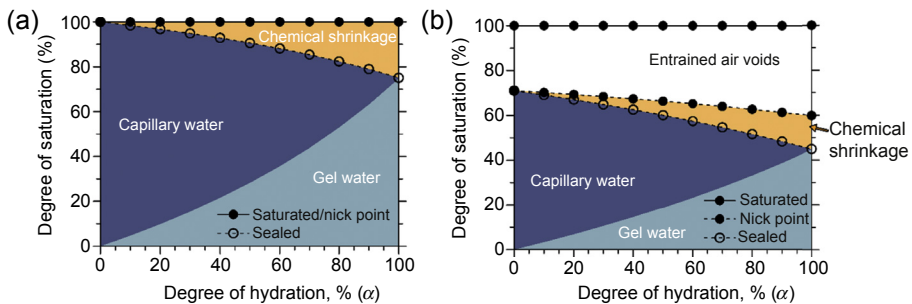
Figure 11.3 Changes in the degree of saturation for a 0.42 w/c ratio (a) paste system or (b) 6.5% air content concrete system. The nick point represents the moment when the paste porosity is filled.
After Weiss et al. (2016).

in the degree of saturation as a function of degree for a sealed system, or when the pores in the paste are saturated (Barrett, 2015; Todak, 2015).

Concrete has three moisture states that are of the most interest when evaluating transport properties. These are a sealed condition; a condition where the porosity in the paste is fluid filled; and one where all the porosity is fluid filled (Barrett, 2015). Calculation of the theoretical degree of saturation in each of these conditions can be accomplished by considering Powers's model and the volume of entrained air voids, noting that the air voids are not fluid filled for a sealed sample or a sample exposed to drying. As such, the air content represents a significant reduction in the degree of saturation even before any chemical shrinkage develops in the paste.

The first condition is the sealed case, where no moisture is allowed to enter or leave the specimen. The degree of saturation in this case would be the sum of the gel and capillary pores divided by the gel and capillary pores, chemical shrinkage volume, and volume of air voids. The second moisture state, the condition where the air voids remain empty but the porosity in the paste is filled, has been termed the nick point, as it corresponds to a kink in water absorption behavior (Todak et al., 2015). The degree of saturation in this case is calculated as the porosity in the paste (chemical shrinkage, and gel and capillary pores) divided by the paste porosity and the volume of air. The last is the complete saturation. This does not just mean submerged in a tank, but vacuum-saturated to allow for complete degassing and for the fluid to fill in all voids in the concrete (Bu et al., 2014).

11.3   Experimental techniques

11.3.1   Concrete resistivity

The three most common methods for measuring the resistivity of concrete include uniaxial, surface, and embedded geometries that are discussed in detail in this section. Common testing geometries for the surface and uniaxial configurations are shown in Figure 11.4. Resistivity is a material property independent of specimen size or shape and testing configuration. Values of resistivity are obtained from measurements of resistance and related by Eqn (11.6), where ρ is the resistivity and k is the geometry factor, which depends on specimen size and shape and testing configuration:

$$\rho = R \cdot k \tag{11.6}$$

Other configurations utilize embedded sensors. These have been used extensively in the literature (e.g., Raupach and Schiessl, 1997; Weiss, 1999; Schiessel et al., 2000; Polder, 2001; Rajabipour et al., 2005; Rajabipour, 2006; Poursaee and Weiss, 2010; Castro et al., 2010; McCarter et al., 2015). These are often sensors that can be placed directly into the fresh concrete and cast in place. These have the benefit that they can be placed into a specimen that is then sealed, and testing would not necessitate removal from the sealed condition and thus create a risk of extensive loss of moisture. This would be ideal for the monitoring of sealed specimens.
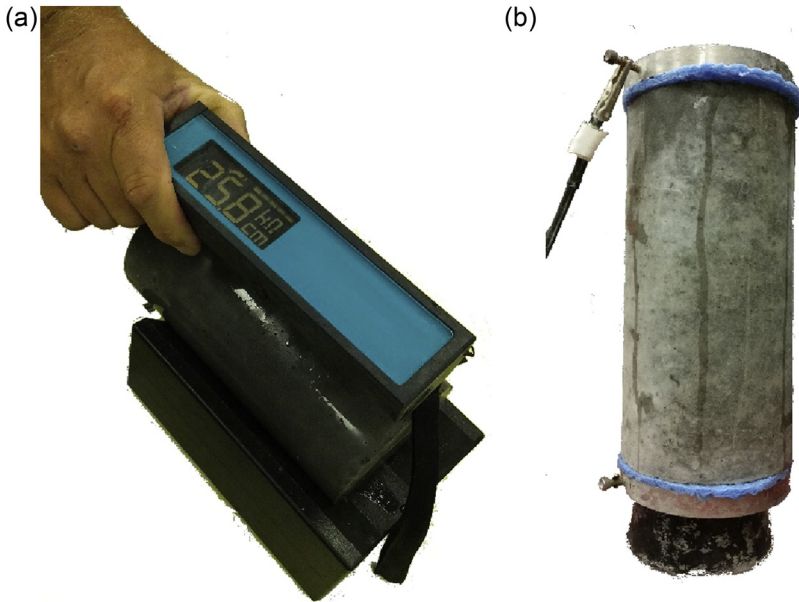
Figure 11.4 Common testing geometries used on standard 100 mm × 200 mm test cylinders in the (a) surface and (b) uniaxial configurations.

As discussed previously, *resistivity* is a material property that is independent of specimen geometry and electrode configuration. However, the *re*sistivity is determined from a test of *resistance*. This resistance must be corrected for specimen size and electrode configuration to determine the resistivity. This correction has traditionally been termed the geometry factor, denoted using k in Eqn (11.6).

Geometry factors can be determined experimentally by comparing with the measurement of a solution of known resistivity, or numerically (Morris et al., 1996; Rajabipour, 2006; Spragg et al., 2013b). The units of resistivity are typically ohm·length, where the ohm comes from the measure of resistance, and the measure of length comes from the geometry factor.

When the resistance is multiplied by the correct geometry factor, resistivity tests that are performed using samples of differing geometry will show consistent results between samples of different geometries (Spragg et al., 2012, 2013b). Also, resistivity measurements are temperature sensitive. The measurements discussed in this chapter were conducted at 23 ± 1 °C. If measurements are conducted at other temperatures, they should be corrected for temperature back to the 23 °C reference temperature before they are used to compute the formation factor (Chrisp et al., 2001; Sant et al., 2008; Spragg et al., 2013b).

11.3.1.1   Surface configuration: Wenner test

The surface resistivity test, often termed the Wenner test, was initially developed for use in soil testing by Frank Wenner at the National Bureau of Standards in the 1910s

(Wenner, 1916). A schematic of the four-point surface resistivity test applied to a concrete cylinder is shown in Figure 11.5.

In the development of the equations used to interpret the results from this test, an assumption of an infinite half-space was assumed—that is, the spacing of the electrodes is much smaller than the depth of the material being measured ($a \ll d, L$). If this criterion is satisfied, the geometry factor is given by $\widehat{k}_1$ in Eqn (11.7):

$$\widehat{k}_1 = 2\pi a \tag{11.7}$$

where a represents the spacing of the electrodes. Many commercial surface resistivity meters make this correction automatically.

However, when testing is conducted on a cylindrical concrete test specimen, the assumption of infinite half-space is not completely satisfied, because of the small testing geometry and large probe tip spacing required to prevent interferences with coarse aggregates (Presuel-Moreno et al., 2010; AASHTO TP95-11, 2011; Morris et al., 1996). An additional factor is often needed to account for constricted current flow in the material. Morris et al. (1996) have shown, using finite element simulations, the magnitude of additional corrections needed when using surface resistivity tests on various cylindrical geometries. These data have been digitized and can be described by Eqn (11.8) (Spragg et al., 2013b):

$$\widehat{k}_2 = 1.10 - \frac{0.730}{(d/a)^1} + \frac{7.34}{(d/a)^2} \tag{11.8}$$
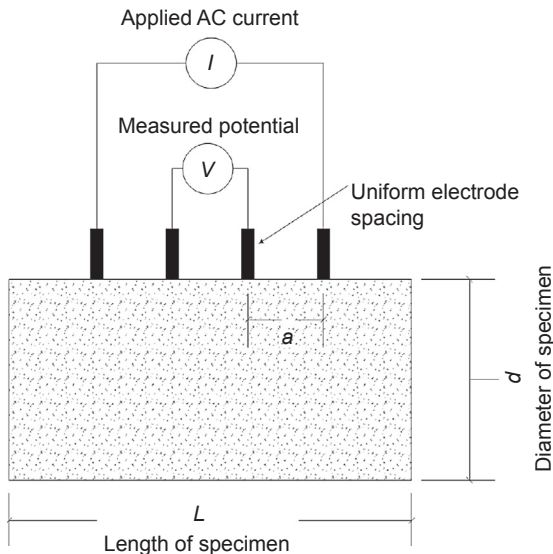
Figure 11.5 Schematic of the surface resistivity test being conducted on a test cylinder. Reproduced from Spragg et al. (2013a).

where a represents the spacing of the electrodes and d is the diameter of the test cylinder. It should be noted that this correction applies only when $d/a \leq 6.0$ and $L/a \geq 6.0$, where L is the length of the cylinder. For testing on a standard 100 mm $\times$ 200 mm test cylinder, this value ranges from 1.8 to 1.9.

Oftentimes, $\widehat{k}_1$ is applied automatically by the resistivity meter before a number is displayed on the machine (Proceq, 2013). In that case, $k = 1/\widehat{k}_2$ should be applied. In the case that the resistivity meter simply shows the measured resistance, the geometry factor for a surface test is given by Eqn (11.9):

$$k = \frac{\widehat{k}_1}{\widehat{k}_2} \tag{11.9}$$

It is also worth noting that Eqn (11.9) is only valid for a (spatially) homogeneous system, and shows good agreement when the material is indeed homogeneous (Spragg et al., 2015a,b).

The surface resistivity test has gained popular usage by the Florida (FM 5-578, 2004; Vivas et al., 2007) and Louisiana (Rupnow and Icenogle, 2012) Departments of Transportation. Many sources in the literature advocate the use of this method because it can allow for measurements in situ, but a dependence on geometry, degree of saturation, leaching of alkalis and ingress of deicing salts applied from deicing operations, temperature, and location of reinforcing steel means that in situ measurements, when assessing concrete quality, should be interpreted carefully (Presuel-Moreno et al., 2009; Spragg et al., 2013a; Salehi et al., 2014).

11.3.1.2 Uniaxial configuration

The uniaxial resistivity test is another resistivity configuration for use on a concrete specimen (McCarter et al., 1981). A schematic of the uniaxial test is shown in Figure 11.6. This configuration typically consists of a set of plates placed at the ends of the specimen with a conductive medium, typically a wet sponge or conductive gel used to create good electrical contact between the specimen and electrodes.

This configuration has the benefit of a more uniform current distribution throughout the sample, and is not as dependent on surface characteristics. The geometry factor for this configuration is shown in Eqn (11.10):

$$k = \frac{A}{L} \tag{11.10}$$

where A is the cross-sectional area of the specimen and L is the length of the specimen.

One important assumption of this test is that there is a good electrical connection between the test specimen and the electrodes, typically accomplished through the use of a conductive medium (Newlands et al., 2007). This can be a conductive gel, paper towel, or sponge wetted with conductive solution (Shane, 2000; Thomas, 2008; Spragg et al., 2012). In some cases, these elements have an associated resistance. A correction has been proposed to the measured resistance to
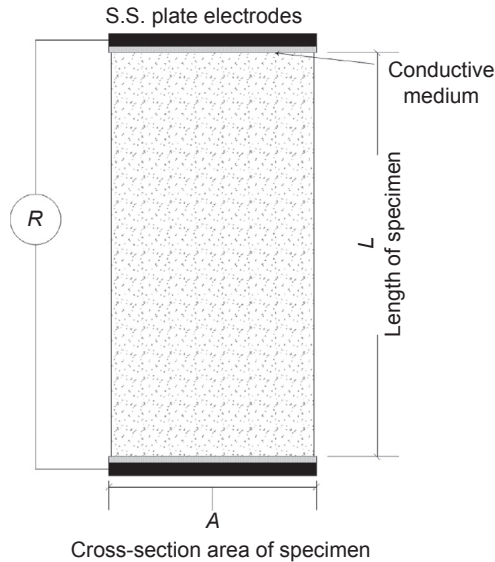
Figure 11.6 Schematic of the uniaxial resistivity test being conducted on a test cylinder. Reproduced from Spragg et al. (2013a).

correct for the resistance of the sponges, as shown in Eqn (11.11) (for resistors in series) (Newlands et al., 2007):

$$R = R_{\text{measured}} - R_{\text{top sponge}} - R_{\text{bottom sponge}} \qquad (11.11)$$

where R is the resistance used in Eqn (11.6); R_{measured} is the measured resistance of the top sponge, specimen, and bottom sponge; and $R_{\text{top sponge}}$ and $R_{\text{bottom sponge}}$ are the resistances of just the top and bottom sponge, respectively. When measuring the resistance of each sponge, it is important to use the pressure that each sponge experiences during the resistivity test. An example is shown in Figure 11.7. Research has indicated that if a solution of low enough resistance is used for the sponges, and the concrete is of high resistivity, the correction tends to be negligible (Spragg et al., 2012).

11.3.1.3 Embedded configuration

The last configuration is the embedded configuration. While the literature has had many successful variants of the embedded sensor, one that has shown particular promise is a set of stainless steel rods in a standard 150 mm × 300 mm test cylinder, shown here in Figure 11.8.

This particular configuration has been described elsewhere in the literature (e.g., Castro et al., 2010; Spragg et al., 2013b).

For this configuration, the geometry factor often needs to be determined numerically or experimentally. The experimental determination can be done using a solution
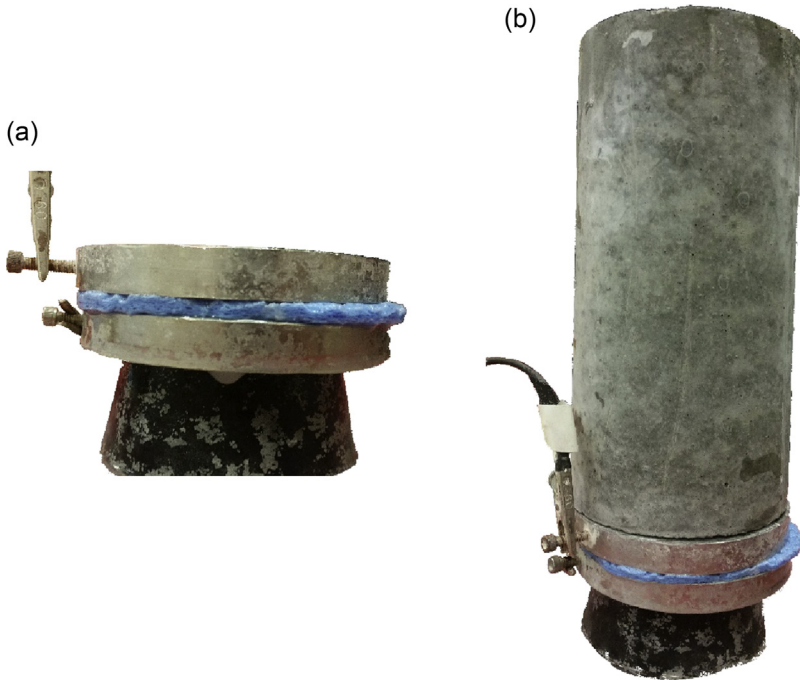
Figure 11.7 Configuration for the measurement of (a) $R_{\text{top sponge}}$ and (b) $R_{\text{bottom sponge}}$.

of known conductivity such as potassium chloride, whose conductivity is presented in many chemistry or physics handbooks, (e.g., Dean and Lange, 1999). It is worth noting that a solution of significantly low resistivity—that is, higher concentration—should be used, as high-resistivity solutions can introduce spurious results.

11.3.2   Pore solution resistivity

The resistivity of the pore solution is an important factor when determining the formation factor. There are typically two methods of obtaining pore solution—experimental and theoretical.

11.3.2.1   Experimental pore solution expression

Experimental pore solution expression can be performed in accordance with a technique discussed by Barneyback and Diamond (1981). This technique uses paste samples made from the cementitious materials of interest, and using their relative proportions from the concrete of interest. The specimens are placed into a high-pressure die system and specimens are squeezed, which expresses the pore solution. The resistivity of the expressed pore solution can then be measured by using a small pore solution cell.

The high-pressure die-and-piston system described by Barneyback and Diamond (1981) is shown schematically in Figure 11.9.
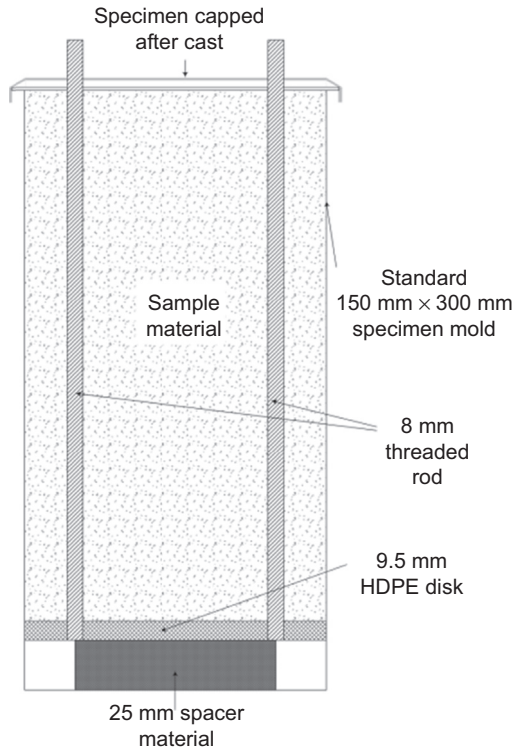
Figure 11.8 Schematic of the embedded configuration in a modified 150 mm × 300 mm test cylinder (HDPE = high-density polyethylene).
Reproduced from Spragg et al. (2013a).

For this approach, approximately 50-mm-diameter samples of cement paste are made, then placed into the die. The apparatus is placed into a press or compression machine and loaded to express the solution from the pores. The fluid is collected in a syringe or small vial. Typically, only a few milliliters of solution are obtained.

Once the solution is obtained, its electrical resistivity can be measured by testing in a pore solution resistivity cell such as the one pictured in Figure 11.10(a) (Castro et al., 2010). A schematic is shown in Figure 11.10(b), and is made from 3/8″ diameter polycarbonate tubing approximately 1″ long with end plates of stainless steel, with a small hole drilled in one of the steel plates. The centers of the plates are slightly milled such that the tube can fit in the end and no solution is lost. The solution is then filled from the hole, and the plates connected to an electrical resistivity meter whose resistance is then measured.

The resistivity of the pore solution can be determined using Eqn (11.6). The geometry factor for the type of cell shown in Figure 11.10 is given by Eqn (11.10)— that is, the ratio of cross-sectional area to length.

Another method of experimentally determining pore solution resistivity is through the use of an embedded pore solution sensing system (Rajabipour et al., 2007;
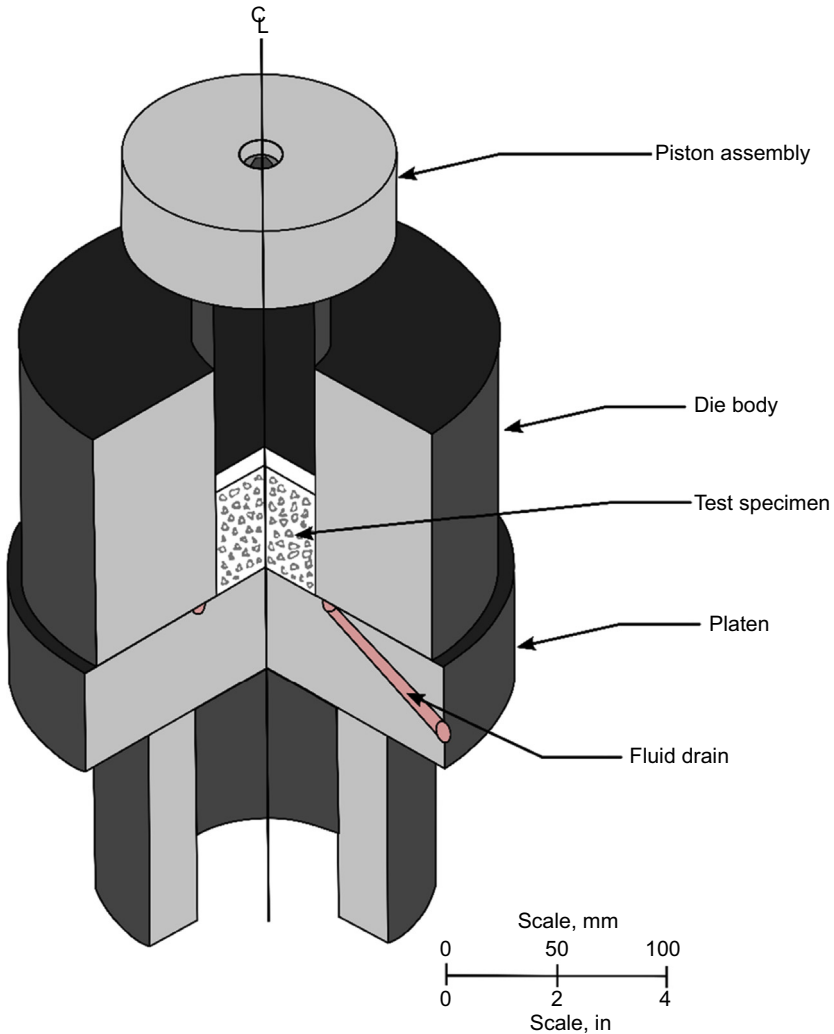
Figure 11.9 High-pressure die-and-piston system for experimentally expressing pore solution from hardened cement pastes.
After Barneyback and Diamond (1981).

Rajabipour and Weiss, 2007). The system consists of two sensors, and prior to use, a calibration curve is developed to account for different relative humidities and solution resistivities. The system can then be embedded into fresh concrete, and the resistivities of the two sensors are measured. Using the resistivities of the sensors and the calibration curve, the pore solution resistivity can be determined (Rajabipour, 2006; Rajabipour et al., 2007).
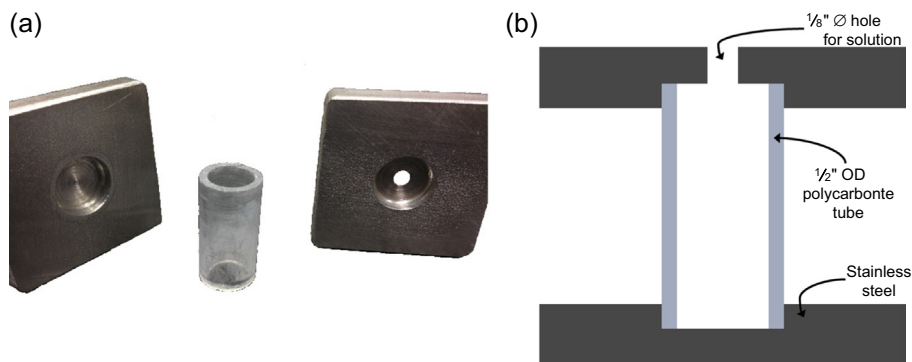
Figure 11.10 Example pore solution cell shown in a (a) photograph or (b) schematic.

11.3.2.2 Theoretical pore solution

An alternative method of approximating pore solution resistivity is estimation based upon the theoretical pore solution composition. The theoretical pore solution composition can be estimated from the chemistry of the cementitious materials, the mixture proportions, and the degree of hydration.

This procedure was originally described by Taylor (1987). It has since been implemented in an online HTML/JavaSscript tool by Bentz (2007), available at http://concrete.nist.gov/poresolncalc.html.

This method initially requires determination of the pore solution composition. For this, the moles (N) of Sodium (Na) and Potassium (K) are determined from the chemistry of the cementitious materials, specifically mass percentages of alkalis, which is the information typically reported in the mill certificate. Also needed is the mass from the mixture design of each cementitious material.

This calculation is based upon the total amount of the alkalis in the cementitious materials; however, not all of these materials are released into the pore solution. This concept has been incorporated into the online tool using the free ion factor (Bentz, 2007), and can be summarized as:

- Of the potentially available Na and K ions from the cement, silica fume, and fly, 75% are present in the pore solution after approximately 24 h. Prior to this time, sulfate reactions are occurring and can impact the pore solution chemistry and pore connectivity (De La Varga, 2013; Spragg et al., 2013b).
- The alkalis present in the slag cement are assumed to be incorporated into slag hydration products, and the alkalis in the slag will not be released into the pore solution.
- Alkalis are strongly absorbed by silica fume, and for mass fractions above 15%, alkalis in the pore solution represent only 45% of total alkalis.
- Electroneutrality must be maintained, so the sum of the cation concentration (i.e., Na^+ and K^+) is used to compute the concentration of OH^- in the pore solution.

For sealed specimens, Powers's model can be used to estimate the volume of pore solution, in terms of L of solution per mass of cementitious materials, as simply the sum of capillary and gel water. The online tool also has an option for what it terms

"saturated" curing, but this specifically means when the matrix is filled, meaning that the volume of pore solution is the sum of the capillary, gel, and chemical shrinkage volumes (Bentz, 2007). This accounts for the dilution of the pore solution concentration by adding the volume of chemical shrinkage, but does not account for alkali leaching that can occur during moist curing (Spragg et al., 2015b).

Previous research has shown good agreement between experimentally expressed measured solutions and theatrical pore solution resistivity values (De La Varga, 2013; Spragg et al., 2013b; Bu and Weiss, 2014) for sealed cured paste samples. The best agreement comes after about a 20% degree of hydration. It has been suggested that this is due to aluminate reactions that can cause variations in the pore solution composition, specifically the presence of sulfate ions and a lower concentration of hydroxyl ions (Spragg et al., 2013b).

Additionally, air-entrained concretes can present challenges. Previous research has shown that changes in entrained air content—that is, different dosages of air-entraining admixture—have been shown to have little effect on sealed resistivity measurements (Castro et al., 2010). This makes sense, as air-entrained concrete is typically considered non-fluid-filled (and therefore non-conductive) in sealed systems. When concretes are vacuum saturated, the pore solution concentration is diluted, as the fluid-filled volume (in a sealed system) goes from the volume of gel and capillary pores in the matrix to the volume of gel, capillary, and chemical shrinkage of the matrix and the entrained air volume (Barrett, 2015). The amount of dilution for a sealed system can be estimated by the air dilution factor shown in Eqn (11.12) and termed d_{Air}, and can be applied to the ionic concentration of each species—that is, K^+, Na^+, and OH^-. The premise of this factor is reducing the number of ions originally in the volume of gel and capillary pores (termed "water left" in the online Bentz tool) by the volume of gel and capillary pores, chemical shrinkage, and air content, which should be in units of L water/kg cement.

The dilution parameter is shown in Eqn (11.12), and is termed $d_{\text{sealed−saturated}}$ to describe the dilution that takes place when going from a sealed specimen to a specimen vacuum saturated in limewater. The Bentz online tool (Bentz, 2007) has an option for a similar dilution, but only accounts for the volume of chemical shrinkage, not the volume of air (Barrett, 2015).

The dilution parameter, $d_{\text{sealed−saturated}}$, can be calculated according to Eqn (11.12). The terms A, B, and C are defined in Table 11.2, where w/cm is the total w/c ratio by mass and α is the degree of hydration. The 0.23 and 0.06 coefficients that describe the reduction in porosity and chemical shrinkage, as discussed by Bentz, are generally accepted values but could be modified for a specific cement (Powers, 1966; Bentz, 2007). Parameter C describes the volume of air-entrained voids, but converted from a volume percentage to units consistent with those of A and B. For this equation, the percentage of air should be used along with the total weight of cementitious materials per cubic yard. The factor of 16.878 is used to make the conversion, when using % and lb of cementitious materials to L of water per kg of cementitious materials:

$$d_{\text{Air}} = \frac{A}{A + B + C} \qquad (11.12)$$

Table 11.2 Description of terms used in the calculation of the dilution parameter to account for dilution of the pore solution when vacuum saturating an air-entrained concrete

Letter	Description	Calculation	Units
A	Volume of gel and capillary porosity	$\text{w/cm} - 0.23\alpha$	L per kg cementitious
B	Volume of chemical shrinkage	0.06α	L per kg cementitious
C	Volume of air	$\dfrac{\frac{\text{Air (\%)}}{100} \cdot 27\left(\frac{\text{ft}^3}{\text{yd}^3}\right) \cdot 28.3\left(\frac{\text{L}}{\text{ft}^3}\right)}{\text{Total cementitious (lb)} \cdot 0.453\left(\frac{\text{kg}}{\text{lb}}\right)}$ or $\dfrac{\text{Air (\%)}}{\text{Total cementitious (lb)}} \cdot 16.878$	L per kg cementitious

The dilution factor, d_{Air}, is applied to the ionic concentration given by the online tool. From there, the resistivity can be calculated as described by literature (Snyder et al., 2003; Bentz, 2007).

The dilution of the pore solution due to filling of the air voids can be significant, and in the case of 6.5% air content and a 0.42 w/c ratio, the dilution can represent a pore solution resistivity nearly double that of the pore solution that is present when the air voids are not filled.

11.3.3 Determining the formation factor

The experiments described in Section 11.4 evaluate the resistivity of two conditions, sealed and vacuum saturated. As discussed in Section 11.2.4 for concrete materials, these evaluate the matrix pores (sealed condition) or the entire pore system (saturated condition), including entrained air voids (Barrett, 2015).

For sealed measurements, it is important to ensure that test specimens are sufficiently sealed to prevent moisture loss from hydrating concrete to the environment. To accomplish this, the work has utilized specimens that were left sealed in their original cylinder molds and placed in an additional 6 mil sealed plastic bag. When incorporated into a specification, in an effort to ensure that the specimens are adequately sealed, a mass change criterion for the period between arrival at the testing lab and the time of testing could be specified (Spragg et al., 2013a; Barrett, 2015).

The sealed formation factor F_{sealed} can be calculated by the ratio of concrete resistivity measured in a sealed condition, ρ_{sealed}, to the resistivity of the pore solution in a sealed condition, $\rho_{\text{o-sealed}}$, as shown in Eqn (11.13):

$$F_{\text{sealed}} = \frac{\rho_{\text{sealed}}}{\rho_{\text{o-sealed}}} \tag{11.13}$$

Specimens for saturated formation factor, $F_{\text{saturated}}$, testing should first be oven dried, then vacuum saturated using limewater at an absolute pressure of 6 Torr for a period of 3 h, adding de-aired limewater for an additional 1 h at the 6 Torr vacuum level, and allowed to sit under limewater for an additional 18 h (Bu et al., 2014). The specimens can then be measured for their saturated resistivity, $\rho_{\text{saturated}}$. The pore solution at saturation, $\rho_{\text{o-saturated}}$, can be calculated as described in Section 11.3.2.2. From these two parameters, $\rho_{\text{saturated}}$ and $\rho_{\text{o-saturated}}$, the saturated formation can be calculated using Eqn (11.14):

$$F_{\text{saturated}} = \frac{\rho_{\text{saturated}}}{\rho_{\text{o-saturated}}} \qquad (11.14)$$

11.4 Microstructural parameters

11.4.1 Formation factor at saturation for concrete materials

This study evaluated a portland cement concrete at an age of 91 days, with the mixture proportions listed in Table 11.3. The samples were sealed cured in their original cylinder molds inside a 6 mil sealed plastic bag.

At an age of 91 days, the specimens were demolded and prepared for testing. Specimens were oven dried and then vacuum saturated with two different solutions: (a) limewater and (b) artificial pore solution. The specimens were tested 24 h after vacuum saturation for resistivity.

The pore solution was approximated for the lime-water-saturated specimens by the procedure described in Section 11.3.2.2, accounting for dilution due to air content. The short amount of time under water was assumed to have negligible effects on the leaching of alkalis. The second set of specimens was saturated with artificial pore solution, with concentrations determined from the procedure discussed in Section 11.3.2.2. The pore solution for this system would be twice the concentration—that is, the alkalis that were initially in solution that remained when the specimen was oven dried and the ions

Table 11.3 Mixture proportions of concrete evaluated for formation factor, in SSD condition

Constituent	Proportion (lb/yd^3)
Cement	658
Water	267
Fine aggregate	1178
Coarse aggregate	1780
Air content	**6.3%**
w/c	**0.40**

Table 11.4 **Experimental data from concrete electrical measurements**

Specimen	Resistivity		Formation factor (unitless)
	Pore solution (m$\Omega \cdot$m)	Specimen ($\Omega \cdot$m)	
OPC-1a	95	21.6	227
OPC-1b	95	22.8	240
OPC-2a	40	8.6	215
OPC-2b	40	9.4	235
		Average	**229.3**
		St Dev	**10.8**

that were present in the artificial pore solution. This would result in a pore solution that is less than half the resistivity. This is summarized in Table 11.4.

It is seen that while concrete specimens saturated with different solutions—that is, different pore solutions—had a drastically different resistivity, their formation factor was relatively constant. A standard deviation was measured and corresponds to a coefficient of variation of 4.7%.

11.4.2 Influence of mixture proportions

The influence of mixture proportions on the formation factor was also investigated as a part of this work. Specifically, a concrete with a paste volume fraction of 28.2% was investigated using the proportions given in Table 11.5. The cement used in this portion of the study was a type I OPC with 0.16% Na_2O and 1.24% K_2O content by mass.

Specimens were sealed cured for a period of 1 year, demolded, and resistivity was measured in a sealed condition. The sealed pore solution resistivity was estimated using the online tool discussed by Bentz (2007). The specimens were oven dried and then vacuum saturated in limewater, and the saturated pore solution concentration was

Table 11.5 **Mixture proportions for different w/c mixtures with a constant paste content, in SSD lb/yd^3**

w/c	0.42	0.48	0.54
Fresh air content	5.0%	5.2%	6.5%
Cement	645	596	554
Water	271	286	300
Fine aggregate	1178	1178	1178
Coarse aggregate	1780	1780	1780

Table 11.6 Estimated pore solution resistivities for sealed cured concretes at 90% degree of hydration, in mΩ·m

w/c	0.42	0.48	0.54
Sealed pore solution	48	60	71
Vacuum saturated	83	97	117

estimated using the measured air contents and the sealed pore solution concentration. As shown in Table 11.6, the resistivities were then calculated from the concentrations as described by literature (Snyder et al., 2003; Bentz, 2007).

The resistivity and calculated formation factors for the three different w/c mixtures are shown in Figure 11.11. The sealed measurements shown in Figure 11.11(a) were conducted immediately following the sample being demolded from a sealed condition. Figure 11.11(b) shows measurements that were conducted on the same specimens after being vacuum saturated in limewater. Testing was conducted at $23 \pm 1\,°C$.

First, it can be seen that the values of both the resistivity and the formation factor change quite significantly between sealed and vacuum-saturated measurements. This has been well documented and shown to follow an approximate power curve with degree of saturation between high values at low degrees of saturation and the saturated value (Schiessel et al., 2000; Weiss et al., 2013). Furthermore, recent research has shown that the fitting coefficient is a relatively constant value, except when considering air-entrained concrete (Barrett, 2015). The volume and spacing of the air-entrained voids control the amount of reduction in sealed resistivity.

It is worth noting that for this study, there is a clear trend with resistivity and the w/c ratio. The concretes in this study are made with the same Type I OPC, have similar air contents, and are made with a constant paste volume fraction. This trend in resistivity and w/c ratio has often been observed in literature (e.g., Henkensiefken et al., 2009), which makes resistivity good at seeing variations in water content of a concrete batch using consistent materials, specifically for use as a quality control test.
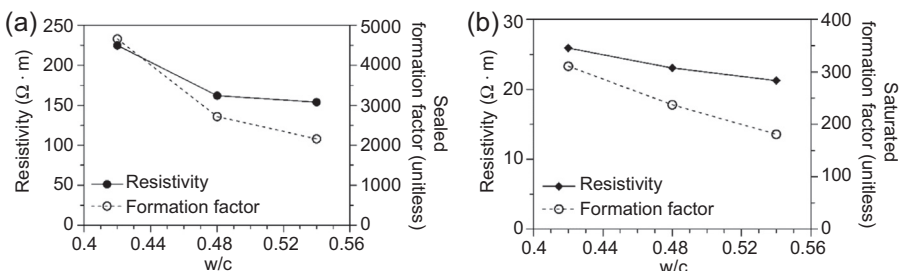
Figure 11.11 Plain concretes made with the same Type I OPC shown as (a) sealed measurements and (b) saturated factor at an age of 1 year.

11.5 Specifying formation factor

11.5.1 Why measure formation factor

Many studies have evaluated the relationship between concrete resistivity and diffusion properties, and see that these relationships are often empirical and mixture specific (Berke and Hicks, 1992). One primary reason for this is because each binder system has its own pore solution properties. By normalizing the concrete resistivity to the pore solution resistivity, the formation factor can be determined.

The formation factor, F, described in Eqn (11.2), is the microstructural characterization parameter that describes the conductive volume and connectivity of the volume. While simple resistivity tests describe pore characteristics and pore solution resistivity, normalizing by the pore solution gives a numerical quantification of the pore network independent of pore solution resistivity.

While this is important for OPC concretes, it becomes especially important for binder systems with supplementary materials. Research has shown that different supplementary cements can exhibit large variations in pore solution properties (Feng et al., 2004).

Furthermore, a test of the formation factor can be accomplished relatively easily, with an electrical testing taking only a few minutes. Alternative tests such as a standard diffusion test can take upward of months for testing and data analysis.

11.5.2 Relating formation factor to life cycle

Recall that the formation factor is a microstructural material property, as described in Section 11.2. The Nernst−Einstein relationship relates the formation factor to a measure of resistivity, but also to an effective diffusion coefficient. This means that the formation factor can be used to obtain a target value for use in quality control testing—that is, resistivity—but can also be related to an estimated time to corrosion (Barrett, 2015; Weiss et al., 2016).

One approach that would provide a conservative estimate of the relationship between the formation factor and the time-to-corrosion life cycle would be the use of the error function solution to Fick's second law. This is termed conservative because the use of this equation does not account for the aging effects of the transport properties, effects of chloride binding or pore blocking reactions that would slow ionic ingress, multimodal transport of chlorides, effects of temperature, or gradual buildup of surface chlorides (Boddy et al., 1999; Bentz et al., 2014).

The goal of the procedure, described below, is to allow for quantitative comparison of microstructure quality. As it is a tool to measure the microstructure of the matrix phase of concrete, it is suggested that it be conducted not on saturated specimens, but on specimens that have been sealed from initial hydration, or on specimens where only the matrix phase is filled with fluid (Bu et al., 2014; Todak et al., 2015; Barrett, 2015). The benefit of this method is that it would assess the durability of the matrix phase and allow for the air void system to be assessed separately.

An estimated time to corrosion can be calculated using the error function solution to Fick's second law, shown in Eqn (11.15):

$$\frac{C(x,t) - C_{o}}{C_{s} - C_{o}} = 1 - \text{erf}\left(\frac{x}{2\sqrt{Dt}}\right) \qquad (11.15)$$

where $C(x, t)$ is the concentration at a depth x at an exposure time t and is typically taken as 0.05% by weight of concrete (a value typically recognized as corresponding to corrosion of reinforcing steel), C_{o} is the background chloride content and is typically taken as 0.02% by weight of concrete, C_{s} is the surface concentration, and D is the apparent chloride diffusion coefficient. The surface concentration C_{s} can be varied depending on the exposure class—taht is, the level of chloride exposure at the surface during in-service conditions.

The apparent diffusion in Eqn (11.15) can be replaced by the ratio of the self-diffusion coefficient of a chloride ion, 19.3×10^{-10} m^2/s at 23 °C, to the formation factor. Specifically, in Eqn (11.15), $D = D_{o}/F$.

Figure 11.12 shows the calculation for time to corrosion initiation for a 50 mm cover depth and a series of three different surface concentrations. These values were selected based upon surface concentrations from around the country given by Life-365 (Life-365, 2012). The values of 0.1%, 0.5%, and 1% by weight of concrete represent low, moderate, and severe exposure categories, respectively. This approach allows for the quantification of relative improvement with an increase in formation factor for a mixture.

The use of the formation factor to specify durable concrete shows promise, because it can be consistently applied to a wide range of systems; this is primarily because many times, the pore solution chemistries of these systems change. While the approach
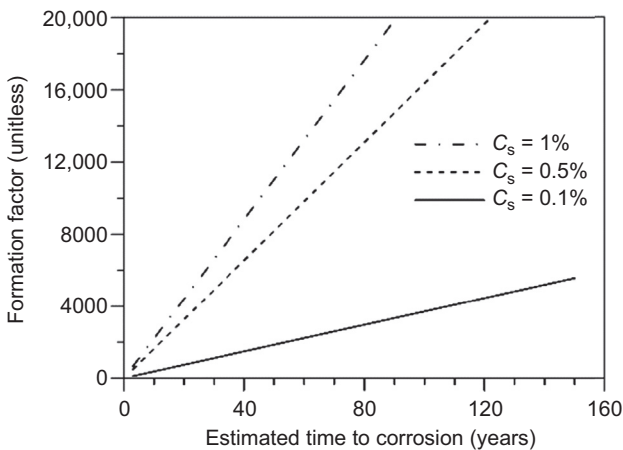
Figure 11.12 Influence of formation factor for a 50 mm cover on estimated time to corrosion. Exposure classes of surface concentrations of 0.1%, 0.5%, and 1% represent low, medium, and severe exposure classes.

taken here provides a conservative estimation of the time to corrosion, a more detailed analysis could be done, if needed, that could account for variation in temperature, the effects of chloride binding, and aging of the formation factor (as shown by Glasser et al., 2008; Barrett, 2015; Weiss et al., 2016).

11.6   Conclusions

Assessing a concrete's resistance to ion penetration is primarily a function of pore characteristics. While electrical tests provide some measure of the pore structure, electrical measurements are highly dependent on the pore solution. In cementitious systems, the pore solution can change quite appreciably depending on the mixture proportions, chemistry of the cementitious materials, and degree of hydration.

By normalizing the measured concrete resistivity by the resistivity of the pore solution, the formation factor parameter can be obtained. This is a numerical quantification of the microstructure. The use of the formation factor will help to make a specification that is applicable to a wide range of cementitious systems with variations in their pore solution properties. Furthermore, the formation factor can be obtained in a few days of testing. This is contrasted with other microstructural characterization tests such as a diffusion test, which can take weeks or even months.

The Nernst−Einstein relationship demonstrates how the formation factor can be used to determine the effective diffusion coefficient for a series of different ionic species. Using Fick's second law, a conservative estimate of the time to corrosion initiation can be estimated for a series of different exposure classes and bar depths. Recent studies have shown that by properly accounting for ionic binding, aging, and temperature, the formation factor can serve as an input to life cycle models that have accurately predicted chloride profiles of laboratory-ponded specimens.

The formation factor can also be related to a simple measure of resistivity. This means that a formation factor specification can be used to establish target values for resistivity during concrete production by simply multiplying the specified formation factor by the pore solution resistivity (Barrett, 2015; Weiss et al., 2016). This would make the specification generic, and it would thus apply for a wide range of cementitious materials.

References

AASHTO TP95-11, 2011. Standard Method of Test for Surface Resistivity Indication of Concrete's Ability to Resist Chloride Ion Penetration. American Association of State Highway and Transportation Officials, Washington, DC.

Andrade, C., 1993. Calculation of chloride diffusion coefficients in concrete from ionic migration measurements. Cement and Concrete Research 23, 724−742. http://dx.doi.org/10.1016/0008-8846(93)90023-3.

Barneyback, R.S., Diamond, S., 1981. Expression and analysis of pore fluids from hardened cement pastes and mortars. Cement and Concrete Research 11, 279−285. http://dx.doi.org/10.1016/0008-8846(81)90069-7.

Barrett, T., 2015. Improving Service Life of Concrete Structures through the Use of Internal Curing: Impact on Practice. Purdue University, Indiana.

Bentz, D.P., 2007. A virtual rapid chloride permeability test. Cement and Concrete Composites 29, 723−731. http://dx.doi.org/10.1016/j.cemconcomp.2007.06.006.

Bentz, D.P., Guthrie, W.S., Jones, S.Z., Martys, N.S., 2014. Predicting service life of steel-reinforced concrete exposed to chlorides. Concrete International 55−64.

Berke, N., Hicks, M., 1992. Estimating the life cycle of reinforced concrete decks and marine piles using laboratory diffusion and corrosion data. In: Chaker, V. (Ed.), Corrosion Forms and Control of Infrastructure, ASTM STP 1137. ASTM International, Philadelphia, Pennsylvania, pp. 207−231.

Boddy, A., Bentz, E., Thomas, M., Hooton, R., 1999. Overview and sensitivity study of a multimechanistic chloride transport model. Cement and Concrete Research 29, 827−837. http://dx.doi.org/10.1016/S0008-8846(99)00045-9.

Bu, Y., Spragg, R., Weiss, J., 2014. Comparison of the pore volume in concrete as determined using ASTM C642 and vacuum saturation. Advances in Civil Engineering Materials. http://dx.doi.org/10.1520/ACEM20130090.

Bu, Y., Weiss, J., 2014. The influence of alkali content on the electrical resistivity and transport properties of cementitious materials. Cement and Concrete Composites 51, 49−58. http://dx.doi.org/10.1016/j.cemconcomp.2014.02.008.

Castellote, M., Andrade, C., 2006. Round-Robin test on methods for determining chloride transport parameters in concrete. Materials and Structures 39, 955−990. http://dx.doi.org/10.1617/s11527-006-9193-x.

Castro, J., Spragg, R., Kompare, P., Weiss, J., 2010. Portland Cement Concrete Pavement Permeability Performance. West Lafayette, Indiana.

Chrisp, T.M., Starrs, G., McCarter, W.J., et al., 2001. Temperature-conductivity relationships for concrete: an activation energy approach. Journal of Materials Science Letters 20, 1085−1087. http://dx.doi.org/10.1023/A:1010926426753.

Christensen, B.J., Coverdale, T., Olson, R.A., et al., 1994. Impedance spectroscopy of hydrating cement-based materials: measurement, interpretation, and application. Journal of the American Ceramic Society 77, 2789−2804. http://dx.doi.org/10.1111/j.1151-2916.1994.tb04507.x.

De La Varga, I., 2013. Increased Fly Ash Volume and Internal Curing in Concrete Structures and Pavements. Purdue University, Indiana.

De La Varga, I., Spragg, R.P., Di Bella, C., et al., 2014. Fluid transport in high volume fly ash mixtures with and without internal curing. Cement & Concrete Composites 45, 102−110. http://dx.doi.org/10.1016/j.cemconcomp.2013.09.017.

Dean, J., Lange, N., 1999. Lange's Handbook of Chemistry. McGraw-Hill, New York, NY.

Dullien, F., 1992. Porous Media: Fluid Transport and Pore Structure, second ed. Academic Press, San Diego.

Feng, X., Garboczi, E., Bullard, J., et al., 2004. Expanding a Tool for Predicting Chloride Diffusivity in Concrete so It Can Be Used by Manufacturers to Evaluate the Durability of Concrete Made with Blended Cements. Part I: Characterizing Blended Cement Materials. Gaithersburg, MD.

FM 5-578, 2004. Florida Method of Test for Concrete Resistivity as an Electrical Indicator of Its Permeability. Tallahassee, FL.

Forde, M.C., McCarter, J., Whittington, H.W., et al., 1981. The conduction of electricity through concrete. Magazine of Concrete Research 33, 48−60. http://dx.doi.org/10.1680/macr.1981.33.114.48.

Garboczi, E.J., 1990. Permeability, diffusivity, and microstructural parameters: a critical review. Cement and Concrete Research 20, 591−601. http://dx.doi.org/10.1016/0008-8846(90)90101-3.

Glasser, F.P., Marchand, J., Samson, E., 2008. Durability of concrete − degradation phenomena involving detrimental chemical reactions. Cement and Concrete Research 38, 226−246. http://dx.doi.org/10.1016/j.cemconres.2007.09.015.

Gu, P., Xie, P., Beaudoin, J.J., Brousseau, R., 1992. A.C. impedance spectroscopy (I): a new equivalent circuit model for hydrated portland cement paste. Cement and Concrete Research 22, 833−840. http://dx.doi.org/10.1016/0008-8846(92)90107-7.

Hall, C., Marchand, J., Gerard, G., Sosoro, M., 1997. Transport of fluids in homogenous isotropic cementitious composites. In: Reinhardt, H. (Ed.), Penetration Permability Concr. RILEM Rep., vol. 16, pp. 5−79.

Hammond, E., Robson, T., 1955. Comparison of electrical properties of various cements and concretes. I−II. The Engineer 199, 78−80.

Henkensiefken, R., Castro, J., Bentz, D.P., et al., 2009. Water absorption in internally cured mortar made with water-filled lightweight aggregate. Cement and Concrete Research 39, 883−892. http://dx.doi.org/10.1016/j.cemconres.2009.06.009.

Jensen, O.M., Hansen, P.F., 2001. Water-entrained cement-based materials − I. Principles and theoretical background. Cement and Concrete Research 31, 647−654. http://dx.doi.org/10.1016/S0008-8846(01)00463-X.

Lamond, J., Pielert, J. (Eds.), 2006. Significance of Tests and Properties of Concrete and Concrete-Making Materials, STP 169D, STP 169D. ASTM International, West Conshohocken, PA.

Life-365, 2012. Life-365 User Manual, pp. 1−80.

Lucero, C.L., 2015. Quantifying Moisture Transport in Cementitious Materils. Purdue University, Indiana.

McCarter, W., Forde, M., Whittington, H., 1981. Resistivity characteristics of concrete. ICE Proceeding 71, 107−117. http://dx.doi.org/10.1680/iicep.1982.1993.

McCarter, W.J., Chrisp, T.M., Starrs, G., et al., 2015. A durability performance-index for concrete: developments in a novel test method. International Journal of Structural Engineering 6, 2. http://dx.doi.org/10.1504/IJSTRUCTE.2015.067966.

McCarter, W.J., Starrs, G., Chrisp, T.M., 2000. Electrical conductivity, diffusion, and permeability of Portland cement-based mortars. Cement and Concrete Research 30, 1395−1400. http://dx.doi.org/10.1016/S0008-8846(00)00281-7.

McGrath, P.F., Hooton, R.D., 1999. Re-evaluation of the AASHTO T259 90-day salt ponding test. Cement and Concrete Research 29, 1239−1248. http://dx.doi.org/10.1016/S0008-8846(99)00058-7.

Mindess, S., Young, J., Darwin, D., 2003. Concrete, second ed. Prentice Hall, Upper Saddle River, NJ.

Morris, W., Moreno, E.I.I., Sagüés, A.A., 1996. Practical evaluation of resistivity of concrete in test cylinders using a Wenner array probe. Cement and Concrete Research 26, 1779−1787. http://dx.doi.org/10.1016/S0008-8846(96)00175-5.

Newlands, M., Jones, R., Kandasami, S., Harrison, T., 2007. Sensitity of electrode contact solutions and contact pressure in assessing electrical resistivity of concrete. Materials and Structures 41, 621−632. http://dx.doi.org/10.1617/s11527-007-9257-6.

Nokken, M.R., Hooton, R.D., 2007. Using pore parameters to estimate permeability or conductivity of concrete. Materials and Structures 41, 1−16. http://dx.doi.org/10.1617/s11527-006-9212-y.

Olson, R.A., Christensen, B.J., Coverdale, R.T., et al., 1995. Interpretation of the impedance spectroscopy of cement paste via computer modelling − part III microstructural analysis of frozen cement paste. Journal of Materials Science 30, 5078−5086. http://dx.doi.org/10.1007/BF00356052.

Polder, R.B., 2001. Test methods for on site measurement of resistivity of concrete − a RILEM TC-154 technical recommendation. Construction and Building Materials 15, 125−131. http://dx.doi.org/10.1016/S0950-0618(00)00061-1.

Poursaee, A., Weiss, J., 2010. An automated electrical monitoring system (AEMS) to assess property development in concrete. Automation in Construction 19, 485−490. http://dx.doi.org/10.1016/j.autcon.2009.12.016.

Powers, T.C., 1966. The Nature of Concrete. Portland Cement Association, Skokie, IL.

Powers, T.C., Brownyard, T.L., 1946. Studies of the physical properties of hardened Portland cement paste. Journal of the American Concrete Institute. http://dx.doi.org/10.14359/15301.

Presuel-Moreno, F., Liu, Y., Paredes, M., 2009. Understanding the effect of rebar presence and/or multilayered concrete resistivity on the apparent surface resistivity measured via the four-point wenner method. Corrosion, NACE International. Corrosion 2009, Atlanta Georgia. https://www.onepetro.org/conference-paper/NACE-09217.

Presuel-Moreno, F., Suares, A., Liu, Y., 2010. Characterization of New and Old Concrete Structures Using Surface Resistivity Measurements. Florida Atlantic University−Sea Tech Campus, Dania Beach, FL. http://www.dot.state.fl.us/research-center/Completed_Proj/Summary_SMO/FDOT_BD546-08_rpt.pdf.

Proceq, 2013. Resipod Family Operating Instructions. Schwerzenbach.

Radlinski, M., Olek, J., Nantung, T., 2010. Development and application of maturity method for prediction of concrete's resistance to chloride ion penetration. Transportation Research Record Journal of the Transportation Research Board 2164, 105−112. http://dx.doi.org/10.3141/2164-14.

Rajabipour, F., 2006. In situ Electrical Sensing and Material Health Monitoring in Concrete Structures. Purdue University, Indiana.

Rajabipour, F., Sant, G., Weiss, J., 2007. Development of electrical conductivity-based sensors for health monitoring of concrete materials development of electrical conductivity-based sensors for health monitoring of concrete materials. In: Proc. Transp. Res. Board, Washington, DC, pp. 1−16.

Rajabipour, F., Weiss, J., 2007. Electrical conductivity of drying cement paste. Materials and Structures 40, 1143−1160. http://dx.doi.org/10.1617/s11527-006-9211-z.

Rajabipour, F., Weiss, J., Shane, J.D., et al., 2005. Procedure to interpret electrical conductivity measurements in cover concrete during rewetting. Journal of Materials in Civil Engineering 17, 586−594. http://dx.doi.org/10.1061/(ASCE)0899-1561(2005)17:5(586).

Raupach, M., Schiessl, P., 1997. Monitoring system for the penetration of chlorides, carbonation and the corrosion risk for the reinforcement. Construction and Building Materials 11, 207−214. http://dx.doi.org/10.1016/S0950-0618(97)00039-1.

Rupnow, T., Icenogle, P., 2012. Evaluation of Surface Resistivity Measurements as an Alternative to the Rapid Chloride Permeability Test for Quality Assurance and Acceptance. Louisiana Department of Transportation, Baton Rouge, LA.

Rupnow, T.T., Icenogle, P., 2011. Evaluation of Surface Resistivity Measurements as an Alternative to the Rapid Chloride Permeability Test for Quality Assurance and Acceptance. Louisiana Department of Transportation, Baton Rouge, LA.

Salehi, M., Ghods, P., Burkan Isgor, O., 2014. Numerical investigation of the role of embedded reinforcement mesh on electrical resistivity measurements of concrete using the Wenner probe technique. Materials and Structures. http://dx.doi.org/10.1617/s11527-014-0498-x.

Sant, G., Bentz, D.P., Weiss, J., 2011. Capillary porosity depercolation in cement-based materials: measurement techniques and factors which influence their interpretation. Cement and Concrete Research 41, 854–864. http://dx.doi.org/10.1016/j.cemconres.2011.04.006.

Sant, G., Rajabipour, F., Fishman, P., et al., 2006. Electrical Conductivity Measurements in Cement Paste at Early Ages: A Discussion of the Contribution of Pore Solution Conductivity, Volume, and Connectivity to the Overall Electrical Response, pp. 213–222.

Sant, G., Rajabipour, F., Weiss, J., 2008. The influence of temperature on electrical conductivity measurements and maturity predictions in cementitious materials during hydration. The Indian Concrete Journal 82, 7–16.

Schiessel, A., Weiss, J., Shane, J.D., et al., 2000. Assessing the moisture profile of drying concrete using impedance spectroscopy. Concrete Science and Engineering 2, 106–116.

Shane, J., 2000. Electrical Conductivity and Transport Properties of Cement-Based Materials Measured by Impedance Spectroscopy. Northwestern University, Illinois.

Snyder, K., Feng, X., Keen, B., Mason, T., 2003. Estimating the electrical conductivity of cement paste pore solutions from OR^-, K^+ and Na^+ concentrations. Cement and Concrete Research 33, 793–798.

Snyder, K.A., 2001. The relationship between the formation factor and the diffusion coefficient of porous materials saturated with concentrated electrolytes: theoretical and experimental considerations. Concrete Science and Engineering 3, 216–224.

Spragg, R., Bu, Y., Snyder, K.A., et al., 2013a. Electrical Testing of Cement-Based Materials: Role of Testing Techniques, Sample Conditioning, and Accelerated Curing. FHWA/IN/JTRP-2013/28. http://dx.doi.org/10.5703/1288284315230.

Spragg, R., Villani, C., Snyder, K., et al., 2013b. Factors that influence electrical resistivity measurements in cementitious systems. Transportation Research Record Journal of the Transportation Research Board 2342, 90–98. http://dx.doi.org/10.3141/2342-11.

Spragg, R., Villani, C., Weiss, J., 2015a. Electrical properties of cementitious systems: formation factor determination and the influence of conditioning procedures. Advances in Civil Engineering Materials (submitted).

Spragg, R.P., 2013. The Rapid Assessment of Transport Properties of Cementitious Materials Using Electrical Methods. Purdue University, Indiana.

Spragg, R.P., Castro, J., Nantung, T., et al., 2012. Variability analysis of the bulk resistivity measured using concrete cylinders. Advances in Civil Engineering Materials 1, 104596. http://dx.doi.org/10.1520/ACEM104596.

Spragg, R.P., Jones, S.Z., Bu, Y., et al., 2015b. Alkali-leaching in cementitious systems: implications to measurements of electrical resistivity. Construction and Building Materials (submitted for publication).

Taylor, H.F.W., 1987. A method for predicting alkali ion concentrations in cement pore solutions. Advances in Cement Research 1, 5–17. http://dx.doi.org/10.1680/adcr.1987.1.1.5.

Thomas, M., 2008. Personal Communication Regarding the use of Conductive Gel in Resistivity Tests.

Thomas, M., Fournier, B., Folliard, K., et al., 2006. Test methods for evaluating preventive measures for controlling expansion due to alkali-silica reaction in concrete. Cement and Concrete Research 36, 1842–1856. http://dx.doi.org/10.1016/j.cemconres.2006.01.014.

Todak, H., 2015. Durability Assessments of Concrete Using Electrical Properties and Acoustic Emissions. Purdue University, Indiana.

Todak, H., Lucero, C., Weiss, W.J., Spring 2015. Why is the air there? Thinking about freeze-thaw in terms of saturation. Concrete inFocus 27−33.

Torquato, S., Haslach, H., 2002. Random heterogeneous materials: microstructure and macroscopic properties. Applied Mechanics Reviews. http://dx.doi.org/10.1115/1.1483342.

Tumidajski, P.J., Schumacher a, S., Perron, S., et al., 1996. On the relationship between porosity and electrical resistivity in cementitious systems. Cement and Concrete Research 26, 539−544. http://dx.doi.org/10.1016/0008-8846(96)00017-8.

Vivas, E., Hamilton, H., Boyd, A., 2007. Permeability of Concrete − Comparison of Conductivity and Diffusion Methods. Gainesville, FL.

Weiss, J., Barrett, T., Qiao, C., Todak, H., 2016. Toward a specification for transport properties of concrete based on the formation factor of a sealed specimen. Transportation Research Record, to accepted for publication.

Weiss, J., Shane, J., Mieses, A., et al., 1999. Aspects of Monitoring Moisture Changes Using Electrical Impedance Spectroscopy. Lund, Sweden, pp. 31−48.

Weiss, J., Snyder, K., Bullard, J., Bentz, D.P., 2013. Using a saturation function to interpret the electrical properties of partially saturated concrete. Journal of Materials in Civil Engineering 25, 1097−1106. http://dx.doi.org/10.1061/(ASCE)MT.1943-5533.0000549.

Weiss, W.J., 1999. Prediction of Early-age Shrinkage Cracking in Concrete Elements. Northwestern University, Illinois.

Wenner, F., 1916. A method of measuring earth resistivity. Bureau of Standards Bulletin 12, 469. http://dx.doi.org/10.6028/bulletin.282.

Xie, P., Gu, P., Zu, A., Beaudoin, J.J., 1992. A rationalized AC impedance model for the microstructural characterization of hydrating cement systems. Cement and Concrete Research 23, 359−367.

Yuan-Hui, L., Gregory, S., 1974. Diffusion of ions in sea water and in deep-sea sediments. Geochimica et Cosmochimica Acta 38, 703−714. http://dx.doi.org/10.1016/0016-7037(74)90145-8.

Corrosion protection methods of steel in concrete

12

Amir Poursaee
Clemson University, Clemson, SC, USA

12.1   Cathodic protection

The first example of cathodic protection applied to concrete structures was reported in 1957 (Stratfull, 1957), and widespread use of the technique for protecting bridge decks contaminated by deicing salts began in 1973 in North America (Stratfull, 1973, 1974). Cathodic protection, as schematically illustrated in Figure 12.1, is based on changing the electrochemical potential of the steel to more negative values. This potential change can be obtained by connecting an external anode to the steel and impressing direct electrical current (DC) through the rebar using a rectified power supply. This external anode is mounted on the surface of the concrete. The positive terminal of a low-voltage DC source is connected to the mesh, and the negative terminal is connected to the steel bars.

In order to stop the corrosion of the reinforcing steel bar completely, the potential would have to be lowered to values more negative than ~ -1200 mV CSE (immunity region in Pourbaix diagram for iron (Pourbaix, 1974)). However, at those values, the cathodic reaction would result in hydrogen evolution that could cause hydrogen embrittlement of any prestressed steel in the structure. Consequently, the potential is carefully controlled to a level (typically -1000 mV CSE) at which the corrosion is negligible but not actually stopped. Alternatively, the process can rely on the galvanic effect, and a less noble metal can be used as sacrificial anodes. In this case, metals such as zinc and zinc—aluminum alloys are applied to the concrete surface by flame spray, or as a mesh or sheet adhered via a conductive gel (Polder, 2005). Cathodic protection must be monitored regularly. For this purpose, the potential of the steel should be monitored with respect to a reference electrode before and after disconnecting the
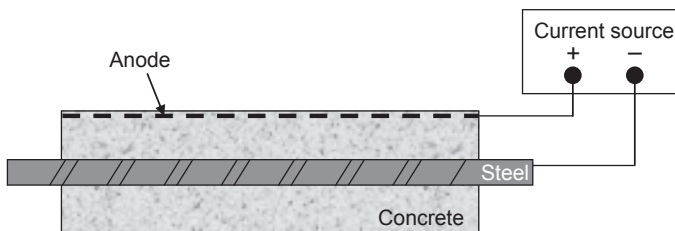
Figure 12.1 Schematic illustration of the cathodic protection (impressed current method) of steel reinforcing bars in a concrete structure.

system to make sure that the system is depressing the potential from the open-circuit potential. The limits and standard practices are outlined in NACE (1990) and briefly explained in Section 12.2.2.

12.1.1   Anode system in impressed current method

The anode system consists of the anode material and its overlay. This system must be able to supply the required current and distribute it to the steel reinforcing bar that is to be protected. On the anode surface, oxygen or chlorine evolution can take place. Both reactions decrease the pH and cause an acidic environment, and as a result the pH of the concrete in contact with steel decreases. Thus, anodic current densities have to be limited (Pedeferri, 1996). The anode can be: a mesh that is fixed and covered with a cementitious overlay; a conductive and electroactive layer applied directly to completely cover the concrete surface; or a wire or strip placed in holes or slots, and backfilled with either cementitious or electroactive material or conductive tiles placed on the concrete surface (Bertolini et al., 1994). Titanium expanded mesh activated with mixed metal oxides (iridium, ruthenium, cobalt, etc.) is the most widely used and successful type of anode. Conductive organic coatings containing a carbon conductor and a series of conductors (capable of resisting anodic reaction) are another common type of anode. A variety of other anode types (such as overlays containing either granular carbon and carbon fiber with a metallic coating, conductive ceramics, thermally sprayed zinc coating, etc.) are suitable for use in cathodic protection in concrete, but have few long-term applications (Pedeferri, 1996).

12.1.2   Monitoring system in impressed current method

As mentioned above, permanent monitoring systems must be installed in order to determine the performance of a cathodic protection system. Monitoring systems are essentially based on potential measurements of the reinforcing steel bar with respect to a reference electrode. Reference electrodes should be buried in concrete and located in the most critical areas, or where the control of the potential is of most importance. The most common reference electrodes for permanent embedment are Ag/AgCl, Mn/MnO, and activated titanium with or without cementitious backfill (Pedeferri, 1996). For steel in concrete, the protection potential depends on chloride content, pH, cement type, etc., and the criteria utilized to indicate practical conditions are empirical. The most widely used is called the 100 mV day criterion: "protection or prevention conditions are reached when a potential decay of at least 100 mV over a period between 4 and 24 h from instant of potential is measured" (NACE, 1990).

12.1.3   Cathodic protection using embedded galvanic anodes (Liao, 2014)

Galvanic anodes provide protection using dissimilar metals and operate naturally without the need of external power. Galvanic systems can be used different steel reinforced concrete structures including abutment overbuild, deck overlay, jackets for

columns, piers and marine piles. Galvanic system can also be used for targeted corrosion protection, such as concrete repairs, expansion joint repair and bridge widening. In a galvanic anode system, the current is generated by the potential difference between the zinc anode (-1100 mV vs SCE) and the steel reinforcement (typically at $350-500$ mV vs. SCE for corroding steel). One commercially available galvanic anode, puck-like anode, is produced from zinc metal encased in a specially formulated porous cementitious mortar saturated in a high alkaline environment. Such an environment, maintaining a constantly high pH that is corrosive to zinc and protective of steel, was shown to sustain the zinc in an active condition, producing soluble zinc corrosion products that do not stifle the corrosion process of the metal.

12.1.4 Negative impacts of cathodic protection in steel-reinforced concrete

Theoretically, the increase in alkalinity around the reinforcement can cause damage if the concrete contains alkali-reactive aggregates (Page, 1992). Thus, if the structure to be protected contains aggregates that may be sensitive to alkali, the risk of alkali–aggregate reaction has to be considered. Another negative effect is that at very negative potentials (i.e., at high current densities), loss of adhesion between rebar and concrete can occur (Pedeferri, 1996). The most important side effect is the embrittlement of steel caused by the hydrogen evolution that is critical in prestressed concrete. In the alkaline environment of concrete, hydrogen evolution can occur only at potentials more negative than about -950 mV versus saturated calomel electrode (SCE), and embrittlement effects are not produced at potentials more positive than -900 mV (vs SCE). Therefore, to avoid hydrogen embrittlement risk of susceptible steel, a lower limiting potential of -900 mV (vs SCE) should be fixed for steel. Low-carbon steels, used for reinforced concrete construction are generally not susceptible to hydrogen embrittlement; only high-strength steels utilized for prestressed construction are considered susceptible to hydrogen embrittlement. This type and degree of susceptibility depend on many metallurgical and electrochemical variables and thus vary with factors such as composition, heat and mechanical treatments, presence of notches or defects due to corrosion, value of load and its variations giving a low strain rate, and environmental conditions (Pedeferri, 1996).

12.2 Electrochemical chloride extraction (ECE)

In ECE, the goal is to repel the negatively charged chloride ions from the rebar and out of the surface of the concrete by applying a negative charge to the rebar, as illustrated schematically in Figure 12.2. ECE is similar to cathodic protection, but there are two important differences. First, the current density used for ECE is much higher than that for cathodic protection. Second, the surface anode for ECE is temporary and remains in place only for the duration of the process (typically a few weeks) (Liu and Shi, 2009). During the treatment, any corrosion products are electrochemically reduced at the

$$4OH^-_{(aq)} \rightarrow 2H_2O_{(l)} + O_{2,(g)} + 4e^-$$

$$2H_2O_{(l)} \rightarrow 4H^+_{(aq)} + O_{2,(g)} + 4e^-$$

$$2Cl^-_{(aq)} \rightarrow Cl_{2,(g)} + 2e^-$$

External anode

Anions (e.g., OH⁻, Cl⁻)

Power supply

Concrete

Cations (e.g., K⁺, Na⁺, Ca²⁺, Mg²⁺)

Reinforcing steel

Reduction of corrosion products

$$2H_2O_{(l)} + O_{2,(g)} + 4e^- \rightarrow 4OH^-_{(aq)}$$

$$H_2O_{(l)} + 2e^- \rightarrow 2OH^-_{(aq)} + H_{2,(g)}$$
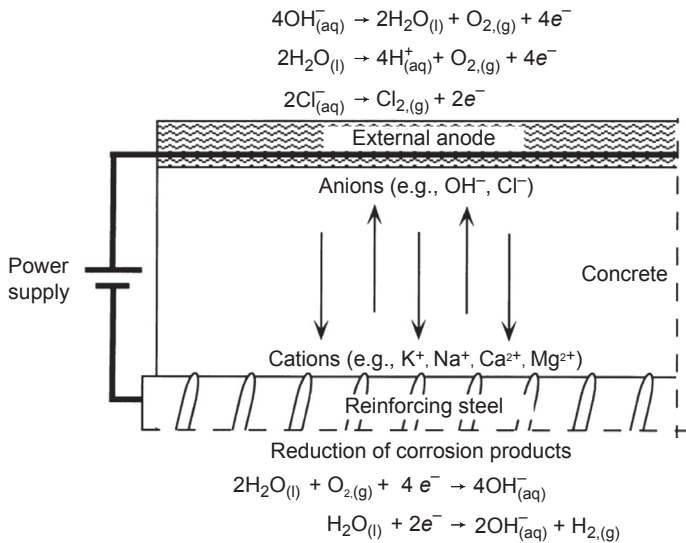
Figure 12.2 Schematic illustration of the application of ECE treatment to a corroding reinforced concrete structure.

reinforcing steel (Marcotte et al., 1999b). While both cathodic protection and chloride extraction have proven to extend the service life of the treated structure, ECE offers the advantage of not requiring long-term regular maintenance.

Ihekwaba et al. (1996) investigated the effect of carbonation on ECE. Their study showed that higher chloride extraction was obtained in noncarbonated concrete than in carbonated concrete irrespective of the configuration of the reinforcement system. Accumulations of alkali ions were greater in the noncarbonated concrete specimens. These effects illustrate interesting features of chloride diffusion as a function of concrete carbonation. This observation was attributed to the precipitation of carbonates in the pores. This precipitation decreased concrete permeability and increased electrical resistivity, both of which affected the current density distribution in the concrete and thus the performance of ECE.

Hope et al. (1995) studied the effect of rebar configuration on ECE. It was observed that concrete reinforced with multiple layers of steel having the rebar directly placed over each other showed better chloride removal than those in which the rebar were displaced with respect to one another. Since the chloride ions within the concrete between the layers had to pass between the negatively charged top rebar in order to reach the anode, there was a significant reduction in chloride content in the top region.

Siegwart et al. (2003) investigated the effect of ECE on the average pore size and pore size distribution of concrete. During ECE, an increase in the concrete resistance was observed, and the results indicated that the average pore size and pore size distribution of concrete were altered by the ECE treatment. The pores in the control samples occurred less frequently and were larger than those in the treated samples.

Orellan et al. (2004) investigated the efficiency and side effects of ECE, and their experimental results indicated that total chloride content was reduced by about 40% near the steel, where as Na^+ and K^+ concentrations increased. The presence of sodium-rich crystals and an alkali—silica rich gel at the steel—concrete interface was detected. Alkali metals were accumulated around the steel, which led to the formation of sodium-rich crystals and a recrystallization of Friedel's salt on the steel—concrete interface. In laboratory tests on steel in mortar, it has also been shown that the applied current during ECE can significantly alter the composition and morphology of the mortar at the steel/mortar interface, and the steel/concrete bond strength (Marcotte, 1996; Marcotte et al., 1999a).

ECE is best applied when the chlorides are almost reaching the reinforcing steel but have not yet initiated active corrosion. It cannot stop the damage if the process of deterioration is advanced. Therefore, the extraction treatment may be considered an appropriate preventive method, but strictly speaking should not be considered a rehabilitation method (Miranda et al., 2007).

12.3 Inhibitors

Corrosion inhibitors are defined as chemical compounds, both inorganic and organic, that are added to water or other liquids or gases in small amounts to reduce the corrosion rate by affecting the anodic half-cell reaction, the cathodic half-cell reaction, or both. Inhibitors have been classified in many ways, including by composition and mechanism of action. Materials that hinder corrosion by forming protective precipitates or by removing an aggressive constituent from the environment are also considered inhibitors (Virmani and Clemena, 1998). However, the substances that affect the transportation mechanism of the aggressive species to the reinforcing steel bars are not considered inhibitors, but as pore blockers (Buchler, 2005). A corrosion-inhibiting admixture to concrete can function by increasing the resistance to breakdown by chlorides of the passive film on the steel, creating a barrier film on the steel, increasing the degree of chloride binding in the concrete, scavenging the oxygen dissolved in the pore solution, and blocking the ingress of oxygen (Hansson et al., 1998). The mechanism of inhibition is often complex, and varies according to inhibitor type. For simplicity, the major inhibitor classifications are (Virmani and Clemena, 1998):

- Anodic inhibitors: These inhibitors passivate the metal by forming an insoluble protective film on anodic surfaces or by adsorption on the metal. Examples of this type of inhibitor are chromates, nitrites, molybdates, alkali phosphates, silicates, and carbonates. Certain anodic inhibitors (e.g., nitrites) can cause accelerated corrosion and pitting attack if used in insufficient concentrations.
- Cathodic inhibitors: These inhibitors are generally less effective but safer than anodic inhibitors, and function by forming an insoluble or adsorbed film on cathodic surfaces of a metal. Examples of cathodic inhibitors are zinc and the salts of antimony, magnesium, manganese, and nickel.
- Organic inhibitors: These inhibitors function by blocking both anodic and cathodic reactions by adsorption on the entire surface of the metal. This type of inhibitor includes amines, esters, and sulfonates.

Numerous compounds have been investigated in the laboratory as potential corrosion-inhibiting admixtures to concrete, and the most widely used ones are:

- Calcium nitrite that is added to the mixing water of concrete. Due to the negative charge of nitrite, it migrates into the pit and enhanced passivation by its oxidative properties (Mammoliti, 2001; ACI, 2010).
- Calcium nitrate that is added to the mixing water of concrete. In the presence of corrosion products, nitrate is reduced to nitrite. This reaction in an alkaline environment is fast enough to provide sufficient nitrite to inhibit corrosion (Buchler, 2005).
- Sodium monofluorophosphate (MFP) that is added to the mix or applied to the surface of concrete. The inhibition mechanism of MFP is unknown (Elsener, 2001; Ngala et al., 2003; Chaussadent et al., 2006).
- Hydroxyalkylamines that are added to the mix or applied to the surface of concrete. Generally, they are produced in a gas phase and migrate relatively quickly to the surface of concrete and reduce the corrosion rate. No detailed information is available regarding the protection mechanism (Buchler, 2005)

At present, there are four commercially available corrosion-inhibiting admixtures (Thompson et al., 2000):

- Darex Corrosion Inhibitor (DCI and DCI-S), manufactured by W.R. Grace: The active ingredient in this admixture is calcium nitrite at approximately 30%. The typical dosage is approximately $10-30$ L per cubic meter ($2-6$ gallons per cubic yard) of concrete, depending on the expected extent of chloride exposure. This inhibitor provides "active" protection of reinforcing steel by facilitating the formation of a passive oxide film on the steel surface through the following reaction:

$$2Fe^{2+} + 2OH^- + 2NO^{2-} \rightarrow 2NO\uparrow + Fe_2O_3 + H_2O \qquad (12.1)$$

- Rheocrete 222^+, manufactured by BASF: The active ingredient of this corrosion-inhibiting admixture is a water-based combination of amines and esters. According to its manufacturer, this organic mixture forms a protective film on the reinforcing steel to serve as a barrier that actively inhibits both anodic and cathodic reactions. In addition, this mixture also lines the pores in the concrete with hydrophobic chemical compounds that provide a screen to "passively" reduce the ingress of chloride ions into the concrete (Nmai et al., 1992). The recommended dosage is 5 L/m^3 (1 gal/yd^3) of concrete, irrespective of the severity of the exposure environment.
- Ferrogard 901, manufactured by Sika: This is a water-based blend of surfactants and an amino alcohol (or alkanolamine), specifically dimethyl ethanolamine. Its manufacturer showed that the amino alcohol absorbs onto the steel bars by forming a bond between its amino functional group and the hydroxide group on the steel surface. This leads to the formation of insoluble iron oxide complexes that stabilize the oxide surface and inhibit further corrosion. The recommended dosage is 10 L/m^3 (2 gal/yd^3) of concrete irrespective of the severity of the corrosive and exposure environments.
- Catexol 1000 CI, manufactured by Axim Concrete Technologies: It appears that this corrosion-inhibiting admixture combines both an organic film-forming inhibitor, specifically an amine derivative, and a nitrite-based inhibitor. No specific data are available for this admixture.

Some inhibitors may cause adverse effects in concrete, such as low concrete strength, erratic setting times, efflorescence, and enhanced susceptibility to alkali

aggregate reaction. The long term efficiency of the inhibitors in steel reinforced concrete structures has not yet been proved, and there are many discussions in this area. Lack of understanding of the mechanisms, environmental aspects, and safety aspects are some of the major limitations of using inhibitors in reinforced concrete structures properly (Mammoliti, 2001; Buchler, 2005). Despite the risks and uncertainty, the use of corrosion inhibitors, both inorganic and organic, as admixtures for the corrosion protection of steel in reinforced and prestressed concrete has increased in recent years. Research is continuing to identify other corrosion inhibitors that will provide long-lasting corrosion protection to steel reinforced concrete structures.

References

ACI Committee 222, 2010. Corrosion of Metals in Concrete.

Bertolini, L., Bolzoni, F., Cigada, A., Pastore, T., Pedeferri, P., 1994. Cathodic protection of new and old reinforced concrete structures. Corrosion Science 35 (1633), 16−39.

Buchler, M., 2005. Corrosion inhibitors for reinforced concrete. In: Bohni, H. (Ed.), Corrosion in Reinforced Concrete Structures. Woodhead Publishing Ltd., Cambridge, England and CRC Press LLC, Boca Raton, pp. 190−214.

Chaussadent, T., Nobel-Pujol, V., Farcas, F., Mabille, I., Fiaud, C., 2006. Effectiveness conditions of sodium monofluorophosphate as a corrosion inhibitor for concrete reinforcements. Cement and Concrete Research 36, 556−561.

Elsener, B., 2001. Corrosion Inhibitors for Steel in Concrete-State of the Art. Report, European Federation of Corrosion Publication, London.

Hope, B.B., Ihekwaba, N.M., Hansson, C.M., 1995. The Influence of multiple reinforcing mats on electrochemical chloride removal from concrete slabs. Electrochemical Methods in Corrosion Research V, Lisbon, Materials Science Forum.

Hansson, C.M., Mammoliti, L., Hope, B.B., 1998. Corrosion inhibitors in concrete—Part I: The principles. Cement and Concrete Research 28 (12), 1775−1781.

Ihekwaba, N.M., Hope, B.B., Hansson, C.M., 1996. Carbonation and electrochemical chloride extraction from concrete. Cement and Concrete Research 26, 1095−1108.

Liao, H.X., 2014. Concrete bridge corrosion protection with embeded galvanic anodes. In: Chen, A., Frangopol, D.M., Ruan, X. (Eds.), Bridge Maintenance, Safety, Management and Life Extension. Taylor and Francis Group, London, pp. 1951−1957.

Liu, Y., Shi, X., 2009. Electrochemical chloride extraction and electrochemical injection of corrosion inhibitor in concrete: state of the knowledge. Corrosion Reviews 27 (1−2), 53−81.

Miranda, J.M., Cobo, A., Otero, E., González, J.A., 2007. Limitations and advantages of electrochemical chloride removal in corroded reinforced concrete structures. Cement and Concrete Research 37 (4), 596−603.

Mammoliti, L., 2001. Examination of the Mechanism of Corrosion Inhibition by $Ca(NO_2)_2$- and $Ca(NO_3)_2$- Based Admixtures in Concrete (Ph.D. thesis in Mechanical Engineering). University of Waterloo.

Marcotte, T.D., 1996. The Effect of Electrochemical Chloride Extraction on the Microstructure of Steel-Reinforced Mortar (Ph.D. thesis in Mechanical Engineering). Queen's University.

Marcotte, T.D., Hansson, C.M., Hope, B.B., 1999a. The effect of the electrochemical chloride extraction treatment on steel-reinforced mortar—Part II: Microstructural characterization. Cement and Concrete Research 29, 1561−1568.

Marcotte, T.D., Hansson, C.M., Hope, B.B., 1999b. The effect of the electrochemical chloride extraction treatment on steel-reinforced mortar—Part I: Electrochemical measurements. Cement and Concrete Research 29, 1555−1560.

Nmai, C.K., Farrington, S.S., Bobrowski, G.S., April 1992. Organic-based corrosion-inhibiting admixture for reinforced concrete. Concrete International 14, 45−51.

NACE, 1990. RP0290-90: Cathodic Protection of Reinforcing Steel in Atmospherically Exposed Concrete Structures. NACE, Houston, Texas.

Ngala, V.T., Page, C.L., Page, M.M., 2003. Corrosion inhibitor systems for remedial treatment of reinforced concrete, Part 2: Sodium monofluorophosphate. Corrosion Science 45, 1523−1537.

Orellan, J.C., Escadeillas, G., Arliguie, G., 2004. Electrochemical chloride extraction: efficiency and side effects. Cement and Concrete Research 34 (2), 227−234.

Page, C.L., 1992. Interfacial Effect on Electrochemical Protection Methods Applied to Steel in Chloride Containing Concrete. Rehabilitation of Concrete Structures. RILEM, Melbourne.

Pourbaix, M., 1974. Atlas of Electrochemical Equilibria in Aqueous Solutions. National Association of Corrosion Engineers, Houston, Texas.

Pedeferri, P., 1996. Cathodic protection and cathodic prevention. Construction and Building Materials 10 (5), 391−402.

Polder, R.B., 2005. Electrochemical techniques for corrosion protection and maintenance. In: Bohni, H. (Ed.), Corrosion in Reinforced Concrete Structures. Woodhead publishing Ltd., Cambridge, England and CRC Press LLC, Boca Raton, pp. 215−241.

Siegwart, M., Lyness, J.F., McFarland, B.J., 2003. Change of pore size in concrete due to electrochemical chloride extraction and possible implications for the migration of ions. Cement and Concrete Research 33 (8), 1211−1221.

Stratfull, R.F., 1957. Corrosion of steel in a reinforced concrete bridge. Corrosion 13 (3), 43−48.

Stratfull, R.F., 1973. Preliminary Investigation of Cathodic Protection of a Bridge Deck. California Department of Transportation, Sacramento, California.

Stratfull, R.F., 1974. Experimental Cathodic Protection of a Bridge Deck. California Department of Transportation, Sacramento, California.

Thompson, N.G., Yunovich, M., Lankard, D.R., 2000. Procedures for Evaluating Corrosion-inhibiting Admixtures for Structural Concrete. National Cooperative Highway Research Program, Washington, DC, p. 216.

Virmani, Y.P., Clemena, G.G., 1998. Corrosion Protection-concrete Bridges. Turner-Fairbank Highway Research Center, McLean, VA.

Modeling corrosion of steel in concrete

O. Burkan Isgor

Oregon State University, School of Civil and Construction Engineering, Corvallis, OR, USA

13.1   Introduction

The corrosion of steel reinforcement is the most common cause of deterioration of reinforced concrete structures (Bertolini et al., 2000; Bohni, 2005; Broomfield, 2007; Kurtis and Mehta, 1997; Mehta and Monteiro, 2005). Therefore, identifying steel corrosion in reinforced concrete structures early, before extensive corrosion-induced cracking and delamination occur, is essential for assessing their safety and for prioritizing repairs. Existing corrosion rate monitoring techniques for reinforced concrete elements, on the other hand, lack the accuracy to provide reliable measurements when they are used on real structural members in the field (Feliu et al., 1995; Gepraegs and Hansson, 2005; Gulikers, 2005; Hansson, 1984; Poursaee and Hansson, 2008; Wojtas, 2004). These techniques have been shown to work for simple structural elements, typically in laboratory conditions, when the locations and sizes of anodic and cathodic areas can be isolated accurately. For reinforced concrete elements in service, the locations and sizes of the anodic and cathodic surfaces are mostly unknown because embedded steel surfaces in concrete are inaccessible for direct measurement as a result of electrically resistive and thick concrete cover. This limitation yields existing corrosion rate measurement techniques inaccurate, unreliable, and in many cases unusable in field applications with large and complex reinforcement detailing (Feliu et al., 1995; Gepraegs and Hansson, 2005; Gulikers, 2005; Poursaee and Hansson, 2008; Wojtas, 2004).

Even when nondestructive corrosion rate measurement techniques provide accurate readings, these data represent instantaneous corrosion rates that are influenced greatly by environmental conditions over time. In order to accurately predict the mass or cross-sectional area loss of steel reinforcement in concrete, one needs to monitor the corrosion rates continuously or rather frequently for extended periods of time so that temporal environmental and material variations can be captured. Although existing corrosion rate measurement techniques might be practical for instantaneous monitoring of structures, they become rather expensive and impractical if the monitoring is to be performed continuously over long periods. Therefore, accurate modeling of steel corrosion in concrete structures is an important tool that can help solve this problem. Even though it is rather challenging, if not impossible, to completely replace nondestructive testing methods with corrosion rate prediction models, accurate simulations combined with relatively infrequent, and hence inexpensive, corrosion rate measurements can be used in the health monitoring of reinforced concrete infrastructure.

However, it should be noted that the modeling of active steel corrosion in concrete has its own challenges, which can be summarized under the following broad categories: (1) difficulty and uncertainty in the estimation of the parameters and environmental variables that are necessary for simulations; (2) computational difficulties in the solutions of governing equations due to nonlinear boundary conditions; and (3) challenges in modeling complicated geometries, dense reinforcement details, and nonhomogeneous material properties. Several researchers have made considerable progress with respect to overcoming these challenges in the past two decades (Warkus et al., 2006; Sagues, 2003; Kranc and Sagues, 2001; Gulikers and Raupach, 2006; Ghods et al., 2007; Isgor and Razaqpur, 2006a,b). This chapter provides an overview of modeling the corrosion of steel in concrete in order to elaborate these challenges and present the current state of the art on the subject.

13.2   Kinetics of steel corrosion in concrete

The corrosion of steel reinforcement in concrete is an electrochemical process at the concrete/steel interface in which iron in steel is oxidized in the concrete pore solution by the following anodic half-cell reaction (Bertolini et al., 2000; Broomfield, 2007; Revie and Uhlig, 2008):

$$\text{Fe} \rightarrow \text{Fe}^{2+} + 2e^{-} \tag{13.1}$$

The electrons that are produced in this anodic reaction must be consumed at the cathodic sites on the steel surface to preserve electrical neutrality. The type of cathodic reaction depends on the availability of oxygen around the steel reinforcement. When there is enough oxygen, as in the case of most unsaturated or partially saturated reinforced concrete elements, the cathodic reaction takes the form of oxygen reduction, namely (Bohni, 2005; Broomfield, 2007):

$$\frac{1}{2}\text{O}_2 + \text{H}_2\text{O} + 2e^{-} \rightarrow 2\text{OH}^{-} \tag{13.2}$$

In the absence of oxygen around steel reinforcement, as commonly seen in structural elements that are submerged in water, cathodic reaction might take the form of hydrogen evolution via (Broomfield, 2007; Jones, 1992):

$$2\text{H}^{+} + 2e^{-} \rightarrow \text{H}_2 \tag{13.3}$$

Since most reinforced concrete structures in practice are in a partially saturated state, for the purpose of demonstrating the modeling process of steel corrosion in concrete in this chapter, oxygen reduction will be assumed as the cathodic reaction complementing the anodic iron dissolution process. When the two half-cell reactions occur at widely separated locations, they are termed a macrocell. When they occur close together, or essentially at the same location, they are termed a microcell (Broomfield, 2007).

The electrode potentials of the anodic and cathodic reactions given in Eqns (13.1) and (13.2) can be represented respectively by the Nernst equations (Revie and Uhlig, 2008; Jones, 1992):

$$\phi_{\text{Fe}} = \phi_{\text{Fe}}^{\text{o}} - \frac{2.303RT}{z_{\text{a}}\text{F}} \log\left(\text{Fe}^{2+}\right) \tag{13.4}$$

$$\phi_{\text{O}_2} = \phi_{\text{O}_2}^{\text{o}} - \frac{2.303RT}{z_{\text{c}}\text{F}} \log \frac{\left(\text{OH}^-\right)^2}{P_{\text{O}_2}^{1/2}} \tag{13.5}$$

where $\phi_{\text{Fe}}^{\text{o}}$ (volt) and $\phi_{\text{O}_2}^{\text{o}}$ (volt) are the standard half-cell potentials of iron dissolution and oxygen reduction processes, respectively, R is the universal gas constant (8.3114 J/K mol), T is the absolute temperature, (Fe^{2+}) and (OH^-) are the activities of the iron and hydroxyl ions, respectively, z_{a} and z_{c} are the number of electrons involved in the anodic and cathodic reactions, respectively, and P_{O_2} is the fugacity of O_2, which can be approximated as the partial pressure of oxygen.

At equilibrium at any given point on the metal surface, the rate of the forward and reverse reactions given by Eqns (13.1) and (13.2) are equal to each other, and the rate of these equilibrium reactions can be represented by the anodic and cathodic exchange current densities, i_{oa} (A/m^2) and i_{oc} (A/m^2), respectively. When anodic and cathodic half cells are ionically (through the concrete pore solution) and metallically (through the reinforcement) connected, a net current flows between the anodic and cathodic sites, and the equilibrium potentials change through polarization. The basis of the polarization theory is well established (Revie and Uhlig, 2008); therefore, a detailed explanation of the phenomenon will not be given here. Anodic sites on the steel surface mainly polarize through activation polarization (Warkus et al., 2006; Kranc and Sagues, 2001; Gulikers and Raupach, 2006; Isgor and Razaqpur, 2006b), namely:

$$\phi_{\text{a}} = \phi_{\text{Fe}} + \beta_{\text{a}} \log \frac{i_{\text{a}}}{i_{\text{oa}}} \tag{13.6}$$

where ϕ_{a} (volt) is the polarized anodic potential and β_{a} (volt/dec) is the Tafel slope of the anodic reaction. It should be noted that the corrosion of steel in partially saturated concrete can be considered a catholically controlled process (Broomfield, 2007) during which greater polarization occurs at the cathodic sites. Therefore, some modeling studies make the assumption that anodes on the steel surface do not polarize during the corrosion process; however, this may be an oversimplification of the problem (Isgor and Razaqpur, 2006b).

Cathodic sites on the steel surface can polarize through activation and concentration polarization via (Warkus et al., 2006; Kranc and Sagues, 2001; Gulikers and Raupach, 2006; Isgor and Razaqpur, 2006b):

$$\phi_{\text{c}} = \phi_{\text{O}_2} + \beta_{\text{c}} \log \frac{i_{\text{c}}}{i_{\text{oc}}} - \frac{2.303RT}{2\text{F}} \log \frac{i_{\text{L}}}{i_{\text{L}} - i_{\text{c}}} \tag{13.7}$$

where ϕ_c (volt) is the polarized cathodic potential, i_c (A/m^2) is the cathodic current density, β_c (volt/dec) is the Tafel slope of the cathodic reaction, and i_L (A/m^2) is the limiting current density. In Eqn (13.7), the second term on the right-hand side represents the activation and the third term represents the concentration polarization components. The concentration polarization occurs when oxygen that is consumed by the cathodic reaction (Eqn (13.2)) cannot be replenished adequately from the surface of the structure through the concrete cover to sustain the oxygen reduction process. In this situation, the current density of the electrochemical process is controlled by a limiting current density, i_L, which is an indicator of oxygen availability at the cathodic sites. The limiting current density can be determined using (Bohni, 2005):

$$i_L = z_c F \frac{D_{O_2} C_{O_2}^s}{d} \tag{13.8}$$

where D_{O_2} (m^2/s) is the oxygen diffusion coefficient of concrete, C_{O_2} (mol/m^3 pore solution) is the concentration of dissolved oxygen on the concrete surface, and d (m) is the concrete cover thickness. As can be observed from Eqn (13.8), the limiting current density increases, with increasing oxygen concentration around the steel, and the increasing rate of oxygen can be replenished through the concrete cover. When the limiting current density is large (indicating oxygen availability at the cathodic sites), the concentration polarization term in Eqn (13.7) (Gulikers, 2005) approaches unity; hence, the cathodic polarization is mainly controlled by activation polarization. In other words, during modeling of steel corrosion in partially saturated concrete structures, the concentration polarization term in Eqn (13.5) can generally be ignored, which simplifies the solution process considerably.

When anodic and cathodic half cells are ionically and metallically connected, the established electrochemical cell operates at a corrosion current, I_{corr} (A), namely:

$$I_{corr} = i_a A_a = i_c A_c \tag{13.9}$$

where A_a (m^2) and A_c (m^2) are the anodic and cathodic surface areas on the steel surface, respectively. As can be observed in Eqn (13.7), when anodic and cathodic areas are equal to each other, as can be approximated for uniform corrosion, anodic and cathodic current densities are the same. Other cases (e.g., in the case of pitting corrosion) depend on the anode-to-cathode area ratio (A/C).

Since iron dissolution (i.e., metal loss) occurs at the anodic sites, the corrosion rate is related to the anodic current density (Gulikers, 2005):

$$p = 31.56 \times 10^6 \frac{W i_{corr}}{zFG} \tag{13.10}$$

where W is the atomic weight of iron (56 g/mole), G is the density of iron (7874 kg/m^3), and i_{corr} (A/m^2) is the corrosion current density, which is equivalent to the anodic current density, namely:

$$i_{corr} = i_a = \frac{I_{corr}}{A_a} \tag{13.11}$$

Once the current density at any unit area along the steel reinforcement is calculated, the determination of the rate and amount of corrosion becomes a straightforward task.

The determination of the anodic current density (or the corrosion current density) can be achieved through theoretical/numerical modeling, empirical equations, or other practical approaches. In the following section, the numerical solution of the corrosion current density at the anodic sites is described. Empirical and other practical approaches for the prediction of corrosion current density for steel reinforcement in concrete are presented in Section 13.5.

13.3 Theoretical/numerical modeling of corrosion current density

The corrosion of steel in concrete can take the form of microcell or macrocell corrosion depending on how anodic and cathodic half cells are separated from one another. In the case of microcell corrosion, the anodic and cathodic half cells are essentially at the same location with an A/C ratio approaching unity. After the equilibrium between anodic and cathodic half-cell reactions is reached, at any point on the steel surface, the rates of anodic and cathodic reactions, i_a and i_c, respectively, will be equal to each other and to the microcell corrosion current density, i_{corr}. Since the distance between the anodic and cathodic sites on the steel surface is very small for microcell corrosion, the effect of concrete resistivity can be ignored, and consequently, the potentials of anode and cathode can be considered equal. Therefore, the microcell corrosion current density of corroding steel in concrete can be obtained by numerically solving the following nonlinear equation, which assumes that the polarized anodic and cathodic electrode potentials (i.e., Eqns (13.6) and (13.7)) at any given point on the steel surface are equal to each other:

$$\phi_c^0 - \phi_a^0 + \beta_c \log\left(\frac{i_{corr}}{i_{oc}}\right) - \beta_a \log\left(\frac{i_{corr}}{i_{oa}}\right) + \frac{2.303RT}{z_cF}\log\left(\frac{i_L}{i_L - i_{corr}}\right) = 0$$

(13.12)

When the corrosion is in the form of macrocell corrosion, the determination of corrosion current density on the steel surface requires a more advanced approach. In this scenario, the current density can be predicted if the electrochemical potential (abbreviated henceforth as "potential") distribution around that point is known. Once the potential distribution along the reinforcement is known, the current density at any point on the steel surface can be calculated by Ohm's law (Munn and Devereux, 1991a,b):

$$i = -\frac{1}{r}\frac{\partial \phi}{\partial n}$$

(13.13)
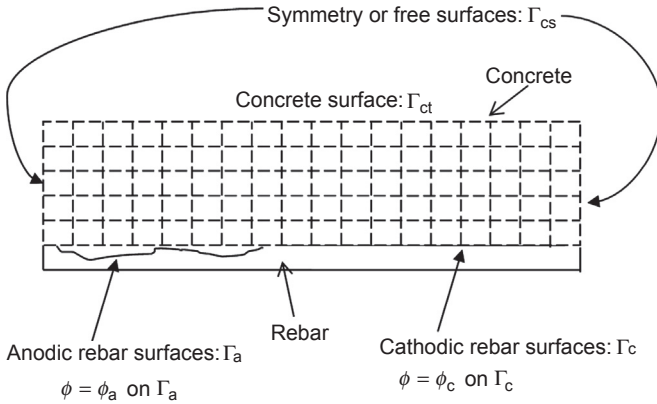
Figure 13.1 Analysis domain and boundary conditions for a simplified two-dimensional problem.

where ϕ (volt) is the potential, r (ohm-m) is the resistivity of the pore solution, and n is the direction normal to the equipotential lines. The potential distribution in concrete due to corroding rebar can be determined by solving Laplace's equation (Munn and Devereux, 1991a,b):

$$\nabla^2 \phi = 0 \tag{13.14}$$

where ∇^2 is the harmonic operator. For a three-dimensional problem, Eqn (13.14) takes the following form:

$$\frac{\partial^2 \phi}{\partial x^2} + \frac{\partial^2 \phi}{\partial y^2} + \frac{\partial^2 \phi}{\partial z^2} = 0 \tag{13.15}$$

Calculation of the potential distribution on the surface of the steel involves the solution of Eqn (13.14) subject to prescribed boundary conditions. These boundary conditions comprise the relationship between potential and current density for the anodic and cathodic regions as well as prescribed current densities. For the anodic and cathodic regions of the steel for a simplified two-dimensional domain as shown in Figure 13.1, the boundary conditions are defined as:

$$\phi = \phi_a \text{ on } \Gamma_a \tag{13.16}$$

$$\phi = \phi_c \text{ on } \Gamma_c \tag{13.17}$$

where ϕ_a and ϕ_c are polarized anodic and cathodic potentials that can be expressed in Eqns (13.6) and (13.7). Along free surfaces and axes of symmetry, no flux boundary conditions need to be defined via:

$$\frac{\partial \phi}{\partial n} = 0 \text{ on } \Gamma_{cs} \text{ and on } \Gamma_{ct} \tag{13.18}$$
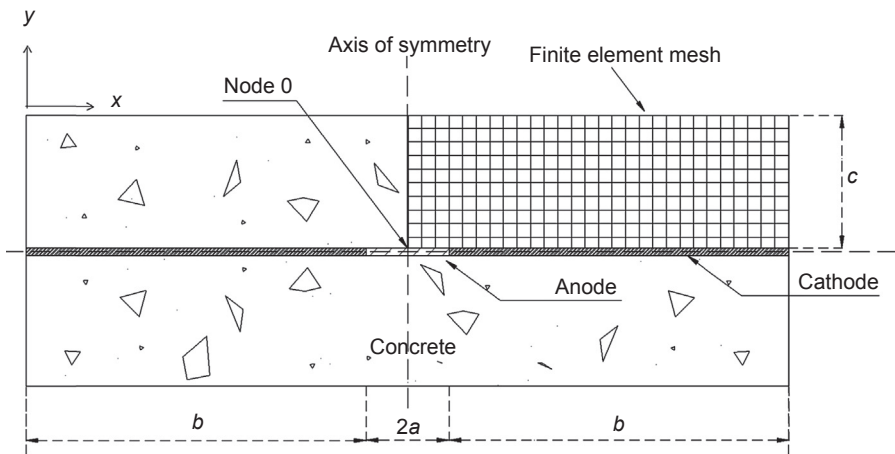
Figure 13.2 Analysis domain finite element discretization for the demonstration example.

Since the polarization Eqns (13.6) and (13.7) requires the knowledge of the current densities i_a and i_c on the steel surface, and these current densities can only be calculated using Eqn (13.13) after the solution of Eqn (13.14), the problem is nonlinear and requires the implementation of a nonlinear solution algorithm. The solution of this nonlinear problem can be achieved through numerical techniques such as finite element, finite difference, or boundary element methods (Kranc and Sagues, 2001; Isgor and Razaqpur, 2006b). In addition to the ability to provide corrosion rates on steel surface, this numerical approach can also be used to simulate half-cell potential experiments, as demonstrated by Pour-Ghaz et al. (2009a).

As a demonstration example, a typical finite element solution of a simplified two-dimensional problem, illustrated in Figure 13.2, is presented here. The analysis parameters of the example are provided in Table 13.1. The analyzed case has a rather large limiting current density (i.e., high oxygen availability), indicating that cathodic polarization is in the form of activation polarization only. The domain represents a single rebar experiencing macrocell corrosion with a single anodic region. Due to the symmetry of the system, only a quadrant of the domain needs to be analyzed. The analysis domain is discretized with 600 four-noded Lagrangian finite elements.

Figure 13.3 illustrates the current density distribution along the rebar length for different A/C ratios. The zones with positive corrosion current density correspond to the corrosion current density of the anodic surfaces. It is clear in this figure that corrosion current density is not a constant value along the reinforcement, and that it increases with decreasing A/C ratio when all other parameters remain the same. This implies that the accurate solution of Laplace's equation for current densities along the reinforcement requires knowledge of the A/C ratio, which will be discussed further in Section 13.4.

Another important point to note is that the solution of Laplace's equation provides instantaneous values of current densities along the reinforcement, which depend on several factors such as temperature, electrical resistivity, and the degree of

Table 13.1 Analysis parameters for the presented numerical demonstration example

Parameter	Value
Rebar length, $a + b$ (mm)	300
Cover thickness, c (mm)	100
Finite element size (mm)	5×5
Standard half-cell potential of Fe (mV vs SCE[a])	-780
Tafel slope of the anode, β_a (mV)	60
Anodic exchange current density, i_{oa} (A/mm^2)	3×10^{-10}
Standard half-cell potential of oxygen (mV vs SCE[a])	160
Tafel slope of the cathode, β_c (mV)	-180
Cathodic exchange current density, i_{oc} (A/mm^2)	1×10^{-11}
Temperature, T (K)	298
Resistivity, r (ohm-mm)	140,000
Limiting current density, i_L (A/mm^2)	1×10^{-6}

[a]SCE, Saturated calomel reference electrode.
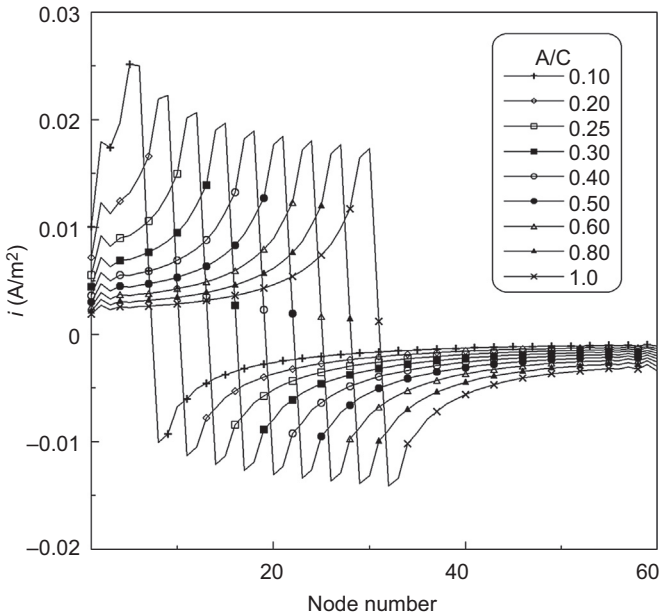
Figure 13.3 Distribution of current density along the reinforcement for various A/C ratios (demonstration example).
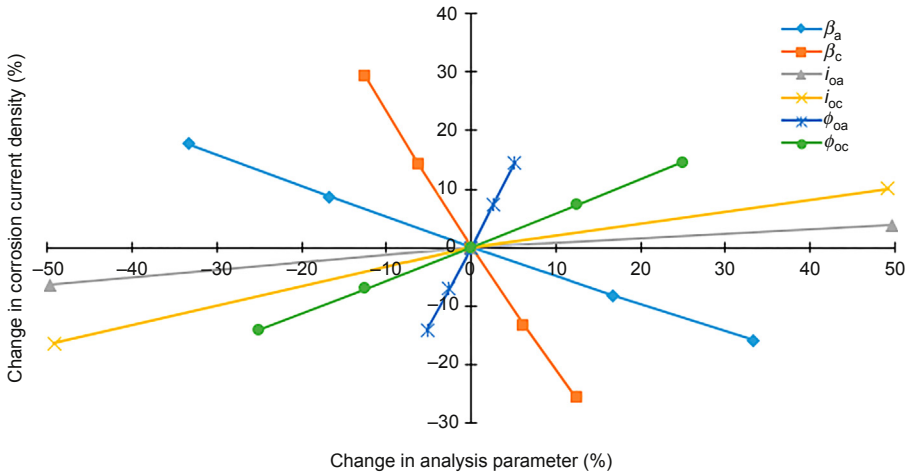
Figure 13.4 Sensitivity of corrosion current density to changes in main corrosion modeling parameters (base case is provided in Table 13.1; A/C = 0.1).

saturation; therefore, in order to calculate mass (or cross-sectional area) loss from steel reinforcement, Laplace's equation should be solved at different instances in time to perform time-dependent corrosion rate predictions. Once the corrosion rates are known over time, the mass (or cross-sectional area) loss can be calculated at any point on the reinforcement over time in performing service or remaining life prediction studies.

The solution of Laplace's equation with the nonlinear polarization boundary conditions through equations as described in this section requires the assumption of a number of corrosion parameters, specifically anodic and cathodic exchange current densities, anodic and cathodic standard electrode potentials, and anodic and cathodic Tafel slopes. These properties are mostly governed by the properties of the corroding system, and reasonable assumptions can be made for reinforcement corrosion in concrete (Gulikers and Raupach, 2006; Isgor and Razaqpur, 2006b; Kranc and Sauges, 2006; Hassanein et al., 2002). However, it is important to note that there is some degree of variability in these parameters originating from the fact that every concrete is different with a different pore solution composition. Figure 13.4 illustrates the sensitivity of corrosion current density on the changes of these six parameters for a case with an A/C ratio of 0.1. The base value for each parameter is provided in Table 13.1. The figure illustrates that variability in these parameters has an effect on corrosion rate predictions, albeit to different degrees. For example, for the demonstration example provided here, the corrosion rate is rather sensitive to changes in the anodic half-cell potential and the cathodic Tafel slope. A change of 10% in the cathodic Tafel slope results in about a 25% change in the predicted maximum corrosion current density along the reinforcement. Similarly, a 10% change in anodic half-cell potential causes about a 20% change in the predicted maximum corrosion current density along the reinforcement. These effects will be different for different A/C ratios, concrete resistivities, and macrocell configurations. Therefore, corrosion modeling exercises for

reinforced concrete elements need to be accompanied by sensitivity studies to develop an understanding of the role of parameter variability on corrosion rate predictions. A more comprehensive investigation of the effect of variability of corrosion analysis parameters on corrosion current density is provided by Ge and Isgor (2007).

A final remark regarding the prediction of corrosion current densities on steel reinforcement can be made regarding cases with simultaneous microcell and macrocell processes. In structures with complex reinforcement detailing, it is possible that some parts of the reinforcement might experience microcell corrosion locally, albeit at different rates, while they also connect to each other through macrocell corrosion cells. The modeling approach described here can be used to simulate such scenarios as demonstrated by Soleimani et al. (2010).

13.4   Environmental conditions and material/chemical properties of concrete around steel reinforcement

The corrosion modeling approach presented in Section 13.3 relies on knowledge of environmental conditions (e.g., temperature, the degree of saturation, and relative humidity) and material/chemical properties (e.g., electrical resistivity, pH or OH^- concentration, chloride concentration) of the concrete cover surrounding the steel reinforcement. Temperature, for instance, affects almost all aspects of the corrosion process, from main corrosion analysis parameters (e.g., Tafel slopes, electrode potentials and exchange current densities) to other critical factors such as electrical resistivity of concrete (Ge and Isgor, 2007; Pour-Ghaz et al., 2009b,c). The determination of chloride and pH profiles within the concrete cover has particular importance in modeling, because these parameters are used to identify corrosion initiation, the type of corrosion (i.e., microcell vs macrocell), and in particular for the case of macrocell corrosion, the locations of anodic and cathodic sites that serve as boundary conditions in the solution of Laplace's equation to solve for current densities on steel reinforcement.

In the case of chloride-induced corrosion, when the chloride concentrations at the steel/concrete interface exceed a threshold value, either represented as chloride concentration or as a ratio of chloride to hydroxide ions, it can be assumed that such locations on the steel surface lose their passivity and become active anodic sites. The remaining steel surfaces act as cathodic sites. When depassivation occurs nonuniformly, current density predictions on the reinforcement surface can be made assuming macrocell corrosion with defined anodic and cathodic boundary conditions as described in Section 13.3. In situations where the chloride concentration around the reinforcement shows a uniform distribution and the chloride threshold is exceeded at every point on the steel surface, it can be assumed that corrosion takes place uniformly in the form of microcell corrosion, which does not require the identification of exact locations of anodic and cathodic sites as discussed in Section 13.3. In the case of carbonation-induced corrosion, the identification of corrosion initiation and the type of corrosion, and in the case of macrocell corrosion the locations of the anodic

and cathodic surfaces, can be achieved by comparing the pH of the pore solution around the reinforcement with a user-defined pH threshold.

The main challenge in this exercise lies with the variability and uncertainty involved in reported chloride thresholds rather than the actual corrosion modeling process. Whether they are represented in terms of total or free chloride concentrations or the chloride-to-hydroxide concentration ratio, Cl^-/OH^-, reported values of chloride thresholds for carbon steel reinforcement in concrete cover a wide range and have a large degree of uncertainty (Ann and Song, 2007; Alonso et al. 2000; Angst et al., 2009). It has been shown that the reported variability of chloride thresholds is the result of a number of factors including the chemistry of the concrete pore solution (Goni and Andrade, 1990; Andrade and Page, 1986), rebar surface conditions (Mammoliti et al., 1996; Li and Sagues, 2001; Pillai and Trejo, 2005), and properties of the rebar—concrete interface (Ghods et al., 2011). This variability associated with chloride thresholds can be mitigated through probabilistic approaches that do not use deterministic values for chloride thresholds; however, at the time of the writing of this chapter, research toward the development of such approaches was still ongoing.

In a comprehensive approach, the determination of environmental conditions and material/chemical properties of the concrete cover surrounding steel reinforcement can be achieved through the coupled solution of heat, moisture, and ionic transport equations, which have been widely studied by several researchers part of initiation stage modeling investigations (Samson and Marchand, 1999, 2007; Samson et al., 2005; Ideker et al., 2014; Isgor and Razaqpur, 2004; Martin-Perez et al., 2001). Comprehensive models include the simulation of reactive-transport processes, which are based on the numerical solution of the extended Nernst—Plank equation for various ionic species in concrete (Samson and Marchand, 1999, 2007). These models treat the transport phenomenon as a coupled process that involves advection, diffusion, and electrical migration. Due to the inclusion of the electrical migration mechanism, these models have the ability to incorporate the effect of polarized boundary conditions on electrical distribution within the concrete cover. A major disadvantage of these models is their dependence on a large number of input parameters, some of which cannot be easily determined in practical applications. Less comprehensive models focus on the uncoupled or loosely coupled transport of individual species (e.g., chloride, hydroxide, oxygen) by approximating the multimechanism phenomena with diffusion-based (Fickian) processes (Isgor and Razaqpur, 2004; Martin-Perez et al., 2001). These models allow for the solution of the governing differential equations of the transport problem using numerical techniques such as the finite element method in two or three dimensions, with smaller computational effort and a relatively small number of input parameters. In one-dimensional problems, the solution of these governing equations becomes trivial—in most cases, closed-form equations can be obtained. Although this approach has a number of advantages over models based on the coupled solution of the extended Nernst—Plank equation for different ionic species, in these models chemical interactions with ions and the effect of electrical potential distribution on the ionic transport phenomenon cannot be simulated. The main disadvantages of these simplified models are presented in detail by Marchand and Samson (2009).

13.5   Empirical models and other practical approaches for predicting corrosion current density

Empirical models for predicting corrosion current density are based on the observed relationship between the corrosion rate of steel and different parameters that affect it, such as concrete properties and environmental conditions. These models are easy to use, since they do not require a wide range of assumptions to be made as in theoretical modeling approaches. However, because they are derived from limited experimental data and do not consider the fundamental mechanisms of corrosion from a theoretical point of view, their general applicability and reliability can be rather limited. Nevertheless, these models can provide accurate predictions when the simulated case is similar to the experiments from which the empirical relationships are obtained. In this section, selected empirical models and other practical approaches for the determination of corrosion current density of steel in concrete are presented without providing extensive details.

In one of the earlier studies, Alonso et al. (1988) developed an empirical model correlating the electrical resistance of mortar to the corrosion rate of steel. The experimental study consisted of steel-reinforced specimens produced with mortar with different types of cement and with and without different supplementary cementitious materials. The corrosion was achieved by carbonating the mortar. The corrosion rate of the steel was measured by means of the polarization resistance method at 50% and 100% relative humidity (RH), as well as in partial water immersion. Equation (13.19) represents the model that shows that corrosion rate is proportional to the reciprocal of the concrete resistance:

$$i_{corr} = \log(i_{const}) + C_{coef} \log(R_{con}) \tag{13.19}$$

where i_{corr} ($\mu A/cm^2$) is the corrosion current density as measured by a polarization resistance method, R_{con} (Ω) is the mortar resistance, i_{const} ($\approx 10^4$ $\mu A/cm^2$) is a constant, and C_{coef} is a coefficient that is a function of the cement type, which is given for each mortar tested in this study (Alonso et al., 1988). Although the model is simple and practical, it is also rather limited in its application. First, electrical resistance is a geometry-dependent property; hence, the application of the model to elements with different geometries is rather challenging. In addition, corrosion was initiated by carbonation; therefore, the model's applicability to chloride-induced corrosion can be debated. Due to extensive carbonation, the steel can be considered uniformly depassivated; therefore, it might not be possible to extrapolate the results to pitting corrosion.

Morinaga (1990) developed an empirical model for predicting corrosion current density of chloride-induced steel corrosion using specimens that were exposed to an outdoor environment for about a 10-year period. The corrosion rate of steel in each specimen was determined by the mass loss method in accordance with ASTM G1. The following relationship was developed by regression analysis using the results of these experiments:

$$i_{corr} = \left[-0.51 - 7.60 C_{Cl} + 44.97(w/c)^2 + 67.95 C_{Cl}(w/c)^2 \right] \times (d_{st}/d^2) \times 10^4 \tag{13.20}$$

where i_{corr} was represented in terms of g/cm^2/year, w/c is the water-to-cement ratio of the concrete, C_{Cl} (% by weight of mixing water) is the chloride content, d_{st} (mm) is the diameter of reinforcing steel, and d (mm) is the concrete cover thickness. The main advantage of Morinaga's model is that input parameters are mostly known design properties of the concrete element, and the only environmental variable that requires an assumption is the chloride content. However, this practical benefit is also a disadvantage, since the model does not include critical effects such as temperature or RH in corrosion current density predictions. Considering this caveat, Morinaga proposed an additional empirical equation that is mainly based on environmental parameters, namely:

$$
\begin{aligned}
i_{corr} = {}& 2.59 - 0.05T - 6.89(h - 0.45) - 22.87C_{O_2}^{air} - 0.99C_{Cl} \\
& + 0.14T(h - 0.45) + 0.51TC_{O_2}^{air} + 0.01TC_{Cl} + 60.81(h - 0.45)C_{O_2}^{air} \\
& + 3.36(h - 0.45)C_{Cl} + 7.32C_{O_2}^{air}C_{Cl}
\end{aligned}
$$

$$(13.21)$$

where i_{corr} is the corrosion current density presented in ($\times 10^{-4}$ g/cm^2/year), T is in $^\circ$C, h (%) is the RH, and $C_{O_2}^{air}$ (%) is the concentration of oxygen in air. It should be noted that this model does not include any concrete design parameter, such as the w/c ratio, in its formulation.

Liu and Weyers (1998a,b) developed an empirical model by testing large reinforced concrete slabs simulating concrete bridge decks. A total of 44 specimens were produced with different values of chloride content and cover thickness. The w/c ratio of the specimens varied between 0.41 and 0.45. The corrosion rate and electrical resistance of the specimens were measured regularly. Temperature was monitored with a thermocouple embedded at rebar depth. At the final stage of the experiment, metal mass loss measurements were performed in accordance with ASTM G1. During the five-year outdoor exposure of the specimens, a total of 2927 measurements were recorded. The following relationship to be used for predicting corrosion current density of steel reinforcement in bridge decks was developed by a regression analysis on the collected data:

$$
\ln 1.08i_{corr} = 7.89 + 0.7771 \ln 1.69C_t - \frac{3006}{T} - 0.000116\,R_{con} + 2.24t^{-0.215}
$$

$$(13.22)$$

where C_t (kg/m^3 of cement) is acid soluble chloride content as determined by ASTM C1152, T (K) is temperature, R_{con} (ohm) is the resistance of concrete, and time, t, is given in years. Unlike Morinaga's model, Liu and Weyers do not use any design parameters in their model, but rely on measurement data such as temperature, electrical resistance, and chloride content.

An empirical model correlating the effect of the water-to-cement ratio (w/c), cement content, and chloride content to the steel corrosion rate was developed by Ahmad and Bhattacharjee (2000). Three values of each parameter (using a total of 27 specimens)

were considered to capture quadratic, bilinear, and linear variation of the corrosion rate with each parameter. The result was the model given in the following equation:

$$i_{corr} = 37.726 + 6.120\left(\frac{C_{Cl} - 2.5}{1.25}\right) - 2.231\left(\frac{C_{cement} - 300}{50}\right)^2\left(\frac{w/c - 0.65}{0.075}\right)$$

$$+ 2.722\left(\frac{w/c - 0.6}{0.075}\right)^2\left(\frac{C_{Cl} - 2.5}{1.25}\right)^2$$

(13.23)

where i_{corr} is corrosion current density (nA/cm^2), C_{cement} (kg/m^3) is the cement content, and C_{Cl} (% by mass of cement) is the chloride content in the form of CaCl$_2$. Although the parameters considered in developing this model affect the corrosion rate significantly, the applicability of the model is somewhat limited, since no environmental factors such as RH or temperature were considered.

Due to the apparent relationship between the corrosion rate of reinforcement and the electrical resistivity of concrete, there has been growing interest in developing models based on the relationship between corrosion current density and electrical resistivity of concrete. One of these models was proposed as part of the European DuraCrete project. Since electrical resistivity of concrete is a parameter that can be determined relatively accurately in situ, and within seconds, these resistivity-based corrosion rate models have been gaining increasing attention. Some resistivity-based models, on the other hand, are not empirical but obtained through theoretical studies. For example, Gulikers (2005) used equivalent circuit modeling and Butler−Volmer kinetics to obtain a theoretical relationship between corrosion current density and the electrical resistivity of concrete, namely:

$$i_{corr} = \frac{F_G^{-0.8125} 98.696 \times 10^{-3}}{\rho^{0.8125}}$$

(13.24)

where i_{corr} is in A/m^2 and F_G (m^{-1}) is the geometry factor.

Pour-Ghaz et al. (2009b,c) investigated the effect of temperature on the corrosion rate of steel corrosion in concrete using virtual experiments. These numerical experiments are based on the finite element solution of Laplace's equation with predefined boundary conditions of the problem, and have been designed to establish independent correlations among corrosion rate, temperature, kinetic parameters, concrete resistivity, and limiting current density for a wide range of possible A/C distributions on the reinforcement. The virtual experiment approach allowed the researchers to perform over 15,000 simulations, which were used to develop the following closed-form regression model for the prediction of the corrosion current density:

$$i_{corr} = \frac{1}{\tau \rho^\gamma}\left(\eta T d^\kappa i_L^\lambda + \mu T \nu^{i_L^{\varpi}} + \theta(T i_L)^\vartheta + \chi \rho^\gamma + \zeta\right)$$

(13.25)

Table 13.2 The constants of the model given in Eqn (13.25)

Coefficient	Value
τ	1
H	0.32006292
ζ	-53.1228606
κ	0.00550263686
λ	0.120663606
γ	0.787449933
μ	$-3.73825172 \times 10^{-7}$
θ	47.2478753
ϑ	0.00712334564
χ	0.003482058
ν	784,679.23
ϖ	0.0102616314

where ρ (Ω m) is the concrete resistivity, T (°K) is temperature, d (m) is concrete cover thickness, and i_L (A/m^2) is the limiting current density. The coefficients of the equation (i.e., τ, γ, η, κ, λ, μ, ν, ϖ, θ, ϑ, χ, ζ) are provided in Table 13.2.

As a demonstration of the models presented in this section, a hypothetical comparative study is presented here. Although a wide range for each parameter affecting corrosion of steel in concrete can be considered in constructing the hypothetical case, the parameters in this section are chosen to represent a reinforced concrete structure encountered in usual civil engineering practices. The design parameters are summarized in Table 13.3. The structure is assumed to be in an environment experiencing

Table 13.3 Concrete and structural design parameters for the hypothetical comparison study

Parameter	Value
w/c	0.5
Aggregate-to-cement ratio	3.0
Cement type	OPC Type I
Cement content	400 kg/m^3
Air content	3%
Cover thickness	45 mm
Rebar diameter	20 mm
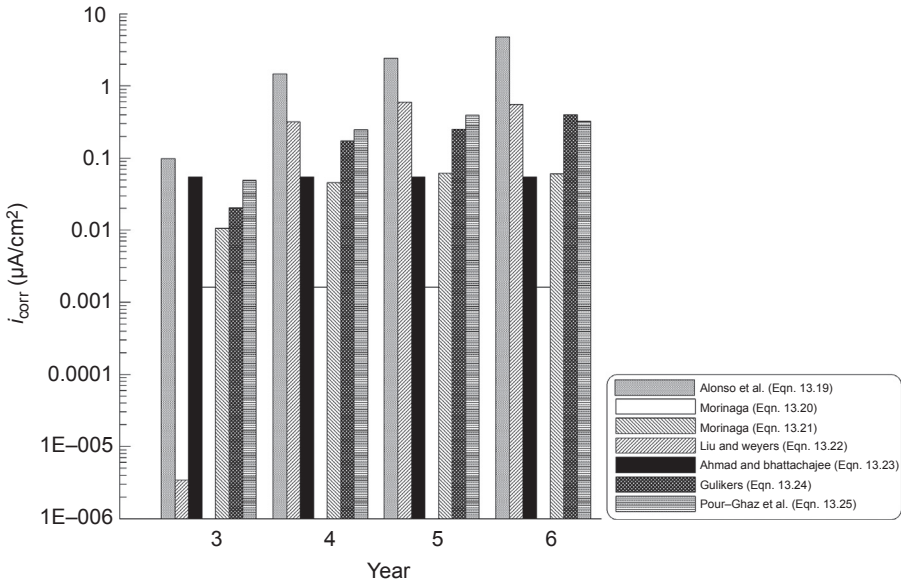
Figure 13.5 Comparison of the corrosion current densities predicted by selected models.

seasonal variations (average temperature: $20-40\,^{\circ}C$; average RH: $65\%-90\%$) (Pour-Ghaz, 2007). Furthermore, it is assumed that uniform depassivation has occurred due to chloride contamination (2% by cement mass) after 2 years of exposure. The values of concrete resistivity, dissolved oxygen content, and oxygen diffusion coefficient are calculated based on design parameters and exposure conditions using the same procedures described by Pour-Ghaz (2007).

Figure 13.5 illustrates the corrosion current density for the hypothetical case using the models presented in this section. It is important to note the variation in the predictions of the models even though they use the same set of data. It is also clear that the selection of empirical models requires a careful analysis of the specific case and simulated conditions. As an example, it can be observed from this figure that the model proposed by Alonso et al. (1988) overestimates the corrosion current density compared with other models, in all exposure periods. One of the reasons for this overestimation could be because the Alonso model was developed specifically for carbonation-induced corrosion. In the hypothetical case, the corrosion was induced as a result of chloride ingress. Carbonated concretes typically have higher electrical resistivity than chloride-contaminated concretes, which can explain the overestimation of the corrosion current densities by the model developed by Alonso et al. (1988). Similar problems associated with empirical models can be avoided when theoretical models, such as the approach described in Section 13.3 or the practical model developed by Pour-Ghaz et al. (2009b,c), are used. However, as discussed earlier, these theoretical models require assumptions about the parameters affecting corrosion and confirmation of the variability associated with these parameters.

13.6 Conclusions

Accurate modeling of steel corrosion in concrete structures is an important tool that can help in structural health monitoring, scheduling/prioritization of repair operations, and better interpretation of data from corrosion measurement techniques. Accurate simulations combined with relatively infrequent, and hence inexpensive, corrosion rate measurements can be used in health monitoring of reinforced concrete infrastructure. Theoretical corrosion modeling approaches that are based on fundamental principles of steel corrosion in concrete can be quite powerful; however, they also require assumptions about the parameters affecting corrosion and consideration of the variability associated with these parameters. Empirical models, on the other hand, are easy to use, since they do not require a wide range of assumptions to be made as is the case with theoretical modeling approaches. However, because they are derived from limited experimental data and do not consider fundamental mechanisms of corrosion from a theoretical point of view, their general applicability and reliability can be rather limited. Nevertheless, these models can provide accurate predictions when the simulated case is similar to the experiments from which the empirical relationships are obtained.

References

Ahmad, S., Bhattacharjee, B., 2000. Empirical modelling of indicators of chloride-induced rebar corrosion. Journal of Structural Engineering 27, 195−207.

Alonso, C., Andrade, C., Gonzalez, J.A., 1988. Relation between resistivity and corrosion rate of reinforcements in carbonated mortar made with several cement types. Cement and Concrete Research 18, 687−698.

Alonso, C., Andrade, C., Castellote, M., Castro, P., 2000. Chloride threshold values to depassivate reinforcing bars embedded in a standardized OPC mortar. Cement and Concrete Research 30, 1047−1055.

Andrade, C., Page, C.L., 1986. Pore solution chemistry and corrosion in hydrated cement systems containing chloride salts - a study of cation specific effects. British Corrosion Journal 21, 49−53.

Angst, U., Elsener, B., Larsen, C.K., Vennesland, O., 2009. Critical chloride content in reinforced concrete - a review. Cement and Concrete Research 39, 1122−1138.

Ann, K.Y., Song, H.-W., 2007. Chloride threshold level for corrosion of steel in concrete. Corrosion Science 49, 4113−4133.

Bertolini, L., Elsener, B., Pedeferri, P., Polder, R., 2000. Corrosion of Steel in Concrete: Prevention, Diagnosis, Repair. Wiley-VCH, Weinheim.

Bohni, H., 2005. Corrosion in Concrete Structures. CRC Press, New York.

Broomfield, J.P., 2007. Corrosion of Steel in Concrete. Taylor & Francis, New York.

Feliu, S., Gonzalez, J.A., Andrade, C., 1995. Effect of current distribution on corrosion rate measurements in reinforced-concrete. Corrosion 51, 79−86.

Ge, J., Isgor, O.B., 2007. Effects of Tafel slope, exchange current density and electrode potential on the corrosion of steel in concrete. Materials and Corrosion-Werkstoffe Und Korrosion 58, 573−582.

Gepraegs, O.K., Hansson, C.M., 2005. A comparative evaluation of three commercial instruments for field measurements of reinforcing steel corrosion rates. Journal of ASTM International 8.

Ghods, P., Isgor, O.B., Pour-Ghaz, M., 2007. A practical method for calculating the corrosion rate of uniformly depassivated reinforcing bars in concrete. Materials and Corrosion-Werkstoffe Und Korrosion 58, 265−272.

Ghods, P., Isgor, O.B., McRae, G.A., Li, J., Gu, G.P., 2011. Microscopic investigation of mill scale and its proposed effect on the variability of chloride-induced depassivation of carbon steel rebar. Corrosion Science 53, 946−954.

Goni, S., Andrade, C., 1990. Synthetic concrete pore solution chemistry and rebar corrosion rate in the presence of chlorides. Cement and Concrete Research 20, 525−539.

Gulikers, J., Raupach, M., 2006. Numerical models for the propagation period of reinforcement corrosion - comparison of a case study calculated by different researchers. Materials and Corrosion-Werkstoffe und Korrosion 57, 618−627.

Gulikers, J., 2005. Theoretical considerations on the supposed linear relationship between concrete resistivity and corrosion rate of steel reinforcement. Materials and Corrosion-Werkstoffe und Korrosion 56, 393−403.

Hansson, C.M., 1984. Comments on electrochemical measurements of the rate of corrosion of steel in concrete. Cement and Concrete Research 14, 574−584.

Hassanein, A.M., Glass, G.K., Buenfeld, N.R., 2002. Protection current distribution in reinforced concrete cathodic protection systems. Cement and Concrete Composites 24, 159−167.

Ideker, J., Isgor, O.B., Li, C., Jafari, V., Verba, C., Rodriguez, D.E., 2014. Experimental and numerical modeling approach to elucidating damage mechanisms in cement-well casing-host rock settings for underground storage of CO_2. In: NETL Technical Report Series. U.S. Department of Energy, National Energy Technology Laboratory, Albany, Oregon, USA.

Isgor, O.B., Razaqpur, A.G., 2004. Finite element modeling of coupled heat transfer, moisture transport and carbonation processes in concrete structures. Cement and Concrete Composites 26, 57−73.

Isgor, O.B., Razaqpur, A.G., 2006a. Advanced modelling of concrete deterioration due to reinforcement corrosion. Canadian Journal of Civil Engineering 33, 707−718.

Isgor, O.B., Razaqpur, A.G., 2006b. Modelling steel corrosion in concrete structures. Materials and Structures 39, 291−302.

Jones, D.A., 1992. Principles and Prevention of Corrosion. Macmillan.

Kranc, S.C., Sagues, A.A., 2001. Detailed modeling of corrosion macrocells on steel reinforcing in concrete. Corrosion Science 43, 1355−1372.

Kranc, S.C., Sagues, A.A., 2006. A numerical method for the recovery of local potentials and currents due to corrosion of steel in concrete, electrochemical techniques for evaluating corrosion performance and estimating service-life of reinforced Concrete. Journal of ASTM International 3, 11.

Kurtis, K.E., Mehta, P.K., 1997. A critical review of deterioration of concrete due to corrosion of reinforcing steel. ACI Special Publication 170, 535−554.

Li, L., Sagues, A.A., 2001. Chloride corrosion threshold of reinforcing steel in alkaline solutions - open-circuit immersion tests. Corrosion 57, 19−28.

Liu, T., Weyers, R.W., 1998. Modeling the dynamic corrosion process in chloride contaminated concrete structures. Cement and Concrete Research 28, 365−379.

Liu, Y.P., Weyers, R.E., 1998. Modeling the time-to-corrosion cracking in chloride contaminated reinforced concrete structures. ACI Materials Journal 95, 675−681.

Mammoliti, L.T., Brown, L.C., Hansson, C.M., Hope, B.B., 1996. The influence of surface finish of reinforcing steel and pH of the test solution on the chloride threshold concentration for corrosion initiation in synthetic pore solutions. Cement and Concrete Research 26, 545−550.

Marchand, J., Samson, E., 2009. Predicting the service-life of concrete structures - limitations of simplified models. Cement and Concrete Composites 31, 515−521.

Martin-Perez, B., Pantazopoulou, S.J., Thomas, M.D.A., 2001. Numerical solution of mass transport equations in concrete structures. Computers and Structures 79, 1251−1264.

Mehta, P.K., Monteiro, P.J.M., 2005. Concrete: Microstructure, Properties, and Materials. McGraw-Hill Professional, New York.

Morinaga, S., 1990. Prediction of service life of reinforced concrete buildings based on the corrosion rate of reinforcing steel. In: 5th International Conference on Durability of Building Materials and Components, Brighton, U.K.

Munn, R.S., Devereux, O.F., 1991a. Numerical modeling and solution of Galvanic corrosion systems: 1. Governing differential-equation and electrodic boundary-conditions. Corrosion 47, 612−618.

Munn, R.S., Devereux, O.F., 1991b. Numerical modeling and solution of Galvanic corrosion systems. Part 2: finite-element formulation and descriptive examples. Corrosion 47, 618−634.

Pillai, R.G., Trejo, D., 2005. Surface condition effects on critical chloride threshold of steel reinforcement. ACI Materials Journal 102, 103−109.

Pour-Ghaz, M., Isgor, O.B., Ghods, P., 2009a. Quantitative interpretation of half-cell potential measurements in concrete structures. Journal of Materials in Civil Engineering 21, 467−475.

Pour-Ghaz, M., Isgor, O.B., Ghods, P., 2009b. The effect of temperature on the corrosion of steel in concrete. Part 2: model verification and parametric study. Corrosion Science 51, 426−433.

Pour-Ghaz, M., Isgor, O.B., Ghods, P., 2009c. The effect of temperature on the corrosion of steel in concrete. Part 1: simulated polarization resistance tests and model development. Corrosion Science 51, 415−425.

Pour-Ghaz, M., 2007. A novel approach for practical modelling of steel corrosion in concrete. In: Department of Civil and Environmental Engineering. Carleton University, Ottawa, p. 247.

Poursaee, A., Hansson, C.M., 2008. Galvanostatic pulse technique with the current confinement guard ring: the laboratory and finite element analysis. Corrosion Science 50, 2739−2746.

Revie, R.W., Uhlig, H.H., 2008. Corrosion and Corrosion Control, fourth ed. Wiley-Interscience, New York.

Sagues, A.A., 2003. Modeling the effects of corrosion on the lifetime of extended reinforced concrete structures. Corrosion 59, 854−866.

Samson, E., Marchand, J., 1999. Numerical solution of the extended Nernst-Planck model. Journal of Colloid and Interface Science 215, 1−8.

Samson, E., Marchand, J., 2007. Modeling the transport of ions in unsaturated cement-based materials. Computers and Structures 85, 1740−1756.

Samson, E., Marchand, J., Snyder, K.A., Beaudoin, J.J., 2005. Modeling ion and fluid transport in unsaturated cement systems in isothermal conditions. Cement and Concrete Research 35, 141−153.

Soleimani, S., Ghods, P., Isgor, O.B., Zhang, J., 2010. Modeling the kinetics of corrosion in concrete patch repairs and identification of governing parameters. Cement and Concrete Composites 32, 360−368.

Warkus, J., Raupach, M., Gulikers, J., 2006. Numerical modelling of corrosion - theoretical backgrounds. Materials and Corrosion-Werkstoffe Und Korrosion 57, 614−617.

Wojtas, H., 2004. Determination of polarization resistance of reinforcement with a sensorized guard ring: analysis of errors. Corrosion 60, 414−420.

Future trends in research on reinforcement corrosion

14

C. Andrade
Institute of Construction Science "Eduardo Torroja" (IETcc) of the National Research Council of Spain; Consejo Superior Investigaciones Científicas (CSIC), Madrid, Spain

14.1   Introduction

Experience on the durability of reinforced concrete extends 100−150 years, a period during which the material has been demonstrated to have multiple applications and to adapt to different uses and types of elements and structures, despite being made with cements from different locations and using local aggregates. Structural concrete resists well in many environments, but in ambient environments that are marine or chloride bearing, reinforcement corrosion may appear as premature damage, and reaching a 100-year lifetime without corrosion does not seem likely. Studies to extend reinforcement passivity are numerous worldwide; in spite of this, many aspects are still not well known, and there is the need to incorporate present knowledge into engineering education.

In present chapter, several aspects are commented that, in author's opinion, need further scientific and technical advances. The chapter is organized in thematic sections in a broad manner, with particular comments for some of the gaps identified. In each case, an attempt is made not to repeat what has been described in previous chapters of this book, but rather to identify gaps needing further development. Selected topics are logically limited by the extension of the chapter. The sections are:

1. Causes of reinforcement corrosion:
   a. Carbonation
   b. Chloride ingress
   c. Stress corrosion cracking (SCC)
   d. Corrosion onset and chloride threshold
   e. Corrosion propagation period
2. Modelling of service life
3. Preventive methods
4. Repair materials and techniques
5. Corrosion measurement techniques

14.2   Processes leading to reinforcement corrosion

The two most frequent processes leading to reinforcement corrosion are carbonation of concrete cover and chloride ingress (Tuutti, 1982). In both types of attack, the aggressive substances penetrate through the pores and react with the hydrated cement phases.

Then, the processes always have two simultaneous steps, *transport* and *reaction*. These are used in emphasizing the needs for future research, together with analyzing the impact of processes in the concrete *microstructure*. Finally, needs in *testing* and *modelling* complete the analysis.

14.2.1   Carbonation

Carbonation supposes the dissolution of CO_2 gas into the pore solution and the reaction of its dissolved species with the Portlandite and the rest of the cement hydrates to produce calcite, and less frequently vaterite and aragonite. Several important studies were performed to clarify the evolution of the microstructure, the degree of reaction in the carbonation front and the manner in which the front progresses in the function of the porosity (Houst and Wittmann, 1994; Thiery et al., 2007; Glasser et al., 2008).

The aspects that need further clarification related to carbonation are:

1. **Transport phase**. It is assumed to proceed by diffusion of the CO_2 gas through the empty pore spaces and is characterized by the diffusion coefficient, D_{CO_2}. This coefficient, however, can only be indirectly characterized or measured in carbonated specimens. Measurement methods for D_{CO_2} are necessary in order to progress in clarifying porosity's role in the whole carbonation process.
2. **Reaction**. It is in general assumed that: (a) all calcium oxide (OCa) can react with carbon dioxide and (b) carbonation is better resisted as the amount of Portlandite increases (i.e. a higher tricalcium silicate (SC_3) content and higher degree of reaction). However, very little information exists on:
   a. *Rate of reaction* between dissolved carbon dioxide and several cement phases (the alkali and calcium hydroxide, calcium silicate hydrate (C−S−H) and AFm phases)
   b. *Amount of bound CO_2 or calcium carbonate formed* − studies were done on this subject from which it can be deduced that not all of the OCa present in the paste carbonates. Uncarbonated Portlandite may remain due to geometrical restrictions or lack of accessibility of the CO_2.
   c. *Pore humidity content*, which has a central role not only for the transport but also for the reaction ability
   d. *Alkali content.* The alkalis have an opposite role, as their presence in the pore solution induces higher pH values that require more CO_2 to be neutralized, but simultaneously the higher pH leads to higher $CO_3=$ contents in the pore solution and then more profound carbonation degrees.
3. **Testing**. *Natural* and accelerated conditions are usually employed; however, controversy remains as to the maximum CO_2 concentration that gives similar values to those of natural exposure. It seems that 3% (Castellote et al., 2009) as shown in Figure 14.1 is a frontier, although it may be influenced by the type of cement. Below this amount of CO_2 in the carbonation chamber, the amount of silica gel formed during carbonation is similar to that produced under natural conditions. Higher proportions lead to a higher production of silica gel, likely due to partial pressure in the chamber that produces more bicarbonate species in the pore solution, which reduces pH and starts to attack the C−S−H liberating silica gel while forming higher proportions of calcite (Castellote et al., 2009).

14.2.2   Chloride ingress

Chloride ingress is the main cause of reinforcement corrosion (Page and Treadaway, 1982; Climent et al., 2000; Martín-Pérez et al., 2000; Mangat and Molloy, 1994; Bamforth
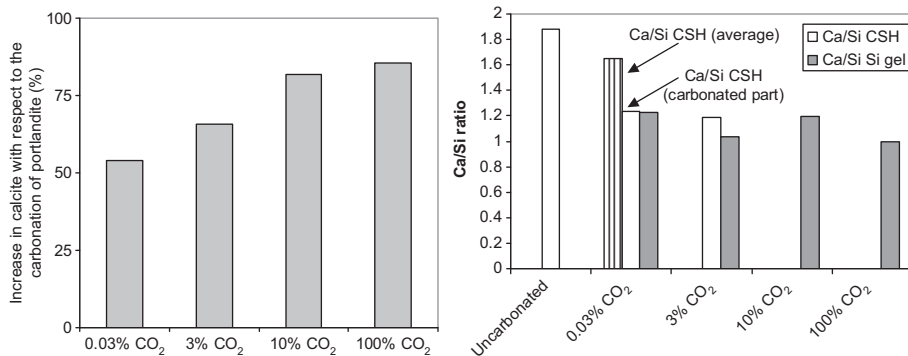
Figure 14.1 Left: Amount of formed calcite above the stoichiometry of Portlandite; Right: Ca/Si ratio of the C−S−H and the Ca-modified silica gel. In the case of natural carbonation (0.03%), two values are given, that of the whole sample and that of only the carbonated zone (Castellote et al., 2009).

and Chapman-Andrews, 1994; Andrade, 1993; Whiting, 1981; Meira et al., 2007; Page and Lambert, 1987; Glasser et al., 1999; Baroghel-Bouny et al., 2010). While carbonation implies the need to have the pore network partially empty for the gas to get through, chloride ions penetrate if the pores have evaporable water. In partially saturated concrete, chloride penetration slows down due to low humidity content, although the chlorides also can penetrate dissolved in the water vapour (marine fog) through the empty pore space in marine atmospheres. In spite of numerous studies published on this subject, several challenges remain, as most of the publications deal with testing different additions to the clinker, with very few addressing the fundamentals of the process and its controlling parameters. Further, diffusion depending on cation type or chloride binding are key aspects very seldom studied from a basic perspective.

In the case of chloride ingress, special attention has been paid to the knowledge of the profile shape, the surface concentration evolution in natural conditions and the chloride binding regime. In these aspects, the collection of data and the analysis made have enabled important advances and a deeper understanding of the process.

Related to the transport of chlorides into concrete and their reaction, there are many aspects needing further study:

1. **Transport phase**. Transport depends on the porosity and external concentration of chlorides (driven force). From the basic clarification of the acceleration effect of external electrical fields, migration is used together with natural diffusion for studying the effect of several variables on the velocity and mode of chloride ingress.
   a. *Unsaturated conditions* − Chloride penetration is usually measured in saturated concrete; however, numerous structures are in environments polluted with chlorides in the air (in the water vapour of the air), as they are placed near the sea but are not water saturated. Basic studies in the laboratory have been made by Climent et al. (2000), Figure 14.2, and studies in real conditions have been made by Meira et al. (2007) in several site stations on the east coast of Brasil, in which the rate of deposition of the chlorides on the concrete surface, and the influence of the wind regimes and the cost of border distance have been established. However, it is necessary to collect similar data from many other places in the world and to establish a general trend.
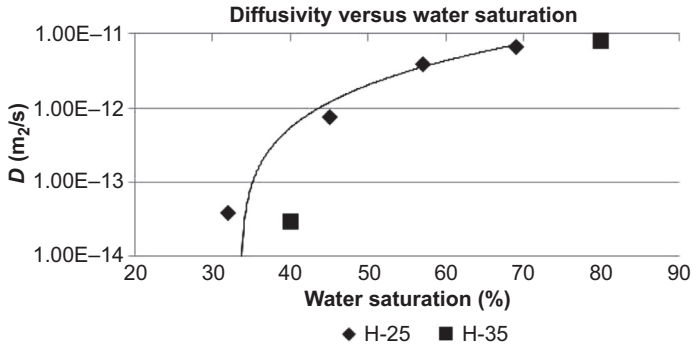
Figure 14.2 Relationship between Cl⁻ diffusion coefficients with binding consideration and the degree of water saturation of the specimens (Climent et al., 2000).

    b. *Tortuosity* − The relation between the pore volume and the diffusion coefficient is not lineal, which is attributed to pore *tortuosity and 'constrictivity'*, but until now its quantification has not been fully successful. Its clear definition and role is a key aspect in prediction from the concrete microstructure.

    c. Effect of *zeta potential of the pore walls* − The *zeta potential* (the potential induced by the double layer appearing due to the surface charge of the pore surfaces) should play a role in the ion transport in concrete as illustrated by Page and Lambert (1987), but its quantification is far from being clear and particularized for each ion.

2. Reaction. In *chloride binding*, AFm phases are the preferential compounds that form chloroaluminates (Glasser et al., 1999) that retard the chloride threshold's advance towards the reinforcement.

    a. *Chloride isotherms* − The study of chloride binding has been made in the last few years, modelled by means of mathematical expressions called 'chloride isotherms', which relate bound chlorides to total or 'free' chlorides remaining in the pore solution. Two isotherms are used for modelling: Langmuir and Freundlich (Figure 14.3). The use of the equilibrium constants should be explored in order to try to rationalize more the binding process.
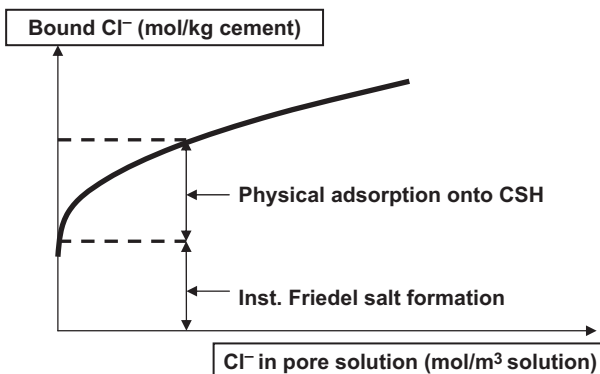
Figure 14.3 Simplified shape of chloride 'isotherms'.
Reproduced from Baroghel-Bouny et al. (2010).

    b. *Chloride binding kinetics* − The isotherms are empirical relations that substitute more appropriate thermodynamic expressions and also do not take into account the rate of reaction.

    c. *Mineral additions* − It additionally remains, in spite of the many publications around the subject, to fully clarify how the chlorides react with the different aluminate and sulfoaluminate phases present in pure Portland cements and in *cements with mineral additions.*

    d. The role of the *pH of the pore solution*, as well as cycling of *temperature* in hot and cold seasons, also needs to be quantified.

3. Aging and changes in the concrete microstructure. It has been noted that due to the penetration of chlorides, a *decrease of the diffusion coefficient* called 'aging' is detected with the progression of time (Mangat and Molloy, 1994). Its quantification as a 'potential' mathematical expression has enabled it to be called an '*age factor*' to the power *n* of the expression

$$D_t = D_0 \left(\frac{t}{t_0}\right)^{-n} \tag{14.1}$$

where D_t is the value of the apparent coefficient at further ages, t, D_0 is the value at the testing time t_0 (usually 28 days of curing plus the testing time of 35 or 90 days) and n is an exponent (the age factor) indicating the slope of decreasing D_{ns} with time. This equation is represented in Figure 14.4 for the hypothetical case of an initial D_{ap} value of 1×10^{-8} cm²/s. In the function of the exponent n, the initial D_{ns} value would decrease one or two orders of magnitude after 100 years, which represents a tremendous impact in the prediction of the time to reinforcement corrosion. Therefore, the most possible exact determination of exponent n is a crucial aspect for the whole reliability of a prediction. This equation is starting to be used also in practice and being adopted in prestandards, with the inherent risk that its misinterpretation could have.

    Information is needed for the causes of the decrease and how long it develops, together with the need to develop a rapid testing method that could help in the reliability of service life predictions. On the other hand, the *type of cement* plays a central role in the decrease noticed, because pure Portland cements present a low decrease while cements with mineral
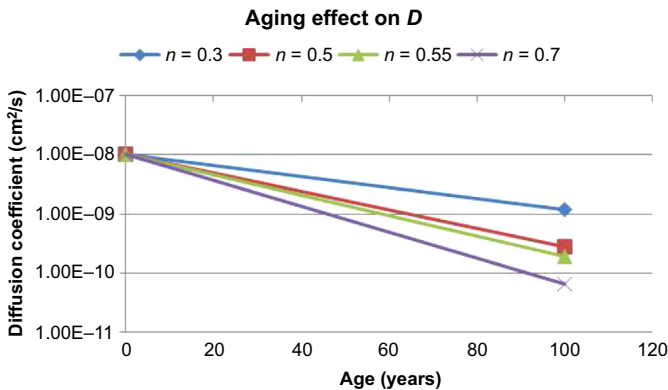
Figure 14.4 Effect of exponent *n* on the decrease of D_{ap} with time calculated by means of Eqn (14.1), assuming $t_0 = 0.0767$ years.

additions show significant decreases, so it is important to note that a small variation can greatly affect the prediction.

4. **Testing**. It is at present very common to use either natural diffusion or migration tests. If the results of the testing are to be used in service life prediction, several aspects need further research, because not only the different external chloride concentrations may aim at different D values, but variations are also found when varying the duration of testing time. The evolution of microstructure is one of the reasons for the differences. In this respect, superior test results have been achieved using natural diffusion, because it is possible to extend the time of contact of the solution with the concrete and then to monitor aging evolution. Migration tests being made in a very short time are not good, because they are made with the concrete out of contact with the salt solution. Work is needed to try to find conditions that could be used to better *reproduce real ones over the long term.* Additionally, it must be mentioned that testing conditions consider only immersion, and *tests considering partial saturation or de-icing salts* are not standardized. For partial saturation, the work of Climent et al. (2000) must be mentioned.

Migration tests allow for significant shortening of testing time and have become very popular (Andrade, 1993; Whiting, 1981). This is because the accelerating factor is ν times the voltage applied, where:

$$\nu = \frac{z \cdot F}{R \cdot T} \tag{14.2}$$

for which $F =$ Faraday's constant, $R =$ gas constant, $T =$ temperature and $z =$ charge. For $T = 293$ K, the value result is 39.6, which multiplied by 10 V means that the testing time is shortened by almost 400 times.

However, as mentioned, these accelerated methods are not suitable to quantify aging factors and should not be used to predict service life (unless no aging is considered or is tested in parallel tests — for instance, by measuring resistivity evolution), because they are measured at a precise moment with the concrete being out of the salt solution.

A solution for the different uncertainties of chloride testing is to use concrete resistivity (Andrade, 2004), which is a nondestructive technique (NDT) that can monitor the evolution of hydration in the same specimen. The resistivity is equivalent to the steady state (effective) diffusion coefficient, then incorporating a 'retard' factor due to the binding, which can be calculated by means of several tests, one of which is the multiregime test to obtain the ratio between the effective and apparent diffusion coefficient. Resistivity enables the recording of the decrease due to concrete 'aging' (Andrade and d'Andrea, 2011) in saturated conditions, as shown in Figure 14.5.

5. **Modeling**. It was extensively reviewed in (Houst and Wittmann, 1994) and several other papers (Saetta et al., 1993; Sagüés, 2003; Berke et al., 1986; Gulikers, 2004), and still is a key subject of research due to the lack of record of long-term data compared with short-term testing. Service life predictions began around 20–30 years ago, and we still lack proper long-term records and calibration. For chloride testing, the most usual model is based on second Fick's law, considering the boundary conditions of constant chloride surface concentration C_s and a semi-infinite medium. Fick's laws are derived from the heat transport (Tuutti, 1982).

$$-J(x) = \frac{\partial C(x)}{\partial t} = D_{ap}\frac{\partial^2 C}{\partial x^2} \tag{14.3}$$
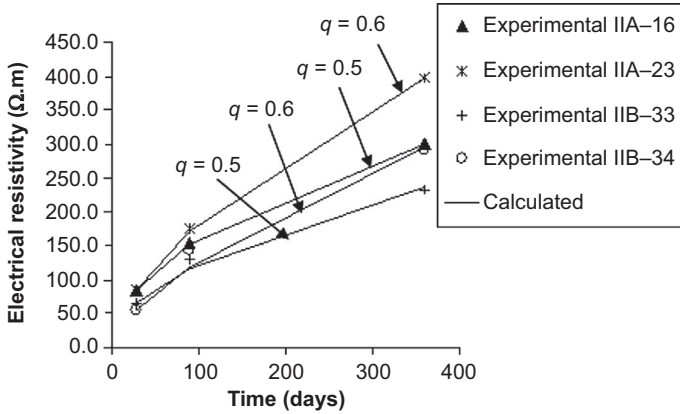
Figure 14.5 The increase in resistivity with time develops in parallel to the decrease of the diffusion coefficient (Mangat and Molloy, 1994; Baroghel-Bouny et al., 2010), and then can be used in the determination of the aging factor.
From Andrade and d'Andrea (2011), where several cement types IIA and IIB were tested.

$$C_x = C_s \left(1 - erf \frac{x}{2\sqrt{D_{ap}t}} \right) \tag{14.4}$$

An alternative to Fick's law is the use of the Nernst−Plank law of mass transport, because it allows the modelling of the external application of an electrical field (Andrade, 1993), and also it enables the consideration of all ions present in the pore solution (multi-ionic transport) or convection conditions:

$$-J_j(x) = D_j \frac{\partial C_j(x)}{\partial x} + \frac{z_j F}{RT} D_j C_j \frac{\partial E}{\partial x} + C_j V(x) \tag{14.5}$$

being: $J(x)$ = unidirectional flux of species (mol/cm^{2}s), D_j = diffusion coefficient of species j (cm^2/s), ∂C = variation of concentration (mol/cm^3), ∂x = variation of distance (cm), ∂E = variation of potential (V), Z_j = electrical charge of species j, F = Faraday's constant (coil/eq), R = gas constant (cal/(V.eq)), T = absolute temperature (°K), C_j = bulk concentration of species j (mol/cm^3) and v = artificial or forced movement of ion (cm/s).

As mentioned, in spite the expansion on the development and use of chloride models, their applicability for predictions of long-term performance remains uncertain because of four main limitations:

1. *Boundary conditions.* The C_s values are crucial because of the impact they have on the calculation. They vary depending on the type of cement and age of the structure together with the exposure class. An additional aspect of the problem that needs to be studied is the fact that a pick (Figure 14.6) is developed in certain structures, which is called a 'skin' effect or the
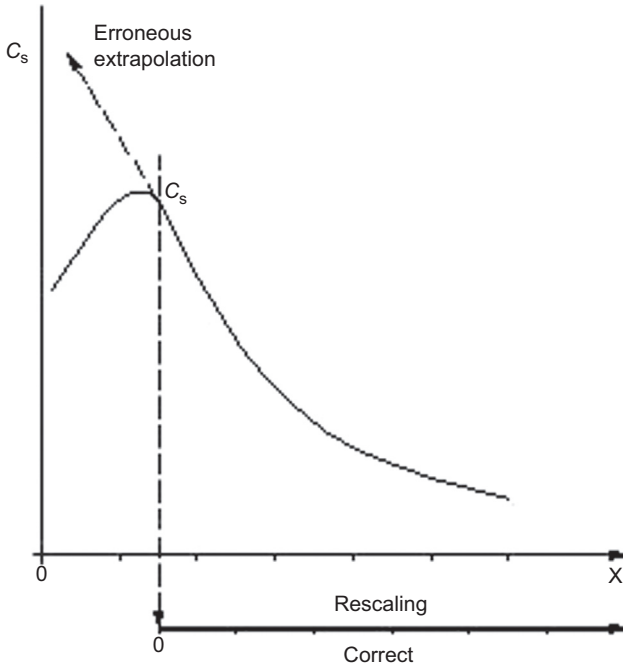
Figure 14.6 Profile showing a pick in the inetrior of the concrete not being the maximum concentration in its surface. Predictions should be made from the pick and not from the 'virtual' surface concentration obtained from the back extrapolation from the pick.

developing of a 'convection' zone. Its progression with time is unknown with reference to concrete quality and exposure class. It has to be emphasized that the prediction for future progression of chlorides should be made from that maximum value (C_{max}) and not from the 'virtual C_s' obtained from the extrapolation.

2. *Modeling of external conditions − climatic events and chloride deposition rates.* For the correct prediction of service life, it is necessary that boundary conditions are well established and determined by the environment. For the case of chlorides transported by air and wind in coastal areas (Meira et al., 2007), a model has been developed in recent years that considers wind velocity and distance from the coast, among other parameters. However, changes in temperature have not yet been considered.

3. *Statistical variability.* Due to the inherent variability involved in the fabrication of concrete and in the climate itself, there is a challenge to establish the statistical variability of model parameters and their characteristic values. This work is very time-consuming and requires interlaboratory testing in addition to calculating the optimum number of samples for the statistical characterization.

4. *Levels of sophistication.* The more sophisticated the model in trying to be more accurate, the more difficult it becomes to validate the parameters involved. This is a general trend for all materials, not just concrete. A reasonable balance between model complexity and applicability should be found in each model. A good compromise can be achieved by establishing levels of sophistication with the same results.

5. *'Multi-ionic' modelling*. Recent efforts (Glasser et al., 2008) have been made to consider all ions in the mass balance equations of transport. Although this is an interesting advance, these efforts share the aspect mentioned, that complexity is not always an advantage unless all parameters are well characterized. Multi-ionic transport requires the constitutive and activity values for all ions, which is not always feasible. If approximations are adopted, then errors can be of the same order as other less sophisticated models. On the other hand, the main important ion is chloride, and if its transport number is known, the rest of the ion concentrations are not strictly necessary.

SCC. Although only two causes of corrosion are usually mentioned, carbonation and chloride induced corrosion, there is another type, the stress corrosion cracking (SCC) phenomenon, which is more risky because it induces metal brittleness failures. SCC occurs only when the following three factors are simultaneously present (Galvele, 1987; Sánchez et al., 2007): (1) the use of a susceptible material (such as prestressing wires), (2) a certain level of stress and (3) an aggressive environment (still not well identified in concrete). The process starts by the nucleation of microcracks in the surface of the steel. One of them may progress to a certain depth from which the crack velocity is very high, and the wire breaks in a brittle manner in relatively short time. The mechanism of nucleation and its progression to SCC is still a controversial issue. There are numerous unknown basic aspects of SCC that need further clarification, but models that can indicate the risk in posttensioned or prestressed elements are urgently needed.

14.3 Corrosion onset and chloride threshold

In alkaline media, the steel develops the so-called 'passive layer' that maintains the metal in passive state for decades unless aggressive substances reach the reinforcement (Elsener et al., 2011; Ghods et al., 2011). When the carbonation front or the chloride threshold reaches the rebar level, corrosion may start with the disappearance of the passive layer existing in the alkaline media. The phenomenon of depassivation and the start of corrosion seems to be much studied; however, there are numerous aspects in addition to the chloride threshold (Gouda and Monfore, 1965; Glass and Buenfeld, 1997; Hausmann, 1964; Lambert et al., 1991; Izquierdo et al., 2004; Markeset, 2009), which is the most commonly mentioned, that remain not fully elucidated. The most important to be emphasized are the following:

1. **Passive layer**. Very interesting papers have been published by Elsener et al. (2011) and Ghods et al. (2011) on this subject. It remains to establish a clearer link of the characteristics of the passive layer to the chloride threshold.
2. **Depassivation by chloride and chloride threshold**. Study of the chloride threshold's ability to induce corrosion has generated more heat than light, but still is a valid consideration for a limit of 0.4% of Cl^- based on a simple calibration of the bound Cl^- of an ordinary Portland cement. It can be deduced from recent work that the chloride threshold depends on the rest potential. The chloride threshold is higher as the potential becomes more cathodic. The best manner to handle chloride threshold is to consider the statistical distribution for
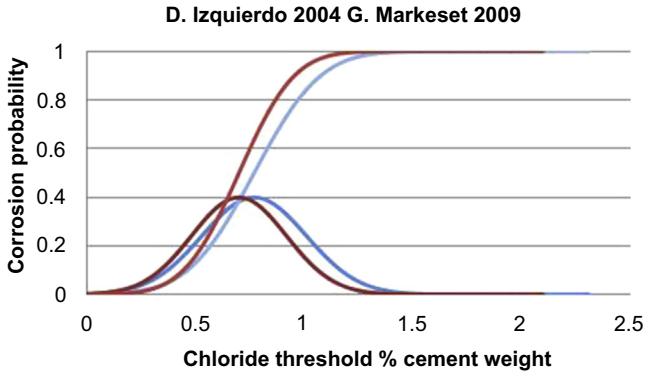
Figure 14.7 Different statistical distributions of the probability of depassivation as a function of the amount of chlorides (in black that of Iquierdo et al. and in blue that of Markeset).

depassivation obtained from the results shown in Figure 14.7 (Izquierdo et al., 2004), where the distribution of (total) chloride thresholds for potential values more anodic than -200 mV SCE is presented. The result for chloride threshold (Cl_{th}) in % by cement weight $= 0.771 \pm 0.2$ for total chloride content; that is, at 95% probability the average value is 0.771 with a standard deviation of ± 0.2. In a graphic manner, these can be plotted as the chloride concentration versus the probability of depassivation.

In the same graph has been plotted the results found by Markeset (2009) in real structures in Norway. The accordance in the shape of the distribution indicates that the laboratory data exhibit a lower chloride threshold and can be used as a reference. Then, new data in real conditions are needed in order to confirm the statistical distribution found.

In general, the probability of corrosion has to be calculated by taking into account that chlorides reach the external part of the bars first, and that the probability and amount of corroded surface increases with the passage of time following a rate controlled by the diffusion coefficient. The sequence is given in Figure 14.8. In it is expressed that depassivation, for practical purposes, is not an instantaneous event but a period, and the limit or chloride threshold will depend on the amount of corrosion produced at a certain time. The limit results not in a unique value, but is linked to the limit state to be verified.
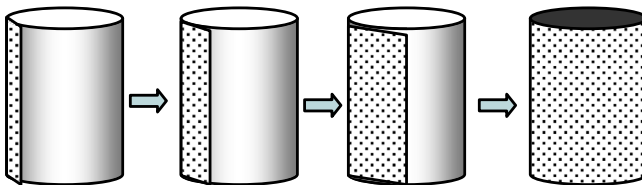
Figure 14.8 Progressive depassivation of the perimeter of the bar due to the arrival of the corrosion threshold.

14.4 Corrosion propagation

After corrosion starts and remains in active condition, oxides are generated that diffuse through the pore system and induce pressures leading to cracking of the concrete cover. In submerged structures, though, oxides may have a low degree of oxidation so that cracking is often not produced. The 'rust' has an expansive character, because iron oxides occupy a higher volume than parent steel. The four structural consequences of corrosion are: (1) the loss of steel section, (2) the decrease in steel ductility, (3) the loss of the steel/concrete bond and (4) concrete cover cracking, all of which result in decreases in the load-bearing capacity of the element. The time to reach a certain limit state depends on the rate of corrosion. The corrosion propagation period has been modeled by assuming a constant corrosion rate (an average obtained annually) by dividing the corrosion penetration, P_{corr}, or loss in radius by the corrosion rate V_{corr} (or I_{corr} if expressed in µA/cm^2) (Andrade et al., 1988):

$$t_p = \frac{P_{corr}}{V_{corr}} \tag{14.6}$$

Three main challenges related to the calculation of accumulated corrosion are (Andrade et al., 1988, 2000, 2002; Andrade and Castillo, 2003; Molina et al., 1993; Torres and Sagüés, 2000):

1. **Relation between corrosion and climatic parameters**. The corrosion rate depends on concrete's porosity and water content. These concrete characteristics are well represented by concrete resistivity, and a corrosion rate model based on resistivity was published some time ago (being the Icorr in micro-A/cm2 and the Resistivity in Kohm.cm).

$$I_{corr} = \frac{30}{\rho} \tag{14.7}$$

   Most studies are made under laboratory conditions or in chambers with controlled conditions, but actual structures are exposed to the atmosphere and the impacts of rain, changing temperature, snow and wind, have hardly been studied. Under these conditions, all corrosion parameters evolve over time, as Figure 14.9 shows for the corrosion rate of the reinforcement of a beam contaminated with chlorides. The daily and seasonal evolution imposes changes in the water content that cannot be straightforwardly modeled. It is necessary to undertake the recording of data in natural exposures in order to have a general formulation.

2. **Representative annual corrosion rate**. The changes in the corrosion rate make it necessary to define an annually averaged or representative corrosion rate, $I_{corr,REP}$, that could facilitate the prediction of corrosion progression. The accumulated corrosion enables such a representative value to be obtained if there are enough data. Thus, the right side of Figure 14.9 shows the accumulated corrosion P_{corr} in a concrete beam contaminated with chlorides exposed to atmospheric events. The corrosion rate results are certainly constant, although in the case of the figure, there are two clearly different periods in the life of the element: during the first two years, and after. The two-year mark was identified as the time when the cover cracked.
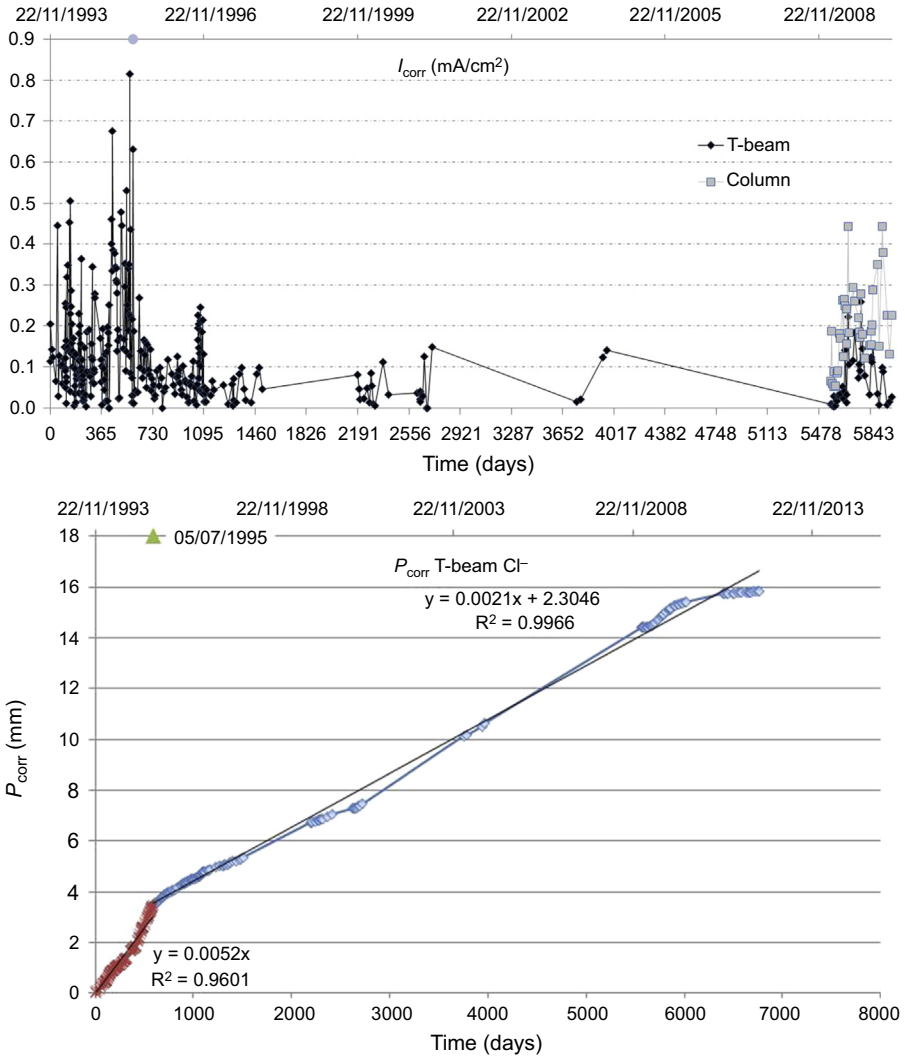
Figure 14.9 Evolution of corrosion rate with atmospheric climatic events. Corrosion current density and accumulated corrosion for a T-beam (Andrade et al., 2002).

In outdoor exposition, it seems that when the cover cracks, the corrosion rate decreases due to the quicker drying that the crack allows.

3. **The relation between corrosion penetration and cover cracking**. It is very popular at present to develop studies on numerical or analytical modelling of the crack width generated by corrosion; however, very few experimental studies have been made, and it must be recognized that few advances from the initial studies have been obtained (Molina et al., 1993; Torres and Sagüés, 2000). The most interesting need in the future is to continue the experimental studies with different concrete types and under different humidity conditions.

14.5   Modelling of service life

Service life is usually modelled from Tuutti's work (Tuutti, 1982) by a two-step process of initiation and propagation:

$$t_1 = t_i + t_p \tag{14.8}$$

The need to approach the calculation with computational methods has resulted in the proposal of different models (Saetta et al., 1993; Sagüés, 2003; Berke et al., 1986; Gulikers, 2004); these models, however, lack proper calibration because they are relatively new. During the last decade, computers have enabled the expansion of modelling in such a manner that not only unidirectional transport of moisture and ions have been published, but even 3-D representations of the progression of hydration and the formation of the microstructure are feasible (Garboczi et al., 2004; van Breugel, 2008).

1. **Multilevel modeling**. The several approaches (van Breugel, 2008; Andrade, 2006; Baroguel-Bouny et al., 2004) to modeling and verifying service life have induced the need for classification. Table 14.1 (Andrade, 2006) shows that three levels of verification are being developed. *Level 1* is deterministic and comprises deemed-to-satisfy rules that are the traditional prescription of concrete mix proportioning. *Level 2* is semiprobabilistic and based on either (1) the use of 'durability indicators' and performance tests that are related to durability, but without the explicit use of time or (2) prediction models in which time is explicit. *Level 3* is the fully probabilistic level.

2. **Probabilistic treatment and safety limits**. This is the usual approach for structural calculations, and should be for durability. It is necessary that data are collected and treated probabilistically in order to apply these concepts in a rigorous manner to structures at risk of suffering from deterioration (Rackwitz, 2000; Duracrete, 1998; Frangopol, 1997). In this respect, it must be emphasized that the level of optimum safety in deteriorating structures is far from being solved, because it has yet to be analysed in comparison with failure consequences and economic costs. That is, the reliability index β has to be optimized by comparison of different technical solutions with their associated costs in order to establish optimum safety levels. Currently, there is a lack of real data that could help to advance the state of the art in this subject. Life cycle analyses or safety calculations should be based on recorded data in real structures, rather than being simply interesting computational exercises.

Table 14.1 Levels for durability design formats (Andrade, 2006)

Levels of durability verification				
1	2		3	
Deterministic	Semiprobabilistic		Probabilistic	
Time implicit	Time implicit	Time explicit	Time implicit	Time explicit
Standards & codes	Durability indicators	Prediction models	Durability indicators	Prediction models

3. **Performance approach**. Efforts have been made to apply this approach to current standards in order to define objectives more than specifications. The indicators are characteristics or properties of the concrete that are classified in categories or levels, and can be better applied in daily practice (Andrade, 2006).

4. **Electrical resistivity as a corrosion indicator or controling parameter of a model**. Electrical resistivity is a parameter that informs simultaneously on a material characteristics, such as porosity with the degree of water saturation (Andrade, 2004; Andrade and d'Andrea, 2011). Assuming it is measured in specimens of concrete at 28 days wet curing, its values can be used as a corrosion indicator by ranking the values and relating them with time to depassivation, or it can be introduced in a mathematical expressions of a type of square root law based on its relation to diffusivity. The model based on resistivity requires certain complementary parameters related to the binding of chlorides or carbon dioxide (reaction factor), and ambient factors. The resulting model can be applied to the initiation and propagation period. It needs experimental validation, but its application is promising. The present expression of the model is:

$$t_l = \frac{x^2 \cdot \rho_{ef} \left(\frac{t_t}{t_0}\right)^q}{k_{Cl,CO_2}} \cdot r_{Cl,CO_2} + \frac{P_c \cdot \left(\rho_{ef} \cdot \left(\frac{t_t}{t_0}\right)^q \cdot \xi\right)}{K_{\text{corr}}} \tag{14.9}$$

where t_l = time life, x = cover thickness, ρ_{ef} = concrete resistivity at 28 days wet curing, t_0 = time at which the first resistivity measurement is made, t_t = 28 days, r_{Cl,CO_2} = reaction factor, k_{Cl,CO_2} = ambient factor, P_c = corrosion penetration, ξ = ambient factor applied to the corrosion rate and K_{corr} = corrosion constant (see Eqn (14.7)).

5. **The modeling of the structural consequences of material degradation**. Important advances have been made in recent years (Rodriguez et al., 1995; Contecvet, 2001), and at present are the basis for the structural recalculation of elements deteriorated by reinforcement corrosion, at least with simplified models, although numerical modeling also is being developed in the subject.

6. **Management of service life**. Concrete structures are designed and built to comply with the design requirements of safety, serviceability and aesthetics. Apart from mechanical stability and resistance to fire covered by the standards, concrete structures must comply with other essential requirements of both a technical and a nontechnical nature. They can be grouped into four main headings: (1) economical and financial, (2) social and cultural, (3) environmental and (4) functional. These requirements should be maintained during the entire service life, and an important step is the establishment of periodic inspections with corrective measures. Although life cycle analysis has been applied to concrete structures, it is far from being a tool capable of helping owners to maintain their inventories of structures (ConRepNet, 2007).

14.6   Additional preventive measures

The most efficient methods to extend the corrosion onset of the reinforcement are (Figure 14.10):

1. **Cathodic protection** (Lazzari and Pedeferri, 2006), which needs to develop anodes that could last longer and be incorporated in existing structures without changing their aesthetics
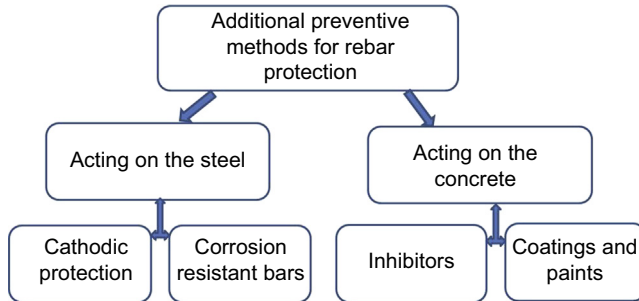
Figure 14.10 Additional preventive methods for corrosion protection of the reinforcements.

2. **More corrosion-resistant reinforcements** such as stainless steel (Nurnbeger, 2005), galvanized (Yeomans, 1994) or composite rebars (Malvar, 1995) — that is, changing normal steel by use of corrosion-resistant materials
3. **Inhibitors** added (Berke, 1989) to the mix or applied from the surface are also efficient in extending the service life.

All these methods are efficient but render the concrete more expensive. Their analysis in a life cycle cost approach could help to introduce them more efficiently into new structures.

14.7   Repair techniques

The most common repair techniques are patching and cosmetic repair of the concrete (Vennesland, 1997; Mailvaganam, 1992; Raharinaivo and Pollet, 2003). Numerous cement-based materials for repair and patching have been developed. They are quite resistant to the penetration of aggressive substances, but their thermal and mechanical characteristics are different from those of the parent concrete, and failures resulting from these differences are often prematurely produced. The challenge will be to develop materials that could be more easily applied while functioning with the same basic characteristics as the initial concrete.

Regarding other repair techniques, the most efficient is cathodic protection, which is well established, and the challenge is in adapting to the existing structure by developing flexible anodes of easy application. The other two electrochemical repair techniques, re-alkalization and chloride extraction (Raharinaivo and Pollet, 2003), also have advanced very remarkably in the last decade. Being more complex than cathodic protection, these still need more time before they become more widely used, indicating the need for more technical developments.

14.8   Corrosion measurement techniques

Proper techniques were used from very early studies (Gouda and Monfore, 1965) in the laboratory and so, corrosion potential and corrosion rate (through the polarization resistance technique) measurements have enabled to understand many of the basic

phenomena (Andrade and Gónzalez, 1978; Feliú et al., 1990; Andrade et al., 2004) The application of these techniques to the measurement in large real structures was made at the beginning of the 90s (Lazzari and Pedeferri, 2006; Nurnbeger, 2005; Yeomans, 1994; Malvar, 1995; Berke, 1989; Vennesland, 1997; Mailvaganam, 1992; Raharinaivo and Pollet, 2003; Andrade and Gónzalez, 1978; Feliú et al., 1990; Andrade et al., 2004) after solving the calculation of the steel area polarized by the current applied from a small counter electrode or 'critical length'. This length is not a constant and therefore requires an intelligent mode of confining the cement applied to a predetermined area. This can be achieved by the so-called 'modulated confinement' by means of a second annular counter that surrounds the principal one and maintains the current confined between both: central disc and guard ring. An alternative to the modulated confinement is the direct measurement of the critical length by means of placing reference electrodes in the surface of the concrete at precise distances and follow the attenuation of the potential with the distance. Their use is well established from many years ago but still several aspects need further research: (1) the search for an NDT that could give information on the actual loss of metal and (2) the developing of smart interpretation of monitoring by sensors (Vennesland et al., 2007). The monitoring of data in real structures reports important information but, on the other hand, demands the management of a huge amount of data and their processing and incorporation into engineering models. The filtering of erroneous data and the interpretation of them still will need development.

14.9   Final comments

In reviewing the challenges for future reinforcement corrosion work, the *modeling* of processes should be mentioned as the most important subject studied during the last few years. For the future, the challenge is the integration of partial models into more comprehensive ones in a 'multiscale and multilevel' approach. The modeling needs to be fed with reliable data measured under real conditions. The expressions must be scientifically based and experimentally validated, in order to position concrete research as a high-tech field with tailored solutions adapted to local materials.

On the other hand, being that it is the steel reinforcement that corrodes, trends should shift to develop more resistant reinforcing bars, such as by galvanizing or manufacturing with stainless steel. Fibre-reinforced polymeric bars are also a choice, although their mechanical characteristics and bond to the concrete are not yet optimized, and their durability should be better studied over the long term. As to repair methods, identifying so-called 'migrating inhibitors' that can penetrate from outside without the necessity of removing non-cracked-due-to-deterioration zones is conceptually an important goal.

Acknowledgements

References

Andrade, C., Castillo, A., 2003. Evolution of reinforcement corrosion due to climatic variations. Materials and Corrosion 54 (6), 379−386.

Andrade, C., d'Andrea, R., April 2011. Chloride aging factor of concrete measured by means of resistivity. In: Proceedings of the XII DBMC, International Conference on Durability of Building Materials and Components. Oporto, Portugal.

Andrade, C., Gónzalez, J.A., 1978. Quantitative measurements of corrosion rate of reinforcing steels embedded in concrete using polarization resistance measurement. Werkstoffe und Korrosion 29, 515.

Andrade, C., Alonso, M.C., González, J.A., June 1988. An attempt to use the corrosion rate measurements for estimating rebar durability. In: Proceedings of the Conference on Corrosion Rate of Steel in Concrete (ASTM) Baltimore (USA).

Andrade, C., Fullea, J., Alonso, C., 2000. The use of the graph corrosion rate-resistivity in the measurement of the corrosion current. In: Andrade, C., Alonso, C., Fullea, J., Polimon, J., Rodriguez, J. (Eds.), Proceedings of the International Workshop on Measurement and Interpretation of the On-site Corrosion Rate. MESINA- RILEM Proc. No. 18. Rilem Publications S.A.R.L, pp. 157−166.

Andrade, C., Alonso, C., Sarría, J., 2002. Corrosion rate evolution in concrete structures exposed to the atmosphere. Cement and Concrete Composites 24, 55−64.

Andrade, C., Alonso, C., Gulikers, J., Polder, R., Cigna, R., Vennesland, Ø., Salta, M., Raharinaivo, A., Elsener, B., 2004. Test methods for on-site corrosion rate measurement of steel reinforcement in concrete by means of the polarization resistance method. Materials and Structures 37, 623−643.

Andrade, C., 1993. Calculation of chloride diffusion-coefficients in concrete from ionic migration measurements. Cement and Concrete Research 23 (3), 724−742.

Andrade, C., 2006. Multilevel methodology for durability design. In: International Workshop RILEM on Perfomance Based Evaluation and Indicators for Concrete Durability, Madrid-Spain, pp. 101−108.

Andrade, C., 2004. Calculation of initiation and propagation periods of service-life of reinforcements by using the electrical resistivity. In: International Symposium on Advances in Concrete through Science and Eng., RILEM Symposium, March 22−24, Evanston (Illinois, USA).

Bamforth, P., Chapman-Andrews, J., 1994. Long term performance of RC elements under U.K. coastal exposure conditions. In: Swamy, N. (Ed.), International Conference on Corrosion and Corrosion Protection of Steel in Concrete. Sheffield Academic Press, pp. 139−156.

Baroghel-Bouny, V., Wang, X., Thiéry, M., October 2010. Prediction of chloride binding isotherms by analytical model or numerical inverse analysis. In: Proceedings of the 2nd Symposium on Service Life Design for Infrastructures. (DBMC Service life). Delft University of Technology.

Baroguel-Bouny, V., et al., July 2004. Concrete Design for a Given Structure Service Life. Durability Control with Respect to Reinforcement Corrosion and Alkali-silica Reaction. State-of-the-art and Guide for the Implementation of a Performance-type and Predictive Approach Based upon Durability Indicators-Scientific and Technical Documents of AFGC, p. 252.

Berke, N.L., Dallaire, M.P., Hicks, M.C., MacDonald, A.C., 1986. Holistic approach to durability steel reinforced concrete. In: Dhir, R.K., Hewlett, P. (Eds.), Proceedings of the International Conference "Concrete in the Service of the Mankind. Radical Concrete Technology". E&FN Spoon, UK, pp. 25−45.

Berke, N.S., October 1989. A review of corrosion inhibitors. Environmental Treatment and Control 41−44.

van Breugel, K., 2008. Beyond multiscale modeling. In: Schlangen, E., et al. (Eds.), Proc. Int. RILEM Symposium on Concrete Modeling − CONMOD'08, Delft, pp. 37−46.

Castellote, M., Fernandez, L., Andrade, C., Alonso, C., 2009. Chemical changes and phase analysis of OPC pastes carbonated at different CO_2 concentrations. Materials and Structures 42, 515−525.

Climent, M.A., de Vera, G., Lopez, J.F., Garcia, C., Andrade, C., 2000. Transport of chlorides through non saturated concrete after an initial limited chloride supply. In: Andrade, C., Kropp, J. (Eds.), Proceedings of the 2nd International Workshop on Testing and Modeling the Chloride Ingress into Concrete. RILEM Publications, Cachan, France, pp. 173−187.

ConRepNet, 2007. Thematic Network on Performance Based Remediation of Reinforced Concrete Structures. BRE Press, London.

Contecvet, 2001. A Validated User's Manual for Assessing the Residual Life of Concrete Structures. DG Enterprise, CEC. The manual can be downloaded from the website of www.ietcc.csic.es.

Brite EuRam Project Duracrete -Probabilistic Performance Based Durability Design of Concrete Structures, 1998, pp. 95−1347.

Elsener, B., Addari, D., Rossi, A., 2011. Nickel-free manganese bearing stainless steel in alkaline media—electrochemistry and surface chemistry. Electrochimica Acta 56, 4489−4497.

Feliú, S., González, J.A., Feliú Jr., S., Andrade, C., 1990. Confinement of the electrical signal or in-situ measurement of polarization resistance in reinforced concrete. ACI Materials Journal 87, 457.

Frangopol, D.M., 1997. Application of life cycle reliability-based criteria to bridge assessment and design. In: Thelford, T. (Ed.), Safety of Bridges, Institution of Civil Engineers, Highway Agency.

Galvele, J.R., 1987. A stress corrosion cracking mechanism based on surface mobility. Corrosion Science 27 (1), 1−33.

Garboczi, E.J., Bullard, J.W., Bentz, D.P., 2004. Virtual testing of cement and concrete. Concrete International 26 (12), 33−37.

Ghods, P., Isgor, O.B., Brown, J.R., Bensebaa, F., Kingston, D., 2011. XPS depth profiling study on the passive oxide film of carbon steel in saturated calcium hydroxide solution and the effect of chloride on the film properties. Applied Surface Science 257, 4669−4677.

Glass, G.K., Buenfeld, N.R., 1997. The presentation of the chloride threshold level for corrosion of steel in concrete. Corrosion Science 39 (5), 1001−1013.

Glasser, F.P., Kindness, A., Stronach, S.A., 1999. Stability and solubility relationships in AFm phases Part I. Chloride, sulfate and hydroxide. Cement and Concrete Research 29, 861−866.

Glasser, F.P., Marchand, J., Samson, E., 2008. Durability of concrete. Degradation phenomena involving detrimental chemical reactions. Cement and Concrete Research 38, 226−246.

Gouda, V.K., Monfore, G.E., 1965. A rapid method for studying corrosion inhibiton of steel in concrete. Journal PCA 24. Septiembre, n° 3.

Gulikers, J., 2004. Critical evaluation of service life models applied on an existing marine concrete structure. In: NORECON Seminar 2004: Repair and Maintenance of Concrete Structures, Copenhagen April 19−20, (2004).

Hausmann, D.A., 1964. Electrochemical behaviour of steel in concrete. Journal A.C.I. Febrero 171.

Houst, Y.F., Wittmann, F.H., 1994. Influence of porosity and water content on the diffusivity of CO_2 and O_2 through hydrated cement paste. Cement and Concrete Research 24 (6), 1165−1176.

Izquierdo, D., Alonso, C., Andrade, C., Castellote, M., 2004. Potentiostatic determination of chloride threshold values for rebar depassivation. Experimental and statistical study. Electrochimica Acta 49, 2731−2739.

Lambert, P., Page, C.L., Vassie, P.R.W., 1991. Investigation of reinforcement corrosion. Electrochemical monitoring of steel in chloride contaminated concrete. Materials and Structures 24, 351.

Lazzari, L., Pedeferri, P., 2006. Cathodic Protection-Polipress. Politecnico de Milano Publications, Milan, Italy.

Mailvaganam, N.P., 1992. Repair and Protection of Concrete Structures. CRC Press, Boca Raton, USA.

Malvar, L.J., May−June 1995. Tensile and bond properties of GFRP reinforcing bars. ACI Materials Journal 276−285.

Mangat, P.S., Molloy, B.T., 1994. Predicting of long term chloride concentration in concrete. Materials and Structures 27, 338−346.

Markeset, G., 2009. Critical chloride content and its influence on service life predictions critical chloride content and its influence on service life predictions. Materials and Corrosion 60 (8), 593−596.

Martín-Pérez, B., Zibara, H., Hooton, R.D., Thomas, M.D.A., 2000. A study of the effect of chloride binding on service life predictions. Cement and Concrete Research 30, 1215−1223.

Meira, G.R., Andrade, C., Alonso, C., Padaratz, I.J., Borba Jr., J.C., 2007. Salinity of marine aerosols in a Brazilian coastal area—influence of wind regime. Atmospheric Environment 41, 8431−8441.

Molina, F.J., Andrade, C., Alonso, C., 1993. Cover cracking as a function of bar corrosion: Part II−numerical model. Materials and Structures 26, 532−548.

Nurnbeger, U., 2005. Stainless steel in concrete structures. In: Böhni, H. (Ed.), Corrosion in Reinforced Concrete Structures. Woodhead Publishing Ltd. Condridge, pp. 135−162.

Page, C.L., Lambert, P., 1987. Kinetics of oxygen diffusion in hardened cement pastes. Journal of Materials Science 22, 942−946.

Page, C.L., Treadaway, K.W.J., 1982. Aspects of the electrochemistry of steel in concrete. Nature 297 (5862), 109−115.

Rackwitz, R., 2000. Optimization, the basis of code, ranking and reliability simplification. Structural Safety 22 (1), 27−60.

Raharinaivo, A., Pollet, V., 2003. Chloride extraction and realkalinization. In: Cigna, R., Andrade, C., Nurnberger, U., Polder, R., Weydert, R., Seitz, E. (Eds.), Chapter 3.1. Corrosion of Steel in Reinforced Concrete Structures. COST 521. European Commission Pulbishers. Directorate-General Research, Luxembourg.

Rodriguez, J., Ortega, L.M., Casal, J., 1995. Load carrying capacity of concrete structures with corroded reinforcement. In: Forde, M.C. (Ed.), International Conference on Structural Faults & Repairs, London, UK, 2, pp. 189−198.

Saetta, A., Scotta, R., Vitaliani, R., 1993. Analysis of chloride diffusion into partially saturated concrete24. ACI Materials Journal 90, 441−451.

Sagüés, A.A., October 2003. Modeling the effects of corrosion on the lifetime of extended reinforced concrete structures. Corrosion 854−866.

Sánchez, J., Fullea, J., Andrade, C., 2007. Stress corrosion cracking mechanism of prestressing steels in bicarbonate solutions. Corrosion Science 49, 4069−4080.

Thiery, M., Villain, G., Dangla, P., Platret, G., 2007. Investigation of the carbonation front shape on cementitious materials: effects of the chemical kinetics. Cement and Concrete Research 37, 1047−1058.

Torres, A.A., Sagües, A.A., 2000. Concrete cover cracking with localized corrosion of reinforcing steel. In: Proc., 5th CANMET/ACI Int. Conf. on Durability of Concrete, pp. 591−611.

Tuutti, K., 1982. Corrosion of Steel in Concrete, CBI Research Report 4: 82, Swedish Cement and Concrete Research Institute, Stockholm.

Vennesland, Ø., May 1997. Electrochemical parameters of repaired and non repaired concrete at Gimsoystaumen bridge. In: Blankvoll, A. (Ed.), International Conference on Repair of Concrete Structures from Theory to Practice in a Marine Environment. Svolvaer Norway, pp. 253−262.

Vennesland, Ø., Raupach, M., Andrade, C., 2007. Recommendation of Rilem TC 154-EMC: electrochemical techniques for measuring corrosion in concrete-measurements with embedded probes. Materials and Structures 40, 745−758.

Whiting, D., 1981. Rapid Determination of the Chloride Permeability of Concrete. Report No. FHWA-RD-81-119, NTIS DB No. 82140724. Federal Highway Administration, Washington, DC, p. 174.

Yeomans, S.R., January 1994. Performance of black, galvanized and epoxi-coated. Corrosion Engineering 72−81.

Index